ПУБЛИКАЦИЈЕ АСТРОНОМСКОГ ДРУШТВА "РУЂЕР БОШКОВИЋ" Св. 5
PUBLICATIONS OF THE ASTRONOMICAL SOCIETY "RUDJER BOŠKOVIĆ" No. 5

ЗБОРНИК РАДОВА СРПСКО-БУГАРСКЕ АСТРОНОМСКЕ КОНФЕРЕНЦИЈЕ 2004

Београд, **21-24**. април 2004.
уредник Милан С. Димитријевић

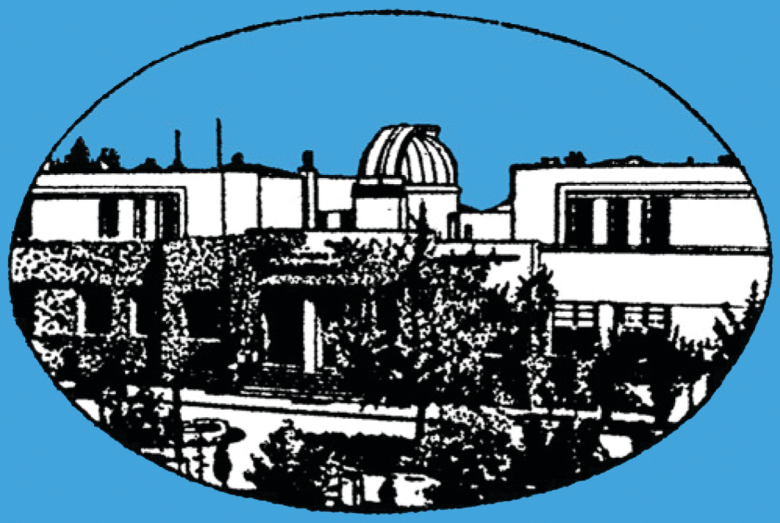

PROCEEDINGS OF THE SERBIAN-BULGARIAN ASTRONOMICAL CONFERENCE 2004

Belgrade, April **21-24**.2004.
ed. by Milan S. Dimitrijević

Belgrade, 2007

Digital copy produced by Žarko Mijajlović
Belgrade
August 2021

UDC 520/524 (082) (0.034.2)

ISSN 0506 4295

ISBN 978-86-906631-3-2

ПУБЛИКАЦИЈЕ АСТРОНОМСКОГ ДРУШТВА "РУЂЕР БОШКОВИЋ"

PUBLICATIONS OF THE ASTRONOMICAL SOCIETY "RUDJER BOŠKOVIĆ"

Sv. 4 **No. 4**

ЗБОРНИК РАДОВА СРПСКО-БУГАРСКЕ АСТРОНОМСКЕ КОНФЕРЕНЦИЈЕ 2004

април 2004.

уредник Милан С. Димитријевић

PROCEEDINGS OF THE SERBIAN – BULARIAN ASTRONOMICAL CONFERENCE 2004

April 18-22, 2004.

ed. by Milan S. Dimitrijević

B E O G R A D

2007

PUBL. ASTRON. SOC. "RUDJER BOŠKOVIĆ" No. 5, 1-294 BELGRADE, JULY 2007

Content

Proc. IV Serbian-Bulgarian Astronomical Conference,
Belgrade 21–24 April 2004,
eds. M. S. Dimitrijević, V. Golev, L. Č. Popović, M. Tsvetkov,
Publ. Astron. Soc. "Rudjer Bošković" No 5, 2005, 9 - 16 *Invited lecture*

3D SPECTROPHOTOMETRY WITH PMAS

P. BÖHM, T. BECKER, A. KELZ, M. M. ROTH and M. A. W. VERHEIJEN
Astrophysical Institute Potsdam,
An der Sternwarte 16, D-14482 Potsdam, Germany

Abstract. Although the method of optical 3D spectroscopy has become more popular in astronomy with the availability of new integral field units (IFUs) for instruments like FLAMES, SINFONI, and VIMOS for the VLT in Chile (ESO), or GMOS at GEMINI North, it has not really become a common tool yet. The main reason for the apparent reluctance in the astronomical community of using IFUs is the difficulty of handling the data.

Here we present the integral field spectrograph PMAS (Postdam Multi-Aperture Spectrophotometer) together with the IDL software tool P3d, developed especially for the reduction of PMAS data. However, with some minor adaptions it is also very useful for the reduction of data taken by other IFUs like VIMOS. We show the capabilities of PMAS with its standard lenslet IFU and its new wide-field IFU module called PPAK, a further development for the observation of low surface brightness objects. Apart from technical details about the instrument and the software, some preliminary scientific results are shown from the observations of Planetary Nebulae.

1. THE PRINCIPLE OF 3D SPECTROSCOPY

3D Spectroscopy (sometimes also called Imaging Spectroscopy, or even more commonly Integral Field Spectroscopy = IFS) is an observational technique to obtain spectra for each point of a 2-dimensional field-of-view in the following way (Fig. 1):

1. the 2D field-of-view on the sky is sampled into discrete spatial elements (so-called SPAXELS) of round, square, hexagonal, ..., shape (depending on the special application of the used IFU instrument)

2. individual spectra are created *simultaneously* for each spaxel over the whole field-of-view

3. the generated set of spectra can be rearranged in a computer to form a 3-dimensional data cube of two spatial coordinates, and one wavelength coordinate

Any column of the data cube represents an individual spectrum at a certain spatial position and any slice corresponds to a monochromatic image at a certain wavelength. Coadding of several columns provides e.g. background or object spectra, and coadding of slices leads to quasi-broadband images.

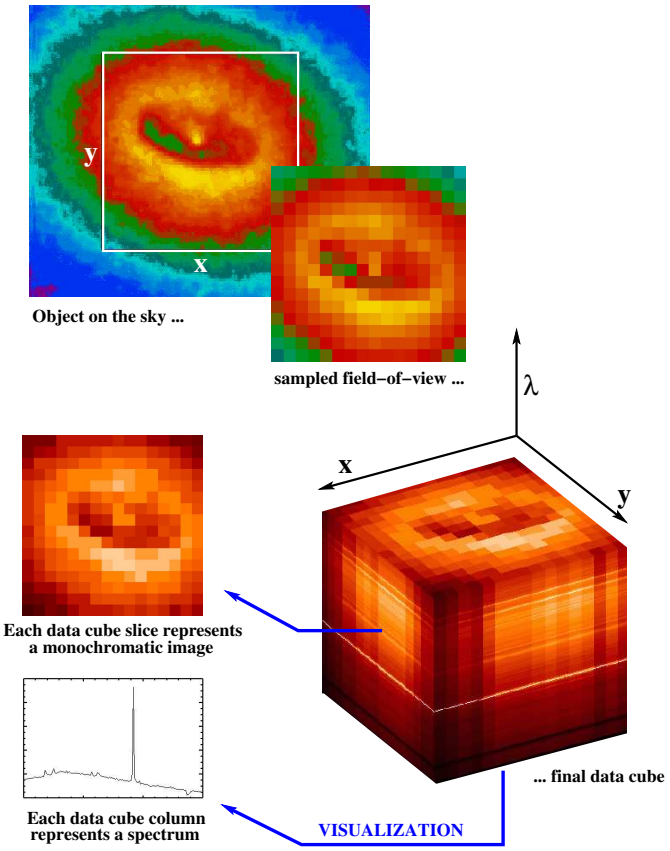

Figure 1: Principle of 3D spectroscopy with square spaxels. In reality, the data cube becomes a *rhomboid* in the presence of atmospheric refraction because of spatial shift as a function of wavelength.

2. PMAS DESIGN AND CHARACTERISTICS

The instrument PMAS, designed and built at AIP, uses a fiber-coupled lensarray to divide the field-of-view into spaxels. A magnified image of the telescope focal plane is projected by foreoptics onto the front surface of a quadratic array of microlenses. Each lens creates a tiny image of the entrance pupil of the optical system (= main telescope mirror), several tens of micrometers in diameter. Optical fibers are attached to the lensarray at the location of these spots, thus providing coupling to a spectrograph at the other end of the waveguides.

The flexibility of fibers is used to rearrange the square format of the input field-of-view into a linear pattern to form a pseudo-slit at the input of the spectrograph collimator. The light from each fiber is dispersed by the grating and is projected as a

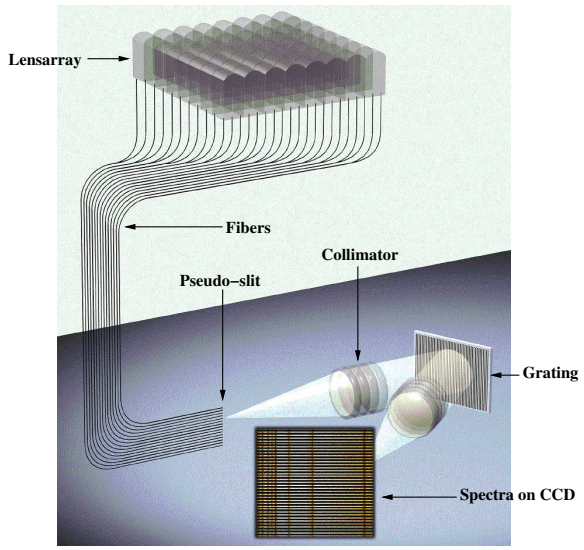

Figure 2: Principle of fiber-coupled lensarray IFS (excluding foreoptics) for a 8×8 lensarray. The recent configuration of the PMAS standard IFU is 16×16 lenses, producing 256 spectra per exposure.

single spectrum on the detector. Since there are many fibers at the pseudo-slit, a family of spectra is generated simultaneously on the CCD, i.e. one exposure produces one CCD-frame containing one set of spectra (Fig. 2).

Apart from the spectrograph CCD, PMAS has a second cryogenic CCD camera for target aquisition and guiding, which can be equipped with up to 4 broad- or narrowband filters.

PMAS was built as a travel instrument that can be mounted to different telescopes with little modification. It has a total weight of roughly 1.5 tons. PMAS has had First Light in 2001, and since 2002 it has been available to the German and Spanish astronomical community and their collaboration partners as a common user instrument at the 3.5 m telescope at Calar Alto Observatory (Spain).

For a complete technical overview of PMAS see Roth 2002, a summary is given in (Tab. 1).

3. P3d – THE PMAS REDUCTION SOFTWARE

There has been an enormous progress in the construction of IFU instruments during the last two years. Large IFUs like GMOS for GEMINI North with 1500 (1000 science, 500 sky) spectra per shot, FLAMES, SINFONI, and VIMOS for the VLT, the last one with 80×80 = 6400 spectra per exposure, have come into operation. Nevertheless, the difficulty of handling the complexity and amount of spectra in a proper and effective way has prevented many astronomers from using these powerful instruments. One needs dedicated data reduction software to automatically extract several hundreds spectra and remove instrumental signatures in order to create the final data cube.

Table 1: PMAS characteristics at Calar Alto Observatory

primary mirror diameter	3.5m
focal station	cassegrain
principle of operation	lensarray + fiber-coupled spectrograph
spectrograph type	fully reflective f/3 collimator and f/1.5 camera
wavelenght range	350 – 900 nm (CaF2 optics)
gratings	1200, 600 and 300 gr/mm reflective gratings
linear dispersion	$\approx$ 0.35, 0.8 and 1.7 Å/pixel, resp.
detector size (standard mode)	2048×4096, 15μm pixels, 2048 spectral pixels
detector size (mosaic mode)	2×2048×4096 mosaic, 4096 spectral pixels
standard field size	16×16 square elements (8″×8″ FoV)
spatial sampling	0.5″×0.5″, 0.75″×0.75″, 1″×1″

PMAS data can be reduced with the IDL-based modular data reduction package P3d, developed by Thomas Becker in parallel with the construction of PMAS. All P3d tools provide graphical user interfaces (GUI) for the comfortable, interactive operation plus an active IDL window for the implication of your own commands.

Apart from the full data reduction package there are tools for quick online reduction, data cube visualization, and mosaicing of data cubes (offset exposures).

3.1. THE FULL REDUCTION PROGRAM P3D

P3d is a data reduction tool which offers an automatic reduction of raw images with photometric accuracy, provided all the necessary calibration data are taken. All the several reduction steps like bias and dark subtraction, cosmic removal, spectra tracing and extraction, wavelength calibration and flat fielding can be run for a complete stack of images either as a whole (after dedicated parameter settings), or step by step.

3.2. P3D ONLINE REDUCTION

As an aid for the observer at the telescope, there is a fast program for the online reduction, in order to have a quick look to the data just observed for immediate observing schedule decisions. To use P3d Online one needs to have

(1) one lamp flat exposure (Halogen) to create the trace mask
(2) one bias exposure for bias subtraction (optional)
(3) one calibration lamp exposure (Neon, Mercury, Thorium/Argon - depending on wavelength range) to create the dispersion mask (optional)
(4) one dome or better skyflat exposure to create the fiber flat mask (optional)

Provided the calibration frames were taken prior the science exposure, the extraction of spectra is performed as a matter of a few minutes after CCD readout. It can be seen immediately, if the target is centered, if the exposure time is sufficient, and if the spectrum shows the expected features.

Eight reduced object files can be displayed in one P3d Online GUI in parallel as monochromatic images. Additionallay, raw images can be displayed, the trace mask can be inspected in comparison to the raw image, and the active data cube can be

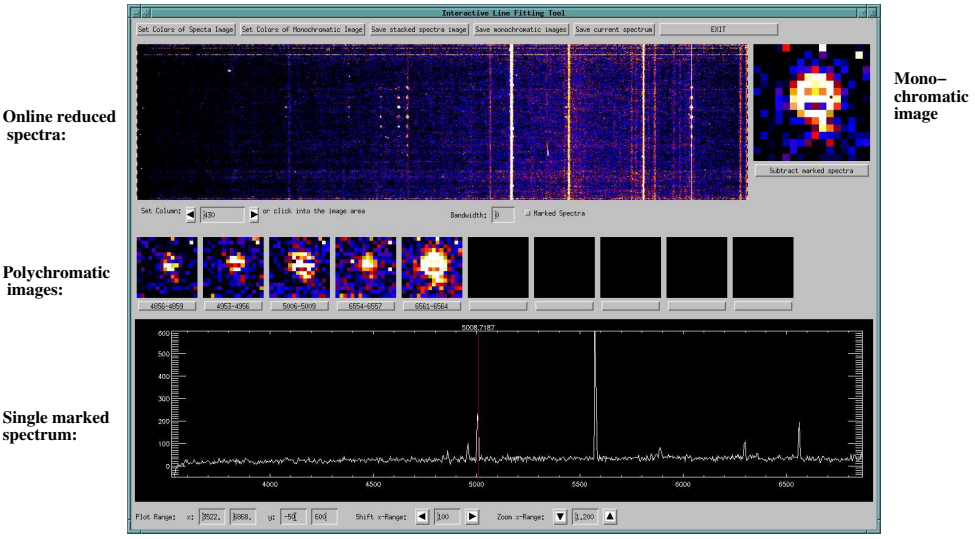

Figure 3: P3d online reduction software, spectra viewer. The object shown is a planetary nebula in LeoA with emission lines in H_β, [OIII], and H_α.

checked by Spectra Viewer and Cube Slider. Last but not least one can display and evaluate telescope focus series taken with PMAS. For more detailed information about the P3d Online tool, see Becker 2003.

3.3. SPECTRA VIEWER

The Spectra Viewer (Fig. 3) displays the extracted 256 spectra of one data cube in a stacked 2D format one by one as lines (dispersion direction) starting from bottom to top (crossdispersion direction). The stacked spectra format gives a first overview of the spectral features in a data cube, and also provides hints to regions of interest in the spatial domain. For example, a distant pointlike planetary nebula appears as emission dots in the spectra of the object spaxels, i.e. in the middle of the y-axis, if the object is centered (upper panel).

A monochromatic image is selected simply by mouse-click onto the column of interest. So-called polychromatic or broadband images are displayed in the middle panel by selection of a certain wavelength region in the panel above.

Clicking onto a certain spaxel in the monochromatic image (upper right) produces the corresponding spectrum plot in the lower panel. The spaxel is marked in the monochromatic image by a black dot. Sky spaxels can be easily recognized by eye, marked on the monochromatic image by mouse-click, and subtracted from the object spectrum.

Although developed especially for the PMAS IFU, the P3d Online software has been successfully adapted for the reduction of VIMOS data.

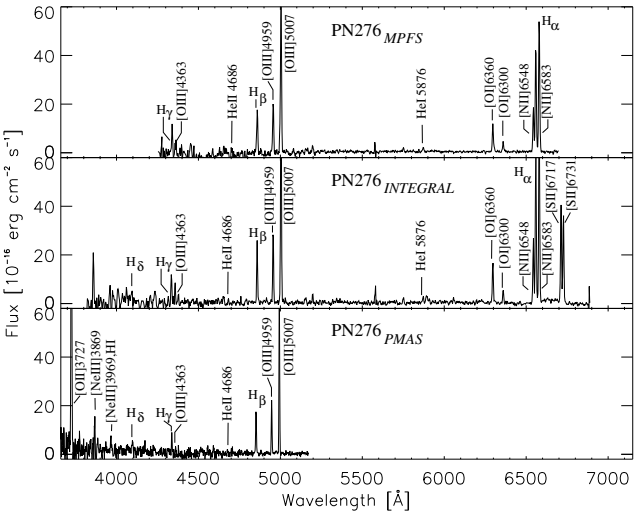

Figure 4: Spectra of the XPN candidate PN276, observed with the 3 IFU instruments MPFS, INTEGRAL, and PMAS. (Roth et al., 2004, Fig. 11).

4. SPECTROPHOTOMETRY OF PLANETARY NEBULAE

The improvement of IFU instruments in comparison to classical slit-spectroscopy is the ability to perform crowded-field spectrophotometry, useful for the study of resolved stellar populations in nearby galaxies. A pilot study of five extragalactic planetary nebulae (XPNe) in M31 of Roth et al. (2004), observed with three different IFU instruments including PMAS, demonstrated the major improvement in the accuracy of background subtraction.

Four of the five candidates were confirmed as XPNe, but with significant differences of the resulting line ratios when compared to other authors, e.g. Jacoby and Ciardullo (1999), or Richer et al. (1999). It was argued that 3D Spectroscopy is the superior method in comparison with classical slit spectroscopy for the spectrophotometry of faint background-limited objects, in particular with regard to systematic errors arising from emission or absorption line features from the background surface brightness distribution. One XPN candidate was found to be a misidentification, and classified as a supernova remnant (SNR) instead, based on the following arguments (Fig. 4):

- the [S II] doublet $\lambda\lambda$6717,6731 line ration of 1.03 implies an electron density of $\approx 400\ e\,\mathrm{cm}^{-3}$, rather low for a typical PN
- $T_e \approx 55000\,\mathrm{K}$, derived from the [O III] line ratio [I(λ4959)+I(λ5007)]/I(λ4363) is too high
- the spatial extension of $\approx 5'' \times 4''$ is incompatible with the typical angular size of an XPN at that distance.

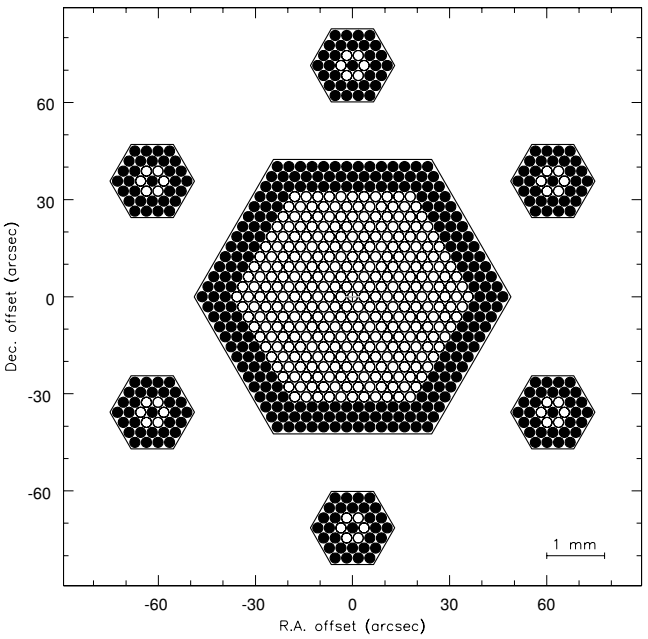

Figure 5: Wide-field IFU PPAK with 331 science fibers (open circles in the center), 36 sky fibers (open circles in the 6 mini IFUs), 15 calibration fibers (not shown because of different location), and 302 buffer fibers (filled circles). The overall FOV is $65'' \times 74''$, with spaxel sizes of $2''.7$ per science fiber core diameter.

5. THE NEW WIDE-FIELD IFU PPAK

For the observation of objects like XPNe, luminous stars in nearby galaxies, QSO host galaxies, gravitationally lensed QSOs, or other pointlike sources a FOV of $8'' \times 8''$ is sufficient. However, for the observation of extended low surface brightness objects it is far too small. Having in mind projects like the determination of galaxy disk masses by measuring the stellar velocity dispersions in the outer disks of spiral galaxies, or for the H_α velocity fields of LSB galaxies, an IFU concept with sparsely packed fibers in a wider FOV was proposed (Verheijen et al., 2004).

In 2003, the new wide-field IFU PPAK was designed and built, providing a FOV of $65'' \times 74''$ from a total of 331 science fibers, forming a bare hexagonal bundle in the focal plane without microlenses (Fig. 5). Additionally, 6 mini IFUs (sky fibers) provide a proper background sampling, and 15 fibers can be illuminated simultaneously by internal lamps for calibration purposes (Kelz et al., 2004).

Commisioning and First Light for PPAK was achieved in January 2004 (Kelz, 2004).

6. OBSERVING TIME PROPOSALS

PMAS is available at the 3.5m telescope of the German-Spanish Calar Alto Observatory, to the north of Almeria (Spain). Applications for observing time have to be sent as electronic proposals till March, 15th, for the autumn semester, and September, 15th, for the spring semester, respectively. For detailed description, LaTeX template and style files see http://www.mpia-hd.mpg.de/Public/CAHA/Applications/.

References

Becker, T.: 2003, `http://www.aip.de/groups/opti/pmas/PMAS_COOKBOOK/P3d_help/P3d_online_help.html`

Jacoby, G.H., Ciardullo, R.: 1999, *Astrophys. J.*, **515**, 169.

Kelz, A. Verheijen, M., Roth, M.M., Laux, U., Bauer, S.: 2004, in SPIE 5492-187.

Kelz, A.: 2004, `http://www.aip.de/highlight_archive/kelz_ppak/`

Richer, M.G., Stasinska, G., McCall, M.L.: 1999, *Astron. Astrophys. Suppl. Series*, **135**, 203.

Roth, M.M., Becker, T., Kelz, A., Schmoll, J.: 2004, *Astrophys. J.*, **603**, 531.

Roth, M.M.: 2002, `http://www.aip.de/groups/opti/pmas/PMAS_OVERVIEW/pmas_overview.html`

Verheijen, M.A.W., Bershady, M.A., Andersen, D.R., Swaters, R.A., Westfall, K., Kelz, A., Roth, M.M.: 2004, *Astron. Nachr.*, **325** (2), 147.

Proc. IV Serbian-Bulgarian Astronomical Conference,
Belgrade 21–24 April 2004,
eds. M. S. Dimitrijević, V. Golev, L. Č. Popović, M. Tsvetkov,
Publ. Astron. Soc. "Rudjer Bošković" No 5, 2005, 17 - 32 *Invited lecture*

EUROPEAN LONGITUDE NETWORK AND A PROJECT FOR BELGRADE INCLUSION

Z. CVETKOVIĆ
Astronomical Observatory, Volgina 7, 11160 Belgrade 74, Serbia
E–mail zcvetkovic@aob.bg.ac.yu

Abstract. The first part of this work is devoted to the investigation of mathematical models for adjusting observations, describing influences of various factors on measurements during the longitude and the longitude difference determinations. Among 12 investigated models, it the model showing the statistically best agreement with the measurement data is accepted. The second part is devoted to the examination of the influence of stellar positions on such determinations during the use of two celestial reference frames: the dynamical one, determined by the FK5 catalogue and the kinematical one, determined by the Hipparcos catalogue. It has been determined the systematic difference of two mentioned bases for the longitude determination, which is annulated in the case of longitude differences. In the third part, the functional model, providing the satisfying precision and high reliability for the Belgrade Astronomical Observatory inclusion in the European longitude network, has been investigated. Such point could be a reference point for the determination of the national longitude network and for the geoid determination for our country. By changing the geometry of a part of ELN, it has been found that this could be achieved by the determination of the Belgrade longitude difference related to only two nearly stations, members of ELN.

1. INTRODUCTION

The determination of the astronomical geoequatorial longitude is based, on the one hand, on the observations of stars with respect to the local plumb line and, on the other hand, on the positions of these stars in a fundamental catalogue which materialise the celestial reference system. Therefore, for the purpose of estimating the accuracy and reliability of longitude determination it is necessary to estimate influences due to the changes of the celestial reference system and to the random and systematic errors in the positions of observed stars in view of the determination methods.

Activities on the formation of the European Longitude Network (ELN) took place in the late XX century (Kaniuth et al. 1988). It was developed for the purpose of an accurate and homogeneous astronomical reference system necessary in both a common adjustment of the European Trigonometric Network and the astrogeodetic and astrogravimetric geoid determination.

Each of the member countries in the European Trigonometric Network should have at least one station in ELN. The campaign for including Astronomical Observatory in

Belgrade (AOB) in ELN, planned for 1990, has not been realised even till nowadays.

For the purpose of ELN establishing in the period 1977-1980, i.e. 1988 precise measurements of longitude differences between national reference stations in Germany, Italy, Spain, the Netherlands, France, Portugal and Austria (Kaniuth and Wende 1980; 1983; Wende 1992) took place. These measurements were done with a Danjon astrolabe by applying the method of equal zenith distances. The whole observational material was put at the present author's disposal due to the courtesy of Academician Prof. Dr R. Sigl and Dr W. Wende.

The last campaign for the longitude-difference determining in the framework of ELN was carried out in 1988. The longitude differences were determined between two Austrian stations, Vienna and Graz and the reference station in Munich. The observer was W. Wende. He observed selected stars from the FK5 Catalogue with declinations between 20^o and 70^o. The measurements from the 1988 campaign are treated and analysed in the present paper.

2. MATHEMATICAL ADJUSTMENT MODEL

The mathematical model for the adjustment of observations requires the relative weights of observations to be determined previously. The study of a weight model is equivalent to the study of a model of variance-components measurements.

Here four models of variance components (VC) are used (Perović and Cvetković 2001):

1. zenith-distance variance as a function of time-registration variance - model VC1; 2. Wende's model of variance components - model VCW; 3. two-component model - VC2 model and 4. three-component model - model VC3.

Due to a common adjustment of all campaign measurements an adequate functional regression model is studied. The functional model of the covariance analysis, i.e. correction equations, is used:

$$\mathbf{v} = \mathbf{A}\mathbf{x} + \mathbf{C}\mathbf{z} + \mathbf{f} \tag{1}$$

where $\mathbf{v}$ is the vector of observation corrections, $\mathbf{A}$ and $\mathbf{C}$ are the matrices of known coefficients of the linear model, $\mathbf{x}$ is the vector of unknown basic parameters, $\mathbf{z}$ is the vector of unknown additional parameters and $\mathbf{f}$ is the vector of free terms of the linear model.

The vector of basic (obligatory) parameters $\mathbf{x}$ is the same in each adjusting model and it has nine components: three increments $d\varphi_j$, $(j = 1, 2, 3)$, three increments $d\lambda_j$, $(j = 1, 2, 3)$ where $j = 1$ corresponds to Station Munich, $j = 2$ to Station Vienna, $j = 3$ to Station Graz and three increments dz_k, $(k = 1, 2, 3)$ for three groups of observed stars 10, 11 and 12 ($k = 1$ for Group 10, $k = 2$ for Group 11, $k = 3$ for Group 12). For this reason the functional models under study differ in the term $\mathbf{Cz}$ representing influences of various factors on the observations.

Besides, with each functional model four adjustment versions are obtained depending on which model of observation weights is used.

2.1. THE FIRST FUNCTIONAL MODEL - FM1

This model is used for describing the influences of eight factors on the observations so that the FM1 model has a total of 17 parameters, i.e. every observation has the following correction equation:

$$\begin{aligned} l_p \; + \; v \; = \; & b_\varphi d\varphi_j \; + \; b_\lambda d\lambda_j \; - \; dz_k \\ & + \; \Delta T b_\varphi \Delta\varphi_G \; + \; \Delta T b_\lambda \Delta\lambda_G \\ & + \; b_{IT} dIT \; + \; b_{IA} dIA \; + \; b_{HD_2} dHD_2 \\ & + \; b_H dH1 \; + \; b_H^2 dH2 \; + \; b_F dF \end{aligned} \tag{2}$$

where the nine obligatory parameters are in the first row. The eight additional parameters are in the other rows: $\Delta\varphi_G$ - time variation of latitude, $\Delta\lambda_G$ - time variation of longitude, dIT - correction for the variation of the instrument temperature, dIA - correction for the variation of the temperature difference between the instrument and the environment, dHD_2 - correction for the human-eye adaptation to light and darkness, $dH1$ and $dH2$ - corrections for the influence of the star apparent magnitude and dF - correction for the influence of star colour.

After adjusting by using the FM1 model the estimates of the corrections $\hat{v}$ are analysed with respect to various regressors (influences): series, nights, azimuth, apparent magnitudes of stars, outer air temperature measured during the observations, atmospheric pressure and instrument temperature. The distribution of correction estimates $\hat{v}$ is given in Figs. 1-7 (left). In these figures the individual correction estimates are presented as dots, whereas the mean values are presented with circles connected in a line. It is seen that there is a systematic variation from series to series, i.e. from night to night, caused, most likely, the varying of the outer temperature and of that of the instrument with night. On account of this instead of two parameters which describe these influences (dIT and dIA) over the entire campaign 23 different ones are introduced, one for each night, i.e. dIT_h and dIA_h, $h = 1, ..., 23$ (Cvetković and Perović 2000) and in this way the functional model FM2 is formed.

2.2. THE SECOND FUNCTIONAL MODEL - FM2

In this adjusting model, with a total of 61 parameters, each observation has the following correction equation:

$$\begin{aligned} l_p \; + \; v \; = \; & b_\varphi d\varphi_j \; + \; b_\lambda d\lambda_j \; - \; dz_k \\ & + \; \Delta T b_\varphi \Delta\varphi_G \; + \; \Delta T b_\lambda \Delta\lambda_G \\ & + \; b_{IT} dIT_h \; + \; b_{IA} dIA_h \; + \; b_{HD_2} dHD_2 \\ & + \; b_H dH1 \; + \; b_H^2 dH2 \; + \; b_F dF \end{aligned} \tag{3}$$

where the nine obligatory parameters are in the first row as in the case of FM1; the other rows contain 52 additional parameters out of which there are six in common

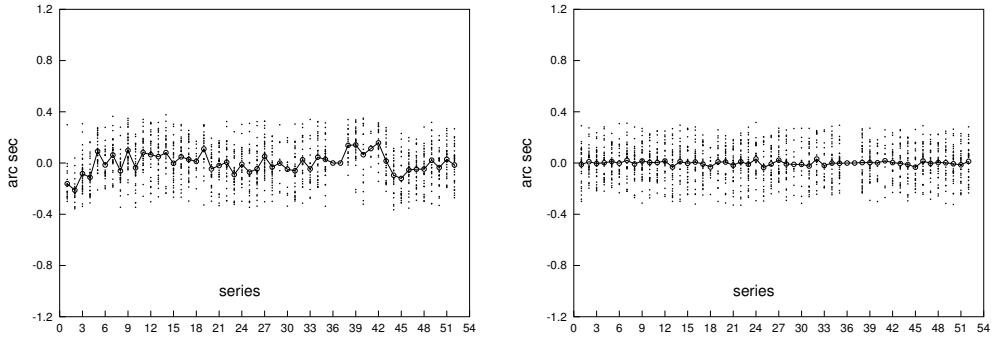

Figure 1: The distribution of correction estimates $\hat{v}$ in series obtained by using FM1 model (on the left) and FM2 (right).

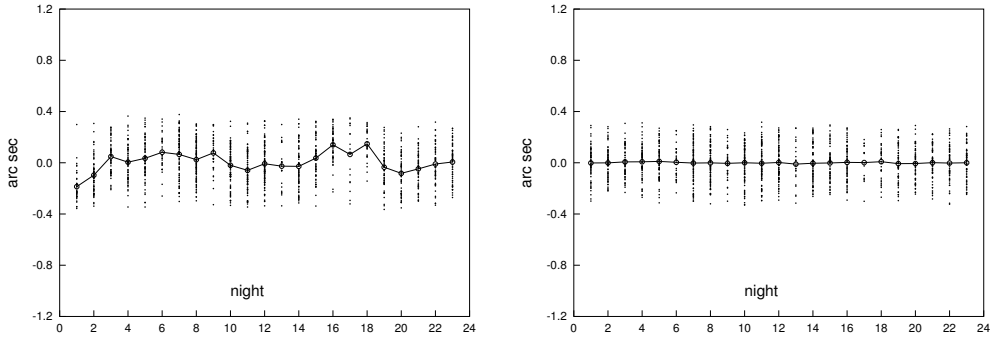

Figure 2: The distribution of correction estimates $\hat{v}$ in nights obtained by using FM1 model (on the left) and FM2 (right).

with FM1. The other 46 additional parameters (dIT_h, dIA_h, $h = 1, ..., 23$) (two for each of 23 observation nights) are introduced instead of two ones (dIT and dIA) for the entire campaign.

After adjusting with the FM2 model the correction estimates $\hat{v}$ are analysed with respect to the same regressors (influences) as the correction estimates obtained after the adjusting by using the FM1 model. The distribution of the correction estimates $\hat{v}$ is given in Figs. 1-7 (right). In these figures the systematic change from night to night cannot be longer seen. This indicates that the augmentation of the model with eight additional parameters to 52 is justified, i.e. the FM2 model yields a better description of the influences of some factors on the observations. The values obtained for $\hat{\mathbf{v}}^T\mathbf{P}\hat{\mathbf{v}}$ (Table 1) are also in favour of this justification. They are by about 35% smaller compared to the corresponding values for the model FM1. Something similar can be also said for the estimates of the variances m_o^2.

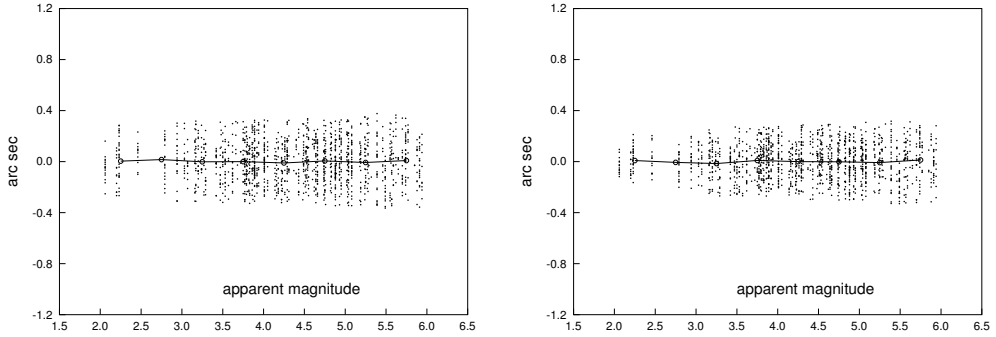

Figure 3: The distribution of correction estimates $\hat{v}$ in apparent magnitude obtained by using FM1 model (on the left) and FM2 (right).

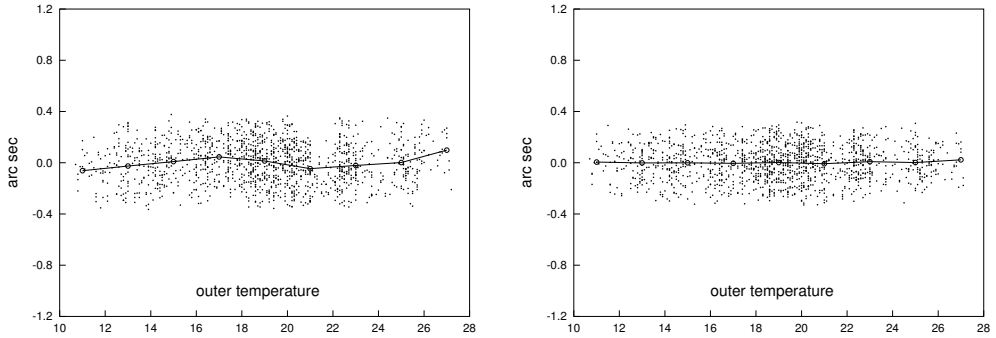

Figure 4: The distribution of correction estimates $\hat{v}$ in outer temperature obtained by using FM1 model (on the left) and FM2 (right).

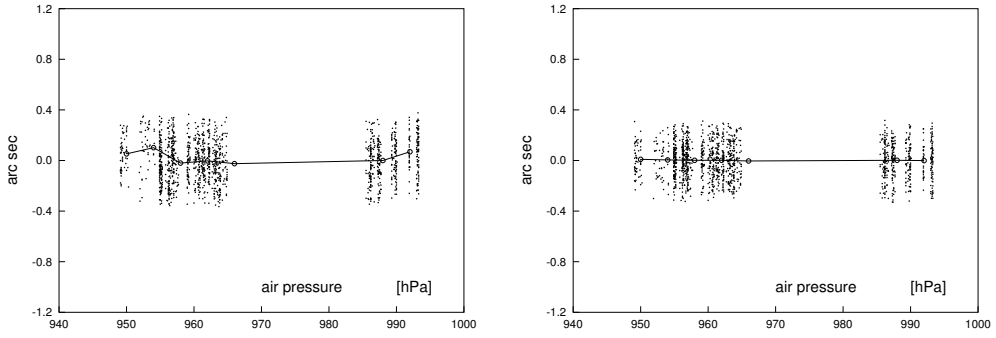

Figure 5: The distribution of correction estimates $\hat{v}$ in air pressure obtained by using FM1 model (on the left) and FM2 (right).

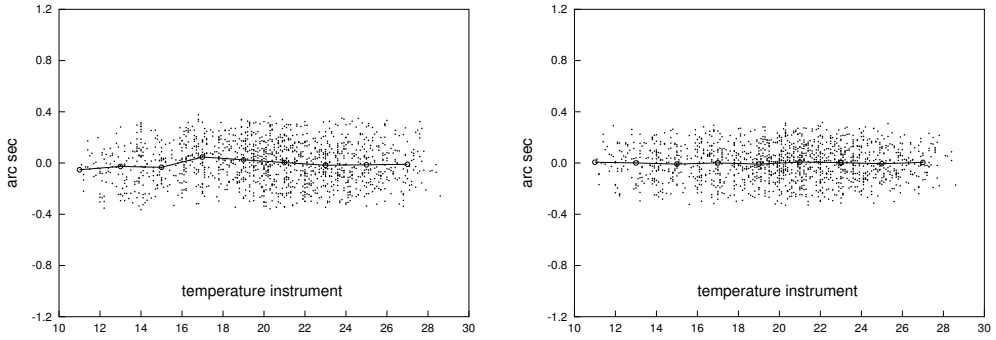

Figure 6: The distribution of correction estimates $\hat{v}$ in temperature instrument obtained by using FM1 model (on the left) and FM2 (right).

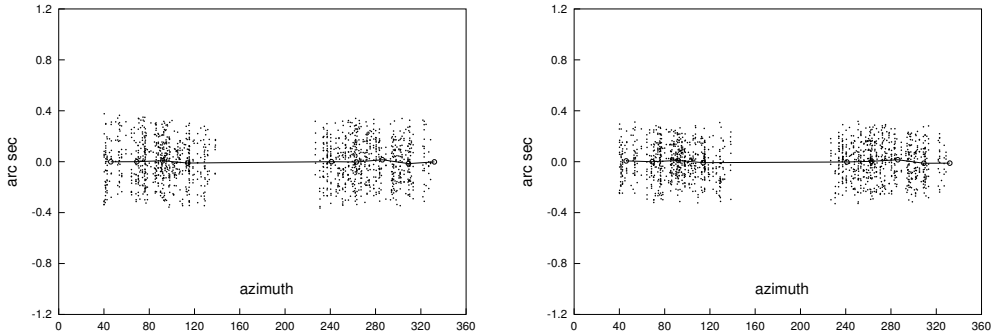

Figure 7: The distribution of correction estimates $\hat{v}$ in azimuth obtained by using FM1 model (on the left) and FM2 (right).

2.3. THE THIRD FUNCTIONAL MODEL - FM3

Compared to the FM2 model the vector of additional parameters **z** is augmented to comprise more parameters which represent corrections of the right ascensions of stars $d\alpha_\nu$, $\nu = 1, ..., m$ where the subscript ν is the number of stars for which right-ascension corrections are necessary.

In the FM3 model the equations of observation corrections have the form:

$$\begin{aligned} l_p \; + \; v \; = \; & b_\varphi d\varphi_j \; + \; b_\lambda d\lambda_j \; - \; dz_k \\ & + \; \Delta T b_\varphi \Delta\varphi_G \; + \; \Delta T b_\lambda \Delta\lambda_G \\ & + \; b_{IT} dIT_h \; + \; b_{IA} dIA_h \; + \; b_{HD_2} dHD_2 \\ & + \; b_H dH1 \; + \; b_H^2 dH2 \; + \; b_F dF \\ & + \sum_{\nu=1}^{m} (-b_\lambda \; d\alpha_\nu) \end{aligned} \tag{4}$$

Table 1: The adjustment results obtained by using three functional models: FM1, FM2 and FM3: P_{KD1} - weights calculated from model KD1; P_{KDW} - weights calculated from model KDW; P_{KD2} - weights calculated from model KD2; P_{KD3} - weights calculated from model KD3; n - number of observations; u - number of model parameters; $\hat{\mathbf{v}}^T\mathbf{P}\hat{\mathbf{v}}$ - sum of correction squares, m_o^2 - variance estimate and f - number of freedom degrees.

Func. Model	Weights	n	u	$\hat{\mathbf{v}}^T\mathbf{P}\hat{\mathbf{v}}$ $[''^2]$	m_o^2 $[''^2]$	f
$FM1$	P_{KD1}	1375	17	38.4551	0.02832	1358
	P_{KDW}	1378	17	37.7076	0.02771	1361
	P_{KD2}	1378	17	36.1434	0.02656	1361
	P_{KD3}	1378	17	34.9085	0.02565	1361
$FM2$	P_{KD1}	1377	61	25.8567	0.01965	1316
	P_{KDW}	1377	61	24.5164	0.01863	1316
	P_{KD2}	1376	61	23.8305	0.01812	1315
	P_{KD3}	1396	61	21.0608	0.01578	1335
$FM3$	P_{KD1}	1375	97	21.6668	0.01695	1278
	P_{KDW}	1377	94	19.5538	0.01524	1283
	P_{KD2}	1377	97	18.2303	0.01424	1280
	P_{KD3}	1377	95	17.4259	0.01359	1282

where the a priori unknown (variable) number m of right-ascension corrections $d\alpha_\nu$ $(\nu = 1, ..., m)$ is in the last row.

At first for every star the right-ascension correction $d\alpha$ is introduced to apply the method of gradual exclusion afterwards. If at the significance level of 0.05, the test statistic does not indicate existence of $d\alpha$ for some star, this parameter is omitted in the next iteration, i.e. the number of additional model parameters is diminished by one.

The final results of adjustment for all the three functional models and their mutual comparison are given in Table 1.

The models of variance components KD1 and KDW, with regard that they have one variance component, the former one for observation, the latter one for a star group, belong to the so-called models yielding a priori positive estimates of variance components. The models KD2 and KD3 yield positive estimates for the variance components only in the case of using the functional model FM3 supposed to describe well the influences of the factors active in the observations, i.e. it is thought to be adequate. The fact that the values obtained for $\hat{\mathbf{v}}^T\mathbf{P}\hat{\mathbf{v}}$ and the estimates of the variances m_o^2 for this functional model are by about 20% smaller compared to the functional model FM2, where the variance estimates are by about 35% smaller than in the case of the functional model FM1, is in favour of this.

Table 2: Longitude values λ for three stations; σ_λ are the errors of longitude determinations.

Station	λ [h m s]	σ_λ [s]
Munich	0 46 16.8747	0.00064
Vienna	1 05 20.9012	0.00076
Graz	1 01 58.5779	0.00080

Table 3: Values of longitude differences $\Delta\lambda$; $\sigma_{\Delta\lambda}$ are the errors of the longitude-difference determination.

From – To	$\Delta\lambda$ [h m s]	$\sigma_{\Delta\lambda}$ [s]
Munich – Graz	−0 15 41.7032	0.00090
Graz – Vienna	−0 03 22.3233	0.00104
Vienna – Munich	0 19 04.0265	0.00096

It is concluded that the use of the FM3 model yields the best description of the influences of the factors present in the observations, i.e. it is justified to introduce the right-ascension corrections.

In the case of all the three functional adjusting models the smallest variance estimates m_o^2 are obtained when the P_{KD3} model for observation weights is applied. These results indicate that it is justified to introduce the third variance component describing the influence of the star apparent magnitude on the observation accuracy. Among the four examined models of variance components, i.e. weights of observations, KD3 yields the best results, as seen from Table 1, so it is thought to be adequate.

On the basis of this analysis the best mathematical model is chosen. This is the functional model FM3 with the weight model P_{KD3}.

With this mathematical model and by using the star positions from the HIPPARCOS Catalogue the longitudes (Table 2), as well as the longitude differences (Table 3), for the three stations participating in the campaign - Munich, Vienna and Graz - are determined.

3. COMPARISON OF ADJUSTMENT RESULTS OBTAINED BY USING STAR POSITIONS FROM TWO CATALOGUES, FK5 AND HIPPARCOS

The influence of star positions on the determination of longitudes and their differences is examined. For this purpose the measurements of the whole campaign are adjusted also by applying the positions of the observed stars in the fundamental catalogue FK5. The functional model FM3 is used, whereas the weights are from the model of variance components KD3.

The results of the longitude determination are given in Table 4, the corresponding

Table 4: Values of longitudes λ for three stations: σ_λ are errors of longitude determination; $\lambda_{FK5} - \lambda_{Hipp}$ are longitude differences obtained by using star positions from catalogues FK5 and HIPPARCOS.

Stations	λ [h m s]	σ_λ [s]	$\lambda_{FK5} - \lambda_{HIPP}$ [s]	$\sigma_{\lambda_{FK5}-\lambda_{HIPP}}$ [s]
Munich	0 46 16.8778	0.00065	0.0031	0.00091
Vienna	1 05 20.9041	0.00077	0.0029	0.00108
Graz	1 01 58.5809	0.00079	0.0030	0.00112

Table 5: Values of longitude differences $\Delta\lambda$; $\sigma_{\Delta\lambda}$ are determination errors for longitude differences; $\Delta\lambda_{FK5} - \Delta\lambda_{HIPP}$ are longitude differences obtained by using star positions from catalogues FK5 and HIPPARCOS.

From – To	$\Delta\lambda$ [h m s]	$\sigma_{\Delta\lambda}$ [s]	$\Delta\lambda_{FK5} - \Delta\lambda_{HIPP}$ [s]
Munich – Graz	−0 15 41.7031	0.00091	0.0001
Graz – Vienna	−0 03 22.3232	0.00104	0.0001
Vienna – Munich	0 19 04.0263	0.00096	0.0002

results concerning the longitude differences are given in Table 5. In these tables the differences following from the values obtained with the HIPPARCOS positions are also given.

It is seen from Table 4 that the longitude differences $\lambda_{FK5} - \lambda_{HIPP}$ are equal for all the three stations, i.e. their amount is 0.0030 seconds of time which is due to the systematic difference between the two reference frames.

The catalogues FK5 and HIPPARCOS have a small rigid-body residual rotation which can be examined from a comparison of the positions and proper motions of the fundamental stars in the two catalogues. The vector of the orientation difference between the two reference frames can be determined from the difference of the positions, whereas the difference of the proper motions offers the possibility to determine the vector of the rotation difference between the two reference frames. The preliminary results obtained from the catalogue differences for all 1535 stars of the fundamental FK5 Catalogue can be found in the Foreword to the HIPPARCOS Catalogue and they are referred to the epoch J1991.25.

The rigid-body rotation (no coinciding of celestial coordinate directions), i.e. the differences in the star positions between FK5 and HIPPARCOS, affects the longitude determination, but not that of their differences which is seen from Table 5. The differences $\Delta\lambda_{FK5} - \Delta\lambda_{HIPP}$ are practically zero.

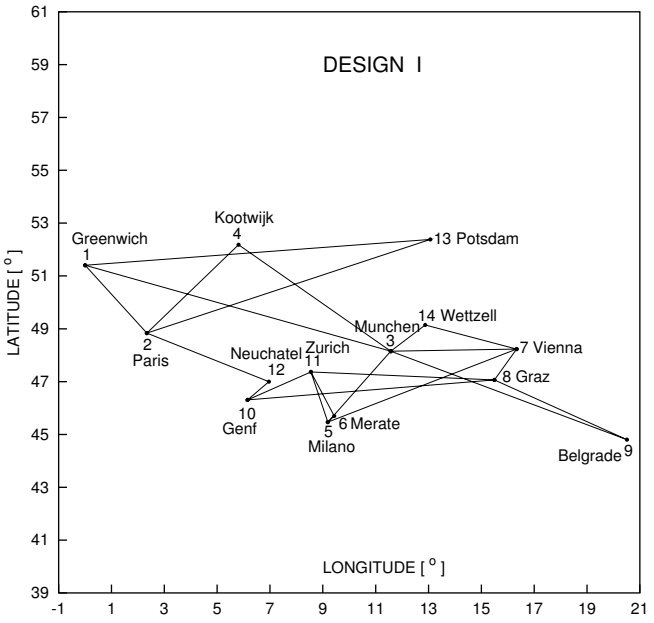

Figure 8: Design I.

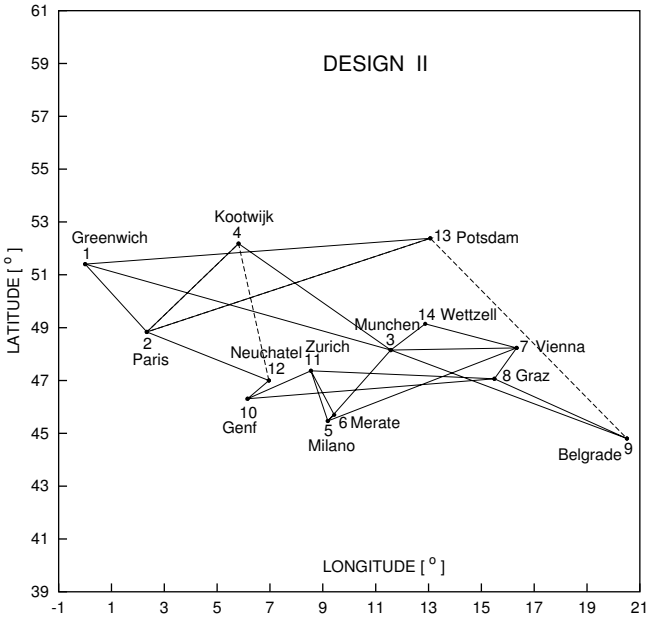

Figure 9: Design II.

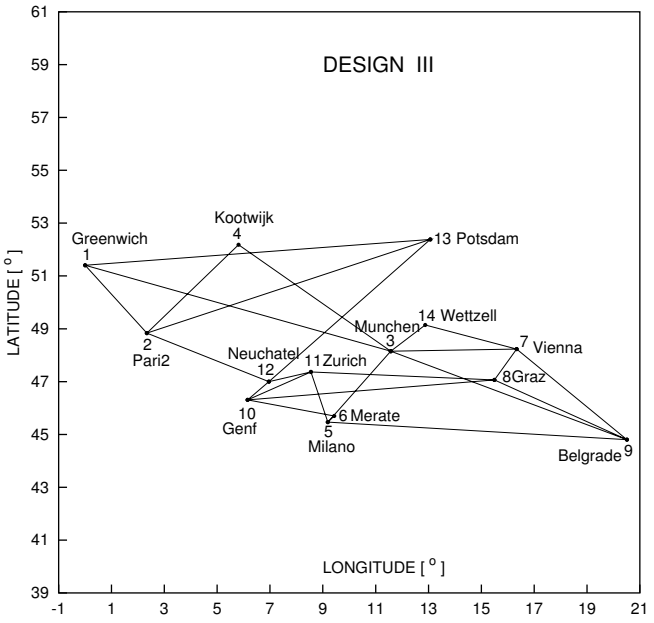

Figure 10: Design III.

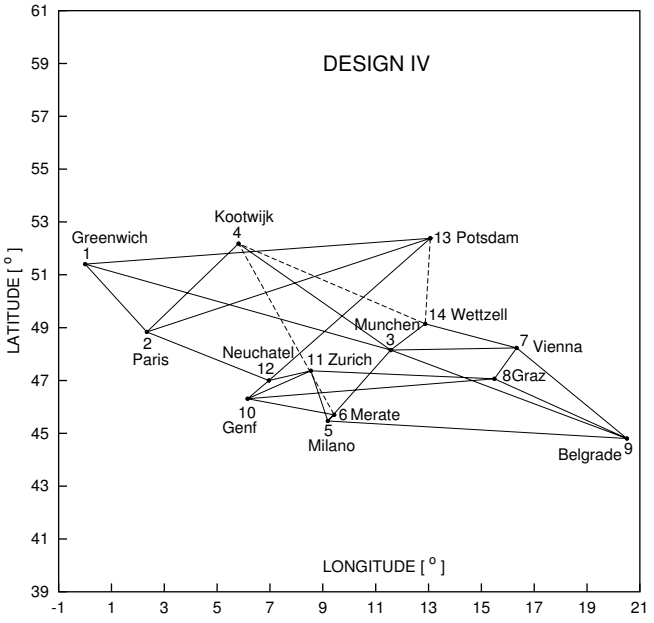

Figure 11: Design IV.

Table 6: Values of reliability measures r_{ii}, G_i^*, $\frac{G_i^*}{\sigma_i}$ and $\sqrt{\lambda_{x,i}}$ longitude differences for Design I.

i	From	To	r_{ii}	G_i^*	G_i^*/σ_i	$\sqrt{\lambda_{x,i}}$
1	1	13	0.2666	0.06713	4.615	4.154
2	13	2	0.2666	0.06713	4.615	4.154
3	2	4	0.3164	0.06163	4.236	3.564
4	4	3	0.3164	0.06163	4.236	3.564
5	3	7	0.6993	0.05116	3.517	2.264
6	7	8	0.5221	0.05676	3.901	3.001
7	8	9	0.3240	0.06090	4.186	3.483
8	9	3	0.3240	0.06090	4.186	3.483
9	3	5	0.5057	0.06056	4.162	3.445
10	5	6	0.3665	0.06798	4.673	4.241
11	6	11	0.4085	0.06798	4.673	4.241
12	11	10	0.5761	0.05932	4.077	3.303
13	10	12	0.2289	0.07244	4.980	4.692
14	12	2	0.2289	0.07244	4.980	4.692
15	2	1	0.6301	0.05258	3.614	2.464
16	1	3	0.4178	0.06021	4.139	3.406
17	3	14	0.3234	0.06095	4.190	3.489
18	14	7	0.3234	0.06095	4.190	3.489
19	7	5	0.4476	0.06245	4.293	3.656
20	5	11	0.4583	0.06193	4.257	3.598
21	11	8	0.5416	0.05673	3.900	2.998
22	8	10	0.5078	0.05802	3.988	3.152

It should be said that in this campaign only one segment of the reference frame is used. The observing programme contains 121 FK5 stars only (out of total of 1535) being less than 10%. Besides, these stars are from one part of the celestial sphere. Their declinations are between 20^o and 70^o, whereas the right ascensions are between 14 and 20.5 hours, i.e. 20 and 25.5 hours for western and eastern transits, respectively. Despite all of this a constant longitude difference $\lambda_{FK5} - \lambda_{HIPP}$ for all the three stations is obtained. This is, on the one hand, a confirmation of the rigid-body rotation between the two reference frames and, on the other hand, a confirmation that the used functional adjustment model and that of observation-weight determination are adequate.

4. THE PROPOSAL OF A PROJECT FOR INCLUDING BELGRADE IN THE ELN NETWORK

One of the objectives, which should have been realised as early as about fifeteen years ago, is to include one of our national stations in the ELN network. The most suitable station for this purpose is the Astronomical Observatory in Belgrade (AOB)

Table 7: Values of reliability measures r_{ii}, G_i^*, $\frac{G_i^*}{\sigma_i}$ and $\sqrt{\lambda_{x,i}}$ longitude differences for Design II.

i	From	To	r_{ii}	G_i^*	G_i^*/σ_i	$\sqrt{\lambda_{x,i}}$
1	1	13	0.3562	0.06439	4.426	3.866
2	13	2	0.4498	0.05986	4.115	3.366
3	2	4	0.5309	0.05447	3.744	2.715
4	4	3	0.4328	0.05799	3.986	3.149
5	3	7	0.7014	0.05100	3.506	2.241
6	7	8	0.5280	0.05641	3.878	2.958
7	8	9	0.4184	0.05862	4.029	3.222
8	9	3	0.5033	0.05544	3.811	2.838
9	3	5	0.5091	0.06028	4.144	3.414
10	5	6	0.3682	0.06770	4.654	4.213
11	6	11	0.4091	0.06770	4.654	4.213
12	11	10	0.5852	0.05878	4.041	3.242
13	10	12	0.3405	0.06734	4.629	4.176
14	12	2	0.4385	0.06200	4.262	3.605
15	2	1	0.6251	0.05238	3.600	2.436
16	1	3	0.4930	0.05670	3.897	2.993
17	3	14	0.3240	0.06090	4.186	3.483
18	14	7	0.3240	0.06090	4.186	3.483
19	7	5	0.4485	0.06233	4.285	3.643
20	5	11	0.4604	0.06176	4.245	3.579
21	11	8	0.5424	0.05670	3.897	2.994
22	8	10	0.5337	0.05702	3.919	3.033
23	12	4	0.3587	0.07939	5.457	5.366
24	13	9	0.3187	0.08377	5.758	5.778

because it was a reference station to astrogeodetic determinations in the framework of the activities aimed at the formation of an astrogeodetic network for our country and, besides, it was a member of BIH during a long time.

This would be of importance to the formation of the basic longitude network in our country. The longitude differences between the points of the basic network would be determined with respect to the reference point, AOB.

With regard that Belgrade is at approximately the same latitude as Munich, Vienna, Graz, Milano and most of the stations included in ELN the same stars can be observed from it as from these stations. Due to this in the proposal of including Belgrade in ELN the same observational design can be used as that used at a majority of stations of the central ELN part.

Let in the campaign aimed at the determining of the longitude differences between Munich, Belgrade and Graz the same stars following the same programme as in 1988 be observed. Then it should be expected to achieve the same accuracy of a single star

Table 8: Values of reliability measures r_{ii}, G_i^*, $\frac{G_i^*}{\sigma_i}$ and $\sqrt{\lambda_{x,i}}$ longitude differences for Design III.

i	From	To	r_{ii}	G_i^*	G_i^*/σ_i	$\sqrt{\lambda_{x,i}}$
1	1	13	0.3549	0.06463	4.442	3.891
2	13	2	0.5042	0.05775	3.970	3.121
3	2	4	0.3301	0.06034	4.147	3.420
4	4	3	0.3301	0.06034	4.147	3.420
5	3	7	0.7084	0.05027	3.456	2.132
6	7	8	0.5861	0.05374	3.694	2.620
7	8	9	0.5494	0.05406	3.716	2.662
8	9	3	0.5877	0.05288	3.635	2.504
9	3	5	0.6369	0.05612	3.857	2.922
10	5	6	0.3788	0.06850	4.708	4.295
11	6	10	0.3565	0.06850	4.708	4.295
12	10	11	0.4940	0.05099	4.193	3.494
13	11	12	0.4936	0.06080	4.180	3.472
14	12	2	0.5277	0.05931	4.077	3.303
15	2	1	0.6370	0.05212	3.583	2.401
16	1	3	0.4711	0.05764	3.962	3.107
17	3	14	0.3275	0.06057	4.163	3.446
18	14	7	0.3275	0.06057	4.163	3.446
19	7	9	0.4807	0.06015	4.134	3.398
20	9	5	0.4787	0.06024	4.141	3.409
21	5	11	0.5185	0.05772	3.968	3.116
22	11	8	0.6092	0.05449	3.745	2.717
23	8	10	0.4895	0.06001	4.125	3.383
24	10	12	0.4111	0.06376	4.383	3.798
25	12	13	0.4110	0.07755	5.331	4.091

transit and the same accuracy in the determination of longitudes and longitude differences as in the campaign Munich-Vienna-Graz.

Based on this and observational geometry for the longitude network the precision and reliability of the network for including AOB in ELN can be examined.

Four functional models are considered (observational designs) for the purpose of estimating the reliability of including Belgrade in ELN. They differ according to the linear-model design, whereas the stochastic model for describing individual observations (in this case estimation of longitude differences) is the same.

4.1. FUNCTIONAL MODELS

The network comprises 14 stations, 13 stations included in ELN and Belgrade, with 22 longitude differences (Design I), 24 (Design II), 25 (Design III) and 28 (Design IV).

Table 9: Values of reliability measures r_{ii}, G_i^*, $\frac{G_i^*}{\sigma_i}$ and $\sqrt{\lambda_{x,i}}$ longitude differences for Design IV.

i	From	To	r_{ii}	G_i^*	G_i^*/σ_i	$\sqrt{\lambda_{x,i}}$
1	1	13	0.3805	0.06384	4.388	3.806
2	13	2	0.5515	0.05639	3.876	2.955
3	2	4	0.5105	0.05557	3.820	2.855
4	4	3	0.5925	0.05293	3.638	2.512
5	3	7	0.7137	0.05013	3.446	2.111
6	7	8	0.6073	0.05309	3.649	2.533
7	8	9	0.5543	0.05380	3.698	2.628
8	9	3	0.5908	0.05269	3.622	2.479
9	3	5	0.6689	0.05253	3.611	2.457
10	5	6	0.5146	0.05773	3.968	3.118
11	6	10	0.4527	0.06102	4.194	3.496
12	10	11	0.4998	0.05896	4.053	3.262
13	11	12	0.5305	0.05892	4.050	3.257
14	12	2	0.5560	0.05789	3.980	3.137
15	2	1	0.6370	0.05181	3.561	2.357
16	1	3	0.5044	0.05602	3.851	2.911
17	3	14	0.6844	0.05111	3.513	2.257
18	14	7	0.5149	0.05642	3.878	2.959
19	7	9	0.4961	0.05900	4.055	3.266
20	9	5	0.4872	0.05937	4.081	3.310
21	5	11	0.5254	0.05744	3.948	3.083
22	11	8	0.6143	0.05430	3.733	2.694
23	8	10	0.5055	0.05832	4.009	3.187
24	10	12	0.4661	0.05997	4.122	3.378
25	12	13	0.4573	0.06100	4.193	3.494
26	13	14	0.4389	0.06186	4.252	3.590
27	14	4	0.4776	0.06015	4.134	3.398
28	4	6	0.4664	0.06065	4.169	3.455

For each linear model one calculates the local-reliability coefficients of observations r_{ii}, the marginal gross errors G_i^*, the normed marginal gross errors G_i^*/σ_i and distorsion parameters $\sqrt{\lambda_{x,i}}$. The obtained values are given in Tables 6, 7, 8 and 9.

For all linear models: Design I, Design II, Design III and Design IV the local-reliability coefficients are higher than 0.2, a value assumed as a lower limit in the case of such networks (optimal value 0.4). The normed marginal gross errors are also less than the limit of 7.65 indicating that all these designs satisfy reliability criteria.

The reliability measures show that among the four examined linear models the maximal homogeneity of the observed longitude differences is achieved with linear model IV. In the case of this model the individual determinations of longitude dif-

ferences are not included and every network station is included with at least three longitude differences.

Since all the stars of the observing programme corresponding to the 1988 campaign can be observed from Belgrade, for the stochastic model it is possible to take the data from the campaign of determining the longitude differences Munich-Vienna-Graz. The reliability of including Belgrade in ELN depends then on the geometry of the linear model.

5. CONCLUSION

The best (adequate) mathematical adjustment model, functional - FM3 and stochastic (weight model) - P_{KD3}, is obtained so that the systematic and random influences in the measurements and star positions on the determining of longitudes and longitude differences are reduced to a negligible value compared to the standard errors of these quantities.

There is a systematic difference between the two reference frames given by the catalogues FK5 and HIPPARCOS.

The difference of the reference frames affects the longitude determination, but not also that of the longitude differences.

The including of Belgrade in ELN can be achieved with a high reliability and satisfactory precision through a campaign of the longitude-difference determining with two nearby stations, ELN members.

Acknowledgements

This research has been supported by the Serbian Ministry of Science and Environmental Protection (Project No 1221 "Investigation of Double and Multiple Stars").

References

Cvetković, Z., Perović, G.: 2000, *Publ. Astron. Obs. Belgrade*, **67**, 9.

Kaniuth, K., Wende, W.: 1980, Bestimmung astronomischer Längendifferenzen für das europäische Längennetz in den Jahren 1977 bis 1979, *Deutsche Geodätische Kommission*, **250**, 1.

Kaniuth, K., Wende, W.: 1983, Bestimmung astronomischer Längendifferenzen für das europäische Längennetz im Jahr 1980, *Veröffen. der Bayerischen Kommission für die Internationale Erdmessung*, **44**, 1.

Kaniuth, K., Sigl, R., Soltau, G.: 1988, Adjustment of the European Longitude Network (ELN), *IAG Section I - Positioning, Subcommission for the New Adjustment of the European Triangulation (RETrig), Publication*, **17**, 163.

Perović, G., Cvetković, Z.: 2001, *Serb. Astron. J.*, **164**, 3.

Wende, W.: 1992, Bestimmung astronomischer Längendifferenzen im Europäischen Längennetz zwischen den Stationen München - Wien - Graz im Jahr 1988, *Veröffen. der Bayerischen Kommission für die Internationale Erdmessung*, **50**, 1.

Proc. IV Serbian-Bulgarian Astronomical Conference,
Belgrade 21–24 April 2004,
eds. M. S. Dimitrijević, V. Golev, L. Č. Popović, M. Tsvetkov,
Publ. Astron. Soc. "Rudjer Bošković" No 5, 2005, 33 - 38 *Invited lecture*

TWO SIMPLE PROBLEMS IN SEMICLASSICAL DENSE MATTER PHYSICS

V. ČELEBONOVIĆ

Inst. of Physics, Pregrevica 118, 11080 Zemun-Beograd, Serbia
E–mail vladan@phy.bg.ac.yu

Abstract. Physics of dense matter is an extremely rich and complex scientific field, mixing laboratory experiments and astronomical observations with complex calculations. The aim of this lecture is to discuss in some detail two simple but important problems which have considerable importance for the developement of theoretical work in semiclassical dense matter physics.

1. INTRODUCTION

The first historically known attempt to study experimentally a material under high presssure dates from the $XVIII$ century. An english "gentleman" named Mr. Canton tried to compress water to a pressure of the order of 0.1 GPa (Block et al., 1980). To his astonishement, he observed a "transformation" of water into ice. In the vocabulary of modern condensed matter physics this would be called a phase transition. For a recent example of a study of water and ice under high pressure see Sundberg and Lazor (2004). We can only wonder what would Mr. Canton say today, when 15 different phases of water ice are known. Systematic laboratory high pressure studes started near the end of the XIX century owing to the efforts of P. W. Bridgman at Harvard University (Bridgman, 1964). High pressure experiments have been revolutionized by the discovery of the diamond anvil cell (for a recent review see for example Struzhkin, Hemley and Mao, 2004). Experimental and theoretical research in high pressure (or, more generally, dense matter physics) is pursued throughout the world.

Scientific research in high pressure physics has started in Serbia at the beginning of the sixties (Savić, 1961). In that paper, which was short and simple but initiated an important series of publications, he pointed out an interesting fact: namely, the mean densities of the planets, as derived from observational data known at the time, could be related to the mean solar density by an extremely simple equation. He did not make any hypothesis about the physical nature of this correlation. In the next four years Savić in collaboration with Kašanin (Savić and Kašanin, 1962/65) developed a theory of the behaviour of materials under high pressure. It was later nick-named the SK theory for short; another synonim is "the semiclassical theory". This last term is justified by the fact that this theory uses only the basic notions of atomic and molecular physics, while it is largely founded on laws of classical physics.

The value of this theory is that it offers the possibility of preforming in a simple way calculations which would be prohibitively complex in rigorous statistical mechanics. Logically, this simplicity very often diminishes the precision of the results.

The basic physical idea of their theory is that subduing a material to sufficiently high pressure leads ultimately to excitation and ionisation of the atoms and molecules which constitute it.

At the time when they were starting to develop their theory, the study of the influence of external fields on atoms and molecules was not a theoretically well developed subject. However, Savić and Kašanin used experimental data known at the time to support their idea.

Namely, Bridgmann's experiments were showing that in some materials under certain values of external pressure first order phase transitions occur. It was also known from the analysis of the propagation of seismic waves that their speed changes abruptly a certain depths in the interior of the Earth. Details on their theory are readily available in the literature (for example, Čelebonović, 1995).

In the remainder of this contribution, we shall discuss at some length two problems of considerable importance for the foundations of the SK theory:

– the relationship between the mean planetary densities derived from observation and the mean solar density, and:

– the calculation of the phase transition points in this theory.

2. THE DENSITY PROBLEM

The basic aim of Savić (1961) was to derive some form of relationship between the solar density and the mean planetary densities. The densities were calculated from the values of planetary masses and radii known at the time. It was shown in that paper that it was possible to fit the values of ρ by the following simple expression:

$$\rho = \rho_0 2^{\phi} \tag{1}$$

where $\rho_0 = 4/3$ is the value of the mean solar density known at the time expressed in CGS units. By suitably assigning to the exponent ϕ various **integral** values it turned out to be possible to reproduce known values of the planetary densities. This fit is extremely important for the complete developement of the SK theory because it determines the ratio of densities in two successive phases of a material under high pressure. However, as Eq. (1) was derived more than 40 years ago, the logical question about the possibilities of its improvement or even change has started to appear. In the meantime the values of planetary and solar densities have been improved, so this also presented a challenge to Eq. (1).

The following table contains modern values of the mean densities of various objects within the Solar System. All the values given in the table were taken from the internet address `http://nssdc.gsfc.nasa.gov/planetary/planetary home.html`. The column denoted by ρ_{mean} contains densities of all the planets of the Solar System and their most important satellites derived from their observed masses and diameters. The values of the ϕ in the third column of Table 1 have been obtained by rounding off values calculated from Eq. (1).

Table 1: Densities of planets and satellites

object	ρ_{mean}	ϕ	ρ_{calc}
Sun	1408	0	1408
Mercury	5427	2	5632
Venus	5243	2	5632
Earth	5515	2	5632
Moon	3350	5/4	3349
Mars	3933	3/2	3982
Phobos	1900	2/5	1858
Deimos	1750	1/3	1774
Jupiter	1326	-1/10	1314
JI	3530	7/5	3716
JII	3010	1	2816
JIII	1940	1/2	1991
JIV	1840	2/5	1858
Saturn	687	-1	704
Titan	1881	2/5	1858
Uranus	1270	- 1/7	1275
Ariel	1670	1/4	1674
Neptune	1638	1/4	1674
Triton	2050	1/2	1991
Pluto	1750	1/3	1774
Charon	2000	1/2	1991

The column with the heading ρ_{calc} contains values of the density calculated by Eq. (1) and the values of ϕ given in the Table.

Several conclusions can be drawn by simple inspection of Table 1.

The aim of this work has been to test Eq. (1) on modern data and on a larger sample of bodies than the one used in Savić (1961). Eq. (1) proposed by Savić and Kašanin more than 40 years ago has been confirmed on a much larger sample of objects. Note that **non-integral** values of the exponent ϕ occur in Table 1. This marks a considerable difference with the original paper by Savić, in which only **integral** values of ϕ occured. A possible interpretation of this result can perhaps be found in considerations of the similarities between atomic sturcture and the structure of the planetary system. The physical meaning of Eq. (1) is still a problem open for discussion, but the important concusion of the present work is that the fit proposed by Savić and Kašanin is valid for a much larger set of objects, under the condition that the exponent ϕ takes on non-integral values.

3. THE PHASE TRANSITION POINTS

The theory proposed by Savić and Kašanin predicts that a material subdued to increasing pressure undergoes a sequence of first order phase transitions, numbered by an integer index i. The algorithm for the calculation of these values of pressure is presented in detail in previous papers on the subject (for example Čelebonović, 1995 or later publications). Just for illustration, the final expression for the phase transition pressure is

$$p_{tr} = 0.5101 p_i^*; i = 1, 3, 5, .. \tag{2}$$

and

$$p_{tr} = 0.6785 p_i^*; i = 2, 4, 6... \tag{3}$$

where

$$p_i^* \cong 1.8077 \beta_i (\overline{V})^{-4/3} 2^{4i/3} MBar \tag{4}$$

where $\overline{V}$ is the molar volume of the material under study, and the symbol β_i denotes a constant determined within the theory for each phase of the material.

However, the problem with Eq. (2), and in general with various calculations within this theory is that they have a weak contact with the well established theories of statistical physics. In the remaining part of this paper one such connection will be proposed.

The starting point of all rigorous considerations in statistical physics is the Hamiltonian of the system under consideration. Starting from it, one can derive the expression for the partition function, and from it all the thermodynamic potentials. Accordingly, in attempting to link the theory proposed by Savić and Kašanin with modern statistical physics, one should start from a Hamiltonian (or a suitable expression for one of the thermodynamic potentials) which can in principle predict a number of phase transitions of first order. The order of the transitions is important here because the theory we are discussing here is limited to first order transitions. In the Landau theory of phase transitions, the expression for the Gibbs potential per unit volume of a system having spontantenous magnetization M has the form (for example, LeBellac, 1988):

$$g(M) = \frac{1}{2!} r_0(T) M^2 + \frac{1}{4!} u_0 M^4 + \frac{1}{6!} v_0 M^6 \tag{5}$$

where $u_0 < 0$, $v_0 > 0$ and r_0 has the form $r_0(T) = a(T - T_0)$; T_0 denotes some critical temperature relevant for the problem under consideration and a is a constant.

It can be shown that $g(M) = 0$ for

$$M^2 = -\frac{15 u_0}{v_0} \mp \frac{[900 u_0^2 - 1440 r_0 v_0]^{1/2}}{2 v_0} \tag{6}$$

Clearly, this expression is real if $u_0 < 0$,$v_0 > 0$ and $u_0 > [(\frac{8}{5}) r_0 v_0]^{1/2}$.

It follows from Eq. (4) that $\partial g / \partial M = 0$ for

$$M^2 = -\frac{10u_0}{v_0} \mp \frac{[400u_0^2 - 480r_0v_0]^{1/2}}{2v_0} \tag{7}$$

which implies that $u_0^2 \geq (\frac{6}{5})r_0v_0$. In a similar way one could determine the position of the points in which the second derivative of $g(M)$ becomes equal to zero.

Replacing the magnetization M in Eqs. (3-5) by the pressure P renders these expressions applicable to the case of materials under high pressure. In this way a link between the theory proposed by Savić and Kašanin and the Landau theory of phase transitions becomes possible. Eq. (2) contains an experimentally known parameter ($\overline{V}$) and another one derived within the theory (β).

Combining Eqs. (2-3) and (6) and multiplying out all the pure numbers, it follows that for $i = 1$:

$$-\frac{15u_0}{v_0} - \frac{[900u_0^2 - 1440r_0v_0]^{1/2}}{2v_0} = 2.14258\beta_1^2(\overline{V})^{-8/3} \tag{8}$$

where value of the constant β_1 is known from the theory of Savić and Kašanin. This means that Eq. (8) gives a direct connection between this theory and the Landau theory of phase transitions. Reasoning in the same way for $i = 2$, one could obtain a similar equation. Solving a system of these two equations one could obtain the values of the parameters of the Landau theory expressed in terms of the parameters of the theory of Savić and Kašanin. This calculation is algebraically tedious but straightforward. As a result one would obtain expressions for u_0 and v_0 in terms of $r_0(T)$ and the parameters which enter the calculations within the SK theory.

4. CONCLUSIONS

In this lecture two apparently simple problems in dense matter physics have been addressed to some extent. Both of the problems discussed are related to the foundations of the theory of behaviour of materials under high pressure proposed by P. Savić and R. Kašanin nearly fifty years ago. The general conclusion is that one of the basic statements of the SK theory is validated with modern data, and that this theory can be connected with modern theories of phase transitions.

The simple expression proposed in Savić (1961) which links the mean planetary densities with the mean solar density was tested on modern data. All the planets and several satellites of each of them were included - 21 object in all. It was shown that the original fit (Eq. (1) of the present paper) is confirmed with modern data. However, the exponent ϕ in Eq. (1) is no longer **integral** but can also take **non integral** values. This conclusion, although important for the SK theory, opens up the problem of the interpretattion of non-integral values of the exponent ϕ.

In order to make a contact between the SK theory and some of the better known theories of phase transitions, it was combined with the Landau theory of first order phase transitions. The result is that the Landau theory also has several first order phase transition points, and that the parameters of the Landau theory can be expressed in terms of the parameters of the SK theory.

References

Block, S., Piermarini, G. et Munro, R.G.: 1980, *La Recherche*, **11**, 806.
Bridgman, P.W.: 1964, *Collected Experimental Papers*, **I-VIII** Harvard Univ. Press. Cambrige Mass.
Čelebonović, V.: 1995, *Bull. Astron. Belgrade*, **151**, 37 and astro-ph/9603135.
LeBellac, M.: 1988, Des phénomènes critiques aux champs de jauge, InterEditions/Editions du CNRS, Paris.
Savić, P.: 1961, *Bull. de la classe des Sci. Math. et natur. de l'Acad. Serbe des Sci et des Arts*, **XXVI**, p.107.
Savić, P. and Kašanin, R.: 1962/65, The behaviour of materials under high pressure, ed. by Serb. acad. sci. and arts, Beograd.
Struzhkin, V.V., Hemley, R.J. and Mao, H.K.: 2004, *J. Phys.: Condens. Matter.*, **16**, S1071-S1086.
Sundberg, S. and Lazor, P.: 2004, *J. Phys.: Condens. Mater*, **16**, S1223-S1233.

Proc. IV Serbian-Bulgarian Astronomical Conference,
Belgrade 21–24 April 2004,
eds. M. S. Dimitrijević, V. Golev, L. Č. Popović, M. Tsvetkov,
Publ. Astron. Soc. "Rudjer Bošković" No 5, 2005, 39 - 50 *Invited lecture*

REDUCTION OF ASTROGEODETIC DETERMINATIONS ON THE UNIQUE SYSTEM

M. DAČIĆ
Astronomical Observatory, Volgina 7, 11160 Belgrade 74, Serbia
E–mail mdacic@aob.bg.ac.yu

Abstract. Determinations in geodetic astronomy, namely, determination of time, longitude, latitude and azimuth from star observations, have been made during a long period by different persons. Positions of observed stars have been taken from different catalogues and in diferent reference systems. In order that results of such determinations will be mutually comparable, it is necessary to make the reduction of stellar positions on the unique reference system. Consequently, results of astrogeodetic determinations will also be reduced to the same system. Starting from the fact that the position of a point is determined only related to something, it is possible to calculate systematic differences of particular catalogues and catalogues used for the materialisation of the chosen reference system. Obtained stellar positions -, and proper movements - systematic errors, enable the changement from standard epoch on another one (the moment of observation), so that stellar positions are reduced to a single system. The proposed model is checked at three clssical methods of geodetic astronomy and applied to results of general Stevan Bošković's astrogeodetic determinations, made in the first decade of the XX century.

1. INTRODUCTION

Measurements in geodetic astronomy, or more precisely, determinations of astronomical time, plumb-line direction (natural coordinates) and of astronomical azimuth of geodetic sides are performed with high-precision instruments also enabling to obtain high-precision results. However, the results of determinations done nowadays indicate a disagreement between precision and accuracy (internal and external accuracy). This disagreement is due, among others, also to the importance of systematic and random errors in the positions of stars used in these determinations.

In order to answer concerning the cause of the disagreement it is necessary to analyse the methods of determination used in geodetic astronomy from the point of view of the presence of star-position errors in the determination results because the same position errors have a different influence on the determination results depending on the applied method and the star position in the horizontal system. On the other hand it is necessary to estimate the systematic and random errors in the positions of stars used in the determinations.

The determinations of geodetic astronomy have been carried out over a sufficiently long time interval and, consequently, any successful use of star coordinates needs their

positions to be reduced to a unified system. In the present case the system of the FK5 Catalogue is of interest. For this reason the subject is the relationship between FK5 and other catalogues.

The main objective of the present work is, on the one hand, to assume a model for reducing star positions from different, already used, catalogues to a unified system, in particular to a system where FK5 serves as its reference frame. On the other hand, the objective of the study is to estimate the star positions reduced to this system, no matter whether they are from FK5, itself, or from another catalogue. In this way a reliable frame of studies for necessities of geodesy, geophysics or geodynamics would be obtained.

In view of the already existing results a hypothesis can be formulated that the errors of star positions given in earlier catalogues are important to the existence of the disagreement between the precision and accuracy for the determinations carried out in earlier epochs where star positions from these catalogues were used. With regard to the high precision of modern instruments used in geodetic astronomy there are also reasons to test the hypothesis concerning the importance of the influence of errors in star positions on the modern determinations of geodetic astronomy.

The present work is based on the assumption that a sufficiently large body of data (results) exists in fundamental and ephemeride astronomy concerning the properties of relevant catalogues, the values and accuracy of astronomical constants and, above all, the accuracy of proper motions so that a reliable estimation of the accuracy of star positions for epochs of interest can be done.

In "Studija o stanju dosadašnjih radova na astrogeodetskoj mreži SFRJ" (Study about the Works on Astrogeodetic Network of the SFRY done up to now) there are tasks solved through astrogeodetic measurements where these measurements are used either independently or combined with gravimetric or satellite ones. An inspection of the works carried out over the territory of Yugoslavia is characterised by a statement that the determinations undertaken before the First World War could be of interest only with the results of latitude determination. Generally, the accuracy of latitude determination, also of azimuth one, is low due to the technological level of that time. This concerns the determinations performed by Stevan P. Bošković between 1900 and 1911. The results were published as "Skretanja vertikala u Srbiji" (Plumb-Line Deflections in Serbia, Bošković 1952) in an edition of the Serbian Royal Academy of Sciences.

It is clear that in the joining of the results of Bošković's determinations the ones of modern astrogeodesy their insufficient accuracy in view of the necessities and facilities of the present epoch should be taken into account. However, if established how large the presence of the errors in star coordinates in the total budget of astrogeodetic determinations is, this part could be removed. In other words, by reducing the star positions to some of the modern systems such as, for instance, FK5 the accuracy is enlarged just in the part which is dependent of the coordiantes of the observed stars.

2. POSITION ERRORS

In a catalogue the data for every star concerning its position, proper motion, number of observations and mean epoch are usually followed by the ones concerning the mean errors in the position and proper motion. These individual mean errors, together with the mean errors of the catalogue system, offer the insight into the accuracy of star positions. (As said above, the term "catalogue system" indicates the comprehensiveness of the data defining star positions also loaded by systematic errors. In view of this the notions of catalogue system and reference system should be distinguished.) Since the system of a catalogue is obtained from numerous star observations during a sufficiently long time interval, it is usual to present the mean errors of catalogue system in special tables through the root-mean-square (rms) errors for the systems of right ascensions, declinations and proper motions, followed by the data on the mean epoch of observations.

The systematic errors are calculated by using stars common to given catalogues and are expressed through the differences of their positions averaged in zones. These differences can be applied for the purpose of changing the catalogue system, i. e. of reducing to the system of a selected catalogue. For instance, by using the systematic differences (FK5 - FK4), (FK4 - FK3) and (FK3 - NFK) the (FK5 - NFK) ones can be calculated in an indirect way. These differences should be understood as corrections to the NFK Catalogue and this is the reducing of the positions of NFK stars to the FK5 system.

The determinations of plumb-line deflections in Serbia performed in the beginning of the XX century by S. P. Bošković are of interest here. Bošković's observing programme contained bright stars only belonging to the Group of so-called Auwers' stars. These stars are in the NFK Catalogue and they are designated as 1 to 925. Due to this in what follows the consideration of random and systematic errors for the positions of these stars will be given.

2.1. RANDOM ERRORS OF POSITIONS OF FUNDAMENTAL STARS

Compared to an ideal system the mean error of a star position will contain the part representing the mean error of the catalogue fundamental system, itself, and the part representing the individual mean position error in the given system (Mueller, 1969)

$$E^2 = m^2 + M^2 \ . \tag{1}$$

Here, the mean error of the system m for epoch T is calculated by using the following formulae

$$(m_\alpha \cos\delta)_T{}^2 = (m_\alpha \cos\delta)_{T_0}{}^2 + \left(\frac{T - T_{s\alpha}}{100}\right)^2 (m_\mu \cos\delta)^2 \ , \tag{2}$$

$$(m_\delta)_T{}^2 = (m_\delta)_{T_0}{}^2 + \left(\frac{T - T_{s\delta}}{100}\right)^2 (m_{\mu'})^2 \ , \tag{3}$$

whereas the mean error of a star position in this system M for the same epoch according to the formulae

$$(M_\alpha \cos\delta)_T{}^2 = (M_\alpha \cos\delta)_{T_0}{}^2 + \left(\frac{T - T_{0\alpha}}{100}\right)^2 (M_\mu \cos\delta)^2 \ , \tag{4}$$

$$(M_\delta)_T{}^2 = (M_\delta)_{T_0}{}^2 + \left(\frac{T - T_{0\delta}}{100}\right)^2 (M_{\mu'})^2 \ . \tag{5}$$

The mean errors of the FK4 (Fricke and Kopff, 1963) and FK5 (Fricke et al., 1991) systems are given in the forewords of these catalogues. Since here the error of the system is numerically approximately equal to the average value of the individual error of the star position in the catalogue, it can be assumed that the same is valid for the NFK (Peters, 1907) and FK3 (Kopff, 1937) systems in view of how these systems were formed. As for NFK, the values are calculated bearing in mind the fact that the position errors for its stars are 1.5 times as large as those in FK3, whereas in the case of the proper motions the corresponding ratio is equal to 1.8. These data are added to the table presenting the mean errors of the coordinates and those of the centennial proper motions in FK3 (Zverev, 1950, p. 78).

The data from the catalogues FK3, FK4 and FK5 enable the calculating of the mean values of individual mean errors in the positions and proper motions of stars for each of the catalogues separately. In the present calcualtion Auwers' stars with declinations greater than -20 are taken because some of them were used by Bošković in his determinations.

Table 1. presents the results obtained by the present author. The catalogue designation is in the first column. The second and the third ones contain the mean values of the mean epochs of star observations $(T_0)_\alpha$ and $(T_0)_\delta$. The mean individual errors of right ascensions and declinations $M_\alpha \cos\delta$ and M_δ are in the fourth and sixth columns, respectively, whereas the corresponding errors of the proper motions over century $M_\mu \cos\delta$ and $M_{\mu'}$ are in the fifth and seventh columns, respectively. It should be mentioned that the errors in NFK are estimated on the basis of those in FK3.

Table 1. Mean values of individual mean errors in positions and proper motions of Auwers' stars with declinations greater than -20

Cat	$(T_0)_\alpha$	$(T_0)_\delta$	$M_\alpha \cos\delta$	$M_\mu \cos\delta/cy$	M_δ	$M_{\mu'}/cy$
NFK	1870	1870	$\pm 0^s.0030$	$\pm 0^s.0200$	$\pm 0''.050$	$\pm 0''.270$
FK3	1901	1897	$\pm 0^s.0019$	$\pm 0^s.0110$	$\pm 0''.031$	$\pm 0''.151$
FK4	1915	1911	$\pm 0^s.0014$	$\pm 0^s.0063$	$\pm 0''.024$	$\pm 0''.097$
FK5	1950	1939	$\pm 0^s.0008$	$\pm 0^s.0028$	$\pm 0''.017$	$\pm 0''.051$

The data from the catalogues and Tables 1. enable to obtain by applying formulae (1)-(5) the average mean errors in positions of the stars used in Bošković's determinations of plumb-line deflections in Serbia. The errors are calculated for the beginning of the XX century: just for the mean epoch of Bošković's works approximately equal to 1906.0.

The average mean errors in right ascension $E_\alpha \cos\delta$ and declination E_δ with respect to an ideal system calculated for the NFK, FK3, FK4 and FK5 catalogues are presented in Table 2.

Table 2. Average mean position errors for stars used in Bošković's astrogeodetic determinations - epoch 1906.0.

Cat	$E_\alpha \cos\delta$	E_δ
NFK	$\pm 0\overset{s}{.}015$	$\pm 0\overset{''}{.}20$
FK3	$\pm 0\overset{s}{.}004$	$\pm 0\overset{''}{.}06$
FK4	$\pm 0\overset{s}{.}004$	$\pm 0\overset{''}{.}03$
FK5	$\pm 0\overset{s}{.}003$	$\pm 0\overset{''}{.}03$

2.2. SYSTEMATIC ERRORS IN POSITIONS OF FUNDAMENTAL STARS

Since the random errors in the positions of the most important stars in the fundamental systems NFK, FK3, FK4 and FK5 are estimated, the next step is to determine the systematic errors of the fundamental catalogue NFK. If FK5 is taken as a reference catalogue, these errors will be as the systematic differences NFK-FK5. With regard that for the purposes of the present paper the reducing of Bošković's observations to the system of the catalogue FK5 is of interest, what is looked for is the corrections of the NFK system. In other words, the differences FK5-NFK in the corresponding parameters are calculated. This calculation is done in the following phases: 1) FK4 reduced to FK5; 2) FK3 reduced to FK4; 3) NFK reduced to FK3. Bearing in mind the mean epoch of Bošković's observations the reducing of NFK to FK5 takes place for the epoch T=1906.0.

1) As for the FK4 system, the first step is to correct the position of the vernal-equinox point following the formula

$$E(T) = +0\overset{s}{.}035 + 0\overset{s}{.}085\left(\frac{T-1950}{100}\right) , \tag{6}$$

to calculate the reducing of FK4 to the FK5 system (differences FK5- FK4). Here the FK4 equator remains unchanged.

The regional differences FK5-FK4, given in the form of tables on pages 87-90 of the FK5 Catalogue, are used for the purpose of finding the differences of right ascensions and declinations according to the classical formulae:

$$\begin{aligned} (\Delta\alpha\cos\delta)_{1950} &= [(\Delta\alpha_\alpha + \Delta\alpha_\delta + \Delta\alpha_m)\cos\delta]_{1950} \\ \Delta\mu\cos\delta &= (\Delta\mu_\alpha + \Delta\mu_\delta + \Delta\mu_m)\cos\delta \ ; \end{aligned} \tag{7}$$

$$\begin{aligned} (\Delta\delta)_{1950} &= [\Delta\delta_\alpha + \Delta\delta_\delta + \Delta\delta_m]_{1950} \\ \Delta\mu' &= (\Delta\mu'_\alpha + \Delta\mu'_\delta) \ . \end{aligned} \tag{8}$$

The reducing of the systematic differences to the epoch T is done without the factor cos

$$\begin{aligned}(\Delta\alpha)_T &= (\Delta\alpha)_{1950} + \Delta\mu \left(\frac{T-1950}{100}\right) \\ (\Delta\delta)_T &= (\Delta\delta)_{1950} + \Delta\mu' \left(\frac{T-1950}{100}\right) .\end{aligned} \tag{9}$$

2) In the reducing of the FK3 system to that of FK4 one should bear in mind that the equator correction is done according to the formula

$$D(T) = -0\overset{''}{.}017 + 0\overset{''}{.}097\left(\frac{T-1928.4}{100}\right) , \tag{10}$$

but this correction is theoretically zero at the poles.

The regional errors for the FK3 Catalogue, i. e. the differences FK4-FK3 for the year 1950 are given on the pages 131-134 of the FK4 Catalogue. For the epoch 1906.0 the calculation is done according to formulae (7), (8) and (9), but it is taken into account that the values $\Delta\alpha$ and $\Delta\mu$ for the stars with declinations exceeding 60 in their modulus are reduced to the equator (multiplied by $\cos\delta$).

3) The corrections of the NFK system are given directly on pages 84 - 87 of the FK3 Catalogue in Table 3 which contains differences from 1800 to 1930. Though not explicitely specified in the tables, it can be concluded from the data-treatment procedure used for the purpose of improving the NFK system that the differences $\Delta\alpha_\delta$ for declinations between -60 and +60 are given directly, whereas for ones beyond this interval are reduced to the equator.

Table 3. Systematic differences $\Delta\alpha$ - reducing of NFK to FK5 system for epoch 1906.0

$\alpha \setminus \delta$	$+70^o$	$+50^o$	$+30^o$	$+10^o$	-10^o
0^h	$-0\overset{s}{.}196$	$-0\overset{s}{.}073$	$-0\overset{s}{.}060$	$-0\overset{s}{.}051$	$-0\overset{s}{.}043$
4^h	$-0\overset{s}{.}201$	$-0\overset{s}{.}073$	$-0\overset{s}{.}064$	$-0\overset{s}{.}057$	$-0\overset{s}{.}049$
8^h	$-0\overset{s}{.}225$	$-0\overset{s}{.}088$	$-0\overset{s}{.}080$	$-0\overset{s}{.}073$	$-0\overset{s}{.}064$
12^h	$-0\overset{s}{.}217$	$-0\overset{s}{.}084$	$-0\overset{s}{.}066$	$-0\overset{s}{.}062$	$-0\overset{s}{.}055$
16^h	$-0\overset{s}{.}217$	$-0\overset{s}{.}087$	$-0\overset{s}{.}070$	$-0\overset{s}{.}064$	$-0\overset{s}{.}059$
20^h	$-0\overset{s}{.}204$	$-0\overset{s}{.}074$	$-0\overset{s}{.}060$	$-0\overset{s}{.}051$	$-0\overset{s}{.}044$
$\Delta\alpha_\delta$	$-0\overset{s}{.}210$	$-0\overset{s}{.}080$	$-0\overset{s}{.}067$	$-0\overset{s}{.}060$	$-0\overset{s}{.}052$

Therefore, the data presented with the fundamental catalogues FK5, FK4 and FK3 are used for the purpose of composing Tables 3. and 4. in which the systematic differences of the positions FK5 - NFK for epoch 1906.0 in declination zones from -20 to +80.

In Tables 3. and 4. the differences $\Delta\alpha$ and $\Delta\delta$ are grouped over zones of declination and right ascension. In this way we have a more detailed insight into the

systematic errors of NFK here compared to FK5. The middle of a 20-degree declination zone is designated in the first row of both tables, whereas the one of a four-hour right-ascension zone is in the first column. The last row in both tables contains the differences in declination averaged over all the six zones of right ascension.

Tables 3. and 4. give the reducing of NFK to the system of FK5 and together with Table 2. they will serve in the estimation of the influences of errors in star coordinates on the results of Bošković's astrogeodetic determinations.

Table 4. Systematic differences $\Delta\delta$ - reducing of NFK to FK5 system for epoch 1906.0

$\alpha \setminus \delta$	$+70^o$	$+50^o$	$+30^o$	$+10^o$	-10^o
0^h	$+0''.10$	$+0''.15$	$+0''.10$	$+0''.25$	$+0''.08$
4^h	$+0''.10$	$+0''.18$	$+0''.09$	$+0''.25$	$+0''.10$
8^h	$-0''.02$	$+0''.04$	$-0''.03$	$+0''.11$	$-0''.01$
12^h	$+0''.05$	$+0''.10$	$+0''.04$	$+0''.18$	$+0''.03$
16^h	$+0''.07$	$+0''.16$	$+0''.11$	$+0''.24$	$+0''.11$
20^h	$+0''.06$	$+0''.05$	$-0''.02$	$+0''.13$	$+0''.02$
$\Delta\delta_\delta$	$+0''.06$	$+0''.11$	$+0''.05$	$+0''.19$	$+0''.06$

2.3. BOŠKOVIĆ'S DETERMINATIONS 1900 - 1911.

In first years of the XX century geodetic determinations aimed at the exact topographic measuring of Serbia. On this occasion significant disagreements concerning the cartographic works of former Austria-Hungary, Romania, Bulgaria and Serbia were discovered, just at the touching point of these states, i. e. in the north-east of Serbia of that time where the Carpato-Balkanic arc intersects these regions detaching longitudinally the Panonian bassein from the Pontic one. On account of this it is very important to solve the problem about the cause of the disagreement. Another important question is how to orientate the triangulation of Serbia and onto which spheroid to project it. Due to the connection between the geodetic works of that time and the activity of the Military Geographic Institute in Vienna, through which a similar connection arose with the analogous activity in the lands of Central Europe, it was decided to realise the orientation according to the activity of the Vienna Institute and following them to project the triangulation onto the Besselian spheroid as was usual then for all geodetic activity in Central Europe.

S. P. Bošković in the late XIX century during his studies in Pulkovo intuitively understood that, probably, the deviation of the plumb line from its normal position with respect to the ideally curved surface of the terrestrial spheroid was the cause for the geodetic, and automatically the cartographic, mostly longitudinal, disagreement in the lands of the Panonic and Pontic baseins. This might be a consequence of a local atraction perturbation in the intensity of gravity force due to the structure of the Carpato-Balkanic mountain arc. For this reason he planned already then geodetic and astronomical activities in order to verify if his intuition was correct.

For the purpose of realising his idea S. P. Bošković prepared two universal instruments for geodetic and astronomical observations, twelve chronometers, aneroids and

thermometers. The ephemerides for star pairs are calculated for the purpose of time determination by using Tsinger's method for the points of all geographic latitudes in Serbia of that time and also the ephemerides for star pairs for the purpose of latitude determination by using Pevtsov's method and the ephemerides for the Polar Star for the purpose of azimuth determination by using the classical method. Bošković's plan was to measure simultaneously horizontal and vertical triangulation angles and astronomical measurements aimed at determining time, latitude and azimuth choosing for this a number of points on our highest mountains, as well as a number of points in our river valleys thinking that this was the best way to examine and discover the local atraction influences on the perturbation of the normal direction of the intensity of Earth gravity and due to this the deviation of the plumb line.

The first determinations at I - northern point of the Paraćin basis and at the highest top of the mountain of Rtanj in 1900 had very good results. Since the expeditions concerning these activities at chosen highest points of our mountains require strong physical efforts, Bošković organised the programme of geodetic and astronomical activities in such a way to be performed during the first years and afterwards points in our river valleys would be treated. In 1901 there were expeditions and measurements on Midžor, Trem and Jastrebac; in 1902 Veliki Streser, Petrova Gora, Kopaonik, Jankov Kamen and Tornik; in 1903 Mali Povlen, Deli Jovan, Veliki Sumorovac, Crni Vrh, Bukulja and Cer. Afterwards, in 1905, at the churches in Niš, Zaječar and Negotin; in 1906 at Pirot, Tija-Bara (near the monument) and at II point (northern) of the Vranje basis in the village of Zlatokop; in 1907 at Hisar (Leskovac), at the churches in Trstenik and Čačak; in 1908 at I point of Loznica basis - Starača and at Ozerovac near the Markovac bridge over the Morava. Later on, in 1909 on Avala, at Podgorica and Kulič (at the junction of the Morava and the Danube); finally in 1911 at Osojna near Kladovo and in Pirot at Tija-Bara. There were no astronomical activities in 1904, when Bošković's occupations were measurements of four bases, and in 1910 when his occupations were measurements of the Drina valley way between Zvornik and Rača in cooperation with the Vienna Military Institute of Geography.

The urgent works on the calculation of the trigonometric triangulation and the ones commenced on the new topographic measurements for the scale of 1:25,000, also the wars in 1912 and 1913, the urgent geodetic works aimed at new topographic measurements of the liberated parts of the country, as well as the wars between 1914 and 1920, made impossible this enormous astronomical material to be treated. However, it, as well as the triangulation, was not lost. It was transported through Albania to the island of Corfu, then to Thessaloniki and finally back to our country - it came to Belgrade in 1919. At that time the Belgrade Military Institute of Geography, in addition to its own specialist staff, got also a new one, Russian topographers who helped very much in the treatment of the astronomical data.

In Table 5. a presentation of points, with the year of astrogeodetic determinations and coordinates, is given. The column of latitudes contains Bošković's values, as well as the last one with the azimuth values.

Table 5. Points at which the plumb-line deflection was determined in Serbia 1900 – 1911 (λ – longitude of place where observations were performed; φ – Bošković's values for latitude; A – Bošković's values for azimuth).

	Place of Observation	year	λ	φ	A
1.	Paraćin	1900.	$-1^h\ 25^m.6$	$+43^\circ\ 50'\ 31''.57$	$277^\circ\ 00'\ 42''.36$
2.	Rtanj	1900.	$-1^h\ 27^m.6$	$+43^\circ\ 46'\ 39''.98$	$250^\circ\ 27'\ 47''.48$
3.	Midžor	1901.	$-1^h\ 30^m.8$	$+43^\circ\ 23'\ 50''.52$	$170^\circ\ 55'\ 05''.48$
4.	Trem	1901.	$-1^h\ 28^m.7$	$+43^\circ\ 11'\ 10''.10$	$64^\circ\ 28'\ 37''.81$
5.	Jastrebac	1901.	$-1^h\ 25^m.8$	$+43^\circ\ 22'\ 58''.37$	$44^\circ\ 16'\ 58''.68$
6.	Streser	1902.	$-1^h\ 29^m.0$	$+42^\circ\ 37'\ 39''.02$	$15^\circ\ 40'\ 28''.03$
7.	Petrova Gora	1902.	$-1^h\ 26^m.1$	$+42^\circ\ 59'\ 55''.41$	$63^\circ\ 15'\ 27''.57$
8.	Kopaonik	1902.	$-1^h\ 23^m.3$	$+43^\circ\ 16'\ 06''.24$	$135^\circ\ 46'\ 21''.21$
9.	Jankov Kamen	1902.	$-1^h\ 21^m.1$	$+43^\circ\ 20'\ 23''.12$	$139^\circ\ 31'\ 56''.68$
10.	Tornik	1902.	$-1^h\ 18^m.7$	$+43^\circ\ 39'\ 10''.12$	$201^\circ\ 16'\ 11''.63$
11.	Mali Povlen	1903.	$-1^h\ 18^m.9$	$+44^\circ\ 07'\ 53''.08$	$29^\circ\ 29'\ 07''.65$
12.	Deli Jovan	1903.	$-1^h\ 28^m.9$	$+44^\circ\ 13'\ 39''.75$	$59^\circ\ 29'\ 26''.37$
13.	Veliki Sumorovac	1903.	$-1^h\ 26^m.6$	$+44^\circ\ 19'\ 01''.08$	$184^\circ\ 53'\ 13''.17$
14.	Crni Vrh	1903.	$-1^h\ 23^m.6$	$+43^\circ\ 51'\ 41''.31$	$199^\circ\ 06'\ 29''.75$
15.	Bukulja	1903.	$-1^h\ 21^m.9$	$+44^\circ\ 17'\ 59''.29$	$188^\circ\ 34'\ 13''.41$
16.	Cer	1903.	$-1^h\ 18^m.0$	$+44^\circ\ 36'\ 14''.77$	$105^\circ\ 00'\ 58''.66$
17.	Church in Niš	1905.	$-1^h\ 27^m.6$	$+43^\circ\ 18'\ 55''.62$	$218^\circ\ 14'\ 31''.58$
18.	Church in Zaječar	1905.	$-1^h\ 29^m.2$	$+43^\circ\ 54'\ 08''.28$	$65^\circ\ 34'\ 25''.86$
19.	Church in Negotin	1905.	$-1^h\ 30^m.1$	$+44^\circ\ 13'\ 39''.12$	$179^\circ\ 05'\ 34''.41$
20.	Pirot	1906.	$-1^h\ 30^m.4$	$+43^\circ\ 09'\ 36''.47$	$288^\circ\ 30'\ 27''.85$
21.	Zlatokop	1906.	$-1^h\ 27^m.3$	$+42^\circ\ 31'\ 03''.04$	$122^\circ\ 02'\ 43''.35$
22.	Hisar	1907.	$-1^h\ 27^m.8$	$+42^\circ\ 59'\ 12''.76$	$221^\circ\ 31'\ 47''.66$
23.	Church in Trstenik	1907.	$-1^h\ 24^m.1$	$+43^\circ\ 37'\ 16''.44$	$190^\circ\ 50'\ 30''.32$
24.	Church in Čačak	1907.	$-1^h\ 21^m.4$	$+43^\circ\ 53'\ 38''.70$	$99^\circ\ 27'\ 12''.55$
25.	Starača	1908.	$-1^h\ 16^m.8$	$+44^\circ\ 34'\ 30''.59$	$232^\circ\ 06'\ 56''.65$
26.	Ozerovac	1908.	$-1^h\ 24^m.4$	$+44^\circ\ 14'\ 08''.20$	$225^\circ\ 02'\ 57''.46$
27.	Avala	1909.	$-1^h\ 22^m.0$	$+44^\circ\ 41'\ 22''.50$	$194^\circ\ 19'\ 50''.30$
28.	Kulič	1909.	$-1^h\ 19^m.6$	$+44^\circ\ 42'\ 52''.08$	$272^\circ\ 02'\ 05''.21$
29.	Podgorica	1909.	$-1^h\ 24^m.1$	$+44^\circ\ 40'\ 59''.45$	$114^\circ\ 27'\ 53''.41$
30.	Osojna	1911.	$-1^h\ 30^m.4$	$+44^\circ\ 35'\ 18''.79$	$74^\circ\ 31'\ 36''.01$

3. THE REDUCING TO THE FK5 SYSTEM

Essentially, the best way of reducing the results of Bošković's astrogeodetic determinations to the FK5 system is to use his original values of apparent star coordinates (right ascensions and declinations) in order to avoid various incertainties and speculations. After enquiring at several places, among others at the Archives of the Serbian Academy of Sciences and Arts, it has been established that Bošković's entire reduction material, more precisely the reduction sheets with Tsinger's and Pevtsov's pairs and Polar-Star observations, is in the Library of the Military Institute of Geography.

Table 6. The Corrections of Bošković's Astrogeodetic Determinations ($\Delta\varphi_c$ - correction in latitude calculation;$\Delta\varphi_{fk5}$ and ΔA_{fk5} - reducing to FK5 system; $\Delta\varphi_{cio}$ and ΔA_{cio} - reducing to CIO pole; $[\xi]$ - corrected component of plumb-line deflection in north-south direction; $[\eta]$ - corrected component of plumb-line deflection in east-west direction).

	Place of Observation	$\Delta\varphi_c$	$\Delta\varphi_{fk5}$	$\Delta\varphi_{cio}$	$[\xi]$	ΔA_{fk5}	ΔA_{cio}	$[\eta]$
1.	Paraćin	$-0''.32$	$+0''.22$	$+0''.05$	$-00''.15$	$-0''.08$	$+0''.07$	$-14''.07$
2.	Rtanj	$+0''.16$	$+0''.30$	$+0''.06$	$+07''.02$	$-0''.49$	$+0''.05$	$-06''.83$
3.	Midžor	$+0''.05$	$+0''.16$	$-0''.12$	$+08''.49$	$-0''.15$	$+0''.17$	$-01''.78$
4.	Trem	$-0''.09$	$+0''.03$	$-0''.08$	$+10''.26$	$-0''.26$	$+0''.18$	$-08''.40$
5.	Jastrebac	$-0''.48$	$+0''.11$	$-0''.06$	$+00''.67$	$-0''.28$	$+0''.18$	$-08''.78$
6.	Streser	$+1''.32$	$+0''.15$	$-0''.16$	$+05''.81$	$+0''.12$	$-0''.20$	$-11''.60$
7.	Petrova Gora	$-0''.13$	$+0''.09$	$-0''.19$	$-00''.93$	$-0''.14$	$-0''.13$	$-06''.94$
8.	Kopaonik	$-0''.21$	$-0''.01$	$-0''.19$	$-02''.81$	$-0''.39$	$-0''.09$	$-02''.85$
9.	Jankov kamen	$+0''.23$	$+0''.17$	$-0''.19$	$+02''.41$	$-0''.47$	$-0''.07$	$+02''.50$
10.	Tornik	$+0''.07$	$+0''.02$	$-0''.18$	$-03''.19$	$-0''.60$	$-0''.01$	$-01''.16$
11.	Mali Povlen	$-0''.29$	$+0''.02$	$-0''.09$	$+02''.94$	$-0''.10$	$-0''.30$	$-07''.32$
12.	Deli Jovan	$+0''.45$	$+0''.04$	$-0''.14$	$+05''.75$	$-0''.08$	$-0''.26$	$+02''.53$
13.	Veliki Sumorovac	$-0''.10$	$+0''.05$	$-0''.15$	$+00''.70$	$-0''.11$	$-0''.24$	$-04''.15$
14.	Crni Vrh	$+0''.29$	$-0''.05$	$-0''.17$	$+02''.37$	$-0''.13$	$-0''.18$	$-06''.05$
15.	Bukulja	$+0''.78$	$-0''.13$	$-0''.18$	$+05''.37$	$-0''.12$	$-0''.17$	$-06''.04$
16.	Cer	$+1''.17$	$-0''.22$	$-0''.19$	$+04''.06$	$-0''.18$	$-0''.12$	$-07''.10$
17.	Church in Niš	$+0''.42$	$+0''.16$	$+0''.01$	$+02''.29$	$-0''.30$	$-0''.24$	$-11''.39$
18.	Church in Zaječar	$+0''.37$	$+0''.01$	$-0''.02$	$+00''.76$	$-0''.07$	$-0''.24$	$+14''.95$
19.	Church in Negotin	$+0''.08$	$+0''.42$	$-0''.05$	$+03''.75$	$+0''.04$	$-0''.23$	$+14''.60$
20.	Pirot	$+0''.09$	$+0''.08$	$+0''.07$	$-02''.06$	$-0''.50$	$-0''.11$	$-00''.01$
21.	Zlatokop	$+0''.17$	$+0''.45$	$+0''.06$	$+00''.78$	$-0''.25$	$-0''.12$	$-17''.20$
22.	Hisar	$-0''.27$	$+0''.20$	$-0''.02$	$+03''.61$	$-0''.07$	$+0''.13$	$-04''.76$
23.	Church in Trstenk	$-0''.30$	$+0''.14$	$+0''.06$	$+02''.40$	$-0''.42$	$+0''.11$	$+45''.11$
24.	Church in Čačak	$+0''.02$	$+0''.29$	$+0''.09$	$+02''.40$	$-0''.52$	$+0''.10$	$-02''.83$
25.	Starača	$+0''.16$	$+0''.26$	$-0''.11$	$+04''.61$	$-0''.32$	$+0''.24$	$-06''.29$
26.	Ozerovac	$+0''.90$	$+0''.09$	$-0''.09$	$+05''.60$	$-0''.08$	$+0''.25$	$-09''.38$
27.	Avala	$+0''.15$	$+0''.35$	$-0''.28$	$+01''.72$	$-0''.23$	$+0''.10$	$-00''.84$
28.	Kulič	$-0''.20$	$+0''.36$	$-0''.24$	$+00''.62$	$-0''.42$	$+0''.20$	$-09''.51$
29.	Podgorica	$+0''.00$	$+0''.10$	$-0''.18$	$+01''.92$	$-0''.30$	$+0''.10$	$-03''.54$
30.	Osojna	$-0''.20$	$+0''.35$	$-0''.15$	$+02''.10$	$-0''.30$	$-0''.38$	$+05''.50$

Due to the putting of the apparent star coordinates at our disposal the work is significantly simplified. The only thing to be done is to calculate the apparent right ascensions and declinations following the procedure described in Part IV. In this part of the work, as already said, one uses the baricentric coordinates of the Solar-System bodies calculated according to the JPL numerical theory DE200/LE200 for the purpose of obtaining the baricentric coordinates of the Earth and its velocity vector. The corresponding data concerning the interval 1899-1924 have been put at

our disposal due to the courtesy of colleague B. Jovanović.

After obtaining the difference between the FK5 positions and the ones in Bošković's reduction sheets it becomes possible to reduce Bošković's results to the FK5 system. In these reductions one calculates the corrections of Bošković's results according to the differential formulae (Dačić 2000).

Table 6. contains the reductions obtained on the basis of the differences in the apparent places of FK5 and Bošković's ones calculated directly for every observation separately. In other words, after reducing the latitudes and azimuths to the FK5 sys-

Table 7. Plumb-Line Deflections reduced to Fk5 System ($[u]$ - corrected total value of plumb-line deflection; $[E]$ - corrected deflection angle; $[\lambda' - \lambda]$ - corrected difference between astronomical and geodetic longitudes; u, E and $\lambda' - \lambda$ - Bošković's numerical values).

	Place of Observation	$[u]$	u	$[E]$	E	$[\lambda' - \lambda]$	$\lambda' - \lambda$
1.	Paraćin	$14''.07$	$14''.1$	$-\ 90^0.61$	$-\ 90^0.4$	$-19''.50$	$-19''.5$
2.	Rtanj	$9''.79$	$9''.1$	$-\ 44^0.21$	$-\ 44^0.6$	$-\ 9''.45$	$-\ 8''.8$
3.	Midžor	$8''.67$	$8''.6$	$-\ 11^0.84$	$-\ 12^0.1$	$-\ 2''.45$	$-\ 2''.5$
4.	Trem	$13''.26$	$13''.3$	$-\ 39^0.31$	$-\ 38^0.6$	$-11''.51$	$-11''.4$
5.	Jastrebac	$8''.81$	$8''.8$	$-\ 85^0.64$	$-\ 82^0.8$	$-12''.08$	$-11''.8$
6.	Streser	$12''.97$	$12''.3$	$-\ 63^0.40$	$-\ 68^0.6$	$-15''.77$	$-15''.7$
7.	Petrova Gora	$7''.00$	$6''.6$	$-\ 97^0.63$	$-\ 96^0.1$	$-\ 9''.49$	$-\ 9''.1$
8.	Kopaonik	$4''.00$	$3''.3$	$-134^0.60$	$-136^0.2$	$-\ 3''.91$	$-\ 3''.2$
9.	Jankov Kamen	$3''.47$	$3''.8$	$+\ 46^0.05$	$+\ 54^0.6$	$+\ 3''.44$	$+\ 4''.2$
10.	Tornik	$3''.39$	$3''.1$	$-160^0.02$	$-170^0.8$	$-\ 1''.61$	$-\ 0''.7$
11.	Mali Povlen	$7''.89$	$7''.6$	$-\ 68^0.12$	$-\ 64^0.4$	$-10''.20$	$-\ 9''.6$
12.	Deli Jovan	$6''.28$	$6''.1$	$+\ 23^0.75$	$+\ 28^0.2$	$+\ 3''.53$	$+\ 4''.0$
13.	Veliki Sumorovac	$4''.21$	$3''.9$	$-\ 80^0.43$	$-\ 76^0.7$	$-\ 5''.80$	$-\ 5''.3$
14.	Crni Vrh	$6''.50$	$6''.1$	$-\ 68^0.61$	$-\ 68^0.0$	$-\ 8''.38$	$-\ 7''.9$
15.	Bukulja	$8''.08$	$7''.5$	$-\ 48^0.36$	$-\ 49^0.3$	$-\ 8''.43$	$-\ 8''.0$
16.	Cer	$9''.33$	$7''.6$	$-\ 60^0.24$	$-\ 64^0.1$	$-\ 9''.97$	$-\ 9''.5$
17.	Church in Niš	$11''.62$	$10''.9$	$-\ 78^0.63$	$-\ 81^0.1$	$-15''.66$	$-14''.9$
18.	Church in Zaječar	$14''.97$	$15''.3$	$+\ 87^0.09$	$+\ 88^0.5$	$+20''.75$	$+21''.2$
19.	Church in Negotin	$15''.07$	$15''.2$	$+\ 75^0.60$	$+\ 77^0.4$	$+20''.37$	$+20''.6$
20.	Pirot	$2''.06$	$2''.4$	$-179^0.72$	$+165^0.4$	$-\ 0''.01$	$+\ 0''.9$
21.	Zlatokop	$17''.22$	$16''.8$	$-\ 87^0.40$	$-\ 89^0.7$	$-23''.34$	$-22''.8$
22.	Hisar	$5''.97$	$6''.1$	$-\ 48^0.99$	$-\ 52^0.4$	$-\ 6''.53$	$-\ 6''.6$
23.	Church in Trstenik	$45''.17$	$45''.5$	$+\ 86^0.95$	$+\ 86^0.8$	$+62''.31$	$+62''.8$
24.	Church in Čačak	$3''.71$	$3''.1$	$-\ 49^0.70$	$-\ 50^0.2$	$-\ 3''.92$	$-\ 3''.3$
25.	Starača	$7''.80$	$7''.5$	$-\ 53^0.76$	$-\ 55^0.3$	$-\ 8''.81$	$-\ 8''.7$
26.	Ozerovac	$10''.92$	$10''.7$	$-\ 59^0.16$	$-\ 63^0.9$	$-13''.09$	$-13''.3$
27.	Avala	$1''.91$	$1''.7$	$-\ 26^0.03$	$-\ 23^0.6$	$-\ 1''.18$	$-\ 1''.0$
28.	Kulič	$9''.53$	$9''.3$	$-\ 86^0.27$	$-\ 85^0.7$	$-13''.39$	$-13''.1$
29.	Podgorica	$4''.03$	$3''.9$	$-\ 61^0.53$	$-\ 58^0.8$	$-\ 4''.98$	$-\ 4''.7$
30.	Osojna	$5''.89$	$6''.5$	$+\ 69^0.10$	$+\ 71^0.3$	$+\ 7''.72$	$+\ 8''.7$

tem it becomes as if Bošković in his reductions had used the star positions from FK5, the new astronomical constants and the new procedure for the calculating of the apparent places.

The random error of results due to the one in star positions is equal to about +0."01 for both latitude and azimuth. Even this error component in the mean latitude value can be even smaller depending on the number of observed Pevtsov's pairs at a given point (where the plumb-line deflection was determined).

The results of Bošković's astrogeodetic determinations are treated by reducing the coordinates of observed stars to the FK5 system. The latitude is calculated again and the results of latitude observations are analysed separately. After reducing to the CIO pole for every point the corrected total value of plumb-line deflection is calculated and the corrected deflection angle is obtained. On the basis of the comparative values from Table 7. it can be concluded that the introduced corrections have not changed Bošković's results significantly. It is of importance that these results are reduced to the modern FK5 reference system. In this way, by introducing corrections for the coordinates of the instantaneous pole a homogenisation in Bošković's results of latitude and azimuth determinations takes place.

4. CONCLUSION

A general conclusion from all presented above is the following:

- in the fundamental catalogues of the FK series there are enough data for the calculation of errors in the star positions reduced to a chosen epoch;

- the differential formulae enable to determine, in addition to the most favourable observational conditions, also the influences of the errors in the star coordinates on the results of geodetic astronomy;

- the corrections do not result in essential changes, but it is important that by introducing the corrected positions for the observed stars the results of Bošković's determinations of plumb-line deflections in Serbia are reduced to the reference system of FK5.

References

Bošković, S.P.: 1952, Skretanje vertikala u Srbiji, SAN, *Posebna izdanja*, **CXCVI**, Geografski inst., knj. 4.

Dačić, M.: 2000, Proceedings of the Second Serbian - Bulgarian Astronomical Meeting, June 23 - 26, 2000, Zaječar , Dimitrijević, M.S., Popović, L.Č. and Tsvetkov M. (eds.), *Publ. Astron. Obs. Belgrade*, **67**, 27.

Fricke, W., Kopff, A.: 1963, *Veröff. Astron. Rechen-Institut Heilderberg*, **10**.

Fricke, W., Schwan, H., Lederle, T.: 1988, *Veröff. Astron. Rechen-Institut Heilderberg*, **32**.

Fricke, W., Schwan, H., Corbin, T.: 1991, *Veröff. Astron. Rechen-Institut Heilderberg*, **33**.

Kopff, A.: 1937, Dritter Fundamentalkatalog des Berliner Astronom. Jahrbuchs. I Teil. Die Auwers-Sterne für die Epochen 1925 und 1950, *Veröff. Astron. Rechen-Institut Berlin-Dahlem*, **54**.

Mueller, I.I.: 1969, Spherical and Practical Astronomy as Applied to Geodesy, Frederick Ungar Publishing Co., New York.

Peters, J.: 1907, Neuer Fundamentalkatalog des Berliner Astronom. Jahrbuchs, *Veröff. Astron. Rechen-Institut*, **33**.

Зверев М.С.: 1950, Успехи астрономических наук, Том **V**, Изд. Акад. наук СССР, Москва – Ленинград.

Proc. IV Serbian-Bulgarian Astronomical Conference,
Belgrade 21–24 April 2004,
eds. M. S. Dimitrijević, V. Golev, L. Č. Popović, M. Tsvetkov,
Publ. Astron. Soc. "Rudjer Bošković" No 5, 2005, 51 - 58 *Invited lecture*

FULLERENES AND ASTRONOMY

M. S. DIMITRIJEVIĆ
Astronomical Observatory, Volgina 7, 11160 Belgrade 74, Serbia
E–mail mdimitrijevic@aob.bg.ac.yu

Abstract. The astrophysically motivated investigations of the chemistry of carbon stars resulted with the discovery of the C_{60} molecule, first and the most interesting representative of fullerenes molecules. Here is presented a review of astronomical researches connected with fullerenes as for example the search for interstellar and circumstellar ones or presence of such molecules in meteorites brechias of impact craters on Earth and impact traces on spacecrafts. Also, their connection with the problem of the diffuse interstellar and circumstellar absorption lines is discussed. Particular attention is payed to the search for polyynes in interstellar space which resulted in the formulation of investigation of chemistry of carbon stars and in discovery of fullerenes.

1. INTRODUCTION

Possibilities which provides the new C_{60} molecule and variety of the possible new compounds with this molecule as the basis, will result possibly in the birth of a new chemistry. The basic impulse, resulting with the discovery of this new molecule, came from astrophysics, from the attempt to explain the origin of unexplained bands and lines in emission and absorption spectra from interstellar space. It was first of all the intensive absorption band at 217 nm. It was supposed that its origin is connected with small graphite particles (Hufman, 1977). Also a group of interstellar diffuse absorption lines in the visible part of the spectrum, was an unexplainable puzzle for more than 70 years (Hufman, 1977; Herbig, 1975; Krätschmaher et al, 1990a). There were as well several intensive emission bands, with polycyclic aromatic hydrocarbons as carriers (Léger et al, 1984; Allamandola et al, 1985).

We will present shortly here, the development of investigations related to the astrophysical spectra, motivating researches resulting in the discovery of fullerenes.

2. INTERSTELLAR MOLECULES

The development of interstellar spectroscopy was particularly stimulated by the question of the origin of life on Earth. Chemists and biologists belived that a lot of complex organic molecules in the warm sea of the young Earth is needed for that. In 1923., russian scientist A. I. Oparin, supposed that the spontaneous creation of the first primitive single-celled organisms two billion years ago, was the result of the accumulation of biologically important molecules in microscopic coloidal droplets. But

which is the origin of such complex organic molecules? Charles Townes, who in the 1964 obtained the Nobel Prize for the invention of the maser, discovered with coworkes (Cheung et al, 1968) in 1968 the ammonia molecule (NH_3) in space. The ammonia molecules in interstellar space, coming from a dense cloud lying in the direction of the galactic center, were discovered with the help of the microwave radiation with a wavelength of 1.25 cm, observed by the Hat Creek radio telescope. It was the first polyatomic molecule (a molecule with more than two atoms) found in the interstellar space, and it was only the beginning. During the next three years approximately twenty molecules have been identified in the interstellar space, water, formaldehyde, hydrogen cyanide, and acetylene among them. The astrochemistry was born, and it was the beginning of the identification of more and more complex organic molecules in space.

It was assumed that the majority of the observed molecules originate in a series of reactions between molecular ions and molecules, combined with reactions on the surfaces of interstellar dust particles (Turner, 1989).

3. CARBON ATOM CHAINES - POLYYNES IN INTERSTELLAR SPACE

The new breakthrough in the investigation of the interstellar polyatomic molecules was when Barry Turner, an astronomer at the National Radio Astronomy Observatory at Green Bank in West Virginia detected microwave signals identified as due to cyanoacetylene HC_3N. The fact that interstellar clouds where such complex organic molecules have been found, are in the same time the places of the condensation of new stars with planetary systems, was in favour of the hypothesis that complex organic molecules, needed for the creation of life, were present in the warm sea of the young Earth, and that they are maybee of cosmic origin. The question was if even more complex molecules are present in interstellar space. Namely the last identified complex molecule belonged to the carbon chain molecules of the general form HC_nN (where n is equal to or larger than three), named cyanopolyynes (see e. g. Bell et al, 1982; Čelebonović, 1992). But in order to answer on this question one needs the good knowledge of their microwave spectra, and exotic cosmic conditions held the promise of the presence of molecules which are not present on Earth and which have not been synthesized in laboratories.

In 1975, Harry Kroto, a young chemistry lecturer at the University of Sussex, who was an expert in microwave spectroscopy, was very interested by the problem of organic molecules in space. Together with his colleague David Walton, he decided to investigate the existence of cyanobutadiyne (HC_5N) in interstellar clouds. An undergraduate student Antony Alexander, was engaged to synthesize cyanobutadiyne under Kroto and Walton's supervision, in order to measure its microwave spectrum and search for similar signals in space. Alexander synthesized cyanobutadiyne and measured its microwave spectrum between 26.5 and 40.0 gigahertz (Alexander et al, 1976). Than, Kroto asked his colleague Takeshi Oka from Ontario in Canada, and Oka with Lorne Avery, Norman Broten and John MacLeod, with the help of Kroto's data discovered HC_5N in Sagittarius B2 using the 43-metre diameter radio telescope

at Algonquin Park in Ontario (Avery et al, 1976).

Does in interstellar space exists and more complexe molecule cyanohexatriyne HC_7N? Kroto and Walton engaged a new graduate student Colin Kirby to synthesize this molecule. It was not an easy task but after a lot of difficulties it was done (Kirby et al, 1980) and the result enabled to identify and this molecule in space (Kroto et al, 1978). How far one can continue in this manner? It was obvious that an attempt to synthesize further members of the series will be an extremely difficult task. But Oka suggested to estimate the microwave spectrum of HC_9N molecule by extrapolation on the basis of the properties of preceeding members of the series. This attempt was successful and this molecule (Broten et al, 1978) and soon $HC_{11}N$ (Bell et al, 1982) as well, joined to the list of molecules identified in space.

4. CHEMISTRY OF THE CARBON STARS AND DISCOVERY OF FULLERENES

It was of little probability that chains of carbon atoms originate in ion - molecule reactions as it is with simpler molecules. Polyynes and small carbon clusters have been found not only in interstellar clouds (C_3) but as well in the shell around carbon star IRC+10^o216 (Turner, 1989). Kroto (1981) assumed that the source of carbon chain molecules and clusters are carbon rich red giant stars, which by radiation pressure pour in interstellar space dust containing carbon grains, mostly in the form of amorphous graphite. Kroto (1982) supposed that carbon chains may be synthesized in reactions between carbon clusters made by the vaporization of graphite from carbon grains, and simpler molecules. Together with Robert Curl and Richard Smalley, Kroto formulated a project on the simulation of carbon star chemistry and included also students Jim Heath and Sean O'Brien. The result of this project was the synthesis of C_{60} (Kroto et al, 1985) which led to the Nobel prize for Chemistry for Kroto, Curl and Smalley in 1996. They showed that by laser vaporization of graphite, carbon clusters C_n with n from 1 up to 190 are formed, with C_{60} as dominant one (Kroto et al, 1987). Due to the similarity of the structure of C_{60} and domes constructed by the architect Buckminster Fuller, such clusters obtained the name buckminsterfullerenes or simply fullerenes.

It is interesting that Andrew Kaldor from an oil company in New Jersey obtained molecules C_{60} and C_{70} during plasma graphite formation, still in 1984, but has not remarked and identified them on the spectrogram (Cheush, 1999).

Krätschmer et al. (1990)demonstrated that in sooth obtained by electric arc with graphite electrodes with helium as the working gas, are present C_{60} and C_{70}. The fullerenes are a new cristal allotropic modification of the carbon, besides graphite and diamond.

We have also hiperfullerenes with onion type structure where e.g. a C_{60} molecule is within C_{240}. This one within C_{540} and this one within C_{960}. Such multishell fullerenes or buckyonions suggested by Kroto and McKay (1988) are firstly synthetized in laboratory by Ugarte (1992, 1993)

In the spherically symmetrical vacuum hole within a C_{60} molecule, one can put different atoms and ions. For example Weiss et al. (1988), obtained with an arc

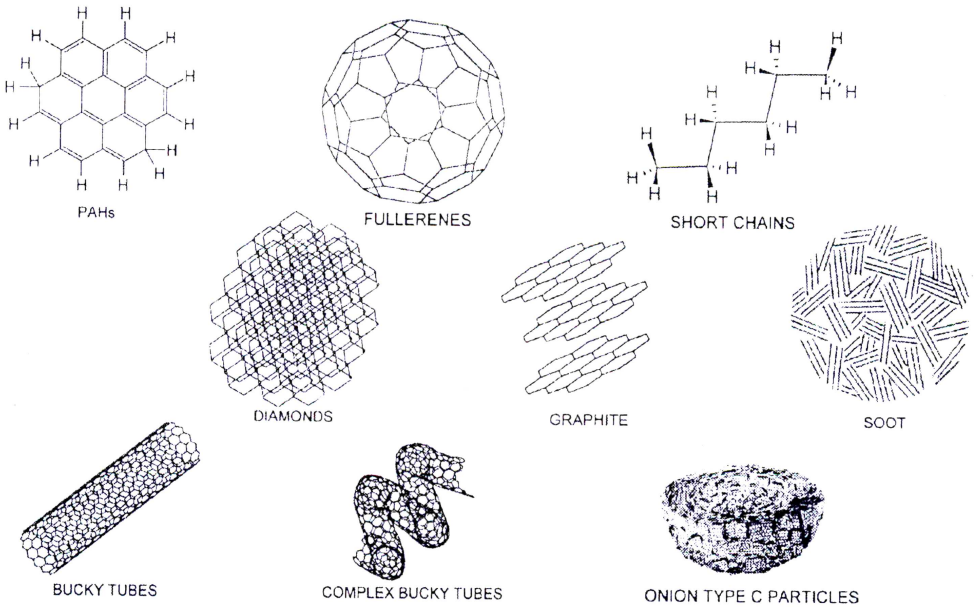

Figure 1: Some of the various forms of carbon that are likely present in gaseous and solide state in the interstellar matter and in solar system material (from Ehrenfreund and Charnley, 2000).

where kalium nitrate has been added to graphite electrodes, that some of K atoms finished in C_{60} molecules and the new compound is named $K@C_{60}$. One of interesting properties of complex carbon forms is also possibility of six angles graphite structure to form nanotubes (see Ebbesen and Ajayan, 1992). Consequently, carbonaceous dust in the interstellar medium may show strong diversity. In Fig. 1 (from Ehrenfreund and Charnley, 2000) are shown the chemical structures of some carbon compounds that are likely present in space.

Later, C_{60} and C_{70} have been identified on Earth in shock produced brechias of the Sudbury impact structure in Ontario (Becker et al, 1994), and in the geological strata of the Cretaceous-Tertiary and the Permian-Triassic boundary layers, associated with bolide impacts (Becker, 1999; Becker et al, 2000, 2001, Botta and Bada, 2002; Pizzarellos et al, 2001). Fullerenes have been detected as well in an impact crater on a spacecraft (Di Brozolo et al, 1994) and in meteorites (see de Vries et al, 1993; Becker et al, 1993; Foing and Ehrenfreund, 1997, Becker and Bunch, 1997; Becker, 1999 and Becker et al. 1999).

The presence of carbon onions in acid residues of the Allende meteorite (see e.g. Ehrenfreund and Charnley, 2000)suggested that higher fullerenes or nanotubes may be present in meteorites. In this meteorite Becker et al. (1999) have found C_{100} and C_{400}. The higher fullerenes have also been isolated from the Murchinson carbonaceous residue, and measurements of noble gases (helium, neon, and argon) in both

the Murchinson and Allende fullerenes by Becker et al. (2000) indicate that these molecules are extraterrestrial in origin.

It was supposed that hydrogen may inhibite the fullerenes growth mechanisms so that one should search C_{60} in hydrogen depleted space regions (Goeres and Sedlmayr, 1992). It has been shown in Gerhardt et al. (1987) however, that fullerenes may be formed when H and O are present. It has been pointed out as well (Kroto and Jura, 1992) the formation of fullerenes in space in relation to carbon dust.

Fullerenes may be formed in small amounts in envelopes of R Coronae Borealis stars (Goeres and Sedlmayr, 1992). Theoretical models show the possible formation of fullerenes in the diffuse interstellar gas with the help of formation of C_2-C_{10} chains from C^+ insertion, ion-molecule reactions, and neutral-neutral reactions (Bettens and Herbst, 1996, 1997).

Interstellar hydrogenated fulleranes (molecules such as family $C_{60}H_m$, m=1,2,...) have been discussed in Webster (1995), and C_{60}^+H was proposed to be most abundant of such molecules in space (Kroto and Jura, 1992). Iglesias-Groth and Breton (2000) suggested that suitable astronomical targets to search for fullerenes are not only carbon stars but also post-AGB stars, protoplanetary nebulae and dusty regions in the Galaxy.

5. DIFFUSE INTERSTELLAR BANDS, SPECTRA AND FULLERENES

One of the great unsolved astrophysical problems is the problem of the identification of the Diffuse Interstellar Bands (DIB) carriers (see Herbig, 1995 for a review). It was proposed in Kroto et al. (1985) and Leger et al. (1988) that the ion C_{60} is a possible DIB carrier. Foing and Ehrenfreund (1994, 1997) searched for C_{60}^+ in the diffuse medium in the infrared. They found two diffuse bands at 957.7 nm and 963.2 nm, in the spectra of 7 carbon rich stars, and in 1997 they proved that the positions of these bands in stellar spectra are coincident within 0.1 percent with laboratory measurements of C_{60}^+ in neon matrix, obtained by Fullara et al. (1993). This was the first evidence of the possible presence of C_{60}^+ around carbon rich stars.

This result motivated Moutou et al. (1999) to use ISO data to search for 7.1 and 7.5 micrometers vibrational emission lines of C_{60}^+ in NGC 7023. They placed an upper limit on C_{60}^+ in NGC 7023 of ¡ 0.3% of interstellar carbon (Moutou et al, 1999; see also Sellgren, 2001). Searches for C_{60} in the interstellar matter througth its UV absorption band at 386 nm, have placed limits of ¡ 0.01% of cosmic carbon abundance in C_{60} (Snow and Seab, 1989; Somerville and Bellis, 1989).

Garcia-Lario et al. (1999) attribute the 21 micrometer dust features observed in the C-rich protoplanetary nebula IRAS 16594-4656 to fullerenes, which may be formed during dust fragmentation. However, many different carrier species have been proposed for this broad strong emission band (e.g. Webster, 1991, 1993, 1995; Hill et al, 1998, see also Ehrenfreund and Charnley, 2000).

Another family of fullerenes which could be relevant to clarify the origin of the DIBs and the unidentified infrared emissions in astronomical objects are the buckyonions or multishell fullerenes (see e.g. Iglesias-Groth and Breton, 2000).

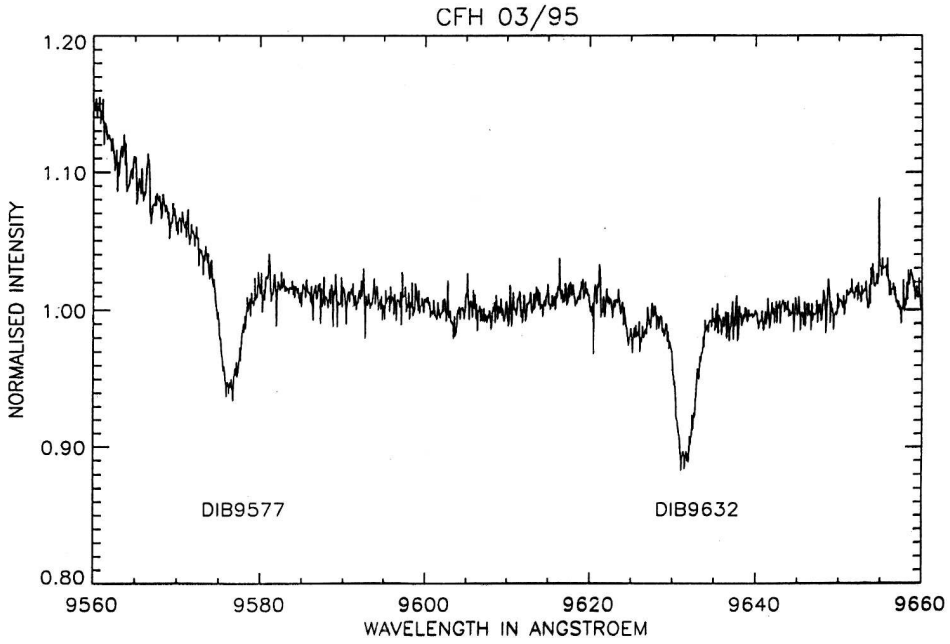

Figure 2: Telluric corrected spectrum of HD183143 carbon rich star observed by Canadian French Telescope at Hawai (CFT) in March 1995. The two DIB's at 9577 and 9632 Å are confirmed with the same width of 2.86 Å consistent with the C_{60}^+ assignment and expected rotational contour broadening with temperature 60±10 K. This Fig. is from Foing and Ehrenfreund (1997) article with the first possible confirmation of the presence of C_{60}^+ ion in carbon rich star spectra.

It was demonstrated as well that doping of C_{60} with C_{70} provokes interesting changements in the spectrum. It has been stated in Pichler et al. (1991), that the optical absorption spectrum of the C_{60}/C_{70} mixture is qualitatively similar with the interstellar extinction curve for photon energies less than 4 eV, so that carbon clusters might be present in space as well as C_{60} and C_{70} mixture. In any case, the investigation of the spectral properties of the C_{60} and C_{70} mixtures in different proportions, with eventual addition of other fullerenes, will contribute to to our knowledge on the fullerene abundance in space.

References

Alexander, A.J., Kroto, H.W., Walton, D.R.M.: 1976, *J. Mol. Spectrosc.*, **62**, 175.
Allamandola, L.J., Tielens, A.G., Barker, J.R.: 1985, *Astrophys. J.*, **290**, L25.
Avery, L.W., Broten, N.W., MacLeod, J.M., Oka, T., Kroto, H.W.: 1976, *Astrophys. J.*, **205**, L173.
Becker, L.: 1999, *Astrophys. Space Sci. Libr.*, **236**, 377.
Becker, L., Bunch, T.E.: 1997, *Meteoritics*, **32**, 479.
Becker, L., Bunch, T.E., Allamandola, L.J.: 1999, *Nature*, **400**, 228.

Becker, L., McDonald, G.D., Bada, J.L.: 1993, *Nature*, **361**, 595.
Becker, L., Poreda, R., Bunch, T.E.: 2000, *Proc. Nat. Acad. Sci.*, **97**, 2979.
Becker, L. et al.: 1994, *Science*, **265**, 642.
Becker, L. et al.: 2000, *Proc. Natl. Acad. Sci. USA*, **97**, 2979.
Becker, L. et al.: 2001, *Science*, **291**, 1530.
Bell, M.B., Kwok, S., Feldman, P.A., Matthews, H.E.: 1982, *Nature*, **295**, 389.
Bettens, P.R., Herbst, E.: 1996, *Astrophys. J.*, **468**, 686.
Bettens, P.R., Herbst, E.: 1997, *Astrophys. J.*, **478**, 585.
Botta, O., Bada, J.L.: 2002, *Surveys in Geophysics*, **23**, 411.
Broten, N.W., Oka, T., Avery, L.W., MacLeod, J.M., Kroto, H.W.: 1978, *Astrophys. J.*, **223**, L105.
Čelebonović, V.: 1992, *Bull. Astron. Belgrade*, **146**, 41.
Cheung, A.C., Rank, D.M., Avery, L.W., Townes, C.H., Thornton, D.C., Welch, W.J.: 1968, *Phys. Rev. Lett.*, **21**, 1701.
Cheush, I.: 1999, *Aerospace Research in Bulgaria*, **15**, 157.
de Vries, M.S., Reihs, K., Wendt, H.R., Golden, W.G., Hunziker, H.E., Fleming, R., Peterson, E., Chang, S,: 1993, *Geochimica et Cosmochimica Acta*, **57**, 933.
Di Brozolo, F.R., Bunch, T.E., Fleming, R.H., Macklin, J.: 1994, *Nature*, **369**, 6475.
Ebbesen, T.W., Ajayan, P.M.: 1992, *Nature*, **358**, 2200.
Ehrenfreund, P., Charnley, S.B.: 2000, *Ann. Rev. Astron. Astrophys.*, **38**, 427.
Foing, B.H., Ehrenfreund, P.: 1994, *Nature*, **369**, 296.
Foing, B.H., Ehrenfreund, P.: 1997, *Astron. Astrophys.*, **317**, L59.
Fulara, J., Jakobi, M., Maier, J.P.: 1993, *Chem. Phys. Lett.*, **211**, 227.
Garcia-Lario, P., Manchado, A., Ulla, A., Manteiga, M.: 1999, *Astrophys. J.*, **513**, 941.
Gerhardt, P., Loffler, S., Homann, K.P.: 1987, *Chem. Phys. Lett.*, **137**, 306.
Goeres, A., Sedlmayr, E.: 1992, *Astron. Astrophys.*, **265**, 216.
Herbig, E.: 1975, *Astrophys. J.*, **196**, 129.
Herbig, G.H.: 1995, *Ann. Rev. Astron. Astrophys.*, **33**, 19.
Hill, H.G.M., Jones, A.P., d'Hendecourt, L.B.: 1998, *Astron. Astrophys.*, **336**, L41.
Hufman, D.R.: 1977, *Adv. Phys.*, **26**, 129.
Iglesias-Groth, S., Breton, J.: 2000, *Astron. Astrophys.*, **357**, 782.
Kirby, C., Kroto, H.W., Walton, D.R.M.: 1980, *J. Mol. Spectrosc.*, **83**, 26.
Krätschmaher, W., Lamb, L.D., Frostiropulos, K., Huffman, D.R.: 1990a, *Nature*, **347**, 354.
Krätschmaher, W. et al.: 1990b, in *Dusty Objects in the Universe*, Kluwer, Dordrecht, 89.
Kroto, H.W.: 1981, *Int. Rev. Phys. Chem.*, **1**, 309.
Kroto, H.W.: 1982, *Chem. Soc. Rev.*, **11**, 435.
Kroto, H.W., Heath, J.R., O'Brien, S.C., Curl, R.F., Smalley, R.E.: 1985, *Nature*, **318**, 162.
Kroto, H.W., Heath, J.R., O'Brien, S.C., Curl, R.F., Smalley, R.E.: 1987, *Astrophys. J.*, **314**, 352.
Kroto, H.W., Jura, M.: 1992, *Astron. Astrophys.*, **263**, 275.
Kroto, H.W., Kirby, C., Walton, D.R.M., Avery, L.W., Broten, N.W., Mac Leod, J.M., Oka, T.: 1978, *Astrophys. J.*, **219**, L133.
Kroto, H.W., Mc Kay, K.: 1988, *Nature*, **331**, 328.
Leger, A., d'Hendecourt, L., Verstraete, L., Schmidt, W.: 1988, *Astron. Astrophys.*, **203**, 415 .
Léger, A., Puget, J.L.: 1984, *Astron. Astrophys. Lett.*, **137**, L5.
Moutou, C., Sellgren, K., Verstraete, L., Léger, A.: 1999, *Astron. Astrophys.*, **347**, 949.
Pichler, K., Graham, S., Gelsen, O.M., et al.: 1991, *J. Phys. Cond. Matter*, **3**, 9259.
Pizzarello, S. et al.: 2001, *Science*, **293**, 2236.
Sellgren, K.: 2001, *Spectrochimica Acta A*, **57**, 627.
Snow, T.P., Seab, C.G.: 1989, *Astron. Astrophys.*, **213**, 291.
Somerville, W.B., Bellis, J.G.: 1989, *Monthly Notices of The Royal Astronomical Society*, **240**, P41.
Turner, B.E.: 1989, *Space Sci. Rev.*, **51**, 235.

Ugarte, D.: 1992, *Nature*, **359**, 707.
Ugarte, D.: 1993, *Europhys. Lett.*, **22**, 45.
Webster, A.S.: 1991, *Nature*, **352**, 412.
Webster, A.S.: 1993, *Monthly Notices of The Royal Astronomical Society*, **263**, 385.
Webster, A.: 1995, in *Diffuse Interstellar Bands*, eds. A. Tielens, T. Snow, Kluwer, 349.
Weiss, F.D. et al.: 1988, *J. Am. Chem. Soc.*, **110**, 4464.

Proc. IV Serbian-Bulgarian Astronomical Conference,
Belgrade 21–24 April 2004,
eds. M. S. Dimitrijević, V. Golev, L. Č. Popović, M. Tsvetkov,
Publ. Astron. Soc. "Rudjer Bošković" No 5, 2005, 59 - 66

Invited lecture

NEW POSSIBILITIES FOR SPACE RESEARCH IN BULGARIA[1]

P. S. GETSOV and P. V. PANOVA
Space Research Institute, Bulgarian Academy of Sciences,
Moskovska Str. No.6, Sofia-1000, Bulgaria
E–mail office@space.bas.bg

1. FIRST PERIOD – HISTORICAL REVIEW.

The organized participation of Bulgarian scientists in space research started in 1969 when the Scientific Group of Space Physics (SGSP) at the Presidium of the Bulgarian Academy of Sciences was created. Years of creative enthusiasm followed the euphoria caused by mankind's grand success in the peaceful study of space at the time. Yet with the first man flown to space and the first spacecraft landed on the moon, targeted studies began in Bulgaria in the field of probe methods for studying of space plasma.

In 1972, after launch of first Bulgarian equipment P-1, Bulgaria became the 18th in order space country.

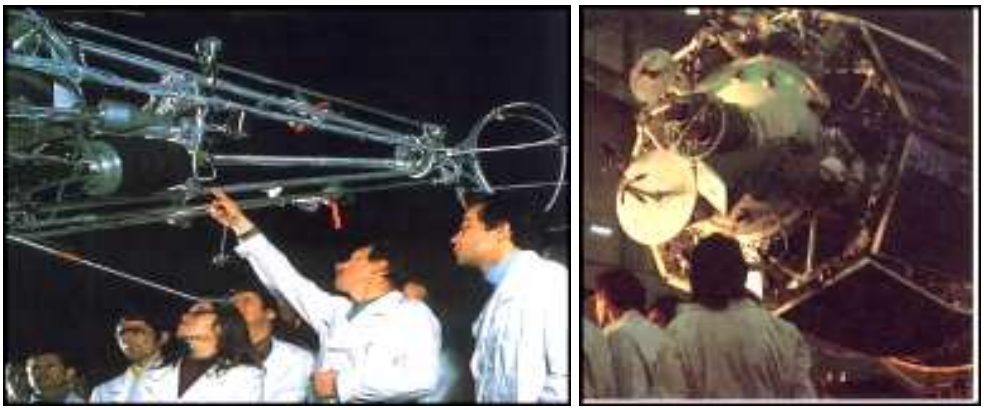

Figure 1a,b: Bulgarian scientists during the preparing of the INTERCOSMOS experiments.

[1]Lecture presented by M. Tsvetkov

In 1975, based on the SGSP, the Central Laboratory for Space Research (CLSR) was founded. Soon, Bulgarian scientists gained significant experience through their successful participation in the INTERCOSMOS Program, preparing experiments and designing equipment for the satellites INTERCOSMOS - 8 (IK - 8, 1972), IK - 12, 14, 19 and the heavy geophysical rockets VERTICAL - 3, 4, 6, 7, 10 (Fig.1a.b.).

In the years that followed, an ever growing number of Bulgarian scientists and institutes joined in the preparation and performance of space experiments. In 1979, the first Bulgarian astronaut Georgi Ivanov (Fig. 2) flew in space on board of SOYUZ - 33 Space Ship. The research program and equipment for his flight were designed entirely by the suggestions of our scientists ("Spectar-15", "Daga", "Sredets", "Vital").

In 1981, through the two satellites INTERCOSMOS "Bulgaria - 1300"(Fig.3.), furnished entirely with Bulgarian equipment, and METEOR - PRIRODA, the National Space Program "Bulgaria-1300" was implemented, aimed at studying the ionospheric-magnetospheric relationship and remote sensing of the Earth from space. These successful experiments consolidated the priority scientific and scientific-application research areas in the country - space physics, remote sensing of the Earth, and space technology.

Figure 2: Astronauts Georgi Ivanov (BG) and N. Rukavishnikov (USSR) on board of SOYUS-33.

The decision of the Government from 1987 for restructuring of the CLSR into a Space Research Institute (SRI) was a manifestation of recognition for the success of space studies and awareness of their future significance. The gained experience and scientific knowledge were the prerequisite for the development of a new research

program for the second manned flight with a Bulgarian astronaut. Under the "Shipka" Program, research teams from the Bulgarian Academy of Sciences, Sofia University, the Academy of Agriculture and other universities and institutes were engaged in the implementation of more than 48 research experiments in the field of space physics, remote sensing of the Earth from space, space biology and medicine, space material science, space equipment. The flight took place in 1988 with astronaut Alexander Alexandrov (Fig. 4). The leading research institute in the implementation of the "Shipka" project was SRI - BAS. For the implementation of this research program the Bulgarian scientists designed 15 research devices and complexes which continue to work even after the Bulgarian flight as part of the equipment on the Russian MIR Orbital Space Station. In parallel with the preparation of this flight, scientists from SRI participated successfully in the international programs VENUS-HALLEY (1985-1986), PHOBOS (1988-1989), AKTIVEN (1989), APEX (1990) (Fig.5).

Figure 3: First Bulgarian Satellite "Bulgaria 1300" lunched in 1981.

Figure 4: The second Bulgarian astronaut Alexander Alexandrov with his russian colleagues.

In the recent years, in the SRI, new programs are elaborated and a number of old programs and complexes are improved, such as: the SVET space greenhouse, the R-400 very high frequency (VHF) radiometer under the PRIRODA project, the NEUROLAB-B system for monitoring the astronauts' psychophysiological status which were flown and operated on board of the MIR orbital space station.

2. SECOND PERIOD – AFTER 1989

One of the greatest achievement of the SRI is the "Neurolab-B" system (Fig.6) which operates on board of the MIR orbital station. It is intended for complex psycho-physiological study of astronauts (electrocardiogram, miogram, electrooculogram, breathing, temperature, blood pressure, skin conductivity etc.).

In the recent years, the small-sized multichannel "Holter" system (Fig.7) was designed for recording of some physiological parameters: electrocardiogram, breathing, blood pressure, temperature etc. The system is used for clinical studies in an English clinic.

Figure 5: Space equipment made at the SRI, BAS and used during different space missions.

Figure 6: The "Neurolab-B" system.

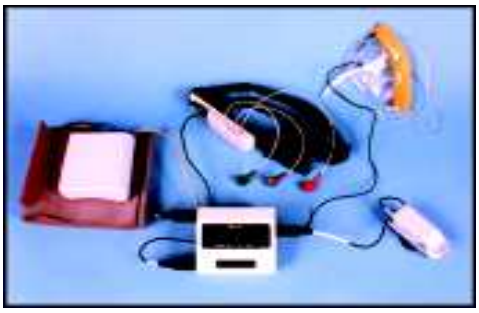

Figure 7: The "Holter" system.

Onboard of the MIR OS were carried out the experiments under the SVET SG space greenhouse project (Fig. 8) with the active participation of Russian and American astronauts during 1990-2000 are as follows: two-month experiments with radishes and Chinese cabbage - June-August 1990; three-month "Super Dwarf" wheat experiments - August-November 1995; six-month wheat experiments with two successive wheat crops – July, 1996 – January, 1997 (with the Utah State University, Logan, USA); four-month experiments with three "Brassica Rapa" generations – May - September, 1997 (with the Louisiana State University, USA); six-month experiments with two successive crops of a new wheat brand – November, 1998 - May, 1999; and three-week experiments with leaf crop - May - June, 2000 (with the IBMP, Moscow).

The project is discussed by the international scientific community which qualifies it as one of the most prestigious ones, carried out in the 1990s on the MIR OS. Plant experiments will continue in the next 21st century on the International Space Station, for which a new generation of SVET-3 SG is being designed, along with similar NASA and ESA equipment.

Figure 8: The "SVET SG" - first space greenhouse successfully tested at MIR OS.

During the project RAPIDS joint workgroup of specialist from NLR and Space Research Institute was formed. An demonstration scenario was developed and coordinated according to the proper test areas concerning schedule activities. The mobile ground receiving station RAPIDS was transported and installed near to the Space Research Institute in Sofia in 22-29 of September 2000. Bulgarian partners have organized a model of Receiving and Processing Center for remote sensing data. As result of the work were received optical (SPOT) and radar (ERS) data.

Figure 9: The mobile ground receiving station "RAPIDS".

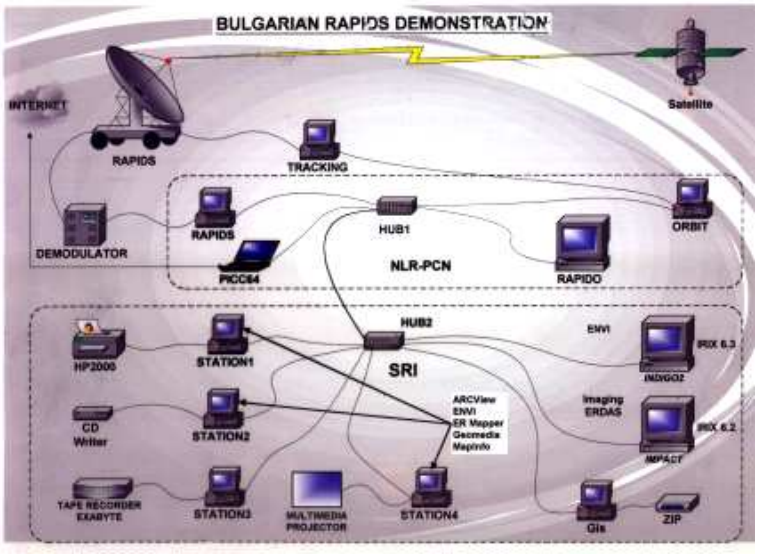

Figure 10. The pipeline structure of "RAPIDS".

SRI perform scientific and applied activity in the field of aviation and space navigation and communication systems and equipment. The team of the Laboratory of Navigation and communication is basically engaged with increasing the effectiveness of the available space or national security communication and navigation systems. Intensive work is underway to design integrated navigation-communication systems with wide practical application in the field of on-line monitoring of movable objects - transportation vehicles and aircraft. The speedy communication modules (Fig. 11) developed in the Laboratory, operating in the range of 2.4 - 5.8 GHz, are applied on a number of ground-based communication systems, using modern protocols and route-defining methods.

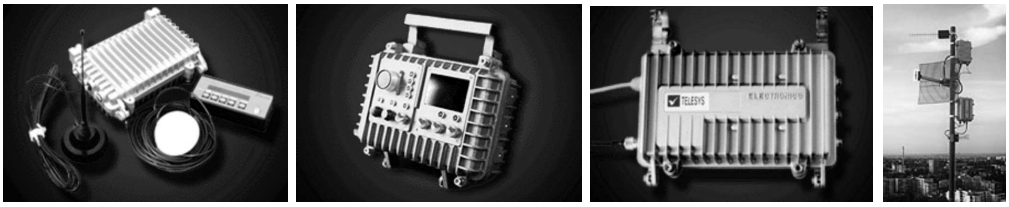

Figure 11: The components from the "RAPIDS" systems made in Space Research Institute, BAS.

3. FUTURE – INTEROPERABILITY BY COOPERATION AND INTEGRATION

The partnership between Bulgaria and a partner countries in Framework Program 6th of EU;

Looking for partners for joint participation in space programs for launching small satellites for Earth observation;

Taking a part in the International Space Station program developing systems and devices for medical and biological investigations;

Take a participation in the field of aircraft onboard systems and unmanned vehicles.

Proc. IV Serbian-Bulgarian Astronomical Conference,
Belgrade 21–24 April 2004,
eds. M. S. Dimitrijević, V. Golev, L. Č. Popović, M. Tsvetkov,
Publ. Astron. Soc. "Rudjer Bošković" No 5, 2005, 67 - 74 *Invited lecture*

THE COMPOSITE Sy2/STARBURST COMPTON-THIN GALAXY NGC 7679 = Mark 534

V. GOLEV and I. YANKULOVA

Astronomy Department of the St. Kliment Okhridski University of Sofia, Bulgaria
E–mail valgol@phys.uni-sofia.bg

Abstract. The Starburst/Sy2 galaxy NGC 7679 (Mrk 534) was observed with the 2m RCC Telescope of the Ukraine National Astronomical Observatory at peak Terskol, Caucasus. The two-channel focal reducer of the MPAe in tunable Fabry-Perot mode was used. The high-luminous IR galaxy NGC 7679 is a low-redshift face-on SB0 galaxy in which starburst and AGN activities co-exist. The ionization structure in the inner central region ($\leq$ 2.5 kpc) is maintained by the AGN continuum whereas outside this region the source of ionization has a clear starburst origin. The SED from IR to X-rays is typical for Sy2 galaxies. NGC 7679 is an unabsorbed X-ray source (i.e. possesses low X-ray column density) for which the simple formulation of the Unified Model for SyGs is not applicable. The maximum of ionization of the starburst region is displaced by 12 arcsec east from the nucleus. The infered ionization anisotropy of the radiation field and the photon deficiency of ionizing photons are suggestive that the central AGN source is observed through dense dusty-gaseous clouds. Such dusty warm absorbers have already been invoked to explain the discrepancy between the amount of X-ray cold absorption and the optical reddening in some SyGs.

1. INTRODUCTION

The high-luminous IR galaxy Mrk 534 is nearby ($z = 0.0171$) nearly face-on SB0 Sy2 galaxy in which starburst and AGN activities co-exist (Della Ceca et al, 2001). Composite Seyfert-starburst galaxies have been recently studied by Levenson et al. (2001). A significant part of the observed FIR-emission of these composites could be associated with circumnuclear starburst events. The circumnuclear starburst should also play a major role in the obscuration processes around the AGN (Levenson et al, 2001, and references therein). NGC 7679 is included in a small sample of unabsorbed Sy2 galaxies (i.e. Seyferts which have an X-ray column density lower than 10^{22} cm^{-2}) for which the simple formulation of the Unified Model for Seyferts is not applicable (Panessa and Bassani, 2002).

NGC 7679 is physically associated by a common stream of ionized gas with the Sy2 galaxy NGC 7682 at $\sim 4.5'$ east. There are also signs of tidal disruption due to the interaction with the faint compagnion that lies $\sim 50''$ at east direction also (see Fig. 1). Together with the existence of a bar in Mrk 534 this could enhance the gas flow towards the nuclear regions and possibly trigger the starburst processes observed (Gu et al, 2001).

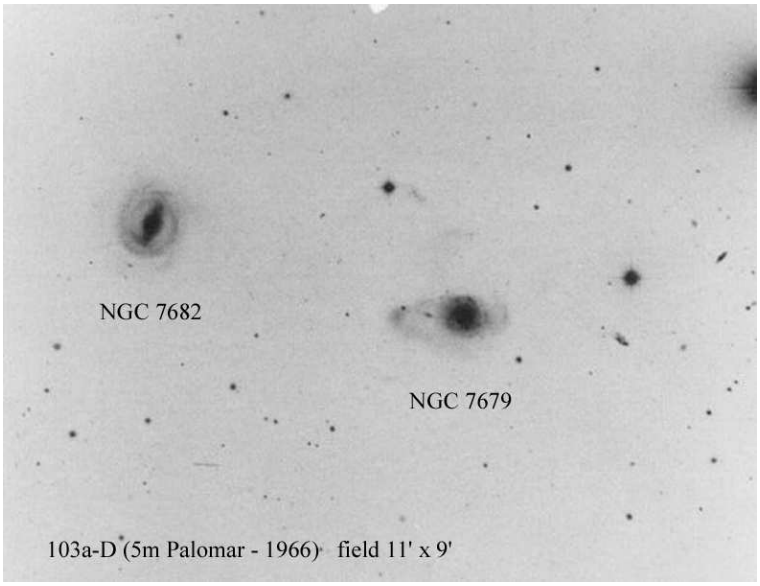

Figure 1: The field of Sy2 pair NGC 7679 and NGC 7682. This broad-band image was downloaded from NED.

NGC 7679 shows quite high IRAS luminosity in the far IR ($\log L_{\rm FIR}/L_{\odot} \approx 11.10$), a ratio $L_{\rm farIR}/L_B \sim 1$, and IR colors typical of a classical starburst galaxy.

2. OBSERVATIONS AND DATA REDUCTION

NGC 7679 was observed by K. Jockers and T. Bonev with the 2m reflector of the Ukraine National Astronomical Observatory at peak Terskol, Caucasus. The observations were carried out on October 1996 with the Two-channel Focal Reducer of the Max-Planck-Institute for Aeronomy (MPAe) designed by K. Jockers and described in Jockers (1997) and Jockers et al. (2000). This instrument was primarily intended for cometary studies but it has repeatedly been used for observations of active galactic nuclei (Yankulova, 1999; Golev et al, 1995, 1996). The technical data and the present capabilities of the MPAe Focal Reducer are described in the paper of Jockers (1997) and Jockers et al. (2000).

All observations are taken in two-channel Fabry-Perot (FP) mode using tunable FP narrow-band imaging with spectral FWHM of the Airy profile $\delta\lambda$ in order of 3 - 4 Å. The overall "finesse" of the system (or $\Delta\lambda/\delta\lambda$) is ≈ 15 which enables quite high contrast of the FP images.

The details of observations are presented in Table 1 where the central wavelengths λ_c and the effective width $\Delta\lambda$ of the interference filters used to separate the Fabry-Perot interference orders, the wavelength $\lambda_{\rm FP}$ at which the Fabry-Perot was tuned, and the exposures are listed. At the distance of Mrk 534 one arcsec corresponds to a

Table 1: NGC 7679 – Observation details

image frame	interference filter[a)] $\lambda_c/\Delta\lambda$ (Å)/(Å)	Fabry-Perot tuned wavelength λ_{FP} (Å)	frames × exposure time (s)
red channel:			
H$\alpha\lambda$6563	6662/55		1 × 1800
			2 × 900
[N II]λ6548	6662/55		1 × 900
continuum	6719/33		1 × 1800
			1 × 900
[O III]λ5007	5094/44		2 × 900
continuum	5002/41		1 × 1200
Gunn r[b)]	6800/1110		1 × 60
blue channel:			
[O III]λ4363	4432/44		1 × 900
			1 × 1200
continuum	4253/32		3 × 900
BG 39/2[b)]	4720/700		2 × 1500

[a)] Used to separate Fabry-Perot working orders.

[b)] Broad-band image taken without Fabry-Perot.

distance of about 340 pc assuming $H_0 = 75$ km sec^{-1} Mpc^{-1}.

Two exposures of Mark 534 were obtained through each filter to eliminate cosmic ray events and to increase the reliability of the measurements. Between exposures the telescope was slightly offset to avoid permanent defects of the CCD. Flatfield exposures were obtained using dusk and dawn twilight for uniform illumination of the detector. No dark correction was required.

The images were reduced following the usual reduction steps for narrowband imaging. After flatfielding the frames were aligned by rebinning to a common origin. The final alignment of all the images was estimated to be better than 0.1 px (the scale is 1 px = 0.8 arcsec). A convolution procedure was performed in order to match the PSFs of each line – continuum pair which unavoidably degrades the final FWHM of the images to the mean value about 3 - 3.5 arcsec.

3. RESULTS

The unpublished Hα images taken from the archives of the Isaak Newton Group of telescopes at La Palma and from the ESO La Silla NTT revealed in the light of pure Hα emission a "double nucleus" unseen in the known broad-band images. The separation between the nuclear counterparts (in fact one is the nucleus itself and the other is an extremely powerfull starburst region close to the nucleus) is $\leq$ 3 arcsec. In Fig. 2 we present our very deep and high-contrast Hα image with numerous starburst regions where because of both seeing and pixel size we are able to see only elliptical central isophotes instead of the "double nucleus". The existence of this "double nucleus" in Mark 534 could enhance the gas flows towards the nuclear regions and possibly trigger the starburst processes.

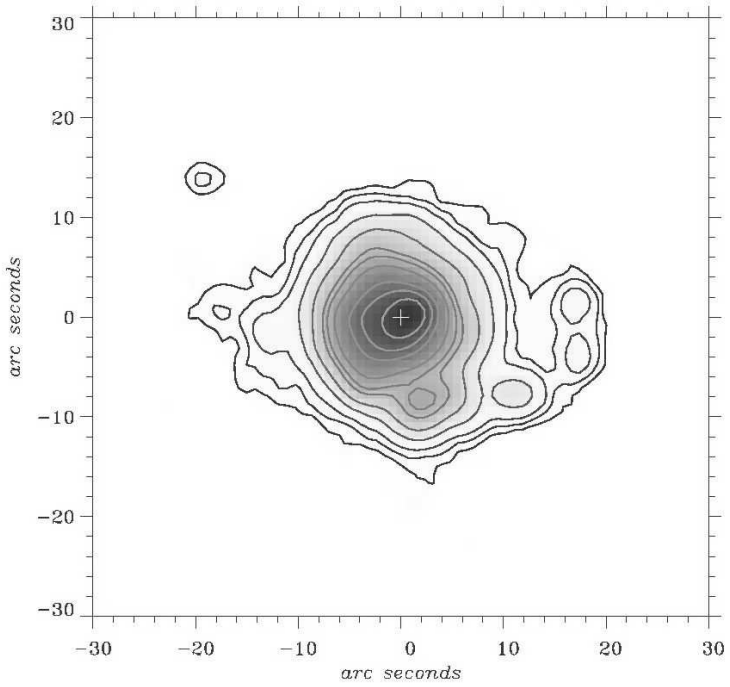

Figure 2: The contours of Hα superimposed on the gray-scale Hα image of the regions around the nucleus of NGC 7679. The image center (0,0) denotes the optical position of the nucleus of NGC 7679 (as given in NED). The resulting FWHM of the seeing after reductions is shown.

The contours of [O III]λ5007 superimposed on the gray-scale [O III]λ5007 image of the regions around the nucleus of NGC 7679 are presented in Fig. 3. The E-W elongation of [O III]λ5007 emission is clearly seen as well as the two extrema decentered of about $\sim$ 4 arcsec from the position of the nucleus.

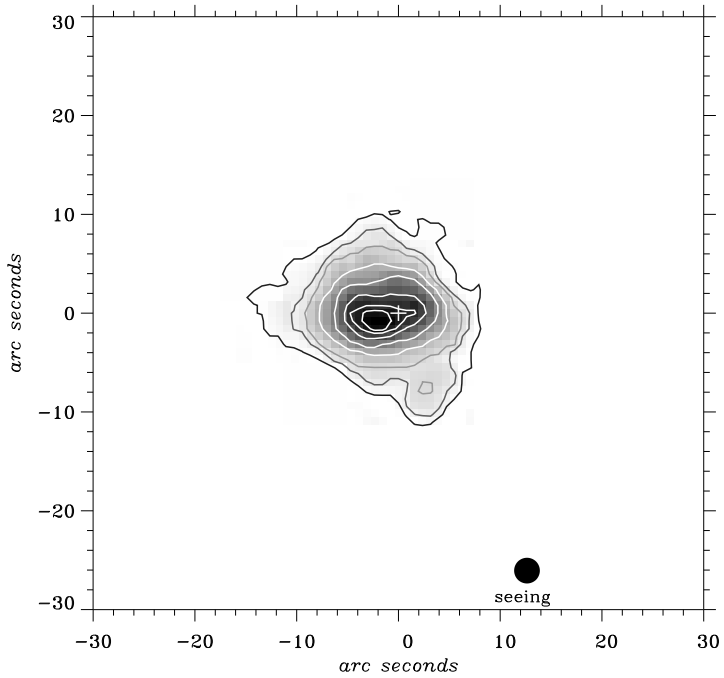

Figure 3: The contours of [O III]λ5007 superimposed on the gray-scale [O III]λ5007 image of the regions around the nucleus of NGC 7679. The image center (0,0) denotes the optical position of the nucleus of NGC 7679.

The [O III]λ4363 emission arises in the innermost nuclear region situated in the valley between both maxima of the [O III]λ5007 emission and does not show any preferred direction. The contours of the [O III]λ4363/[O III]$\lambda\lambda$4959 + 5007 ratio are elongated along the direction perpendicular to the extension of the [O III]λ5007 emission (see Fig. 4). Note the shift of the [O III]λ4363/[O III]$\lambda\lambda$4959+5007 maximum comparing to the maximum of the [O III]λ5007 emission. The former grows between two [O III]λ5007 extrema and reaches its maximum at the position of the nucleus.

The analysis of the [O III]λ4363/[O III]$\lambda\lambda$4959 + 5007 ratio (adopting $T_{\rm e}$ between 1.0×10^4 K and 2.0×10^4 K) shows very high electron densities at the direction of the nucleus ($\log N_{\rm e}$ varies between 6.2 and 7.8 depending on $T_{\rm e}$ adopted).

The [O III]λ5007/Hα ratio or the ionization map (Fig. 5) is a well known idicator of the mean level of the ionization and temperature in the emission-line regions. The E-W elongation with an offset of the peak value is clearly seen. The [O III]λ5007/Hα flux-calibrated ratio infers the highest ionization $\mathrm{F_{5007}/F_{H\alpha}} \approx 2.1$ shifted to the east of about 13 arcsec with respect to the nuclear position defined by the images in the light of the continuum adjacent to Hα. The [O III]λ4363/[O III]$\lambda\lambda$4959 + 5007 ratio

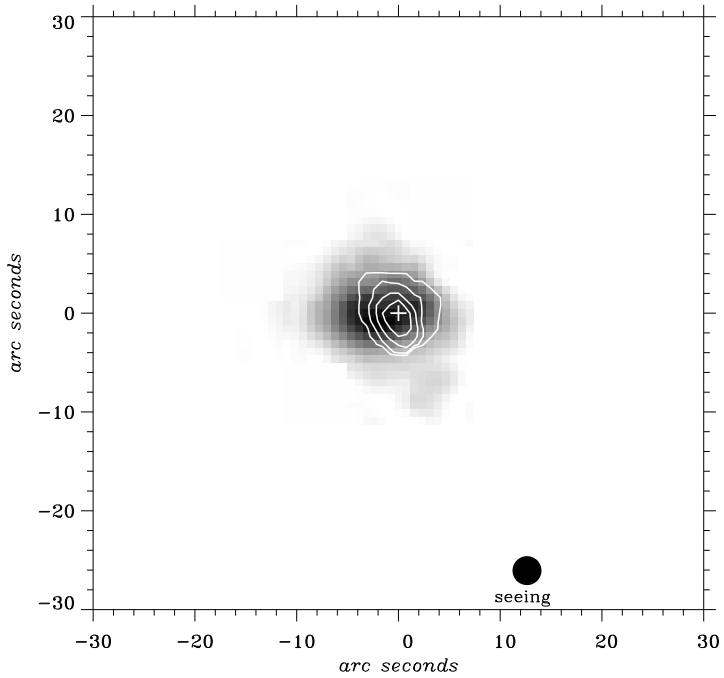

Figure 4: The contours[O III]λ4363/[O III]$\lambda\lambda$4959 + 5007 ratio superimposed on the gray-scale [O III]λ5007 halftone image of the regions around the nucleus of NGC 7679. The image center (0,0) denotes the position of the nucleus.

(dense matter) coincide with the galactic nucleus and the ionization grows to the east of the nucleus.

On the basis of the emission-line fluxes extracted from the central 2 kpc region we estimate the number of the ionizing photons $N_{\rm opt}$ which have to be available in order to exist the observed ionization structure to be $N_{\rm opt} \sim 10^{54} \div 5 \times 10^{54}$ photons s^{-1}. On the other hand the number of ionizing photons $N_{\rm X-ray}$ provided by the central AGN and estimated from the measured flux in soft X-rays (0.1 - 2 keV band) is $N_{\rm X-ray} \approx 10^{53}$ photons s^{-1}).

The morphology both of the inner part of the [O III]λ5007 image and of the [O III]λ5007/Hα ratio suggests an anisotropy of the radiation field. Taking into consideration also the photon deficiency $N_{\rm opt}/N_{\rm X-ray} \approx 0.1 \div 0.5$ we conclude that the central AGN source is observed trough the dust-gas clouds which could be in relation with a dusty torus.

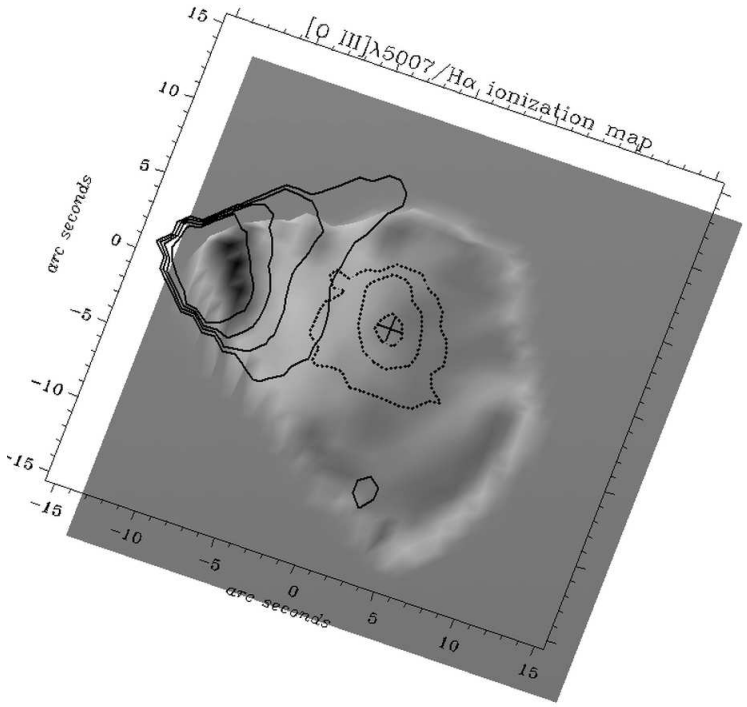

Figure 5: The contours of [O III]λ4363/[O III]$\lambda\lambda$4959 + 5007 ratio superimposed on the gray-scale and contours of the ionization map (or [O III]λ5007Hα ratio). The image center (0,0) denotes the position of the nucleus.

4. CONCLUSIONS

The complex physical picture of NGC 7679 is revealed. Its high FIR luminosity and its IR colors are typical for a classical starburst galaxy. The Hα images show a double nucleus and an extended envelope with bright knots which resembles a starforming ring at about 5 kpc from the center of NGC 7679. The ionization structure in the inner central region (about 3 kpc) is maintained by the AGN-type continuum whereas outside this region the source of ionization has a starburst origin. The SED from IR to X-rays is typical for classical Sy2 galaxies.

(i) The maximum of ionization of the starburst region is displaced by $\sim$ 13 arcsec east from the nucleus.

(ii) The high values around the nucleus of the [O III]λ4363/[O III]$\lambda\lambda$4959 + 5007 ratio are tightly connected with the presence of dense ionized gas with high electron temperature $T_{\rm e}$.

(iii) Both the dense ionized gas in the innermost region (probably dust-mixed in

and outlined by the ratio) and the inferred ionization anisotropy of the radiation field and the photon deficiency of ionizing photons $N_{\rm X-ray}/N_{\rm opt} = 0.1 - 0.5$ (where $N_{\rm opt}$ is the number of ionizing photons needed to maintain the observed ionization structure, and $N_{\rm X-ray}$ is the number of quanta provided in soft X-rays by the central AGN), are suggestive that the central AGN source is observed through dense dust-gas clouds. Such "dusty" warm absorbers have already been invoked to explain the discrepancy between the amount of X-ray cold absorption and the optical reddening in some SyGs (Reynolds 1997).

(iv) There could be a "hole" in the warm absorber of the nuclear source so that the X-ray emission from the accretion disk is unabsorbed and pointed out to the region of the observed [O III]λ5007/Hα maximum at $\sim$ 13 arcsec eastern from the nucleus.

Acknowledgements

We are grateful to Sv. Zhekov, Space Research Institute at Bulgarian Academy of Sciences, for the fruitful discussions of X-ray properties of NGC 7679. We would like to thank Klaus Jockers, Max-Planck-Institut für Aeronomie, and Tanju Bonev, Institute of Astronomy at Bulgarian Academy of Sciences, for securing the Fabry-Perot observations at the 2m telescope of National Astronomical Observatory of Ukraine at peak Terskol, Caucasus, Russia.

This research was partially based on data from the ING and ESO Archives. The research has made use of the SIMBAD database, operated at CDS, Strasbourg, France, and of the NASA/IPAC Extragalactic Database (NED) which is operated by the Jet Propulsion Laboratory, California Institute of Technology, under contract with the National Aeronautics and Space Administration.

We acknowledge the support of the St. Kliment Ohridski University's Science Research Fund by the grant No.80/2004.

References

Della Ceca, R., Pellegrini, S., Bassani, L., Beckmann, V., Cappi, M., Palumbo, G.G.C., Trinchieri, G., Wolter, A.: 2001, *Astron. Astrophys.* **375**, 781.

Golev, V., Yankulova, I., Bonev, T., Jockers, K.: 1995, *Mon. Not. Roy. Astron. Soc.* **273**, 129.

Golev, V., Yankulova, I., Bonev, T.: 1996, *Mon. Not. Roy. Astron. Soc.* **280**, 29.

Gu, Q.S., Huang, J.H., de Diego, J.A., Dultzin-Hacyan, D., Lei, S.J., Benitez, E.: 2001, *Astron. Astrophys.* **374**, 932.

Jockers, K.: 1997, *Experimental Astronomy* **7**, 305.

Jockers, K., Credner, T., Bonev, T., Kiselev, N., Korsun, P., Kulik, I., Rosenbush, V., Andrienko, A., Karpov, N., Sergeev, A., Tarady, V.: 2000, *Kinematika i Fizika Nebesnykh Tel*, Suppl. No. 3, 13.

Levenson, N., Weaver, K., Heckman, T.: 2001, *Astrophys. J.* **550**, 230.

Panessa, F., Bassani, L.: 2002, *Astron. Astrophys.* **394**, 435.

Reynolds, R.: 1997, *Mon. Not. Roy. Astron. Soc.* **286**, 513.

Yankulova, I.: 1999, *Astron. Astrophys.* **344**, 36.

Proc. IV Serbian-Bulgarian Astronomical Conference,
Belgrade 21–24 April 2004,
eds. M. S. Dimitrijević, V. Golev, L. Č. Popović, M. Tsvetkov,
Publ. Astron. Soc. "Rudjer Bošković" No 5, 2005, 75 - 82 *Invited lecture*

STAR COMLEXES IN M33

G. R. IVANOV

Department of Astronomy, Sofia University,
James Bourdier Ave. 5, BG-1164, Sofia, Bulgaria

Abstract. The star complexes have a hierarchical structure in both space and time. A method for indentification of star complxes in M33 is applied. The average size of star clusters is from 11 to 20 pc, while the size of OB associations is ranged 60 - 100 pc. Several OB associations form a star complex with a mean dimension of 0.3 - 1 kpc. In this paper we apply correlation technique in order to compare different stellar populations in M33. Our results confirm the existence of a strong correlation between OB stars, HII regions, and WR stars which indicate the regions of massive star formation. There was confirmed a good correlation between RSGs and WR stars in spiral arms of M33. It can be expected that as the progenitors of WR stars are massive OB stars or RSGs with masses $M \geq 20M_{\odot}$. The massive RSGs as well WR stars probably originate from nearby sites of star formation. We consider this fact as a basis for selecting star complexes in M33. The aim of this paper is to pesent method for indentification of star complexes to be applied for other nearby galaxies.

1. INTRODUCTION

M33 is a nearby galaxy of Sc type with a suitable inclination between galactic disk and the celestial plane, to study the stellar associaton which form star compexes. In this galaxy 143 associations with a mean diameter 200 pc were isolated by Humphreys and Sandage (1980). Efremov (1995) considers the star complex as a slellar group of young stars formed together by fragmentation of a dense molecular cloud, which are initially structured owing to large scale gravitational instability. They consist of objects with total mases about $10^7 M_{\odot}$. The aim of the present paper is to propose a method for indentification of star complexes in M33, using observational data of HII regions which are excited by massive OB stars embedded in them. On the other side, WR stars are objects which are physically associated with HII regions. We suppose that OB, WR stars, and HII regions indicate the star complexes as regions of massive star formation. There was evidence of large scale groupings of RSGs and Cepheids not within OB associations but beyond them (Efremov, 1995). So the possible stellar populations of star complexes may be also red supergiants (RSGs) and Cepheids. Red supergiants (RSGs) in M33 were selected by Vassilev et al. (2002), observed in JHK passbands and published in 2MASS survey. The sample of RSGs was defined by the limit $K > 13$ mag. This criterion removes the brighter stars beacause they should belong to Milky Way background. The sample of RSGs contains 1650 stars selected by criterion $J - K > 1.1$ which are suitable for the purpose of the present

Table 1: General information on M33 galaxy

Center's coordinates (nucleus):
$R.A.(2000) = 23.462042°$
$Dec.(2000) = +30.6601944°$
Distance modulus: m-M = 24.52

paper. Observational data for coordinates of 905 Cepheids are from Mochejska et al. (2001). However the data of latter paper do not cover the total area of M33 since the observational data of Sandage (1983) are also used in the present study. The gas component and the stellar distribution of M33 are well studied. Catalogues of HII regions have been published and by Courtes et al. (1987) and in Ivanov et al. (1993) (hereafter IFM) a catalogue of 2112 OB stars was listed. A list of the Wolf-Rayet stars have been presented by Massey and Conti (1983) and Massey et al. (1987; 1995). Nowadays the number of WR stars in M33 amounts 168.

2. CORRELATION TECHNIQUE

In the present study we combine the surveys of OB stars, HII regions, and WR stars in order to compare the distributions of OB stars, HII regions, WR stars, RSGs and Cepheids in M33. On the other way we also use a correlation technique for comparison between the stellar populations in M33 proposed by Ivanov (1998). Let N1 stars of one population in M33 have surface density δ_1 while another population of N2 stars has a surface density δ_2. The two-dimensional angular distance between the stars of the k-th stellar couple is d_k as defined in the Appendix of Ivanov (1998). Supposing a random distribution of the stellar populations in the galaxy, the distance between the two stars of the k-th couple is exactly d_k, we define the probability (see Ivanov, 1998):

$$P_{12}(k) = [(1 - \exp(-\pi d_k^2 \delta_1)][(1 - \exp(-\pi d_k^2 \delta_2)], \quad (1)$$

a measure for associated stars. The real associated stars of two different populations form couples with $d_k \to 0$ and consequently $P_{12}(k) \to 0$. The couples of foreground stars have great neighbour distances d_k and $P_{12}(k) \to 1$. The quantity $P_{12}(k)$ gives the probability to find one star of population "1" and another star of population "2" within a radius equal to d_k in the case when both populations are randomly distributed. The probabilities $P_{12}(k) \approx 0$ can be used as a good characteristics for associated couples. The present criterion defines the upper and the lower limit of probability P_{min} and P_{max} which can be obtained from observational data. If $P_{12}(k) < P_{min}$, a couple of associated stars is selected. The number of "foreground couples" N_{bgr} we define as ones for which $P_{12}(k) > P_{max}$. Further in this Section we obtain $P_{min} = 0.05$ and $P_{max} = 0.95$. These quantities are generally accepted in the statistics. In case when the associated stars are selected by criterion $P_{12}(k) < 0.05$ the number of associated couples is indicated with N5. A stronger criterion for selecting the associated stars is imposed if the individual probabilities of the couples $P_{12}(k) < 0.01$ and the foreground couples are selected through $P_{12}(k) > 0.99$. Then

Table 2: Correlation parameters between stellar populations in M33. Column 1 gives the name of correlation parameters; column 2 between OB stars and HII regions; column 3 between HII regions WR stars; column 4 between RSGs and WR stars; column 5 between OB stars and WR stars; column 6 between Cepheids and WR stars; column 7 between RSGs and HII regions; column 8 between RSGs and Cepheids.

Correlation parameter	OB-HII	HII-WR	RSG - WR	WR - OB	Ceph- WR	RSG-HII	RSG-Ceph
R5	0.52	0.76	0.70	0.89	0.25	0.09	0.97
R1	0.38	0.54	0.43	0.74	0.14	0.04	0.83
RN5	2.2	7.4	16.3	91	0.74	0.12	135
RN1	1.7	5.5	10	26	0.40	0.06	114
Number of couples	748	140	140	140	140	748	147

the number of associated couples is denoted with N1. A simple way to evaluate the correlation between two populations is to obtain the percentage of associated objects

$$\mathrm{R5} = \mathrm{N5/N}; \qquad \mathrm{R1} = \mathrm{N1/N}. \tag{2}$$

The ratios R1 and R5 are very suitable measures for correlation between the stellar populations. If all stars between two populations are associated, then R5 = 1 or R1 = 1. In the opposite case there are no associated stars between the populations (R5 = 0 or R1 = 0). The ratios given by Eq. 2 are analogous to the conventional coefficient of correlation in the statistics. Another way to evaluate the correlation between two stellar populations is to calculate the ratio of the number of the associated objects to the expected number from random distribution:

$$\mathrm{RN5} = \mathrm{N5/N_{bgr}}; \qquad \mathrm{RN1} = \mathrm{N1/N_{bgr}}. \tag{3}$$

3. CORRELATION BETWEEN STELLAR POPULATIONS IN M33

The data presented in Table 2 can be interpreted as an evidence of tight correlations between WR stars, OB stars and HII regions. About 70 % of the OB stars are associated with the center of HII regions (however, RSGs and cepheids do not show any correlaton with HII regions. The lack of latter corrrelations is expected. Similar is the situation with a comparison between classical stellar asoociation of Humphreys and Sandage (1980) and RSGs, and cepheids. This fact was outlined in the paper ot IFM. About 60 % of associations are without RSGs. The correlation between HII regions, OB stars and WR stars is expected since the source for ionization of the gas in a HII regions are stars earlier than B2, which evolve to RSG. Hence a part of RSGs selected by present study should have a poor correlation with HII regions. We suppose that a fraction of the OB stars which excites the HII regions and belongs to stellar associations is not detected up to now because of the large extinction in the optical part of the spectrum (UBV photometry) of regions for stellar associations, and partly to the extinction in the spectral line H_α for HII regions. There is no correlation between RSGs and HII regions and between cepheids and WR stars. However taking into account that in Vassilev el al. (2002) were selected RSGs with masses 12 - 20

$M_\odot$, we found a strong correlation between RSGs and long period cepheids wih log $P > 1.0$. There is a good correlation beween short period ceipheids and RSGs. This fact shows that the star complex consists of sellar populations with a wide range of stellar masses. It is well known that long period cepheids have masses in the range of RSGs, selected by Vassilev et al. (2002). The correlations between stellar populations in M33 are given in Table 2. The evaluated correlation between RSGs and WR stars is also expected. The ratios R5 ≈ 0.7 given by Eq. 2 for WR stars and RN5 ≈ 16 given by Eq. 3 are high. These results may possibly indicate the existence of a tight correlation between RSGs and cepheids). This can be expected because the progenitors of WR stars are RSGs which have masses M $\geq 20 M_\odot$. On the other hand, the massive RSGs as well as WR stars must originate from nearby sites of star formation. If a star compex is a huge group of clusters, OB associations, HII regions and high luminosity stars, as accepted by Efremov (1995), we have to search the star complexes in the regions of physically associated objects with high surface density comparing to surrouding objects.

4. STAR COMPLEXES IN M33

The clustering method for the identification the stellar groups is described in the paper of Ivanov (1996). The criterion proposes that the objects will be assigned to the one and the same group if they have statistically peak of surface density above the mean level of the neighber objects. In other words the surface density is the main property that can isolate the star complex from the surrounding objects. The data of Table 2 indicate that there are a real physical association between the OB star objects, HII regions and WR stars since we indentify the star complexes in this section as regions of physicaly associated objects with a peak density of 5 times above the surounding density of these objects. When the site of the density peak was defined, we take into account the surface density of additional objects as RSGs and Cepheids in the boundaries of star complexes. The Cepheids and RSGs do not show a considerable association to stellar groups in M33. Moreover, RSGs do not correlate with the main counterpart of star complexes of OB stars and HII regions. For this reason we do not expect many RSGs and Cepheids to belong to the same star complexes. However we found a lot of Cepheids and RSGs in some star complexes while they are in deficite in other ones. We suppose that the presence of these objects in some star complexes gives evidence for the connection between the RSGs and Cepheids through the stellar evolution prosses in parent molecular cloud.

Table 3: Star complexes in M33. Column 1 gives a running number of star complex according to the increasing right ascensions; columns 2 and 3 give the right ascensions and declinations for equoinox 2000.0; columns 4, 6, 8, 10 and 12 give the number of populations within the star complex; columns 5, 7, 9, 11 and 13 give the density of stars within the star complex compared to background stars. The number of cepheids in column 12 denoted with asterisk * is based on the data of Sandage (1983).

1	2	3	4	5	6	7	8	9	10	11	12	13
No	R.A.(2000)	Dec.(2000)	OB_N	OB_F	HII_N	HII_F	WR_N	WR_F	RSG_N	RSG_F	$Ceph_N$	$Ceph_F$
1	23.4297	30.4200	94	5.6	65	6.7	4	5.6	9	4.1	14 *	6.6
2	23.4300	30.3600	129	6.1	51	6.5	4	5.6	32	7.4	9 *	13.0
3	23.4303	30.6450	469	6.8	126	5.6	23	7.4	47	4.6	70	5.5
4	23.4332	30.5850	438	6.8	116	6.6	40	6.8	50	6.5	89	4.7
5	23.4332	30.6400	492	7.1	129	6.3	22	8.5	52	4.3	73	5.7
6	23.4340	30.3995	104	7.5	70	7.2	3	9.9	12	7.0	12 *	5.2
7	23.4370	30.5700	461	8.1	126	6.6	47	7.7	67	4.3	96	4.2
8	23.4375	30.3817	128	8.7	61	8.8	4	9.4	22	6.9	18 *	9.0
9	23.4376	30.4457	97	8.5	54	9.2	6	10.5	6	4.5	4	2.6
10	23.4380	30.6470	500	9.3	138	6.9	24	9.8	51	5.0	70	5.9
11	23.4387	30.5020	206	7.0	71	6.9	19	6.1	21	3.8	70	5.1
12	23.4389	30.7450	308	6.3	85	7.8	20	11.1	40	7.5	84	6.0
13	23.4391	30.8870	140	10.4	60	6.8	0	0.0	16	6.9	11*	6.7
14	23.4402	30.7950	267	6.7	93	7.8	8	6.8	14	4.4	55	6.3
15	23.4409	30.4400	97	7.6	55	9.4	5	7.7	5	4.6	9 *	11.2
16	23.4422	30.6467	5	10.4	138	7.7	25	9.9	52	5.2	73	6.0
17	23.4422	30.6800	478	6.6	133	7.3	38	9.5	54	5.3	47	5.7
18	23.4428	30.5250	315	8.3	105	9.4	30	8.3	40	6.3	104	4.6
19	23.4429	30.5560	451	7.8	124	7.5	48	7.0	57	4.4	112	4.3
20	23.4438	30.8020	241	6.9	96	8.1	7	9.7	13	4.6	54	6.2
21	23.4447	30.6400	513	9.8	134	8.2	23	10.7	54	4.9	77	6.0
22	23.4453	30.8667	142	9.6	60	8.8	0	0.0	19	8.4	12 *	9.1
23	23.4453	30.6050	461	6.2	125	7.4	34	6.1	45	6.7	78	4.8
24	23.4455	30.7150	309	6.9	112	6.6	38	6.2	45	6.2	75	6.1
25	23.4457	30.3775	130	9.0	57	9.1	4	8.1	24	6.2	11 *	9.1
26	23.4458	30.3450	110	8.6	42	6.0	3	20.2	29	5.5	8 *	25.1
27	23.4459	30.7560	339	8.4	93	8.0	21	11.9	36	6.5	99	5.2
28	23.4459	30.6895	389	6.8	124	7.2	34	12.1	55	5.0	56	5.0
28a	23.4465	30.7395	307	7.1	88	8.3	22	9.4	39	7.6	90	6.9
29	23.4468	30.5960	438	7.5	128	6.9	37	7.9	46	6.8	82	4.5
30	23.4480	30.8767	142	12.6	63	8.1	0	0.0	18	8.1	13 *	6.8
31	23.4483	30.6415	523	10.2	133	8.6	23	11.0	58	4.9	75	6.4
32	23.4499	30.7457	322	7.8	92	8.3	21	12.4	38	7.4	92	6.6
33	23.4502	30.5540	441	7.8	127	7.3	47	7.1	53	4.3	99	4.9
34	23.4511	30.6580	522	10.6	146	8.1	36	6.4	56	6.9	70	6.0
35	23.4511	30.7750	321	10.3	95	7.3	19	6.8	32	4.7	97	5.2
36	23.4512	30.5986	443	6.9	131	6.8	38	7.0	50	5.7	76	4.9
37	23.4535	30.7780	320	9.9	98	7.1	19	5.6	34	4.4	93	5.5
38	23.4535	30.6560	515	10.4	143	8.1	36	5.8	54	7.4	77	5.9
38a	23.4539	30.7795	318	9.6	99	7.0	19	5.6	34	4.4	87	5.8
39	23.4555	30.8875	143	12.1	61	7.8	0	0.0	15	6.6	11 *	7.8
40	23.4558	30.6300	532	7.0	135	7.3	25	6.6	51	4.5	91	5.2
41a	23.4559	30.5595	453	7.2	128	6.5	48	7.9	58	4.1	103	4.6

Table 3 (continued)

1	2	3	4	5	6	7	8	9	10	11	12	13
No	R.A.(2000)	Dec.(2000)	OB_N	OB_F	HII_N	HII_F	WR_N	WR_F	RSG_N	RSG_F	$Ceph_N$	$Ceph_F$
41	23.4579	30.7615	338	9.8	97	6.8	22	10.0	41	5.3	109	5.5
42	23.4600	30.9449	59	10.3	37	8.9	2	0.0	8	8.9	8 *	10.7
43	23.4604	30.5965	423	6.1	123	6.0	36	6.3	52	4.9	71	5.4
44	23.4607	30.6802	449	6.2	130	6.3	37	6.9	59	6.3	73	4.4
45	23.4607	31.0095	25	14.4	20	9.2	0	0.0	4	5.1	21*	6..4
46	23.4613	30.7775	317	8.8	94	6.2	18	5.3	36	5.0	99	5.6
47	23.4678	30.6875	360	5.4	110	5.4	30	6.3	58	5.4	68	4.2

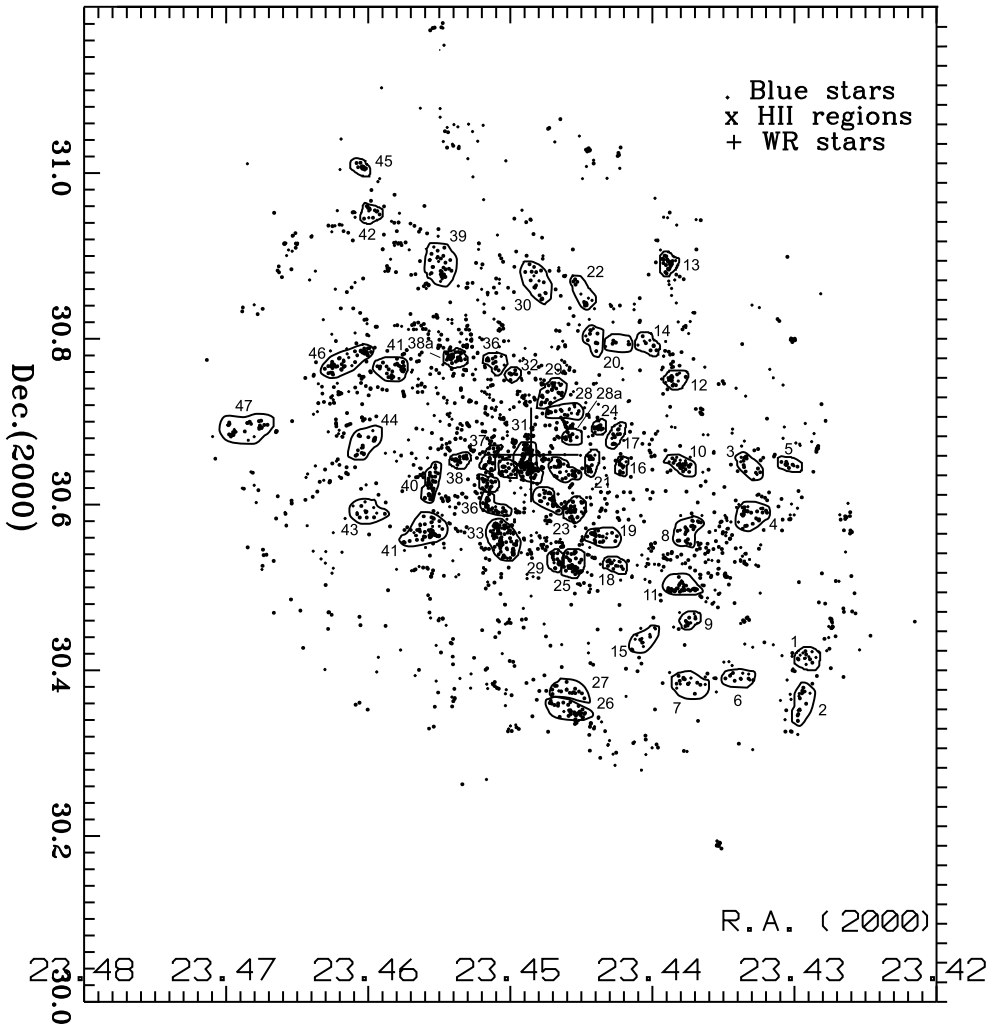

Figure 1: Star comlexes in M33.

5. DISCUSSION

The boundaries of star complexes using the peaks of surface density in OB, WR stars, and HII regions ditribution are defined in Fig 1. The coordinates of the center of complexes and surface densiy of the objects within star complex are given in Table 3. The complexes with numbers: 21, 23, 28, 29, 31, 33, 34, 36, 38, 40, 41a, 43 are located around the center of M33 (outlined by a large plus sign). They consist of lot of OB stars and bright HII objects. There is observational evidence that bright HII regions exibit a strong concentration of OB stars toward their centers. The coincidence of OB stars and HII regions in the same star compex is a good indicator for age estimation of the complex. We suppose that these star complexes indicate the extended central region of M33 with the youngest objects of the galaxy. At the same time these complexes have many WR stars. The pesence of WR stars in the central part of M33 indicate their star complexes as regions of massive star formation. On the other hand the star complexes with the numbers 4, 5, 8, 18, 25, 29, 33, 37, 41, 46, and 47 outline well the two main spiral arms. Their stellar population is different from that of star complexes in the central region of the galaxy M33. There is a good correlation between WR stars and RSGs in them. This fact is discussed by Georgiev and Ivanov (1997) who studied the ditribution of RSGs of IFM and WR stars as a function of galactocentric distance in M33. They suggested, by comparing the two distributions, that the RSGs with the masses higher than 30 $M_{\odot}$ would evolve to to WR stars, whereas the less massive should spend some part of their lives as RSGs. If our sample of RSGs have masses below this limit, in the range of $12-20M_{\odot}$, we expect to find WR stars and their progenitors RSGs at the same sites in the galaxy. The tight correlation between RSG and WR stars in Table 2 confirms their sugestion. This correlation speaks about the disposition of the two populations on the same or nearby sites in the galaxy while the stars disposed on remote regions in the galaxy have a negligible influence on our correlation parameters. The our sample of RSGs confines all regions of the galaxy. Then in the metal rich regions of star complexes, some RSGs would evolve to WR stars and may disapear. But in a less metal rich regions the progenitors may be in the stage of RSGs. So, the correlation between WR stars and RSGs occures in the region of chemical abundance as spiral arm regions. This fact explains because RSGs may exist or lack in some star complexes in Fig. 1. We can conclude from the stellar populations of star complexes in Table 3 that predictions of Maeder et al. (1980) for the influence of metalicity over the star's lifetime are confirmed by observations. The chemical composition in star complexes of M33 is better defined than in other galaxies. However, it should be taken into account the local imhomogenities in the abundance of heavy elements, which may explain the variation of the number of WR stars and RSGs from various star complexes. We combine the distributions of WR stars and RSGs in star complexes. Therefore, if some class of RSGs are protogenitors of WR stars we would have to compare the distribution of WR stars with diffferent samples of RSGs. So, the distribution of of WR stars should be compared with RSGs with different masses. Then we can obtain the sample of RSGs, which are probable progenitors of WR stars. Since, the distribution of WR stars is fixed we have a criterion to evaluate the masses of RSGs

Table 4: Regions of star complexes in M33. Column 1 gives the name of the region; column 2 the numbers of star complexes within the region; columns 3 the stellar population of the region.

Region No	Star complex No	Remark
center	21; 23; 28; 29; 31; 33; 34; 36; 38; 40; 41a; 43	OB + HII regions+WR
S1	4; 5; 8; 18; 25; 29; 33	OB +WR + RSG + Ceph
N1	16; 17;24; 27; 29; 32 36; 37 ; 41; 46; 47	OB + WR + RSG+ Ceph
North	13; 22; 30; 32; 42; 45	Without WR
South	1; 2; 6; 15; 25; 26	Without WR

in spiral arm complexes. The value of magnitude at which the distribution of the classes of the protogenitors and descendants coincide using data of Table 3, will show the mass of RSGs which evolve to WR stars. Then, taking into account data of Table 3 we conclude that RSGs in M33 with masses $15 - 20 M_{\odot}$ evolve to WR stars.

Regions of star complexes may be considered as group of star complexes with violent star formation region.

Acknowledgements

This project was partially supported by grant of the Bulgarian National Science Foundation.

References

Courtes, G., Petet, H., Sivan, J-P., Dodonov, S., and Petit, M.: 1987, *Astron. Astrophys.*, **174**, 28.

Efremov, Yu.N.: 1995, *Astron. J.*, **110**, 2757.

Georgiev, L. and Ivanov, G.R.: 1997, *Revista Mexicana de Astronomia y Astrofisica*, **33**, 117.

Humphreys, R.M. and Sandage, A.: 1980, *Astrophys. J. Suppl.*, **44**, 319.

Ivanov, G.R.: 1996, *Astron. Astrophys.*, **305**, 708.

Ivanov, G.R.: 1998, *Astron. Astrophys*, **337**, 39.

Ivanov, G., Freedman, W. and Madore, F.: 1993, *Astrophys. J. Suppl.*, **89**, 85, (IFM).

Ivanov, G.R., Krastev,K.: 2000, Second Serbian-Bulgarian Astronomical Meeting, June 23-26, 2000, Zaječar, eds. M.S. Dimitrijević, L.Č. Popović and M. Tsvetkov, *Publ. Astron. Obs. Belgrade*, **67**, 81.

Lejeune, T., Cuisinier, F. and Buser, R.A.: 1997, *Astrophys. Space. Sci.*, **125**, 229.

Maeder, A., Lequeux, J. and Azzopardi, M.: 1980, *Astron. Astrophys.*, **490**, L17.

Massey, P., Armandroff, T.E., Pyke, R., Patel, K. and Wilson, C.D.: 1995, *Astron. J.*, **110**, 2715.

Massey, P. and Conti, P.S.: 1983, *Astrophys. J.*, **273**, 576.

Massey, P., Conti, P.S., Moffat, A.F.J. and Shara, M.M.: 1987, *Astron. Soc. Pacific Conf. Series*, **99**, 816.

Mochejska, B.J., Kaluzny, J., Stanek, K.Z., Sasselov, D.D., Szentgyorgyi, A.H.: 2001, *Astron. J.*, **121**, 2032.

Sandage, A.: 1983, *Astron. J.*, **88**, 1108.

Vassilev, O., Vassileva, Ivanov, G.R.: 2002, Third Bulgarian-Serbian Astronomical Meting, May 13-15, Gjolachitsa, eds. G. Ivanov, M.S. Dimitrijević and P. Jovanović, *Publ. Astron. Obs. Belgrade*, **73**, 257.

Proc. IV Serbian-Bulgarian Astronomical Conference,
Belgrade 21–24 April 2004,
eds. M. S. Dimitrijević, V. Golev, L. Č. Popović, M. Tsvetkov,
Publ. Astron. Soc. "Rudjer Bošković" No 5, 2005, 83 - 93

Invited lecture

HIGH ANGULAR RESOLUTION IN MODERN ASTRONOMY: NEW INSIGHTS INTO THE STELLAR PHYSICS

S. JANKOV[1,2], R. PETROV[1], F. VAKILI[1], S. ROBBE-DUBOIS[1] and A. DOMICIANO[1,3]

[1] *Université Nice Sophia-Antipolis, UMR 6525, F-06103 Nice Cedex 2, France*
E–mail Romain.Petrov@unice.fr
E–mail Farrokh.Vakili@unice.fr
E–mail Sylvie.Robbe-Dubois@unice.fr

[2] *Astronomical Observatory, Volgina 7, 11160 Belgrade 74, Serbia*
E–mail sjankov@aob.bg.ac.yu

[3] *Max-Planck-Institut für Radioastronomie,*
Auf dem Hügel 69, 53121 Bonn, Germany
E–mail adomicia@mpifr-bonn.mpg.de

Abstract. The new generation of ground-based instruments for high angular resolution from optical interferometry provides a qualitatively new information for improving our understanding of the physics, structure and evolution of stars through the comparison of observational results with the predictions of theoretical models of stellar interiors and atmospheres. Traditionally, the optical interferometry has been considered as a tool for determination of the fundamental properties of stars, namely their effective temperatures, radii, luminosities and masses, by the combination of angular diameters, with complementary photometric, spectrophotometric and spectroscopic measurements, made with conventional telescopes. However, the influence of stellar interferometry extends beyond classical regimes of stellar diameters and binary orbits. In this contribution we review a selection of outstanding problems in stellar physics showing the potential of new methods which combine the classical techniques (as photometry and spectroscopy) and long baseline interferometry, providing informations that cannot be obtained otherwise with each of these techniques taken at once.

1. INTRODUCTION

An optical long-baseline interferometer is a device that allows astronomers to achieve a higher angular resolution than is possible with conventional telescopes. It is composed of an array of at least two telescopes, which sample the wavefronts of light emitted by a source at separate locations and redirect starlight to a central location in order to recombine the sampled wavefronts. The contrast of interference fringes, or visibility, varies according to the characteristics of the light source (for example, the size of a star or the separation between two stars in a binary system) and according to the length and orientation of the interferometer's baseline, the line connecting the two mirrors. It is possible to take measurements from many different baselines, most

easily by waiting while Earth rotates. In addition, most of the new interferometers have more than two mirrors in the array and can move the mirrors along tracks.

Although the first measurement of a stellar angular diameter was made of the supergiant star α Orionis with Michelson's stellar interferometer in 1920 (Michelson and Pease, 1921), the optical interferometry was slowly evolving from a difficult laboratory experiment to a mainstream observational technique. The real difficulty is to combine the beams in phase with each other after they have traversed exactly the same optical path from the source through the atmosphere, each telescope and down to the beam recombination point. This has to be done to an accuracy of a few tenths of the wavelength, which in the case of visible light is not an obvious task particularly because of atmospheric turbulence which makes the apparent position of a star on the sky jitter irregularly. This jitter often causes the beams in different arms of the interferometer to overlap imperfectly or not at all at any given moment. For this reasons, the optical interferometry requires extreme mechanical stability, sensitive detectors with good time resolution, and ideally an adaptive optical system to reduce the effects of atmospheric turbulence. The development of the required technology allowed to built modern interferometers which are currently operating:

- CHARA Center for High Angular Resolution Astronomy
  Georgia State University Mt Wilson, CA, USA
- COAST Cambridge Optical Aperture Synthesis Telescope
  Cambridge University Cambridge, England
- GI2T Grand Interféromètre à 2 Télescopes
  Observatoire Côte D'Azur Plateau de Calern, France
- IOTA Infrared Optical Telescope Array
  Smithsonian Astrophysical Observatory, Mt Hopkins, AZ, USA University of Massachusetts (Amherst)
- ISI Infrared Spatial Interferometer
  University of California at Berkeley Mt Wilson, CA, USA
- KI Keck Interferometer
  NASA JPL Mauna Kea, HI, USA
- MIRA I Mitake Infrared Array
  National Astronomical Observatory, Japan Mitaka Campus, Tokyo, Japan
- NPOI Navy Prototype Optical Interferometer
  Naval Research Laboratory, Flagstaff, AZ, USA US Naval Observatory
- PTI Palomar Testbed Interferometer
  NASA JPL Mt Palomar, CA, USA
- SUSI Sydney University Stellar Interferometer
  Sydney University Narrabri, Australia

- VLTI VLT Interferometer
  European Southern Observatory Paranal, Chile

2. APPLICATIONS OF STELLAR INTERFEROMETRY

2.1. REVIEW OF SOME OUTSTANDING PROBLEMS

The classical primary goal of interferometry has been the determination of fundamental astrophysical parameters characterizing stars through angular diameter measurements. With the advent of accurate parallaxes from the Hipparcos astrometry satellite *linear radii* can be determined precisely as well as *emergent fluxes* and *effective temperatures* (in conjunction with photometry). Additionally, interferometry can provide a very precise determination of stellar *masses* from binary star orbital motion studies through the application of Kepler's Third Law.

However, stellar interferometry is not limited only to these classical applications. For example, the exact behavior of photospheric limb darkening leads to better insight into the *stellar atmospheres theory* through wavelength dependence of the uniform disk diameter (e.g. Quirrenbach et al., 1996; Wittkowski et al., 2001). Other applications, as well as interferometric techniques, have been reviewed by Quirrenbach (2001), and here we give a non-exhaustive list updated with some more recent developments in the field.

Red giants and *Supergiants* have so far been one of the prime targets for interferometric observations because of their large sizes and brightness. Surface features have been detected on the surfaces of the apparently largest supergiants α Orionis, α Scorpii and α Herculi (e.g. Buscher et al., 1990; Tuthill et al., 1997; Young et al., 2000). For the same reason Optical interferometry has already been successfully used to study *Be star circumstellar environments and winds* (Thom et al., 1986; Quirrenbach et al., 1993; Vakili et al., 1994; Stee et al., 1995).

Spatial resolution in the far infrared is the most promising approach in looking for the complex structures that are expected to be associated with *star forming regions*. Structures associated with *Pre main sequence objects* are of great interest, and require imaging at infrared wavelengths. The study of *Young stellar objects* (YSOs) is one of the exciting topics that can be undertaken now. Different aspects can be tackled by interferometry: circumstellar disks, multiplicity, jets.

The process of *mass-loss* is essential for our understanding of late stages of stellar evolution. Optical and infrared interferometry can provide important observational constraints to the evolution of late-type stars along the *Asymptotic Giant Branch* (AGB) and variability in *Mira* and other variable stars as *P Cygni, R Corona Borealis, Flare stars, Herbig-Haro Objects, Cataclysmic variables, RR Lyrae, Ap and Be stars etc.*. Particularly the *Calibration of Cepheid Period-Luminosity relation* (with progressively increasing accuracy in the mean angular diameter) will improve our knowledge on *Distance scale in the Universe* (e.g. Kervella et al., 2004).

The technique of Interferometric-Doppler Imaging, using the relative phase of the interferometric signal along a spectral line with respect to the continuum (Petrov,

1988), has been developed by Jankov et al. (2001) who treated explicitly (see also Jankov et al., 2002) the case of *non-radial stellar pulsations*, for which the cancellation of opposite sign temperature or velocity fields introduces difficulties, and showed that interferometric constraint introduces the crucial improvement. The effects of *differential rotation* and *gravity darkening* on interferometric observables have been studied by Domiciano de Souza et al. (2004) and Domiciano de Souza (2002) respectively.

2.2. RAPID ROTATION AND STELLAR PHYSICS

In order to perform the following scientific goals:

- Detailed mapping of the star in order to deduce the geometrical deformation due to rapid rotation,
- Gravity darkening
- Accurate determination of equatorial diameter, critical velocity and effective temperature,

Domiciano de Souza et al. (2003) carried out dedicated observations of α Eridani (Achernar) from 11 September to 21 December 2002, with quasi-uniform time coverage, on the VLT Interferometer (VLTI) equipped with the VINCI beam combiner (Kervella et al., 2003). This instrument recombines the light from two telescopes in the astronomical K band centered at 2.2 μm. An array of 35cm siderostats with two interferometric baselines (66m and 140m) was used. The baseline orientations are almost perpendicular to each other giving an excellent configuration for the detection of stellar asymmetries. Moreover, Earth rotation has produced an efficient synthesis effect. The final product of data processing were 60 squared visibility measurements of the object for each baseline projected on the sky, which are directly related to the Fourier transform of the brightness distribution of the object via the Zernike-Van Cittert theorem.

Achernar's pronounced apparent asymmetry (Fig. 1) together with the fact that it is a Be star, raised the question of whether they observed the stellar photosphere with or without an additional contribution from a Circum-Stellar Envelope (CSE). Arguing that the observed asymmetry of Achernar reflects its true photospheric distortion with a negligible CSE contribution, they concluded that the usual Roche approximation does not apply to Achernar, where deviations from gravitational potential and differential rotation must be closely regarded with respect to the internal momentum distribution. One possible scenario is that of the shellular rotation law (Zahn, 1992), in which the angular velocity increases toward the stellar center, implies the oblateness larger than that of a uniformly rotating star (Maeder, 1999). In this context their result on Achernar's surface distortion should also impact other internal mechanisms like meridional circulation, turbulence, transport and diffusion of the chemical elements and angular momentum, increase of mass loss with rotation as well as anisotropies in the mass ejection and wind density from rotating stars.

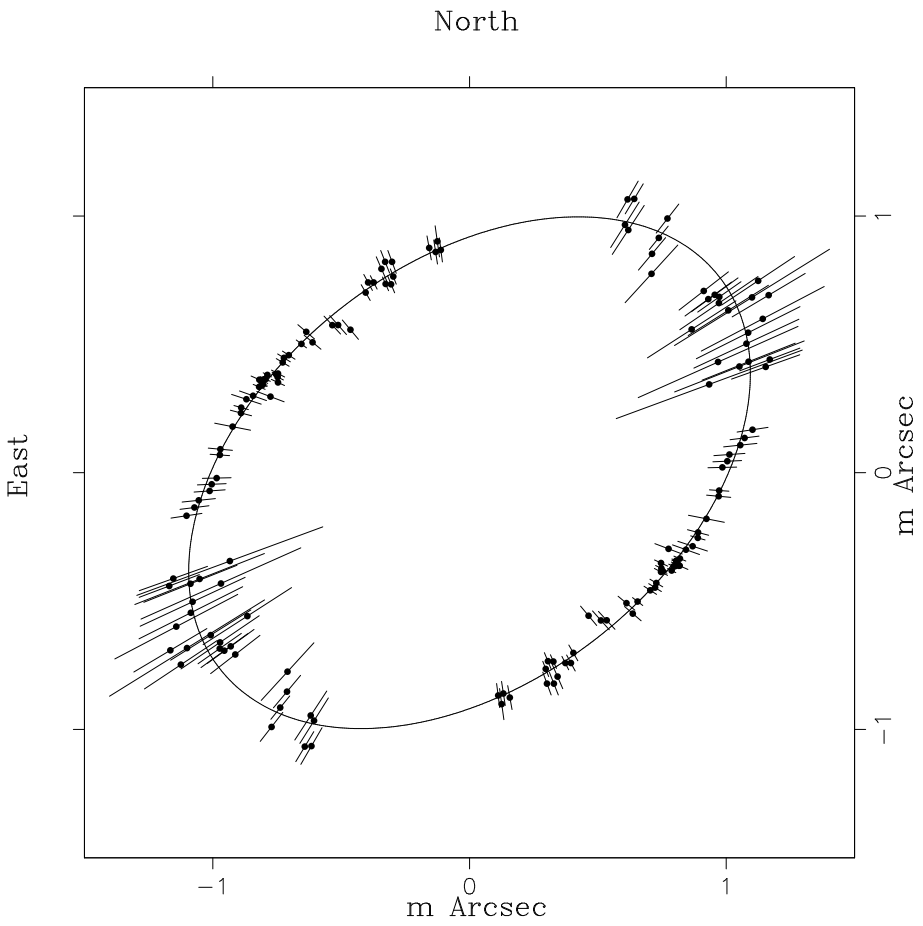

Figure 1: VLTI/VINCI measurements revealing the spectacular oblateness of Achernar.

The highly distorted photosphere of Achernar poses the question of Be stars rotation rate. The formation of out-flowing discs from Be stars remains their central puzzle, where rapid rotation is the crucial piece. Under the Roche approximation the observed oblateness indicates that Achernar should rotate close to its critical velocity since the model solution which implies 96% of the critical velocity is more consistent with the data. Original vision of a critically rotating Roche star, ejecting material from its equator, has been discarded in the past by observing that Be stars rotate at most at 70% to 80% of their critical velocity. However, this statistically observed limit may be biased by the fact that close to or beyond such velocities the diagnosis of Doppler-broadened spectral lines fails to determine the rotation value due to gravity darkening. We believe that only direct measures of Be star photospheres by interferometry can overcome the challenge to prove whether these objects rotate close,

to a few percent, of their critical velocity or not. This will have a profound impact on the dynamical models of Be stars disc formation from rapid rotation combined to mechanisms like pulsation, radiation pressure of photospheric hot spots or expelled plasma by magnetic flares.

2.3. STELLAR SURFACE INHOMOGENEITIES

The study of starspots using classical interferometric techniques requires a very high spatial resolution which, even for RS CVn stars, should be better than 0.2 mas. In parallel to the development of interferometric techniques, the method of Doppler Imaging (Rice, 1996 and references therein) allowed access to the spatial structure of non-resolved stars through observation and interpretation of temporal spectroscopic variability along the stellar rotational phase. Similarly to classical spectroscopy, the differential interferometry (Beckers, 1982) makes it possible to measure the shift of the stellar photometric barycenter (photocenter) of an unresolved star as a function of wavelength. The photocenter is the angular vectorial function and it provides the first order moment of the spatial brightness distribution, in addition to the zero order moment spectroscopic information, allowing better spatial resolution of stellar atmospheres when compared to the classical Doppler Imaging (Jankov et al., 2001).

Doppler Imaging has also been applied to magnetic Ap (CP2) stars, because many of these stars show strong changes of their spectral line profiles due to surface abundance inhomogeneities. The most accepted mechanism in explaining the chemical peculiarities of these stars involves the radiatively driven diffusion of chemical elements in the atmosphere which is influenced by the orientation and strength of a magnetic field, yielding a separation of elements in different layers at the surface of magnetic stars. Observationally, this theory can be verified by comparing the geometry and strength of the magnetic field derived from polarization observations with the structure of "abundance spots" on the stellar surface. Thus, the Doppler Imaging of chemically peculiar stars is an excellent tool for testing theories of elemental diffusion and the origin of magnetic fields in stars with radiative envelopes since the question of the prevalence of magnetic fields among such stars is still open.

However, due to the intrinsic limitations of the Doppler Imaging technique (e.g. Rice et al., 1989) and particularly what concerns the reconstruction of features in the hemisphere in which the rotational pole is hidden, the reliable Doppler maps, which allow to draw physical conclusions, can be obtained only in the narrow range of stellar inclinations. For stars tilted at low inclinations only a small part of the southern hemisphere can be observed and even this small part cannot be reliably reconstructed since it is observed only at the stellar limb. When the inclination of a star approaches 90° the southern hemisphere becomes progressively more visible but for an equator-on star the Doppler Imaging solution is intrinsically non-unique and practically the artifacts due to mirroring effect prevents the mapping for stars with high inclinations.

In order to study this subject Jankov et al. (2003) conducted numerical experiments using an artificial star with a known surface structure. A test pattern for the surface of the star was constructed to reproduce the main pattern of surface maps of the distribution of Chromium (Cr) for ϵ UMa (Rice and Wehlau, 1990). The map of

the surface of the star shows a ring feature about an axis of symmetry where the axis is presumed to represent the magnetic axis of the star. The relative depletion of Chromium by about three orders of magnitude in a belt around the magnetic equator has been found. Fig. 2 displays the artificial star at four rotational phases. The stellar image corresponds to the surface abundance distribution of Chromium on a star with [Cr/H] = -4 and an underabundant ([Cr/H] = -7) ring along the magnetic equator tilted by 30° to the stellar rotation equator. In this example, the artificial star has a rotation axis tilted by $i = 60°$ to the line of sight and rotates with a projected equatorial velocity $V_e \sin i$ of 35 km s^{-1} . Using only the normalized flux spectra with the Gaussian noise $1/\sigma = 1000$ added, the input image (Fig. 3 left) was reconstructed (Fig. 3 right).

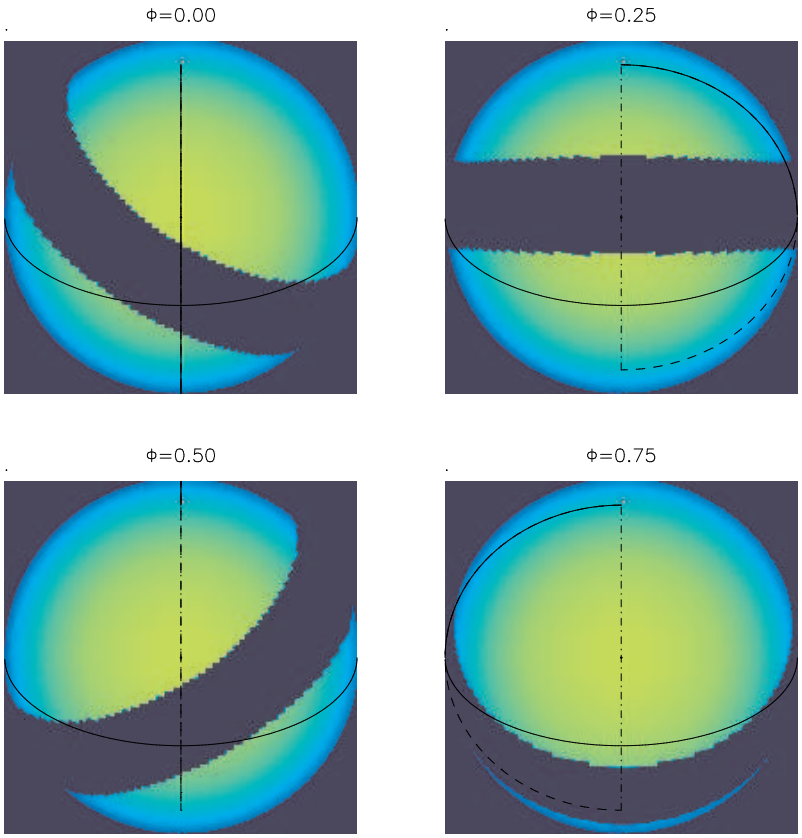

Figure 2: Spherical projections of the inhomogeneous stellar surface for a star tilted at i=60°, and Chromium abundance distribution, in the belt around the magnetic equator tilted by 30° to the stellar rotation equator. The abundance of Chromium in the belt is three order of magnitude less than the abundance in the surrounding regions as observed on the Ap star ϵ UMa (Rice and Wehlau, 1990).

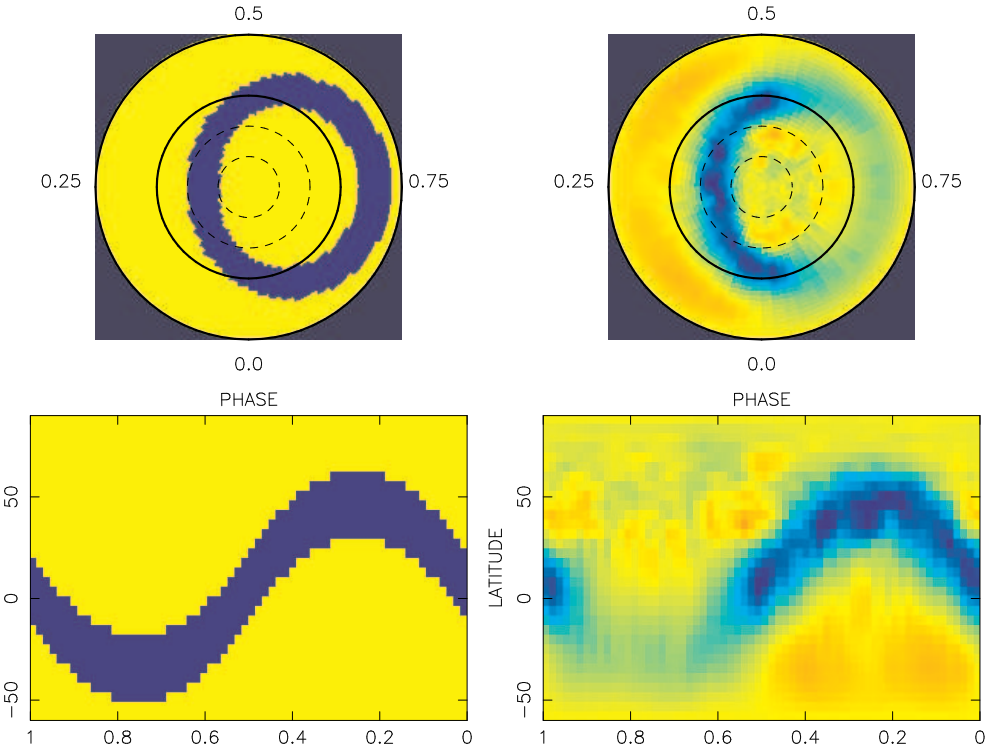

Figure 3: Pole-on (Top) and Mercator (Bottom) projections of the visible surface on a star tilted at $i = 60°$. Left: The input image of the surface temperature distribution as shown in Fig. 2. Right: Maximum Entropy reconstructions from normalized flux spectra alone (Doppler Imaging). Thirty spectra evenly spread throughout the rotational cycle were used as input, with a wavelength step corresponding to a spectral resolution of $\lambda/\Delta\lambda = 15\,000$, Gaussian noise and signal-to-noise ratio ($1/\sigma = 1000$).

This reconstruction shows the loss of contrast of features in the hemisphere bellow the stellar equator (which is the basic limitation of the Doppler Imaging technique). The reasons for this are clear: the contribution to the line profiles in such areas is significantly reduced due to foreshortening and limb darkening effects (see Fig. 2). Moreover, features are visible only briefly, so they contribute to the observed profiles for only a few rotational phases.

The degradation of restored maps is much less present in the reconstructions performed using the moments parallel to rotation in conjunction with normalized flux spectra (Fig. 4 left and right) where Gaussian noise and signal-to-noise ratios ($1/\sigma = 1000$) and ($1/\sigma = 330$) respectively were added.

The recovered maps should be compared to the original one (Fig. 3 left) as well as to the map obtained from flux spectra alone (Fig. 3 right). One can notice a significant improvement since the features in the hemisphere in which the rotational

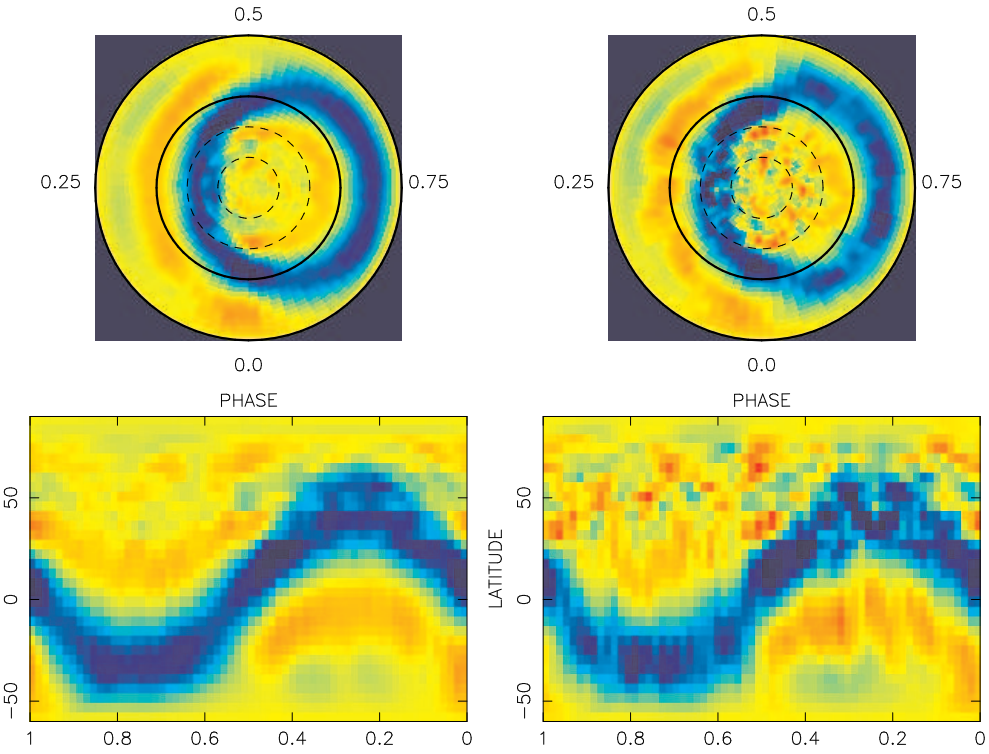

Figure 4: Pole-on (Top) and Mercator (Bottom) projections of reconstructed images from flux spectra and photocenter projection parallel to rotation. Left: Gaussian noise and signal-to-noise ratio ($1/\sigma = 1000$). Right: Signal-to-noise ratio ($1/\sigma = 330$).

pole is hidden are enhanced. When using the moments parallel to rotation, the corresponding stellar regions are reinforced by weighting with coordinate parallel to the stellar rotation axis (as can be seen in Fig. 2), and consequently reproduced in the reconstructed map.

Previous examples show clearly that the interferometric constraint introduces the crucial improvement, making the mapping of stellar surface chemical abundances much more reliable and informative than Doppler imaging alone. *Consequently, the interferometry provides a qualitatively new informations that cannot be extracted from classical spectroscopy alone.*

3. WHAT IS COMING IN THE NEAR FUTURE?

In the following years interferometers of ever increasing sophistication will be operational. Some will develop from current facilities, for example VLTI will introduce the moderate spectral resolution (up to $\lambda/\Delta\lambda = 15\,000$) with AMBER (Petrov et al., 2003) and phase-referenced imaging with PRIMA (Paresce et al., 2003). The future of optical interferometry can be foreseen to evolve in the direction of more ca-

pable arrays boasting significantly larger and more numerous telescope apertures and baselines. The CHARA and NPOI interferometers incorporated six telescopes spread over hundreds of meters, to allow imaging capabilities at milliarcsecond resolution. The VLTI and Keck Interferometer will be extended with auxiliary telescope arrays, allowing many new kinds of science to be pursued.

The Large Binocular Telescope and Interferometer (Mnt Graham, Arizona) is under construction and is in an advanced stage now. Its configuration will allow essentially complete sampling of all spatial frequencies in the image up to 22.8 meters using interferometric imaging between the two 8.4 m apertures. When combined with adaptive optics, the LBT interferometric mode will offer high signal-to-noise imaging on the faint objects, over a relatively wide field.

OHANA (Optical Hawaiian Array for Nanoradian Astronomy) project has carried out initial experiments to couple light from Mauna Kea telescopes into single mode fibers, the first step in a plan to link the existing giant telescopes with optical fiber and to create a powerful optical interferometer with a unique combination of sensitivity and angular resolution. The largest baseline of OHANA (Subaru-Gemini) has a length of 800 meters yielding resolutions of 0.25 and 0.5 milliarcseconds at 1 and 2 microns respectively, thus the sources as small as 30 microarcseconds will be partially resolved (characterized in size). For example, these are typical likely apparent dimensions of accretion disks in a variety of environments

MRO (Magdalena Ridge Observatory) project is shaping up and site (Magdalena mountains, New Mexico) work is expected to begin soon. The 2.4-meter-diameter single telescope will be completed first, followed by the interferometeric array composed of ten telescopes, each approximately 1.4 meters in diameter. The optical/infrared telescopes will be spaced by distances of up to 400 meters and, as a result of the large number of telescopes in the array, the interferometer will be able to make accurate images of complex astronomical objects in optical and infrared domains.

Concerning the near future of space interferometry we can expect, in the next 10 to 20 years, more progress in stellar physics to be possible from the ground. Darwin and TPF (Terrestrial Planet Finder) are respectively ESA and NASA projects dedicated to the search for extra-solar planets, but very probably they will also contribute to the stellar physics. The SIM (Space Interferometry Mission) is in advanced planning stages and is being designed to measure accurate positions of stars with microarcsecond resolution. It will be the first mission to attempt space interferometry, opening the new windows for astronomy. The emergence of future space interferometry facilities, which will benefit from the absence of atmospheric turbulence and much larger baselines, promise to revolutionize the impact of high resolution observations in many areas of astrophysics and particularly in stellar physics.

References

Beckers J.M.: 1982, *Optica Acta*, **29**, 361.

Buscher, D.F., Baldwin, J.E., Warner, P.J., Haniff, C.A.: 1990, *Mon. Not. R. Astron. Soc.*, **245**, 7.

Domiciano, A., Vakili, F., Jankov, S., Janot-Pacheco, E., Abe, L.: 2002, *Astron. Astrophys.*, **393**, 345.

Domiciano de Souza, A., Kervella, P., Jankov, S., Abe, L., Vakili, F., di Folco, E., Paresce, F.: 2003, *Astron. Astrophys.*, **407**, L47.
Domiciano de Souza, A., Zorec, J., Jankov, S., Vakili, F., Abe., L., Janot-Pacheco, E.: 2004, *Astron. Astrophys.*, **418**, 781.
Jankov, S., Vakili, F., Dominiciano de Souza, Jr., Janot-Pacheco, E.: 2001, *Astron. Astrophys.*, **377**, 721.
Jankov, S., Vakili, F., Domiciano de Souza Jr., A., Janot-Pacheco, E.: 2002, *Astronomical Society of Pacific Conference Series*, **259**, eds. C. Aerts, T.R. Bedding and J. Christensen-Dalsgaard, 172.
Jankov, S., Domiciano de Souza, A., Stehle, C., Vakili, F., Perraut-Rousselet, K., Chesneau, O.: 2003, Interferometry for Optical Astronomy II. Edited by Wesley A. Traub. *Proceedings of the SPIE*, **4838**, 587.
Kervella, P. et al.: 2003, Interferometry for Optical Astronomy II. Edited by Wesley A. Traub. *Proceedings of the SPIE*, **4838**, 858.
Kervella, P., Bersier, D., Mourard, D., Nardetto, N., Coudé du Foresto, V.: 2004, *Astron. Astrophys.*, **423**, 327.
Maeder, A.: 1999, *Astron. Astrophys.* **347**, 185.
Michelson, A.A. and Pease, F.G.: 1921 *Astrophys. J.*, **53**, 249.
Paresce, F., Delplancke, F., Derie, F., Glindemann, A., Richichi, A., Tarenghi, M.: 2003, Interferometry for Optical Astronomy II. Edited by Wesley A. Traub. *Proceedings of the SPIE*, Volume **4838**, 486.
Petrov, R.G.: 1988, *Diffraction-Limited Imaging with Very Large Telescopes*, eds. D.M. Alloin, J.M. Mariotti, Kluwer, 249.
Petrov, R.G., Malbet, F., Weigelt, G., Lisi, F., Puget, P., Antonelli, P., Beckmann, U., Lagarde, S., Lecoarer, E., Robbe-Dubois, S. et al.: 2003, Interferometry for Optical Astronomy II. Edited by Wesley A. Traub. *Proceedings of the SPIE*, **4838**, 924.
Quirrenbach, A., Hummel, C.A., Buscher, D.F. et al.: 1993, *Astrophys. J.*, **416**, L25.
Quirrenbach, A., Mozurkewich, D., Buscher, D.F. et al.: 1996, *Astron. Astrophys.*, **312**, 160.
Quirrenbach, A.: 2001, *Ann. Rev. Astron. Astroph.*, **39**, 353.
Rice, J.B.: 1996, In: Strassmeier K.G., Linsky J.L. (eds.) Stellar Surface Structure. *Proceedings of the IAU Symp.* **176**, Kluwer, 305.
Rice, J.B.: 1989, *Astron. Astrophys.*, **245**, 561.
Rice, J.B., Wehlau, W.H.: 1990, *Astron. Astrophys.*, **233**, 503.
Stee, P., de Araujo, F.X., Vakili, F. et al.: 1995, *Astron. Astrophys.*, **300**, 219.
Thom, C., Granes, P., Vakili, F.: 1986, *Astron. Astrophys.*, **165**, L13.
Tuthill, P.G., Haniff, C.A., Baldwin, J.E.: 1997, *Mon. Not. R. Astron. Soc.*, **285**, 529.
Vakili, F., Mourard, D., Stee, P.: 1994, *Proceedings of the IAU Symp.* **162** p. 435.
Wittkowski, M., Hummel, C.A., Johnston, K.J. et al.: 2001, *Astron. Astrophys.*, **377**, 981.
Young, J.S., Baldwin, J.E., Boysen, R.C. et al.: 2000, *Mon. Not. R. Astron. Soc.*, **315**, 635.
Zahn, J.-P.: 1992, *Astron. Astrophys.*, **265**, 115.

Proc. IV Serbian-Bulgarian Astronomical Conference,
Belgrade 21–24 April 2004,
eds. M. S. Dimitrijević, V. Golev, L. Č. Popović, M. Tsvetkov,
Publ. Astron. Soc. "Rudjer Bošković" No 5, 2005, 95 - 100 *Invited lecture*

WEB ACCESS AND IMAGE PROCESSING IN ASTROPHYSICAL DATABASES

D. KALAGLARSKY

Space Research Institute, Bulgarian Academy of Sciences
E–mail damyan@skyarchive.org

Abstract. Web technologies motivate needs for fast access to informative pixel arrays, which are more intuitively understandable than the stellar catalogues alone. The transfer of huge astrophysical images over the web at present is unrealistic in view of hours needed at a typical user bandwidth rate. The current paper aims to preset the development of a system for web-access to image in the Wide-Field Plate Database (WFPDB) (Tsvetkov and Tsvetkova, 1999). The basics of the image compression methods are discussed. The object signal will be stored with noise, background variations, and so on. Different packages of wide-filed astrophysical images compression as Hcompress FitsPress, Independent JPEG Group (IJG) software are mentioned. The access to the WFPDB images has to solve different problems and face various requirements. The effective compression is the key feature to enabling the users to performe the desired image previews as fast as possible. Besides, some basic on-line image processing like noise-filtering, brightness/contrast enhancement should be also applied. The WFPDB users have to be able to see an image at a desired resolution, as well as to get just a part of the image. They can require a preview that is smaller or bigger, with higher level of detailness, depending on their purpose and network bandwidth. One can also get a high level resolution image of a specified region of the plate without having to transfer the whole amount of data.

1. NEED FOR COMPRESSION

The digitization of photographic plates is done by various automatic plate scanning machines (COSMOS, SuperCOSMOS, APS, PMM, PDSs, Flatbed scanners, etc.). These machines allow for the quantification of the truly enormous amount of useful astronomical data represented in a photograph of the sky, and they have realized the full potential of the large area photographic sky surveys. Image information is coded as an array of intensity values, reproducing the geometry of the scanner used for plate digitization.

The storage and simple transfer of such amounts of data over computer networks becomes too cumbersome and in some cases practically impossible. A typical scan in the Wide-Field Plate Database (WFPDB), for example is about 300-600 MB. Its transfer over the Internet would take hours at a typical user bandwidth rate.

The WFPDB contains data for various plate catalogues. It consists both of structured data, describing the plate from astronomical point of view, like center of filed,

observation time, filter used, etc... along with scans of the plate itself. Often the user of the WFPDB on-line search system would like just to have a look at a preview of the plate, rather than to download the whole image, which is usually hundreds of megabytes in size. Thus one can quickly get an idea of the quality of the plate and its usefulness for his/her purposes. Since the WFPDB plate archives consist of wide-filed plate images mostly, it is also very convenient to be able to retrieve an image of only a region of the whole plate, thus not bothering yourself with data you are not interested in. Some on-line image processing techniques would also be of use to the user of the system. It is nice to be able to enhance the brightness/contrast of your image, to apply different filters without using additional software.

2. BASIC PRINCIPLES OF IMAGE COMPRESSION AND STANDARD METHODS USED IN ASTRONOMY

The compression methods make use of the redundancy contained in the image data in order to reduce the number of bits needed to code it. Since astrophysical images show good spatial correlation it is often possible to achieve good compression ratios without almost any visual loss of quality.

2.1. THE TYPICAL COMPRESSION STEPS

1. Apply a transformation to another domain, where in general the entropy of the coefficients is smaller (e.g. using wavelet transform, discrete cosine transform, etc.).

2. Quantize the coefficients obtained.

3. Code the quantized values by a loss-less method (i.e. Huffman tree, RLE, arithmetic coder, etc.) (Stark, TUTORIAL).

The first step is very essential. Choosing the proper transform determines to a great extent the effectiveness of your method for the class of images that are targeted. If we have an image I which pixels are distributed among L intensity levels with probability of the i$^{\text{th}}$ level to appear in the imagep_i, the entropy is given by:

$$H = \sum_{i=1}^{L} -p_i \log(p_i)$$

The smaller the entropy is, the more "compact" your data are.

Step 2, unlike 1 and 3 is irreversible. The distortion of the reconstructed image will depend mostly on the way in which the coefficients are quantized. That's why we have to compromise between the number of bits used for coefficient quantization and the image quality. The desired quality is quite subjective and will depend on the particular application. Since the images in the WFPDB on-line system have to serve for visual previews mostly, without specific astronomical tasks like astrometry and photometry being applied on them, we could make a decent trade-off in this step of the compression.

2.2. SOME STANDARD SOFTWARE PACKAGES

- JPEG: A standard compression algorithm developed by the Joint Photographic Experts Group (JPEG). It decorelates pixels coefficient within 8 x 8 blocks using the Discrete Cosine Transform (DCT) and uniform quantization. There is a free software library by the Independent JPEG Group (IJG).
- FITSPRESS: based on wavelet transform with Daubechies-4 filters.
- HCOMPRESS: based on the Haar wavelet transform.

All of these packages are in some way inappropriate to the purposes of the WFPDB on-line system, since they are not oriented towards very large images (VLI). The handling of VLI involves specific memory management and other software considerations. These packages are also not quite suitable for some WFPDB tasks like partial image reconstruction, visualization of regions of interest, etc. The compression ratios image quality achieved by them are also not quite satisfactory too.

3. METHODS CONSIDERED

Having to face the development of a specific image compression and visualization, different on-line methods have been considered. They have been estimated according to the results shown by their implementations in terms of compression ratio, image quality, computational complexity, resources usage, etc.

3.1. MULTIRESOLUTION APPROXIMATION

By manipulating the resolution of a signal for the purposes of a specific task, one can inspect only the necessary details. The multiresolution pyramid (Mallat, 1999) allows to process an image at a low resolution, and subsequently to increase it, if needed.

Formally, the approximation of a signal f at resolution 2^{-j} is defined as an orthogonal projection of f in a sub-space V_j. V_j consists of all possible projections of approximations of f at resolution 2^{-j}. The orthogonal projection of f is a function $f_j \in V_j$ that minimizes the norm $\|f - f_j\|$. The following formal definitions describe the properties of multiresolution sub-spaces:

1. $\forall (j,k) \in \mathrm{Z}_2, f(t) \in V_j \Leftrightarrow f(t - 2^j k) \in V_j$
2. $\forall j \in \mathrm{Z}, V_j + 1 \subset V_j$
3. $\forall j \in \mathrm{Z}, f(t) \in V_j \Leftrightarrow f(\frac{t}{2}) \in V_j + 1$
4. $\lim_{j \to +\infty} V_j = \bigcap_{j=-\infty}^{+\infty} V_j = \{0\}$
5. $\lim_{j \to -\infty} V_j = \mathrm{Hull}(\bigcup_{j=-\infty}^{+\infty} V_j) = L_2(\mathrm{R})$

These properties are the basis of an apparatus that would make possible to reconstruct a compressed image at resolution 2^{-j}, which would be quite applicable to the purposes of the WFPDB on-line system.

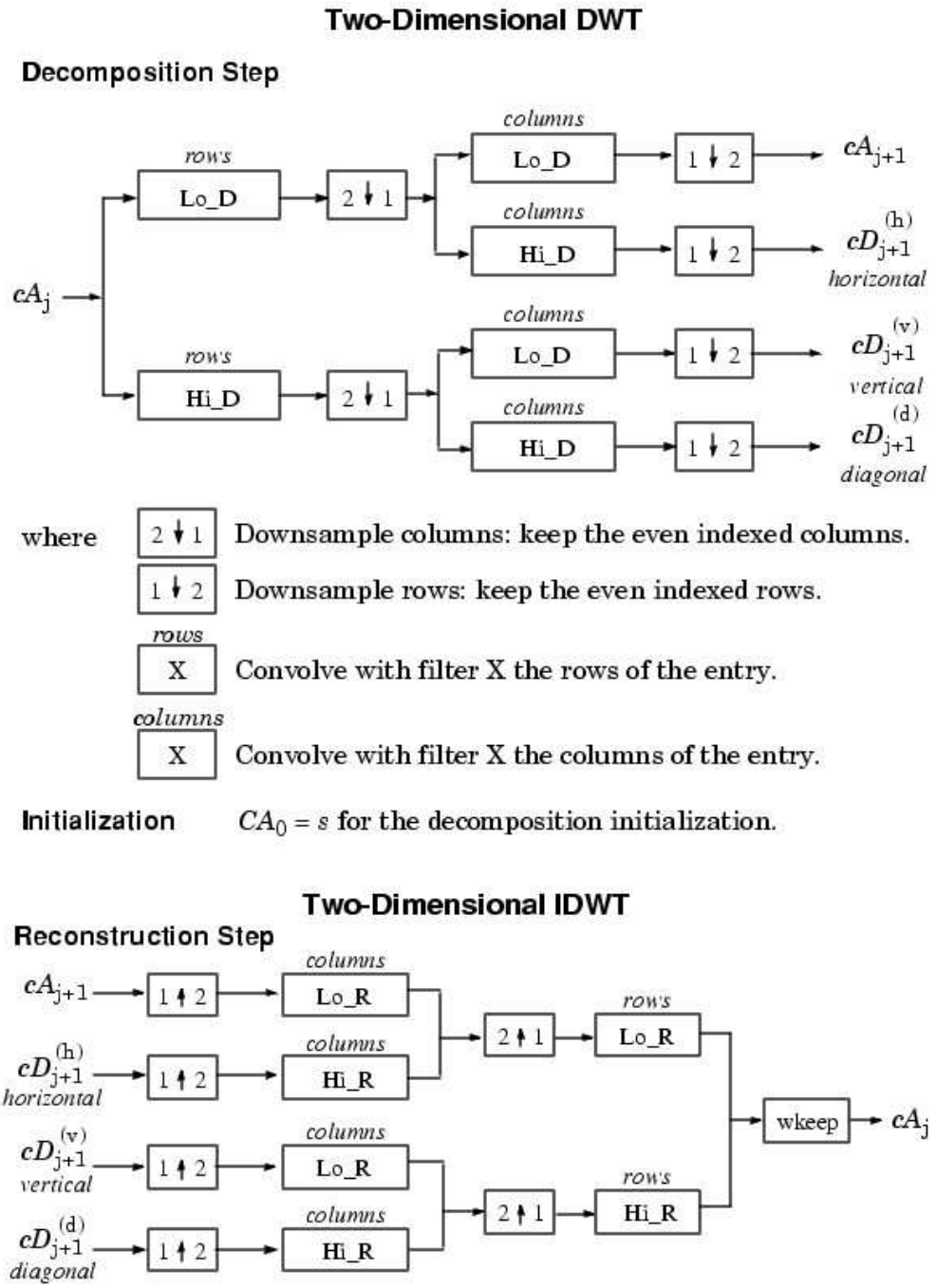

Figure 1: Discrete Wavelet Transform.

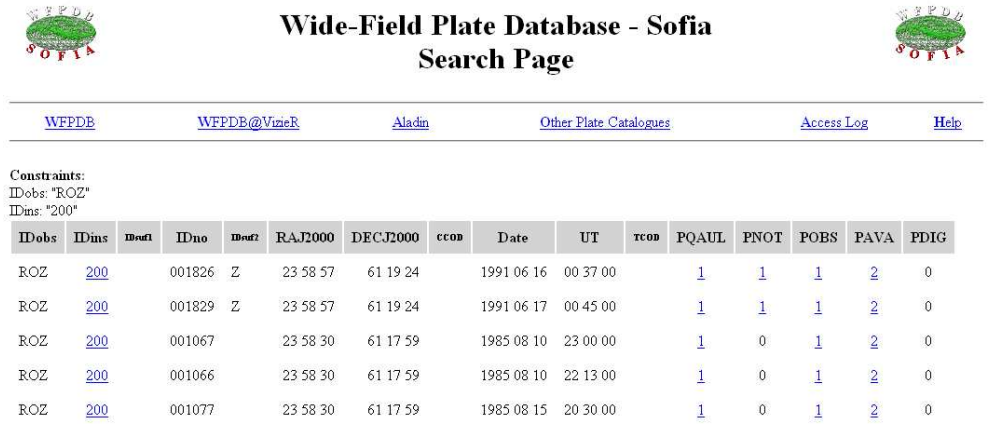

Wide-Field Plate Database - Sofia
Search Page

WFPDB | WFPDB@VizieR | Aladin | Other Plate Catalogues | Access Log | Help

Constraints:
IDobs: "ROZ"
IDins: "200"

IDobs	IDins	IDsuf1	IDno	IDsuf2	RAJ2000	DECJ2000	CCOD	Date	UT	TCOD	PQAUL	PNOT	POBS	PAVA	PDIG
ROZ	200		001826	Z	23 58 57	61 19 24		1991 06 16	00 37 00		1	1	1	2	0
ROZ	200		001829	Z	23 58 57	61 19 24		1991 06 17	00 45 00		1	1	1	2	0
ROZ	200		001067		23 58 30	61 17 59		1985 08 10	23 00 00		1	0	1	2	0
ROZ	200		001066		23 58 30	61 17 59		1985 08 10	22 13 00		1	0	1	2	0
ROZ	200		001077		23 58 30	61 17 59		1985 08 15	20 30 00		1	0	1	2	0

Figure 2: Plate search results (web-browser screenshot).

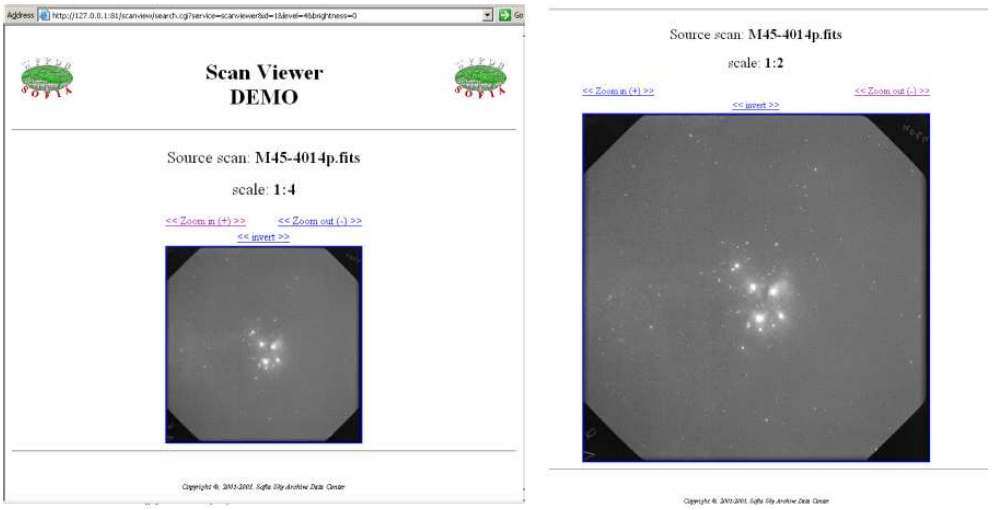

Figure 3: Scan images at different resolution (web-browser screenshot).

3.2. FAST WAVELET TRANSFORM (FWT)

The FWT algorithm presents recursively each approximation $PV_j f$ of a given signal f by a coarser approximation $PV_{j+1} f$ plus the wavelet coefficients $PW_{j+1} f$. The wavelet transform can be computed by consequently convolving the signal with a high-pass h and a low-pass g filters and downsampling. Thus no data redundancy is introduced. N input samples will result in N wavelet coefficients. The reconstruction goes analogously by upsampling the coefficients (Fig. 1).

3.3. CURVELET TRANSFORM

The digital curvelet transform is developed by Candès and Donoho for the needs of image analysis (Donoho and Duncan, 1999). The transform has been designed to represent effectively edges and other singularities along curves.

However, the transform is strongly redundant, thus not very appropriate for the purposes of image compression in WFPDB. The redundancy factor is equal to 16J + 1 whenever J scales are employed in the implementation.

4. DEVELOPMENT OF SOFTWARE

The image presentation system is currently being developed as a module of the WFPDB on-line search system. Having located the plate you are interested in through the interface for searching / navigating in the results (Fig. 2), you can request different previews of the scans of a plate (if available, of course). The presentation module will follow the software architecture of the search system (CGI) and will interact with the other modules of the system. You can choose the resolution of the image you get according to the level of details necessary for your tasks (Fig 3).

5. CURRENT PROBLEMS AND DIRECTIONS FOR FUTURE WORK

Various problems have to be solved in the future development of the system. The implementation has to face plenty of challenges, including enhanced memory management, speed optimization, more profound compression rates analysis. Another open issue is the form in which the generated image is to be transferred to the client node (web-browser). For the moment, JPEG is used. Maybee a native code should to be developed, so that image will not have to be recoded. Some on-line image processing techniques have also to be implemented. Identification of an image with reference to star catalogues is also a problem to be faced.

References

Donoho, D.L., Duncan, M.R.: 1999, Digital Curvelet Transform: Strategy, Implementation and Experiments, `http://www-stat.stanford.edu/~donoho/Reports/1999/DCvT.pdf`.

Mallat, St.: 1999, Wavelet tour, Second Edition, Academic Press.

Stark, J.L: TUTORIAL: Multiscale Methods and Applications, `http://jstarck.free.fr/cours.htm`.

Tsvetkov, M., Tsvetkova, K.: 1999, Treasure-Hunting in Astronomical Plate Archives (THAPA), Proceedings of the International Workshop, Sonneberg, March 4-6, 1999, 88.

Proc. IV Serbian-Bulgarian Astronomical Conference,
Belgrade 21–24 April 2004,
eds. M. S. Dimitrijević, V. Golev, L. Č. Popović, M. Tsvetkov,
Publ. Astron. Soc. "Rudjer Bošković" No 5, 2005, 101 - 104 *Invited lecture*

GLOBULAR CLUSTERS - INTERESTING STELLAR SYSTEMS

S. NINKOVIĆ
Astronomical Observatory, Volgina 7, 11160 Belgrade 74, Serbia
E–mail sninkovic@aob.bg.ac.yu

Abstract. For a long time, globular clusters excite interest of the astronomical community. Here is presented a review, concerning first of all an ensemble of around 150, belonging to the Milky Way. These systems may exist sufficiently long (in comparison with Hubble time), but however, traces of relaxation should be noticeable. It is possible that some of them survived the colapse of their cores.

1. INTRODUCTION

Globular clusters (GCS) are well known stellar systems. They are, especially, known to have shapes closer to perfect spheres than any other kind of stellar systems. Usually the number of stars within a GC is between $10^4 - 10^6$. Many of them seen from the northern hemisphere were known already to C. Messier in the XVIII century. Their distribution in space is, like for many other celestial bodies, not uniform. They mainly form systems identified with galaxies, though it cannot be excluded that some GCS are not bound to any galaxy (for instance, in the case of our own galaxy such cases are known, but they are probably bound to the Local Group of Galaxies). There are even dwarf galaxies having their own globular clusters (e.g. Fornax Galaxy). It may be concluded that globular clusters are very frequent. They can survive over a very long time.

There are several aspects in the studying of GCS. The most important ones are, certainly, the internal structure and the GCS belonging to the Milky Way. One may also mention the studies concerning GCS associated with other galaxies.

2. INTERNAL STRUCTURE OF GCS

The internal-structure studying for GCS starts usually with the examining of their spatial distribution which is based on star counts. First attempts of such kind belong as early as to the beginning of the twentieth century. Plummer's (e.g. 1915) interpretation of star counts, according to which the mass distribution in a typical GC follows the Schuster density law (due to this referred to very often as Plummer-Schuster law), is very well known. However, some later studies (e.g. Kostitsyn, 1922) questioned Plummer's conclusion. Star counts of sufficient quality became available at about 1960. King's (1962) model, today almost generally accepted as explanation

of mass distribution within GCS, is approximately from that time. It should be said that Veltmann (1961), practically at the same time, indicated another mass- distribution model (alternative model) yielding almost an identical fit as King's one. It should be added that this alternative model is also known under the name of modified Hubble-Reynolds formula (e g. Binney and Tremaine, 1987 - p. 39).

In the case of King's model, as well as in the case of the alternative one, the spatial distribution is determined with three parameters: total mass (or central density instead), core radius and limiting or tidal radius. The core radius is very important. It is determined from the run of the surface density since at it the surface density should be one half that at the centre. A comparison of the observed surface-density curve to the one following from the comparison model yields the ratio tidal-to-core radius; the former one is defined as the radius where the surface density vanishes. With regard that in GCS the matter is said to be very strongly concentrated to their centres, as a measure of this concentration one usually uses the logarithm of the ratio of these two radii, the so-called concentration parameter. A comparison between the King model and the alternative one can be found in a paper of the present author (Ninković, 2004). King's model has a disadvantage that from its density formula it is impossible to obtain analytically the corresponding formula for the cumulative mass, i. e. potential. Therefore, the present author (Ninković, 2003) has proposed a formula for the gravitational potential which cannot be applied to the infinity because in it the (volume) density vanishes at a finite distance to the centre. King's model has the same property since there not only the surface density vanishes at a finite distance to the centre, but also the volume one, at the same distance (tidal radius). Unlike King's model in the case of the alternative one at the tidal radius only the surface density vanishes, whereas in the volume one there is a boundary discontinuity. This circumstance seems, in the present author's opinion, more natural because the apocentric distances of stars, clearly, cannot exceed the limiting-radius value, i. e. on the inner side of the boundary the density is still expected to be over zero, whereas on the outer one it should vanish. The potential proposed by the present author (Ninković, 2003) comprises both cases since as the boundary of the system can be assumed also another sphere closer to the centre than that where the density vanishes.

A question to be answered is also the amount of the total mass of a GC. Mass models mentioned above can be useful in such determinations.

3. INTERNAL RELAXATION

The structure of GCS as described above concerns their steady state, as if they were subjects to no evolution. However, the process of internal relaxation consisting of kinetic-energy exchange, usually between stars in pairs, can result in significant changes within a GC. It is characterised by a time interval known as the relaxation time. The calculation of the relaxation time for a typical GC shows that it is significantly shorter than the Hubble time. Therefore, observations with which one can verify theoretical predictions are of interest. The core-radius determinations are among them. Indeed, for some GCS of the Milky Way, the best known example is M15, the core radius strives practically to zero. This phenomenon is referred to as

the core colapse. Its cause is in the fact that massive stars due to the internal relaxation sink towards the centre. In principle the core colapse is the final, extreme, phase of the internal relaxation. For many GCS one can expect the mass segregation. Observations aimed at examining the effects of mass segregation are currently done at many observatories.

4. GCS OF THE MILKY WAY

They are available on the Internet. This sample contains a total of 147 GCS. There are three groups of data. The first one gives the data concerning the internal structure - structural parameters. The concentration parameter is under 1 for 20 GCS (for nine of them no such data), whereas in the case of more than 25 GCS it exceeds the value of 2; its highest value in the sample is 2.5 and it is found for several GCS (about 15). As a final statement one can say that among the GCS with known concentration parameter some 70% have its value in the interval 1-2. As for the GCS with high concentration parameter, say over 2, a majority of them have suffered the core collapse. For example, this is the case with all of them having the highest concentration- parameter value (that of 2.5), nevertheless there are GCS with collapsed cores for which the concentration parameter is less than 2. More precisely for GCS with collapsed cores the core radii are usually estimated to a few seconds of arc. This value is probably near the lower limit of the possibilities of the modern equipment and hence it is not surprising that for so many GCS the concentration parameter is found to be 2.5. This value seems to be an upper limit for the concentration parameter, probably because the tidal or limiting radius is very often between some 15 and 25 arc minutes. In any case the concentration parameter is an important characteristic of a GC. However, there is a question to be answered - how large are its initial amounts - since, no doubt, the internal relaxation contributes to the decreasing of the core radius, i. e. automatically to the increasing of the concentration parameter.

Another important characteristic of a GC is its metallicity. It is seen that for about two thirds of the Milky-Way GCS the metallicity under the value of -1. This value has been very often cited as a limiting one for the objects of the galactic halo with regard to Zinn's (1985) results. It is also known that these metal-poor GCS form a gaussian metallicity distribution with a mean value of about -1.6. A vast majority of them is within limits of -1.3 and -1.9. There are only a few extremely metal-poor GCS in the Milky Way for which the metallicity is lower than -2. However, there is no single GC with metallicity under -2.5. In other words even the most metal-poor GCS are not deprived of metals.

The spatial distribution of the Milky-Way GCS is sufficiently well known. They belong to the halo, i. e. they do not concentrate strongly towards the galactic plane. This is especially true for the metal-poor GCS. However, the metal-rich GCS seem to show a concentration towards the galactic plane so that it is not quite clear if they should be attributed to the halo. There are views (e.g. Nagl, 2000) classifying them, nevertheless, to the halo taking as a criterion the behaviour of their line number density (in projection to the axis of galactic rotation). For some of the Milky-Way GCS the proper motions have been determined. Although their accuracy is not high

(for instance, there are many cases where the discordance in the results obtained by different authors for the same cluster exceeds the indicated error limits), the possibility of calculating the galactocentric orbits have been used. The forms and sizes of these orbits agree well with what can be expected from the spatial distribution (e.g. Ninković et al., 1999). This is a rather qualitative conclusion in view of the comment concerning the accuracy of the proper motions.

5. CONCLUSION

GCS are important stellar systems. Their properties are worth of further studies. Among them are certainly those concerning the distribution of the surface brightness, mass segregation, statistical studies of the Milky-Way sample of GCS including also the search for other, still undiscovered, GCS. Some of these fields are expected to be comprised in the scientific cooperation between Bulgarian and Serbian astronomers.

Acknowledgements

This work is a part of the Project No. 1468 "Structure, Kinematics and Dynamics of the Milky Way" supported by the Ministry of Science and Environmental Protection of Serbia.

References

Binney, J., Tremaine, S.: 1987, Galactic Dynamics, Princeton University Press, Princeton, New Jersey.
King, I.: 1962, *Astron. J.*, **67**, 471.
Kostitsyn, V. A.: 1922, *Trudy Glav. Rossij. Astron. Obs.*, **1**, 28.
Nagl, M.: 2000, *Serb. Astron. J.*, **162**, 47.
Ninković, S.: 2003, *Serb. Astron. J.*, **166**, 39.
Ninković, S.: 2004, *Serb. Astron. J.*, **168**, in press.
Ninković, S, Popović, N., Živkov, V.: 1999, *Publ. Astron. Obs. Belgrade*, No. 65, 135.
Plummer, H.C.: 1915, *Mon. Not. R. Astron. Soc.*, **76**, 107.
Veltmann, Ü.-K.: 1961, *Publ. Tart. Astron. Obs.*, **33**, 387.
Zinn, R.: 1985, *Astrophys. J.*, **293**, 424.

Proc. IV Serbian-Bulgarian Astronomical Conference,
Belgrade 21–24 April 2004,
eds. M. S. Dimitrijević, V. Golev, L. Č. Popović, M. Tsvetkov,
Publ. Astron. Soc. "Rudjer Bošković" No 5, 2005, 105 - 112 *Invited lecture*

BALKAN COLLABORATION IN THE ARCHIVING OF WIDE-FIELD PHOTOGRAPHIC OBSERVATIONS

K. TSVETKOVA[1], M. TSVETKOV[1], K. Y. STAVREV[1], A. BORISOVA[1]
M. STAVINSCHI[2], V. PROTIĆ-BENIŠEK[3]

[1] *Institute of Astronomy, Bulgarian Academy of Sciences,*
72 Tsarigradsko Shosse blvd., 1784 Sofia, Bulgaria
E–mail katya@skyarchive.org

[2] *Astronomical Institute, Romanian Academy,*
5 Cutitul de Argint Str., 75212 Bucharest, Romania
E–mail magda@aira.astro.ro

[3] *Belgrade Astronomical Observatory, Volgina 7, 11160 Belgrade 74, Serbia*
E–mail vprotic@aob.bg.ac.yu

Abstract. We consider the collaboration in the archiving of wide-field photographic observations in the astronomical observatories from the Balkan peninsula region. As a result of the collaboration the descriptive information for 49.2% of all existing wide-field observations in Bulgaria, Serbia and Romania (40 437 plates) is already included in the Wide-Field Plate Database (WFPDB). An on-line access to this information is organized in Strasbourg Data Center and in Sofia Sky Archive Data Center. A digitized plate archive is on the way to be created as a part of the WFPDB with the operating high-speed Epson Expression 1640XL flatbed scanner and high-precision PDS1010 microdensitometer in Sofia Sky Archive Data Center, as well as with UMAX Alfa Vista II flatbed scanner in Bucharest, which provide good opportunities for an effective processing of the archived observations. Another aspect of the collabration is the exchange of experience in development and application of astronomical databases (WFPDB and BELDATA) and organization of mirror sites of the databases.

1. INTRODUCTION

The archiving of the wide-field photographic observations has some obligatory steps: to provide good storage with a suitable temperature and humidity free conditions, to give easy access to the plates, to make an inventory of the plate collection, to prepare computer-readable versions of the plate catalogues, to digitize plates and to assure access to the plate digitized information.

The biggest world plate vaults are in the Harvard College Observatory (USA) and in Sonneberg (Germany). Intention to establish Central Plate Store Unit for the European plate archives arose in Brussels with the project UDAPAC, which still is considered as an initiative. A similar initiative for the north American observatories vaults was raised in January 2004 in the Pisgah Astronomical Research Institute.

The effective use of the archived wide-field observations needs plate logs cataloguing in an uniform database format. Despite of the great difficulties with organizing and funding of the cataloguing an acceleration of this process is needed. Another obligatory condition is the existence of high-speed and high-precision microdensitometers, which provide astrometric and photometric accuracy while generating archival digital data. Last five years commercial flatbed scanners were widely spread in many observatories. In the Harvard College Observatory (USA) only some days ago (April 2004) a project for a flatbed scanner with a CCD camera capable to take 5 frames per second special fixturing to hold different size from plates of size up to 14×17 inch was approved.

Realizing the importance of archived wide-field observations astronomers from some Balkan countries initiated in the 90s of 20th century joint projects on the preservation, digitization and re-usage of plate archives. The work in this direction was greatly stimulated by the on-going project in Sofia for the creaton of an wide-field plate database.

2. THE WIDE-FIELD PLATE DATABASE

The Wide-Field Plate Database (WFPDB, Tsvetkov 1992, Tsvetkov et al. 1998, `http://www. skyarchive.org`), created as a basic source of information for the archived wide-field photographic observations, consists of two parts: (1) Catalogue of Wide-Field Plate Archives (CWFPA) and (2) Catalogue of Wide-Field Plates (CWFP). In the CWFPA (version March 2004) an information for 375 archives with a total of 2 133 912 (2 069 824 direct and 64 088 spectral) plates from 124 observatories can be found. Especially in Europe 256 archives exist with 1 115 468 plates obtained in 74 observatories – more than half of all known wide-field plates world-wide obtained with professional astronomical instruments.

The CWFP up to March 2004 contains descriptive data for 378 187 wide-field photographic observations from 92 plate archives from all over the world.

3. BALKAN OBSERVATORIES, INSTRUMENTS AND PLATE ARCHIVES

In the geographically determined Balkan peninsula region there are astronomical observatories in Bulgaria, Greece, Romania, Serbia and Turkey, but archives of wide-field photographic observations exist only in Bulgaria (Institute of Astronomy, Bulgarian Academy of Sciences), Romania (Astronomical Institute of the Romanian Academy in Bucharest and Cluj) and Serbia (Belgrade Astronomical Observatory). Table 1 presents the astronomical observatories possessing archived wide-field photographic observations.

The main characteristics of the wide-field instruments of the astronomical observatories in Bulgaria, Romania and Serbia are given in Table 2.

As CWFPA (version March 2004) shows, there are 9 Balkan wide-field plate archives obtained with 9 instruments (Table 3). The total number of plates in them is 40 437.

The distribution of the number of wide-field plates obtained in Bulgaria, Romania

Table 1: Balkan astronomical observatories possessing archived wide-field photographic observations

Observatory	Marsden Number	Time Zone [h]	Coordinates λ	ϕ	Altitude [m]
Belgrade	057	+1	20°31′.0 E	+44°48′.2	253
Bucharest	073	+2	26°05′.8 E	+44°24′.8	81
Cluj		+2	23°53′.5 E	+46°46′.5	412
Rozhen	071	+2	24°45′.0 E	+41°43′.0	1759

Table 2: Wide-Field Instruments: Main Characteristics

WFPDB Instrument Identifier	Telescope Original Name	Telescope Type	Aperture [m]	Focal Length [m]	Scale [″/mm]	Field Size [°]
BEL012	Ascania Rfr	Cam	0.12	1.00	206	7.0
BEL016A	Zeiss Ast	Ast	0.16	0.80	258	11.5
BEL016B	Zeiss Rfr	Cam	0.16	0.80	258	11.5
BUC016	16 cm Camera	Cam	0.16	0.80	258	7.4
BUC038	Prin-Merz Ast	Rfr	0.38	6.00	34	2.3
CLU020	Zeiss Rfr	Rfr	0.20	3.00	82.5	2.1
CLU050	Newton	Rfl	0.50	0.25	68.8	2.3
ROZ050	Schmidt	Sch	0.50/0.70	1.72	120	4.5
ROZ200	2 m RCC	RCr	2.00	16.00	12.9	1.0

Table 3: Balkan Wide-Field Plate Archives

WFPDB Instrument Identifier	Years of Operation	Number of Plates	Archive Data Form[1]	Astronomer in Duty
BEL012	1972-1996	4000	T	V.Protić-Benišek
BEL016A	1936-1985	10000	T	V.Protić-Benišek
BEL016B	1936-1941	500	T	D.Olević
BUC016	1930-1961	180	C	Gh.Bocsa
BUC038	1930-1995	10391	C	Gh.Bocsa
CLU020	1932-1976	1179	C	L.Mircea
CLU050	1952-1957	4821	C	L.Mircea
ROZ050	1979-1994	7359[2]	C	M.Tsvetkov
ROZ200	1979-1993	2007	C	K.Stavrev

[1] C – computer-readable form, T – not in computer-readable form
[2] 214 of them are objective prism spectral plates

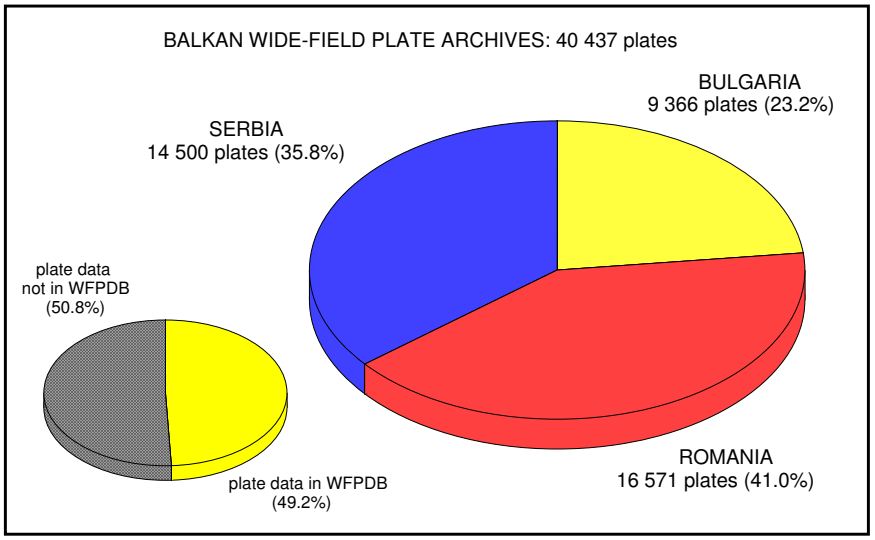

Figure 1: Distribution of the number of wide-field plates among the Balkan countries

and Serbia is shown in Fig. 1. Romania possesses 16 571 plates (41% of all Balkan plates), Serbia – 14 500 (35.8%), and Bulgaria – 9 366 (23.2%).

The data for almost half of all Balkan wide-field plates (19 914) are included in the WFPDB and can be accessed on-line. This concerns the archives of BUC016, BUC038, ROZ050 and ROZ200. The plate data for BEL012, BEL016A BEL016B, CLU020 and CLU050 is not yet included in the WFPDB.

More information about the archives in Table 3 is given in Stavrev and Barzova (1994); Mutafov et al. (1994); Vass (1994); Vass et al. (1994); Tsvetkov et al. (2000a; 2000b); Chis et al. (2000); Blaga et al. (2003).

4. SCANNERS

The Sofia Sky Archive Data Center (SSADC) has at its disposal a PDS 1010plus microdensitometer (the formal ESO one) for precise plate digitization. Since August 2003 SSADC possesses also a flatbed scanner Epson Expression 1640XL with a scanning platform 310×437 mm and resolution 1600×3200 dpi. The duration of the scanning for plate size 16×16 cm is 5 min with a volume of the digitized information 120 Mb. A flatbed scanner UMAX Alpha Vista II with a resolution 1200×2400 dpi is at disposal in the Astronomical Institute of the Romanian Academy (Bucharest). Its scanning platform is 203×254 mm. The duration of the scanning for 9×5 cm plate is 6 min (2 min for prescan and 4 min for real scan) with a volume of the digitized information about 30 Mb for this plate size.

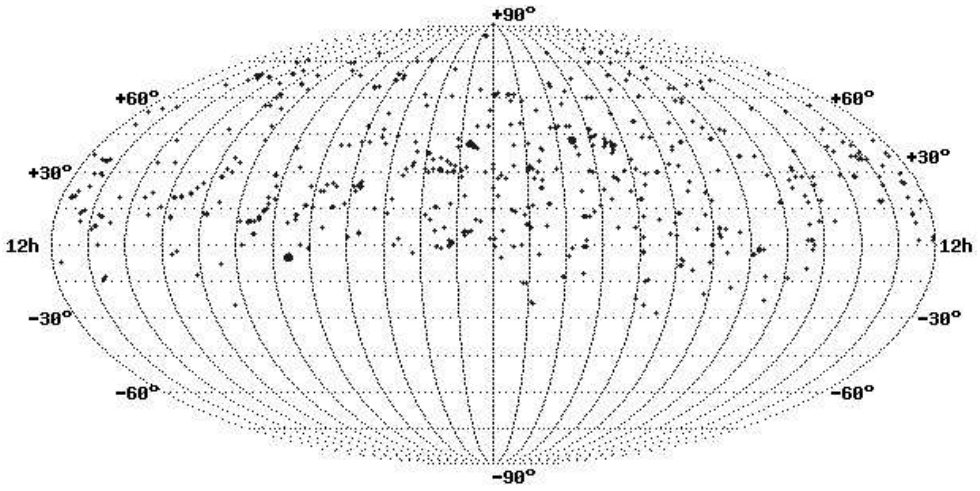

Figure 2: All-sky distribution for the Rozhen 2 m RCC (ROZ200) plates.

5. PROJECTS AND TOPICS

There are two bilateral projects:

– between the Space Research Instutute of the Bulgarian Academy of Sciences and the Astronomical Observatory Belgrade, titled "Development and Application of Astronomical Databases", and

– between the Instutute of Astronomy of the Bulgarian Academy of Sciences and the Astronomical Institute of the Romanian Academy, titled "The Wide-Field Plate Database: Application of the Romanian Photographic Plates".

The number of participants in these projects is : 6 from Bulgaria, 6 from Romania and 11 from Serbia.

The main topics of collaboration can be summarized as follows:

– Cataloguing of wide-field photographic observations,

– Digitization of selected plates,

– Plate processing,

– Application of archived observations,

– Exchange of experience and astronomical data (WFPDB and BELDATA).

6. RESULTS

For the period of the collaboration the descriptive information for the Bucharest wide-field photographic observations was included in the WFPDB. An on-line access to this information for the astronomical community was provided through the VizieR facility in Strasbourg (since 1996, `http://vizier.u-strasbg.fr/cats/VI.htx.`), and the WFPDB updated version in SSADC (since November 2001, `http://www.skyarchive.org`). The results from the analysis of the Bucharest plate archives are

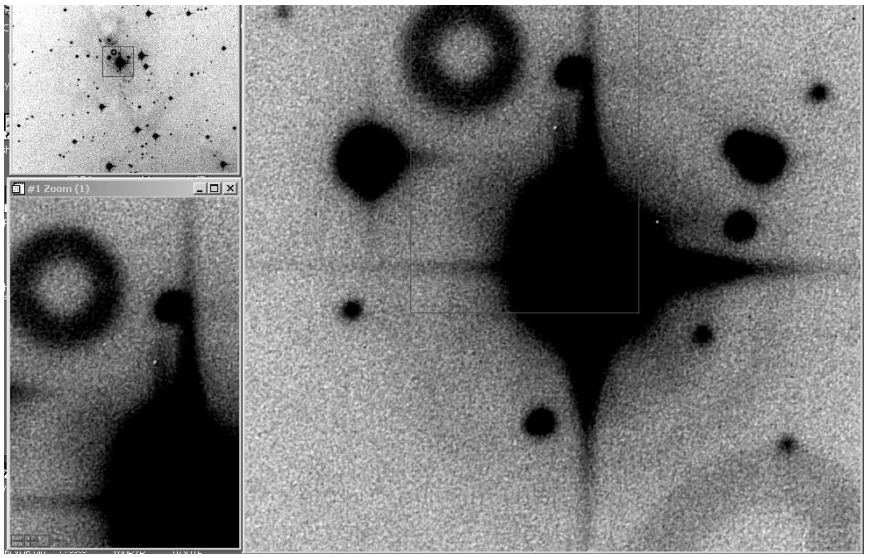

Figure 3: Images of the ROZ200 001655 plate with the variable star KH 15D in the stellar cluster NGC 2264.

presented in Vass (1994), Vass et al. (1994), Tsvetkov et al. (2000a, 2000b). All-sky distribution of the plate centers of the Bucharest plate archives (and of all other archives included in the WFPDB) can be found at `http://draco.skyarchive.org/archives/archives.html`. In Fig. 2 all-sky distribution taken from the same URL address for the Rozhen 2 m RCC (ROZ200) plates is presented.

The information for the Cluj archives (Chis et al., 2000; Blaga et al., 2003) has been added to the CWFPA (version March 2004).

The creation of an archive of digitized preview images of plates as an unseparated part of the WFPDB has started, as well as of an archive of selected digitized plate images to be available on-line. The beginning of this work was the digitization of selected interesting Bucharest plates containing images of more than 4 minor planets. The plates have been scanned with the PDS 1010plus microdensitometer (see Tsvetkov et al., 2000a; 2000b). Fig. 3 shows a part of digitized with the PDS1010 plus microdensitometer ROZ200 001655 plate with the variable star KH 15D in the stellar cluster NGC 2264 (K7 pre-main sequence cluster member with 48 day periodicity and extremely deep $\sim 3.5^{\mathrm{m}}$ minima, caused by eclipse from a circumstellar disk).

Archive of the scanned Pleiades plates obtained in Bucharest, Cluj, Belgrade and Rozhen has been prepared using besides the scanners mentioned above also the flatbed scanner UMAX PowerLook 3000 of Konkoly Observatory with resolution 3048 dpi (8 μm). In Fig. 4 a part of the digitized with the Epson Expression 1640XL flatbed scanner Pleiades ROZ050 000057 plate obtained by multiexposure method (6 exposures of 10 min each) is given.

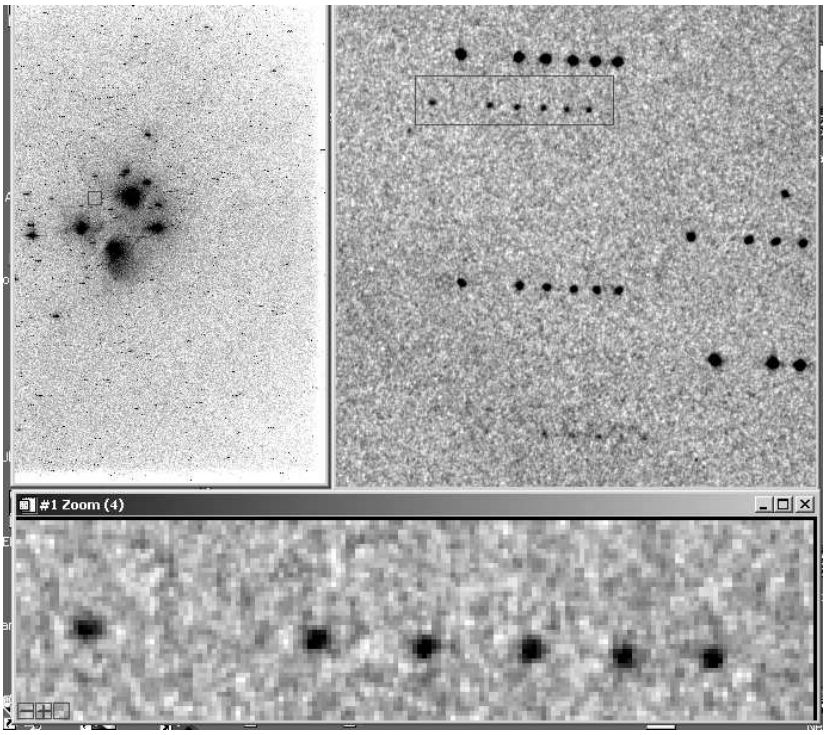

Figure 4: Images of the Pleiades ROZ050 000057 plate obtained by multiexposure method.

Some test scans of the Cluj plates in the Pleiades have been made with the UMAX Alpha Vista II scanner in Bucharest for the joint investigations of the Pleiades red dwarf stars.

7. FUTURE PLANS

The Cluj archive and the last 180 plates, obtained in Bucharest in the period 1993 – 2001 in the frames of the programme for the connection of optical (FK5) and radio (VLBI) observations of reference stars (so called CONFOR project), will be added to the WFPDB. The preparation of a plate catalogue in the WFPDB format for the wide-field photographic observations at the Astronomical Observatory Belgrade will be the final stage for the Balkan archiving. The plate catalogue will be included in the WFPDB and in BELDATA. For both databases mirror sites will be organized.

The creation of an archive of digitized plates with an on-line access will have a main priority in the working programmes of the bilateral projects. Digitized archival wide-field observations will be used for investigations of the Pleiades red dwarf stars, aimed at revealing their long-term behaviour (Borisova et al., 2002; 2003).

References

Blaga, C., Chis, G.-D., Mircea, L.: 2003, *Rom. Astron. J.*, **13**, 83.
Borisova, A.P., Tsvetkov, M.K., Tsvetkova, K.P., Hambly, N., Kalaglarsky, D.G.: 2002, *Publ. Astron. Obs. Belgrade*, **73**, 81.
Borisova, A.P., Tsvetkov, M.K., Tsvetkova, K.P., Hambly, N., Kalaglarsky, D.G, Richter, G.M., Boehm, P., Kelemen, J., Fresneau, A., Argyle, R.W: 2003, *Astronomical and Astrophysical Transactions*, **22**, 487.
Chis, G.-D., Blaga, C., Mircea, L.: 2000, *Rom. Astron. J.*, **10**, 191.
Mutafov, A., Ilcheva, P., Kusheva, M., Michailov, M., Borisov, Z., Lazarov, N.: 1994, in Proc. IAU Symp. 161 "Astronomy from Wide-Field Imaging", 23-27 August 1993, Potsdam, Germany, Eds. H.T. MacGillivray et al., Kluwer, Dordrecht, p. 377.
Stavrev, K.Y., Barzova, I.S.: 1994, in Proc. IAU Symp. 161 "Astronomy from Wide-Field Imaging", 23-27 August 1993, Potsdam, Germany, Eds. H.T. MacGillivray et al., Kluwer, Dordrecht, p. 371.
Tsvetkov, M.: 1992, *IAU WGWFI Newsletter 2*, 51.
Tsvetkov, M.K., Stavrev, K.Y., Tsvetkova, K.P., Semkov, E.H., Mutafov, A.S., Michailov, M.-E.: 1998, in Proc. IAU Symp. 179 "New Horizons from Multi-Wavelength Sky Surveys", Eds. McLean, B. et al., Kluwer, Dordrecht, p. 462.
Tsvetkov, M.K., Stavinschi, M., Tsvetkova, K.P., Stavrev, K.Y., Bocsa, G., Popov, V.N., Cristescu, C.: 2000a, *Baltic Astron.*, **9**, 573.
Tsvetkov, M., Stavinschi, M., Tsvetkova, K., Stavrev, K., Bocsa, G., Popov, V., Cristescu, C.: 2000b, *Rom. Astron. J.*, **10**, 177.
Vass, G.: 1994, *Rom. Astron. J.*, **4**, 183.
Vass, G., Bocsa, G., Ionescu, V., Alexiu, A., Birlan, M.: 1994, *Rom. Astron. J.*, **4**, 179.

Proc. IV Serbian-Bulgarian Astronomical Conference,
Belgrade 21–24 April 2004,
eds. M. S. Dimitrijević, V. Golev, L. Č. Popović, M. Tsvetkov,
Publ. Astron. Soc. "Rudjer Bošković" No 5, 2005, 113 - 127 *Invited lecture*

THEORETICAL $\Sigma - D$ RELATION FOR SUPERNOVA REMNANTS

D. UROŠEVIĆ

Department of Astronomy, Faculty of Mathematics, University of Belgrade,
Studentski trg 16, 11000 Belgrade, Serbia
E–mail dejanu@matf.bg.ac.yu

Abstract. This lecture presents a summary of theoretically-derived relations between the radio surface brightness Σ and the diameter D of supernova remnants (SNRs): such relations are commonly known as $\Sigma - D$ relations. We argue that discrepancies between theoretically-derived relations and valid empirical relations derived, may be at least partially explained by taking into account thermal emission at radio frequencies from two particular types of SNRs.

1. INTRODUCTION

The relation between the surface brightness Σ and the diameter D of supernova remnants (SNRs) – the so-called $\Sigma - D$ relation – provides a convenient way to investigate the radio brightness evolution of SNRs. The $\Sigma - D$ relation relation was first presented and described by Shklovsky (1960ab) in the course of a theoretical analysis of synchrotron radiation from an expanding spherical nebula (that is, a theoretical construct to describe an SNR). Lequeux (1962) generalized the $\Sigma - D$ relation to the shell case to include the well-known shell-type SNR Cas A, and derived a relation which gave a better approximation to empirical relations than the relation derived by Shklovsky (1960ab). As inspired by the work of van der Laan (1962), Poveda and Woltjer (1968) described a modification to the original derivation presented by Shklovsky (1960ab), namely the magnetic field of the SNR was assumed to remain constant as the SNR expands. The $\Sigma - D$ relation derived by Poveda and Woltjer (1968) in this manner closely matched an empirical $\Sigma - D$ relation presented in the same paper. In addition, Kesteven (1968) derived the relation for a shell-type SNR assuming that the thickness of the shell of the SNR remains constant as the SNR expands. Despite the work of Poveda and Woltjer (1968) and Kesteven (1968), however, significant inconsistencies between empirical and theoretical $\Sigma - D$ relations remained. More recently, Duric and Seaquist (1986) derived a $\Sigma - D$ relation based on a theoretical interpretation that paralleled the work of Shklovsky (1960ab): specifically, Duric and Seaquist (1986) adopted both the version of Fermi's accelerating mechanism presented by Bell (1978ab) and the magnetic field model described by Gull (1973) and Fedorenko (1983). The most recent radio observations of SNRs indicate that the surface brightnesses of these sources decrease less rapidly than predicted by theory (e.g.

Case and Bhattacharya, 1998; Urošević, 2002; 2003). Shklovsky (1960b) described how the $\Sigma - D$ relation could be used to determine the distances to radio SNRs based on their surface brightnesses, assuming that this quantity is not distance-dependent. Therefore, the primary application of the $\Sigma - D$ relation is to provide an independent method to estimate the distances to radio SNRs.

Complementary radio observations of SNRs made during the development of theoretical $\Sigma - D$ relations have confirmed the existence of these relations in the form predicted by Shklovsky (1960ab). The first empirical $\Sigma - D$ relation was derived by Poveda and Woltjer (1968): shortly afterward, Milne (1970) derived an empirical $\Sigma - D$ relation and calculated distances to all 97 of the radio SNRs then known to exist in our galaxy. Many observational studies of the $\Sigma - D$ relation were conducted to determine precisely the distances to a specific set of calibrator sources and therefore improve the usefulness of the relation itself (Ilovaisky, 1972; Sakhibov and Smirnov, 1982; Huang and Thaddeus, 1985). Critical analyses of this relation have been conducted since the discoveries by Green (1984). Uncertainties in the distances to certain calibrators are the main weaknesses of the relations derived in this manner: in other words, there are not enough SNRs with precisely calculated distances for the derivation of a proper $\Sigma - D$ relation (Green, 1984). It has also been shown that the derivation of the $\Sigma - D$ relation is meaningful only for shell-type SNRs (Allakhverdiyev et al., 1983; 1986).

From the first studies of this relation, significant differences between theoretical and empirical results were established, with Green (1991) showing that the calibrators are too scattered on the $\Sigma - D$ diagram to derive a valid relation. However, Case and Bhattacharya (1998) derived an empirical $\Sigma - D$ relation – obtaining a much flatter slope than those seen in earlier works – and determined distances for all known shell-type Galactic SNRs. We believe that the discrepancies between theoretical and empirical $\Sigma - D$ relations may be at least partially explained by considering thermal bremsstrahlung emission from SNRs at radio frequencies. Here, we present an updated derivation of the $\Sigma - D$ relation which takes into account this thermal emission at radio frequencies, and we show that the inclusion of this emission helps decrease the discrepancy between theoretical and empirical $\Sigma - D$ relations.

2. THE THEORETICAL $\Sigma - D$ RELATION – A BRIEF REVIEW

2.1. BASIC THEORY (SHKLOVSKY 1960a)

We briefly present the original theory behind the $\Sigma - D$ relation as proposed by Shklovsky (1960a). The vast majority of radio emission detected from Galactic and extragalactic sources is synchrotron radiation produced by relativistic electrons gyrating in magnetic fields. We consider an ensemble of relativistic electrons with an energy distribution in the form of a power law,

$$n(E) = KE^{-\gamma}, \tag{1}$$

where $n(E)$ is the volume density of the relativistic electrons with energies between E and $E + \Delta E$, K is the coefficient of proportionality and γ is the synchrotron spectral

index. The synchrotron emission power (emissivity) ϵ_ν of this ensemble from a unit volume at a given frequency ν may be expressed as

$$\varepsilon_\nu \propto K H^{1+\alpha} \nu^{-\alpha}, \tag{2}$$

where spectral index $\alpha = (\gamma - 1)/2$. The definition of the spectral index is through $S_\nu \propto \nu^{-\alpha}$, where S_ν is the flux density. The synchrotron surface brightness Σ_ν for an ensemble of relativistic electrons and positrons may be expressed as

$$\Sigma_\nu = \frac{S_\nu}{\Omega} = \frac{\varepsilon_\nu V}{D^2 \pi^2} \propto D K H^{1+\alpha} \nu^{-\alpha}, \tag{3}$$

where Ω is the solid angle, D is the diameter of the spherical volume V of the ensemble with a constant volume emissivity ε_ν and ν is the frequency.

Assuming a constant value for γ, after short derivation (Shklovsky, 1960a), we obtain

$$K = K_0 \Big(\frac{D_0}{D}\Big)^{\gamma-1} \Big(\frac{D_0}{D}\Big)^{3}. \tag{4}$$

Here, K represents the time-evolved value of K_0 as the SNR expands. A major assumption in the derivation presented by Shklovsky (1960a) was that as the spherical nebula (here, an SNR) expands, the structure of the magnetic field is approximately conserved. Therefore, the magnetic field flux must remain constant and H will have the following dependence on radius D:

$$H = H_0 \Big(\frac{D_0}{D}\Big)^{2}. \tag{5}$$

Combining the relations given above, we may express the dependence of surface brightness Σ_ν on radius D as

$$\Sigma_\nu \propto D^{-4\alpha-4}. \tag{6}$$

Alternatively, we can express Σ_ν as a function of D as

$$\Sigma_\nu = A D^{-\beta}, \tag{7}$$

where A is a constant and $\beta = 4\alpha + 4$. Shklovsky (1960a) used Cas A to test this theory on the relationship between Σ_ν and D and predicted a 2% relative annual decrease in the observed flux density from this source. Radio observations from that era of Cas A indicated a somewhat lower rate of 1.5% per year. We note that even from the outset of research on the $\Sigma - D$ relation for Galactic SNRs, discrepancies between observation and theory were evident. Assuming an average spectral index of $\alpha = 0.5$ for radio SNRs (Clark and Caswell, 1976), the relation derived by Shklovsky (1960a) predicts a rather steep slope dependence for Σ_ν, namely

$$\Sigma_\nu \propto D^{-6}. \tag{8}$$

2.2. THE LEQUEUX (1962) MODIFICATION

Lequeux (1962) presented another derivation of the $\Sigma - D$ relation where the original relation derived by Shklovsky (1960a) was broadened to include shell-type SNRs. If we once again assume $H \propto D^{-2}$ and a mean spectral index $\alpha = 0.5$ for shell-type SNRs, we obtain

$$\Sigma_\nu \propto D^{-5.8}. \tag{9}$$

The slope predicted by this relation is slightly shallower than the slope predicted by the relation presented by Shklovsky (1960a). When this model is applied to Cas A, an annual relative decrease of 1.7% in flux density is predicted, a value which is approximately 10% lower than the value predicted by Shklovsky (1960a). While this lower value is closer to the value measured by observations, it is still higher than those obtained from empirical relations.

If we assume a shell thickness ηD (where η is a constant such that $0 < \eta < 1$), we again obtain Eq. (3). We conclude that the result from Shklovsky (1960a) can be generalized directly for shell-type SNRs if we assume that the shell thickness remains a constant fraction of the radius of the SNR as the SNR expands.

2.3. THE POVEDA AND WOLTJER (1968) MODIFICATION

Poveda and Woltjer (1968) presented another derivation of the $\Sigma - D$ relation where the magnetic field H was assumed to be constant as the SNR expands, with the particular value of H depending on the amount of compression of the interstellar magnetic field by the SNR shock van der Laan (1962). If a constant H is included in the derivation presented by Shklovsky (1960a), a $\Sigma - D$ relation with a considerably flatter slope is derived as Eq. (3) becomes

$$\Sigma_\nu \propto D^{-2\alpha-2}. \tag{10}$$

If we again assume a value of 0.5 for α, we obtain the following expression for Σ_ν:

$$\Sigma_\nu \propto D^{-3}. \tag{11}$$

This theoretical relation was in good agreement with an empirical relation ($\beta \approx 8/3 \approx 2.67$) derived by Poveda and Woltjer (1968) in the same paper.

2.4. THE KESTEVEN (1968) MODIFICATION

Kesteven (1968) derived another theoretical $\Sigma - D$ relation where the shell thickness was assumed to remain constant as the SNR expands. This assumption produces a new dependence of H on D, namely

$$H = H_0 \frac{D_0}{D}. \tag{12}$$

Adopting this dependence of the magnetic field and repeating the derivation presented by Shklovsky (1960a), the expression for Σ_ν in Eq. (3) may be written as

$$\Sigma_\nu \propto D^{-3\alpha-3}. \tag{13}$$

Once again assuming that $\alpha = 0.5$, we may express Σ_ν as

$$\Sigma_\nu \propto D^{-4.5}. \tag{14}$$

This theoretical $\Sigma - D$ relation was in good agreement with empirically-determined relations of the early 1970s, such as those found by Milne (1970) ($\beta = 4.5$) and Ilovaisky and Lequeux (1972) ($\beta = 4$).

2.5. THE DURIC AND SEAQUIST (1986) MODIFICATION

Finally, we examine the derivation of a theoretical $\Sigma - D$ relation presented by Duric and Seaquist (1986), who considered shell SNRs in the adiabatic expansion phase. By incorporating the Sedov (1959) blast wave solution for SNR expansion, the generation and evolution of a magnetic field as described by Gull (1973) and lastly the acceleration of relativistic electrons by shocks as formulated by Bell (1978ab), Duric and Seaquist (1986) derived a model for the evolution with time of radio emission from an SNR.

Following Gull (1973), we assume that the ambient magnetic field H is amplified in the convection zone: it is the convection zone which provides the environment in which relativistic electrons can radiate efficiently. As the convection zone expands with the SNR, the dependence of H on D may be expressed as

$$H(D) = H_0\Big(\frac{D}{D_0}\Big)^{-\delta}, \tag{15}$$

where $1.5 \leq \delta \leq 2$ (Gull, 1973; Fedorenko, 1983).

Bell (1978b) gives an analytic expression for the synchrotron emissivity arising from such a distribution in a shocked gas. In terms of H and the velocity v (here, equivalent to the expansion velocity), we may express the emissivity ε at a given frequency ν as

$$\varepsilon(H, v) = g(\alpha)\varrho_0 H^{1+\alpha} v^{4\alpha}\Big(1 + \Big(\frac{7\times 10^9}{v}\Big)^2\Big)^\alpha \nu^{-\alpha}, \tag{16}$$

where ϱ_0 is the ambient density, $v \propto t^{-3/5}$ (Sedov, 1959), and

$$g(\alpha) = 0.217 \times 10^{-37\alpha}\Big(\frac{\alpha}{0.75}\Big)(1.435)^{-\alpha}. \tag{17}$$

As in Sect. (2.1), using Sedov (1959) adiabatic solution $D \propto t^{2/5}$, we obtain

$$\Sigma(D) \propto D^{-(6\alpha+\delta\alpha+\delta-1)}\Big(1 + \Big(\frac{3.06\times 10^{18}\rho_0}{x^5 E_0}\Big)D^3\Big)^\alpha, \tag{18}$$

where $x = 2.3$ and $\nu = 1$ GHz. The previous equation can be simplified for $D \ll 1$ pc and $D \gg 1$ pc, which represent two limits of interest to the present work. Applying these limits we finally obtain:

$$D \gg 1\text{pc} \rightarrow \Sigma(D) \propto D^{-(\delta+\delta\alpha+3\alpha-1)}, \tag{19}$$

$$D \ll 1\text{pc} \rightarrow \Sigma(D) \propto D^{-(\delta+\delta\alpha+6\alpha-1)}. \tag{20}$$

We can use this $\Sigma - D$ relation to help determine values for the coefficient A and the exponent β (see Eq. 7). We set $\delta = 2$, consistent with turbulent magnetic field amplification (Gull, 1973; Fedorenko, 1983) and adiabatic expansion of the convection zone: once more we adopt a value of 0.5 for α. Using these values, we obtain a $\Sigma - D$ relation of the following form:

$$D \gg 1\text{pc} \rightarrow \Sigma_{1\text{GHz}} \propto D^{-3.5}, \tag{21}$$

$$D \ll 1\text{pc} \rightarrow \Sigma_{1\text{GHz}} \propto D^{-5}. \tag{22}$$

From Eqs. (19) and (20) we conclude that the exponent β depends only on α and δ. Using $\alpha = 0.5$ and $1.5 \leq \delta \leq 2$ we obtain $2.75 \leq \beta \leq 3.5$. For large diameter SNRs ($D \gg 1$ pc), the $\Sigma - D$ relation may be expressed as

$$\Sigma_{1\text{GHz}} \propto D^{-(2.75 \leq \beta \leq 3.5)}. \tag{23}$$

Updated empirical $\Sigma - D$ relations (Urošević, 2002; 2003) indicate shallower slopes ($\beta \approx 2$) than the slope predicted by this relation.

3. POSSIBLE THERMAL EMISSION FROM SNRS

We present here two models which describe thermal bremsstrahlung emission from SNRs at radio frequencies. The efficiency of the radio emission through the thermal bremsstrahlung process increases as the density increases. There are two basic criteria for the production of a significant amount of radio emission through the thermal bremsstrahlung process from an evolved SNR in the adiabatic phase of evolution: the SNR must be evolving in a dense environment and its temperature must be low (but always greater than the recombination temperature).

3.1. THERMAL RADIATION FROM AN EVOLVED SNR IN THE ADIABATIC PHASE

We first consider an evolved SNR with a diameter D=200 pc, a surface brightness of $\Sigma = 10^{-22}$ W m^{-2} Hz^{-1} sr^{-1} at 1 GHz and a synchrotron shell with a thickness of 10 pc, representing 5% of the SNR diameter. Our adopted values for these properties correspond to those measured or indicated by observations of several evolved Galactic SNRs, such as the four radio loops observed by Spoelstra (1972), the source OA 184, as observed by Routledge et al. (1986) and SNR HB9 (observed by Leahy et al., 1998). For the evolved SNR considered here, the assumed surface brightness corresponds to an emissivity $\varepsilon_{1\text{GHz}} = 1.1 \times 10^{-38}$ ergs cm^{-3} sec^{-1} Hz^{-1} while the total luminosity emitted from the entire volume of the shell at 1 GHz is $L_{1\text{GHz}} = 3.8 \times 10^{23}$ ergs sec^{-1} Hz^{-1}. By integrating over the radio domain from 10^7 to 10^{11} Hz and assuming a spectral index $\alpha = 0.5$, we calculate a luminosity of L=7.5×10^{33} ergs sec^{-1}.

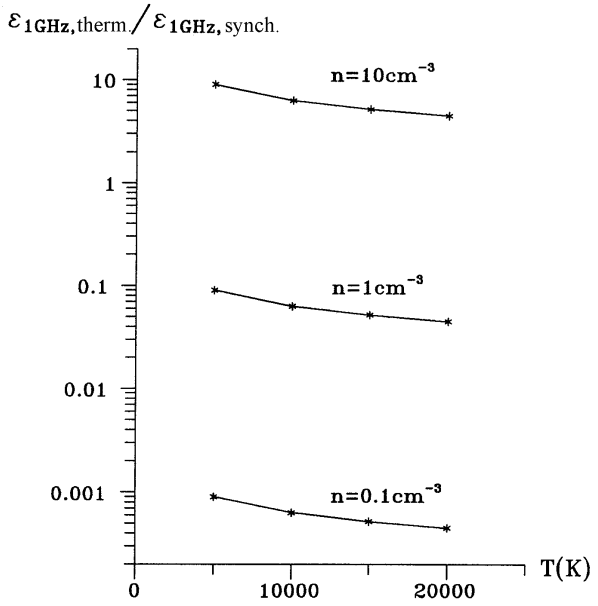

Figure 1: The ratios between the thermal and non-thermal (synchrotron) emissivities at 1 GHz as a function of frequency in the radio domain for the case of a warm ISM. The ratios are plotted for constant gas densities of $n = 0.1$, 1 and $10\,\mathrm{cm}^{-3}$.

We now estimate the amount of thermal bremsstrahlung radiation from the evolved SNR. For a density of $n \approx 1$ cm^{-3} and a temperature $T \approx 10^4$ K, thermal bremsstrahlung provides 10% of the energy ($\varepsilon_{1\mathrm{GHz}} \approx 10^{-39}$ ergs cm^{-3} sec^{-1} Hz^{-1}) at 1 GHz produced by the synchrotron mechanism at that frequency. We argue that thermal bremsstrahlung emission should represent a significant portion of the total radiation produced by SNRs. To illustrate this point, in Fig. 1 we have plotted the ratios of the thermal bremsstrahlung emissivity $\epsilon_{\mathrm{therm}}$ to the synchrotron emissivity $\epsilon_{\mathrm{synch}}$ (that is, the ratio of thermal to nonthermal emission) for the evolved SNR described here as a function of temperature at a frequency of 1 GHz for a range of values of gas density (0.1, 1.0 and 10 cm^{-3}). Notice that this ratio slowly decreases with increasing temperature for each value of the gas density. The thermal bremsstrahlung luminosity of the evolved SNR at 1 GHz is $L_{1\mathrm{GHz}} = 3.4 \times 10^{22}$ ergs sec^{-1} Hz^{-1}. Note that throughout the entire radio domain, the shell of the evolved SNR is optically thin: if we assume a gas density of $n \sim 1\,\mathrm{cm}^{-3}$ and a temperature of $T \sim 10^4$ K and a spectral index $\alpha = 0.5$ and integrate over the entire radio domain (from 10^7 to 10^{11}Hz), we calculate a luminosity of $L = 2.4 \times 10^{33}$ ergs sec^{-1}. The ratio of the thermal bremsstrahlung luminosity to the synchrotron luminosity of an evolved SNR expanding into a warm and dense interstellar medium is approximately one-third: clearly, thermal emission at radio frequencies from such sources should not be neglected.

3.2. THERMAL RADIATION FROM A RELATIVELY YOUNG SNR IN THE ADIABATIC PHASE

We now consider relatively young SNRs in the adiabatic phase of evolution and estimate the amount of thermal bremsstrahlung emission expected from these sources at radio frequencies. Observations have already detected thermal bremsstrahlung absorption or emission at radio wavelengths from four relatively young SNRs: γ Cygni (Zhang et al., 1997), the Cygnus Loop (Leahy and Roger, 1998), HB21 (Zhang et al., 2002) and 3C 391 (Brogan et al., 2002). The typical diameters of these SNRs are 20 pc, the mean thicknesses of their synchrotron shells are 1 pc (that is, about 5% of the SNR diameter) and their average surface brightnesses at 1 GHz are $\sim 10^{-20}$ W m^{-2} Hz^{-1} sr^{-1}. If we consider a young SNR with these typical values for its diameter, synchrotron shell thickness and surface brightness at 1 GHz, respectively, we calculate a synchrotron emissivity of $\varepsilon_{1\mathrm{GHz}} = 1.1 \times 10^{-35}$ ergs cm^{-3} sec^{-1} Hz^{-1} . As in the case of the evolved SNR, we consider thermal bremsstrahlung emission from the young SNR in the adiabatic phase. For a density $n \approx 1\,\mathrm{cm}^{-3}$ and temperature $T \approx 10^6$ K (the electron temperature of a young SNR behind the shock wave) the emissivity of the thermal bremsstrahlung at 1 GHz is ($\varepsilon_{1\mathrm{GHz}} \approx 10^{-40}$ ergs cm^{-3} sec^{-1} Hz^{-1}). Therefore, we can neglect the thermal bremsstrahlung emissivity when compared to the synchrotron emissivity in the case of a young SNR expanding into an ambient medium with a density $n \approx 1\,\mathrm{cm}^{-3}$. However, if the young SNR evolves within a dense molecular cloud with a density $n \approx 300\,\mathrm{cm}^{-3}$ (again assuming $T \approx 10^6$K), the synchrotron emissivity and the thermal bremsstrahlung emissivity are approximately the same ($\varepsilon_{1\mathrm{GHz}} \approx 10^{-35}$ ergs cm^{-3} sec^{-1} Hz^{-1}). Therefore, a young SNR in the adiabatic phase of evolution which is expanding within a very dense medium will produce a significant amount of thermal bremsstrahlung radiation. At 1 GHz, the young SNR is optically thin for $n \sim 1000\,\mathrm{cm}^{-3}$ and $T \sim 10^6$ K and radio emission may be detected from the entire shell of the source. Significant amounts of radio and X-ray emission will not be detected from the interior of the SNR compared to the amounts of radio and X-ray emission from the relatively dense and luminous shell. Note that this medium (with $n \approx 100 - 1000\,\mathrm{cm}^{-3}$ and $T \approx 10^6$ K) is unstable, and this instability leads to a very rapid evolution by the SNR into the adiabatic phase. Furthermore, a young SNR located in a dense molecular cloud will evolve through the adiabatic phase more rapidly than an SNR expanding into a low density medium. The young SNR will also cool rapidly because the shock wave will quickly decelerate via its interaction with the very dense molecular environment. It is possible that we will detect a significant amount of thermal emission in the radio domain only in the case of young SNRs in the adiabatic stage of evolution which are located in regions of high ambient density, such as molecular clouds.

4. THERMAL RADIO EMISSION FROM SNRS AND A MODIFIED THEORETICAL $\Sigma - D$ RELATION

It is clear from the different derivations presented in Sect. 2 that values for the exponent β as determined by empirical $\Sigma - D$ relations are significantly less than values expected by theory. We argue that perhaps the empirical – theoretical inconsistency

can be at least partially explained by the omission of thermal radio emission from SNRs in derivations of theoretical $\Sigma - D$ relations. As noted before, Shklovsky (1960a) derived the $\Sigma - D$ relation (Eq. 7) directly from synchrotron radiation theory: in that derivation, the thermal emission at radio frequencies was neglected even though it probably does influence the $\Sigma - D$ relation and in this Section we will show how thermal radio emission could influence this relation. If we again derive the $\Sigma - D$ relation, this time taking into account thermal radiation from the ionized gas cloud (that is, bremsstrahlung from free electrons moving through the fields established by positively charged ions) and associate it with relations previously derived for the synchrotron mechanism, we may obtain a $\Sigma - D$ relation with a significantly reduced value for β. Discussions on the effects of thermal radio emission on the $\Sigma - D$ relation have already been presented by Urošević et al. (2003ab).

The addition of the bremsstrahlung and synchrotron emissivities (that is, $\varepsilon_{\nu,\mathrm{therm.}} \propto R^{\theta_1}$ and $\varepsilon_{\nu,\mathrm{synch.}} \propto R^{-\theta_2}$, where θ_1 and θ_2 are constants which represent the thermal and synchrotron components of the exponent θ in the $\Sigma - D$ relation, respectively) is complicated because the term $\theta = \theta_1 - \theta_2$ cannot be calculated analytically. If the total emissivity ε_ν is defined to be the sum of the synchrotron emissivity and the thermal bremsstrahlung emissivity (that is, $\varepsilon_\nu = \varepsilon_{\nu,\mathrm{synch.}} + \varepsilon_{\nu,\mathrm{therm.}}$) and if we consider only large radii of the expanding SNR, the total emissivity as determined only by analytic methods is dominated by one of the two emissivities rather than a combination of the two emissivities and the $\Sigma - D$ relations derived in this manner all differ very significantly from the empirical relations. Because an analytic solution does not exist, we use here an approximate method – the convolution method – to combine the two emissivities from the different emission mechanisms. In this Section, the combined emissivity that we derive through the convolution method will yield a new $\Sigma - D$ relation where the slope will be reduced and more closely approximate the empirical relations.

4.1. THE $\Sigma - D$ RELATION FOR THERMAL RADIATION FROM AN IONIZED GAS CLOUD: THE CASE OF CONSTANT TEMPERATURE

For the derivation of the $\Sigma - D$ relation based on thermal emission from an ionized gas cloud, we will apply an algorithm applied by Shklovsky (1960a) for the derivation of the relation for synchrotron emission from SNRs. Based on the theory of the bremsstrahlung radiation applied to an ionized gas cloud, we adopt a volume emissivity of the following form (Rohlfs and Wilson, 1996):

$$\varepsilon_\nu = \frac{4}{3}\frac{Z^2 e^6}{c^3}\frac{N_i N_e}{m^2}\left(\frac{2m}{\pi k T}\right)^{\frac{1}{2}} \ln\frac{p_2}{p_1}, \tag{24}$$

where T is thermodynamic temperature of the medium and N_i and N_e are the volume concentrations of the ions and electrons, respectively. The mass and charge of the electron are denoted as m and e, respectively, while Z represents the atomic number. The collision parameter p represents the shortest distance between an ion and an electron in the course of the electron's accelerated motion in the ion field. The interval (p_1, p_2) spans all of the permitted values for the collision parameter: in this case, the upper limit for p_2 corresponds to the average distance between the ions (in other

words, the Debye length) while limiting values for the parameter p_1 require quantum mechanical considerations, which are traditionally collected in the Gaunt factor. Eq. (24) is derived for interactions with large values of the collision parameter: therefore, considering the typical energy levels, interactions among the particles are weak. For this reason, bremsstrahlung theory has been developed for straight-line motion of the electron in the ion field where the parameter p represents the shortest distance between interacting particles. The $\Sigma - D$ relation derived under these circumstances is applicable for diffuse media where the particles are far away from each other and the energy change of the accelerated particles is small.

We assume that the temperature and density of the particles does not change with changing distance from the center of the object. This is consistent with the model for the hot interstellar medium (HIM) described by McKee and Ostriker (1977) and therefore the collision parameter is independent of the radius. From Eqs. (3) and (24), we obtain

$$\varepsilon_\nu = \text{const} \quad \text{and} \quad \Sigma_\nu \propto D. \tag{25}$$

From inspection of this relation, we notice that as the size of the SNR increases, its surface brightness also increases: this result is consistent with our expectations for an optically thin medium. Urošević et al. (2003a) showed that the medium is transparent for the specific frequency used for the construction of the $\Sigma - D$ relation (that is, 1 GHz).

4.2. THE $\Sigma - D$ RELATION FOR SYNCHROTRON RADIATION AND THERMAL BREMSSTRAHLUNG RADIATION FROM AN IONIZED GAS CLOUD: THE CASE OF CONSTANT TEMPERATURE

The final result of the theory given by Shklovsky (1960a) is $\varepsilon_\nu \propto D^{-7}$. The relation presented by Shklovsky (1960a) is scaled by the maximum value $\varepsilon_{\max}$ of the emissivity of SNRs at the outset of their evolution: we can therefore express the normalized emissivity $\varepsilon_{\text{norm}}$ as

$$\varepsilon_{\text{norm}} = \frac{\zeta_1}{\varepsilon_{\max}} D^{-7}, \tag{26}$$

where ζ_1 is a constant which contains the portion of the synchrotron emissivity which does not depend on D. The maximum value of the emissivity $\varepsilon_{\max}$ corresponds to the minimum radius of the SNR ($D_{\min}$), while the minimum value of the emissivity corresponds to the maximum radius of the SNR ($D_{\max}$) which in turn corresponds to an SNR at the end of its evolution (that is, the dissipation phase). If the emissivity from Eq. (25) is convoluted with emissivity from Eq. (26), we obtain the following integral expression for ε as a function of time:

$$\varepsilon(t) = \frac{\zeta_1}{\varepsilon_{\max}} \int_{D_{\min}}^{D_{\max}} \frac{\zeta_2}{(t-D)^7} dD. \tag{27}$$

Here, ζ_2 is another constant which contains the portion of the thermal bremsstrahlung emissivity which does not depend on D. For a qualitative analysis, this integral may be approximated as

$$\varepsilon(t) \approx \frac{\zeta_3}{\varepsilon_{\max}} \int_0^{\infty} \frac{1}{(t-D)^7} dD. \tag{28}$$

Here ζ_3 is the product of the constants ζ_1 and ζ_2 and the integral is evaluated over the range of D=0 through $D = +\infty$ to describe the expansion of the SNR from very small values (nearly zero) at the beginning of the explosion to very large values (limiting case is ∞) at the end of its lifetime. This integral has the following solution:

$$\varepsilon(t) \propto \int_0^{\infty} \frac{1}{(t-D)^7} dD \propto t^{-6}. \tag{29}$$

Combining this equation and Eq. (3) gives:

$$\Sigma_\nu \propto D^{-5}, \tag{30}$$

Therefore, the introduction of the thermal component to the relation derived by Shklovsky (1960a) leads to a form of the $\Sigma - D$ relation with a significantly flatter slope.

The theoretical interpretation presented by Duric and Seaquist (1986) yields a relation for evolved SNRs in the following form: $\Sigma \propto D^{-3.5}$ ($\varepsilon_\nu \propto D^{-4.5}$). If we assume a synchrotron shell model for the SNR that is consistent with the model of McKee and Ostriker (1977) (that is, for an SNR with low density interior), the thermal flux from the low density interior can be neglected in comparison with the flux from the denser cool X-ray gas (that is, the warm medium with $T \sim 10^4$ K, $n \sim 1$ cm^{-3} located in the inner rim of shell) because the particle concentration is greater in the shell, resulting in greater efficiency in thermal radiation from the shell (Eq. 24). The convolution integral in this case is:

$$\varepsilon(t) \propto \int_0^{\infty} \frac{1}{(t-D)^{4.5}} dD \propto t^{-3.5}. \tag{31}$$

Similar to the previous convolution example, this equation becomes:

$$\Sigma_\nu \propto D^{-2.5}. \tag{32}$$

This relation has a value for β which is closest to the Galactic empirical $\Sigma - D$ relation obtained by Case and Bhattacharya (1998) ($\beta = 2.4$), once again assuming an average value of 0.5 for the spectral index α.

4.3. THE $\Sigma - D$ RELATION FOR THERMAL BREMSSTRAHLUNG RADIATION FROM AN IONIZED GAS CLOUD: THE CASE OF VARIABLE TEMPERATURE

Since the SNR is assumed to be in the adiabatic phase (*i.e.*, the SNR is cooling adiabatically as it expands), we start with the adiabatic equation, expressed as

$$TV^{\gamma-1} = const. \tag{33}$$

In the case of a spherical cloud and assuming $\gamma = \frac{5}{3}$ (*i.e.*, assuming that the gas in the SNR interior behaves like an ideal gas), we obtain the following dependence of temperature with respect to cloud radius:

$$T \propto D^{-2}. \tag{34}$$

Assuming a constant density insures that the collision parameter is independent of the radius of the cloud (once again see Eq. 24). Substituting Eq. (34) into Eq. (24), we may therefore express the emissivity as

$$\varepsilon_\nu \propto D. \tag{35}$$

According to the Eq. (3), we then have:

$$\Sigma_\nu \propto D^2. \tag{36}$$

Since it is well-known that SNRs also possess relativistic electrons which emit synchrotron radiation, we may consider these relativistic particles to derive another constraint on the dependence of emissivity on radius. If the total energy of a particle is much greater than its rest mass, the rest mass may therefore be ignored when considering the particle's total energy. Similar to the case of an ideal gas, if we neglect relativistic corrections for temperatures $T \leq 10^6$K (Rybicki and Lightman, 1979) and set $\gamma = \frac{4}{3}$, we derive the following expression for emissivity with respect to cloud radius:

$$\varepsilon_\nu \propto D^{0.5}. \tag{37}$$

Therefore, following the model presented by McKee and Ostriker (1977), these relations yield a $\Sigma - D$ relation for thermal emission from SNRs of the following form:

$$\Sigma_\nu \propto D^{1.5 \leq -\beta \leq 2.0}. \tag{38}$$

4.4. THE $\Sigma - D$ RELATION FOR SYNCHROTRON RADIATION AND THERMAL BREMSSTRAHLUNG RADIATION FROM AN IONIZED GAS CLOUD: THE CASE OF VARIABLE TEMPERATURE

In this Sect. we derive a $\Sigma - D$ relation based on the combination of synchrotron radiation and thermal bremsstrahlung radiation from an ionized gas cloud (that is, a theoretical construct for an SNR) in the case where the temperature varies throughout the cloud.

The theoretical model described by Duric and Seaquist (1986) yields a $\Sigma - D$ relation in the following form: $\Sigma \propto D^{-3.5}$ (for evolved SNRs) and $\Sigma \propto D^{-5}$ ($\varepsilon \propto D^{-6}$, for young SNRs). As in the case considered in Sect. 4.2, if we assume a shell model for the SNR we can expect thermal flux from the shell. In this case, flux from the low density interior may be neglected because the particle concentration is higher in the shell, resulting in a greater efficiency of thermal radiation from the ionized gas cloud. Relativistic particles in the shell (and probably in the X-ray emitting region) will contribute, thereby introducing the thermal component to the total emissivity as is shown in Eq. (37). The convolution integrals (in the cases of both evolved and young SNRs) are

$$\text{Evolved SNRs} \rightarrow \varepsilon(t) \propto \int_0^\infty \frac{D^{0.5}}{(t-D)^{4.5}} dD \propto t^{-3} \tag{39}$$

$$\text{Young SNRs} \rightarrow \varepsilon(t) \propto \int_0^\infty \frac{D^{0.5}}{(t-D)^{6}} dD \propto t^{-4.5} \tag{40}$$

Similar to the previous convolution, we obtain

$$\text{Evolved SNRs} \rightarrow \Sigma_\nu \propto D^{-2} \tag{41}$$

$$\text{Young SNRs} \rightarrow \Sigma_\nu \propto D^{-3.5} \tag{42}$$

If we once again assume an average spectral index for SNRs of $\alpha = 0.5$, the first relation has a value for β which is closest to the latest "shallower master" empirical $\Sigma - D$ relations (Urošević, 2002; 2003). However, the second relation yields a value for β which is closer to that derived for the very rich young radio SNR population found in M82 (Huang et al., 1994), that is $\beta = 3.4$ (Urošević et al., 2004; Arbutina et al., 2004).

The surface brightness relation given in Eq. (41) for evolved SNRs decreases with an inverse square-law dependence as the radius of the SNR increases, giving a solution for the simple spherical expansion of the SNR as the luminosity remains constant. This effect – the independence of luminosity with respect to SNR diameter – has already been noted and described by Stanković et al. (2003) and Arbutina et al. (2004). The relation $\Sigma_\nu \propto S_\nu/\theta^2$ (where θ is the angular diameter), when combined with $D \propto \theta d$ (where d is distance to the remnant) and $L_\nu \propto S_\nu d^2$ (where L_ν is the radio luminosity of the remnant per unit frequency interval), yields the following relation:

$$\Sigma_\nu \propto L_\nu D^{-2}. \tag{43}$$

In the case where luminosity is independent of radius, this relation simplifies to the relation given in Eq. (37).

5. SUMMARY

(i) We have presented a brief review of theoretical $\Sigma - D$ relations previously published in the literature: this review helps to emphasize the inconsistencies between theoretical and empirical relations.

(ii) We have considered the thermal emission from SNRs at radio frequencies and included this emission in a model of the total radio emission from an SNR. We also developed two models describing young and evolved SNRs in the adiabatic phase of evolution, both of which emit significant amounts of thermal bremsstrahlung emission at radio frequencies.

(iii) By modifying the theory presented in Sect. (2) through the introduction of the thermal bremsstrahlung mechanism to describe SNR evolution in the adiabatic phase, we have derived $\Sigma - D$ relations which are in closer agreement to the empirical results than previous theoretical models.

References

Allakhverdiyev, A.O., Amnuel, P.R., Guseinov, O.H. and Kasumov, F.K.: 1983, *Astrophys. Space Sci.*, **97**, 261.

Allakhverdiyev, A.O., Guseinov, O.H. and Kasumov, F.K.: 1986, *Astrofizika*, **24**, 397.

Arbutina, B., Urošević, D., Stanković, M. and Tešić, Lj.: 2004, *Mon. Not. R. Astron. Soc.*, **350**, 346.

Bell, A.R.: 1978a, *Mon. Not. R. Astron. Soc.*, **182**, 147.

Bell, A.R.: 1978b, *Mon. Not. R. Astron. Soc.*, **182**, 443.

Brogan, C.L., Dyer, K.K., Kassim, N.E., Lazio, J.T. and Lacey, C.K.: 2002, *Bull. Am. Astron. Soc.*, **200**, 15.04.

Case, G.L. and Bhattacharya, D.: 1998, *Astrophys. J.*, **504**, 761.

Clark, D.H. and Caswell, J.L.: 1976, *Mon. Not. R. Astron. Soc.*, **174**, 267.

Duric, N. and Seaquist, E.R.: 1986, *Astrophys. J.*, **301**, 308.

Fedorenko, V.N.: 1983, in IAU Symposium 101, Supernova Remnants and their X-ray Emission, ed. J. Danziger and P. Gorenstein, (Dordrecht: Reidel), p.183.

Green, D.A.: 1984, *Mon. Not. R. Astron. Soc.*, **209**, 449.

Green, D.A.: 1991, *Publ. Astron. Soc. Pacific*, **103**, 209.

Gull, S.F.: 1973, *Mon. Not. R. Astron. Soc.*, **161**, 47.

Huang, Y.-L. and Thaddeus, P.: 1985, *Astrophys. J.*, **295**, L13.

Huang, Z.P., Thuan, T.X., Chevalier, R.A., Condon, J.J. and Yin, Q.F.: 1994, *Astrophys. J.*, **424**, 114.

Ilovaisky, S.A. and Lequeux, J.: 1972, *Astron. Astrophys.*, **18**, 169.

Kesteven, M.J.L.: 1968, *Aust. J. Phys.* **21**, 739.

Leahy, D.A., Zhang, X., Wu, X. and Lin, J.: 1998, *Astron. Astrophys.*, **339**, 601.

Leahy, D.A. and Roger, R.S.: 1998, *Astrophys. J.*, **505**, 784.

Lequeux, J.: 1962, *Ann. d'Astrophys.* **25(4)**, 221.

McKee, C.F. and Ostriker, J.P.: 1977, *Astrophys. J.*, **218**, 148.

Milne, D.K.: 1970, *Aust. J. Phys.* **23**, 425.

Poveda, A. and Woltjer, L.: 1968, *Astron. J.*, **73(2)**, 65.

Rohlfs, K. and Wilson, T.L.: 1996, Tools of Radio Astronomy (second completely revised and enlarged edition), Springer, Heidelberg.

Routledge, D., Landecker, T.L. and Vaneldik, J.F.: 1986, *Mon. Not. R. Astron. Soc.*, **221**, 809.

Rybicki, G.B. and Lightman, A.P.: 1979, Radiative Processes in Astrophysics, John Wiley and Sons, New York.

Sakhibov, F.Kh. and Smirnov, M.A.: 1982, *Pis'ma Astron. Zh.*, **8**, 281.
Sedov, L.I.: 1959, Similarity and Dimensional Methods in Mechanics, Academic Press, New York.
Shklovsky, I.S.: 1960a, *Astron. Zh.*, **37(2)**, 256.
Shklovsky, I.S.: 1960b, *Astron. Zh.*, **37(3)**, 369.
Spoelstra, T.A.Th.: 1972,*Astron. Astrophys.*, **21**, 61.
Stanković, M., Tešić, Lj. and Urošević, D.: 2003, *Publ. Astron. Obs. Belgrade*, **75**, 71.
Urošević, D.: 2002, *Serb. Astron. J.* **165**, 27.
Urošević, D.: 2003, *Astrophys. Space Sci.*, **283**, 75.
Urošević, D., Duric, N. and Pannuti, T.G.: 2003a, *Serb. Astron. J.* **166**, 61.
Urošević, D., Duric, N. and Pannuti, T.G.: 2003b, *Serb. Astron. J.* **166**, 67.
Urošević, D., Pannuti, T.G., Duric, N. and Theodorou, A.: 2004, *Astron. Astrophys.*, submitted.
van der Laan, H.: 1962, *Mon. Not. R. Astron. Soc.*, **124**, 125.
Zhang, X., Zheng, Y., Landecker, T.L. and Higgs, L.A.: 1997, *Astron. Astrophys.* , **324**, 641.
Zhang, X.Z., Qian, S.J., Higgs, L.A., Landecker, T.L. and Wu, X.J.: 2002, *Astrophys. Space Sci.*, **279**, 355.

Proc. IV Serbian-Bulgarian Astronomical Conference,
Belgrade 21–24 April 2004,
eds. M. S. Dimitrijević, V. Golev, L. Č. Popović, M. Tsvetkov,
Publ. Astron. Soc. "Rudjer Bošković" No 5, 2005, 131 - 133 *Contributed paper*

CCD OBSERVATIONS OF SOLAR SYSTEM BODIES FROM BELGRADE ASTRONOMICAL OBSERVATORY

Vl. BENISHEK and V. PROTITCH – BENISHEK
Astronomical Observatory, Volgina 7, 11160 Belgrade 74, Serbia
E–mail vprotitch@aob.bg.ac.yu
E–mail vlaben@yahoo.com

Abstract. Possibilities of "small instruments" with new CCD devices have been discussed as well as the corresponding observational programs on Belgrade Observatory and their improvements with new instruments.

The exceptional success of the Hipparchos Mission and the start of new cosmic programmes such as DIVA, SIM, GAIA, FAME, etc, make the sense and development of terrestrial investigations performed with optical instruments narrower and narrower. In this connection especially the importance of "small instruments" is diminished and as such all instruments with objective diameter less than 1 m are thought. In more rigorous considerations telescopes under 2 m are viewed as "small-dimension" devices. Nevertheless, the case of a majority of observatories all over the world is that instruments under 1 m are still used, but the scientific programmes are aimed at complementing the basic actions carried out actually with telescopes of all essentially large observatories all over the world.

For instance, in the framework of the IAU there is a working group for "Future Development of Ground-Based Astrometry" which has indicated the main possibilities of using "small telescopes" in the future observations of exceptional astrometric importance. This especially concerns the detection of all astronomical phenomena having a higher scientific importance over long time intervals and where the results are still indispensable in the developing of theoretical models and analysing of their dynamical parameters. Observations of Solar-System minor bodies have grown in their importance during the last two decades, besides all Near Earth Objects and those concerning natural satellites of major planets, to be added astrometric and astrophysical observations of comets and observing of extragalactic radio sources aimed at redefining of optical and radio reference networks in the connections of extending the Hipparchos Catalogue towards fainter objects.

Some observing programmes are aimed at correcting of the dynamical parameters for Solar-System minor bodies with respect to ICRF, as well as at improving the mass values for these objects. The search for a transneptunian population, asteroids, binary and multiple stars, variable stars, extrasolar planets, etc is also actual.

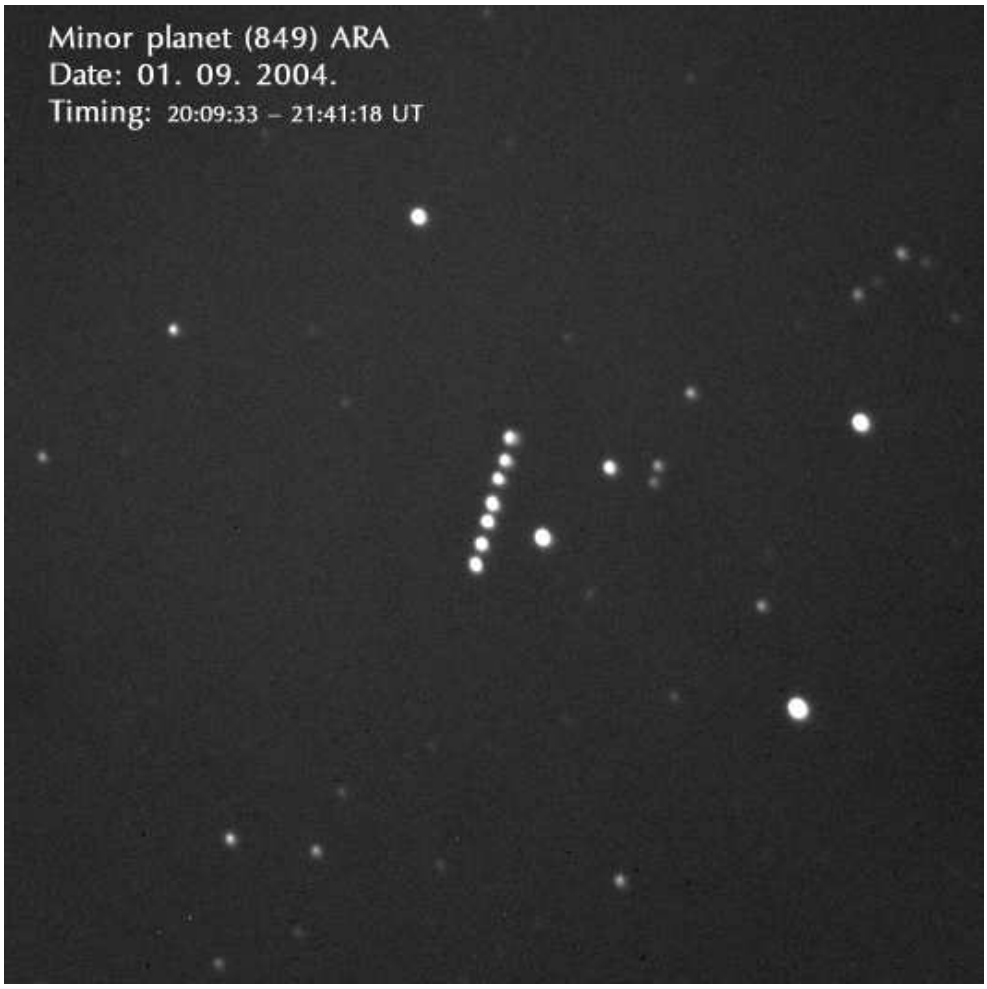

Figure 1: Picture of the globular stellar cluster M 13 obtained by the new instrument.

During the last twenty years an exceptional technological revolution took place in the developing of new CCD detectors which have found application in many sciences, especially in astronomy.

The development of these devices has been followed by a corresponding evolution of hardwares, softwares and programming packets, all of this in order to make the treament of observational material as rapid and efficient as possible.

The Astronomical Observatory in Belgrade has a relatively long and non- interrupted tradition in discovering and observing minor Solar-System bodies - as early as from the distant 1935 - almost over full 70 years.

The first CCD observations were initiated in 1994: a CCD SBIG ST - 6 camera was mounted on the Zeiss 65/1055 cm Refractor and in July in the same year the

disruption of Shoemaker-Levy 9 comet and the falling of its fragments onto Jupiter was observed. During the systematic observation of this exceptionally rare phenomenon by applying the new technique, from Belgrade Observatory, 233 CCD successful records were obtained by L. Č. Popović.

Within the framework of the research project "Positions and Motion of Solar-System Minor Bodies" the following observational activity is carried out:

: follow up of minor planets, especially for the NEO asteroids and objects of unusual dynamical characteristics

: keeping under observations of new and periodic comets

: observations of major planets and their satellites

: participation in international observing campaigns concerning Solar and Lunar eclipses, transits of inner planets across the Solar disc, occultations of stars by the Moon, minor planets and comets, mutual occultations and eclipses among the satellites of Saturn and Jupiter, etc.

The observations done at the Observatory with instruments of relatively modest dimensions have been improved due to the successive use of CCD cameras **SBIG ST 6, ST 7, ST 8** in this decade and during the last two years camera **APOGEE AP 47p 1056 × 1020 pxs (13 × 13 microns).** This camera, having exceptionally good performances when recording of back illuminated objects is the case, combined with an astrograph yields a field of 36.9 × 35.6 arc minutes, i. e. of 4.4 × 4.3 arc minutes in the case of the Zeiss Refractor. Besides, the high quantum efficiency of this camera (90%) contributes significantly to the quality of the obtained images and to the number of objects detectable from the Observatory. The faintest object taken with the Zeiss Astrograph and this camera was a minor planet with an apparent magnitude of **17.2**!

Recently, we expect the new instrument Meade 16" LX 200GPS-SMT fully automatized, which will be used for improved astrometrical work of NEAs as well as for precise photometry of Solar system bodies and stellar systems.

**Proc. IV Serbian-Bulgarian Astronomical Conference,
Belgrade 21–24 April 2004,
eds. M. S. Dimitrijević, V. Golev, L. Č. Popović, M. Tsvetkov,
Publ. Astron. Soc. "Rudjer Bošković" No 5, 2005, 135 - 138** *Contributed paper*

STARK BROADENING PARAMETERS OF THREE O II LINES

S. BUKVIĆ, A. SREĆKOVIĆ and S. DJENIŽE

*Faculty of Physics, University of Belgrade,
Studentski trg 14, 11000 Belgrade, P.O.B. 368, Serbia
E–mail ebukvic@ff.bg.ac.yu*

Abstract. Stark widths and shifts of 3 singly ionized oxygen (O II) spectral lines (327.0856 nm, 327.3434 nm and 327.7561 nm) in the 3p ^{2}F^o- 4s ^{2}D^0 and 3p ^{4}P^o- 4s ^{4}P transitions have been measured in a linear, low-pressure, pulsed arc discharge operated in helium-oxygen mixture (1: 1.1) at a 26 000 K electron temperatures and 1.1 10^{23} m^{-3} electron density. The Stark widths of these lines are the first measured values. The Stark shift of the 327.7561 nm is also the first measured value.

1. INTRODUCTION

The spectral lines of the singly ionized oxygen (O II) are of a great interest in the astrophysical plasma diagnostics (Finn et al., 2004; Kobulnicky and Phillips, 2003, as recent examples). At the electron densities (N) higher than 10 ^{21} m^{-3} the Stark broadening begins to play an important role in the O II line shapes and line center position formation. Thus, the knowledge of the Stark width (FWHM, full-width at half intensity maximum, W) and shift (d) are of an interest. We have measured Stark widths (W) and shifts (d) of 3 singly ionized oxygen (O II) spectral lines (327.0856 nm, 327.3434 nm and 327.7561 nm) in the 3p ^{2}F^o- 4s ^{2}D^0 and 3p ^{4}P^o – 4s ^{4}P transitions in a linear, low-pressure, pulsed arc discharge operated in helium-oxygen mixture (1: 1.1) at a 26 000 K electron temperatures and 1.1 10^{23} m^{-3} electron density. The Stark widths of these lines are the first measured values. The Stark shift of the 327.7561 nm is also the first measured value.

2. EXPERIMENT

The linear pulsed arc, used as plasma source, was described in detail in our previous publications (Djeniže et al., 1992; 2002; Srećković et al., 2001). Thus, only a few details will be given here. A pulsed discharge was occurred in a Pyrex discharge tube of 5 mm inner diameter and had plasma length of 14 cm. The tube had quartz windows. The working gas was helium-oxygen mixture (1: 1.1) at 267 Pa filling pressure with constant flux flowing regime (10 ml/min). A capacitor of 14 μF was charged up to 1.5 kV. Spectroscopic observations of isolated spectral lines were made end-on along the axis of the discharge tube. The complete experimental procedure

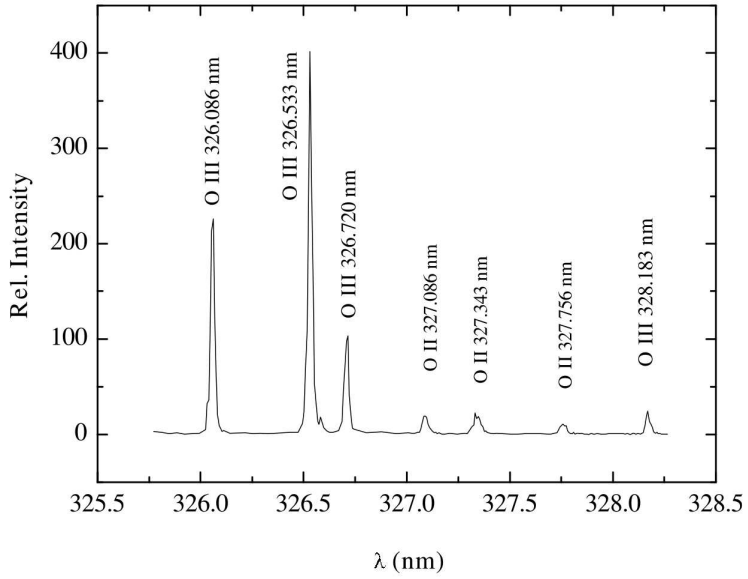

Figure 1: Recorded spectrum with investigated O II lines.

is described in Djeniže et al. (2002). Recorded spectrum, with the investigated O II lines, is presented in Fig. 1.

The plasma parameters are obtained using known diagnostics methods. The electron temperature (T) was determined from the ratios of the relative intensities of the 326.0857, 326.5329 and 326.7204 nm O III to 327.0856, 327.3434 and 327.7561 nm O II spectral lines, assuming the existence of LTE, with an estimated error of ± 6%. The necessary atomic data were taken from Wiese et al. (1966) and NIST (2000).

The electron density (N) was measured using a well-known single laser interferometry technique (Ashby et al., 1965) for the 632.8 nm He-Ne laser wavelength with an estimated error of ± 7%.

3. STARK WIDTHS MEASUREMENTS

The measured profiles were of the Voigt type due to the convolutions of the Lorentzian Stark and Gaussian profiles caused by Doppler and instrumental broadening. For the electron density and temperature in our experiments the Lorentzian fraction was dominant. Van der Waals (Griem, 1974) and resonance (Griem, 1974) broadening were estimated to be smaller by more than one order of magnitude in comparison to Stark, Doppler and instrumental broadening. The standard deconvolution procedure (Davies and Vaughan, 1963) was applied using the least square-algorithm. The absence og the self-apsorption was checked using a method described in Djeniže and Bukvić, (2001). The Stark widths were measured with ± 12% error at a given N and T.

4. STARK SHIFTS MEASUREMENTS

The Stark shifts were measured relative to the unshifted spectral lines emitted by the same plasma using a method established and applied as first by Purić and Konjević (1972). According to this method the Stark shift of a spectral line can be measured experimentally by evaluating the position of the spectral line center (X_C) recorded at two different electron density values during plasma decay. In principle, the method requires recording of the spectral line profile at high electron density (N_1) that causes an appreciable shift and then later when the electron concentration has decreased to a value (N_2) lower by at last an order of magnitude. The difference of the line center positions in these two cases is Δd, so that the shift d_1 at the higher electron density N_1 is

$$d_1 = N_1 \Delta d/(N_1 - N_2). \quad (1)$$

Our Stark shift values have been obtained for line center positions corresponding to the 18^{th} μs and 45^{th} μs after the beginning of the discharge. The Stark shift data are corrected for the electron temperature decay (Popović et al., 1992). The Stark shifts were measured with a $\pm$ 0.6 pm error at a given N and T.

5. RESULTS AND DISCUSSION

Measured Stark FWHM (W_m) and shift (d_m) values at various electron temperatures (T) and densities (N) together with other authors data are given in Table 1.

Table 1: Measured Stark FWHM (W_m) and shift (d_m) values at various electron temperatures (T) and densities (N) together with other authors data. The letters **a** and **b** denote results in this work and from Djeniže at al. (1991), respectively.

Ion	Transition	Multiplet	λ (nm)	T (10^4 K)	N (10^{23} m^{-3})	W$_m$ (pm)	d$_m$ (pm)	Ref.
O II	$2p^2 3p$ - $2p^2(^1D)$ 4s	$^2F^o - ^2D$ (39)	327.0856	2.60	1.10	23.9	-	a
				6.00	0.81	-	2.0	b
			327.3434	2.60	1.10	23.3	1.1	a
	$2p^2 3p$ - $2p^2(^2P)$ 4s	$^4P^o - ^4P$ (23)	327.7561	2.60	1.10	23.7	1.0	a

6. CONCLUSION

Our W data are the first measured values for mentioned O II lines. It turns out that the previously published d value (Djeniže et al., 1991) of the 327.0856 nm O II line have also positive sign.

Acknowledgements

This work is supported by the Ministry of Science and Environment Protection of the Republic of Serbia.

References

Ashby, D.E.T.F., Jephcott, D.F., Malaein, A. and Raynor, F.A.: 1965, *Appl. Phys.*, **36**, 29.
Davies, J.I. and Vaughan, J.M.: 1963, *Astrophys. J.*, **137,** 1302.
Djeniže, S. and Bukvić, S.: *Astron. Astrophys.*, **365**, 252.
Djeniže, S. Srećković, A., Jelisavčić, M. and Bukvić, S.: 2002, *Astron. Astrophys.*, **389**, 1086.
Djeniže, S., Srećković, A., Labat, J., and Platiša, M.: 1991, *Z. Phys.* D, **21**, 295.
Djeniže, S., Srećković, A. and Labat, J.: 1992, *Astron. Astrophys.*, **253**, 632.
Finn, R.A., Zavitsky, D. and McCarthy, D.W.Jr.: 2004, *Astrophys. J.*, **604**, 141.
Griem, H.R.: 1974, Spectral Line Broadening by Plasmas, Academic Press, New York.
Kolulnicky, H.A. and Phillips, A.C.: 2003, *Astrophys. J.*, **599**, 1031.
Lesage, A. and Fuhr, J.R.: 1999, Bibilography of Atomic Line Shapes and Shifts, (April 1992 through June 1999), Observatoire de Paris.
NIST: 2002, Atomic Spectra Data Base Lines `http//nist.physics.nist. Gov.`
Popović, L.Č., Srećković, A. and Djeniže, S.: 1992, Proceed. of the 11^{th} ICSLS, **A25**, Carry de Rouet, France.
Purić, J. and Konjević, N.: 1972, *Z. Physik*, **249**, 440.
Srećković, A., Drinčić, V., Bukvić, S. and Djeniže, S.: 2001, *Phys. Scripta*, **63**, 306.

Proc. IV Serbian-Bulgarian Astronomical Conference,
Belgrade 21–24 April 2004,
eds. M. S. Dimitrijević, V. Golev, L. Č. Popović, M. Tsvetkov,
Publ. Astron. Soc. "Rudjer Bošković" No 5, 2005, 139 - 143 *Contributed paper*

PROBLEM OF CROSS-IDENTIFICATION OF POINT SOURCES

G. DAMLJANOVIĆ
Astronomical Observatory, Volgina 7, 11160 Belgrade 74, Serbia
E–mail gdamljanovic@aob.bg.ac.yu

Abstract. At the Belgrade Astronomical Observatory (AOB) an original programme for the cross – identification of the point sources of any two catalogues with enough data is developed. As an example the results of the cross – identification between HIPPARCOS (HIgh Precision PARallax COllecting Satellite) and 2MASS (Two Micron All Sky Survey) is presented. The programme is based on the 3σ rejection criterion and it is adequate for the cross – identification of new catalogues of millions of stars. In the basic selection of the example there were 117 955 HIPPARCOS stars and 162 195 232 2MASS Second Incremental Data Release ($\sim$ 47% of the sky) ones, and it was found a big amount of common stars by using only the data of catalogues. In the second step, the preliminary calculated systematic error (near $0.''10$) of differences $\Delta\alpha$ and $\Delta\delta$ of detected common stars was included into the programme, and the new result of the cross – identification was significantly better. This paper is the part of nowadays efforts to link big stellar catalogues in the visiblly, infrared and other wavelengths to the ICRF (International Celestial Reference Frame).

1. INTRODUCTION

After a decision of the IAU (International Astronomical Union) General Assembly (Kyoto, 1997) the ICRF was adopted to materialize the ICRS (International Celestial Reference System) from the beginning of 1998. The HIPPARCOS Catalogue (ESA 1997) is considered as the primary optical counterpart of the ICRF from 1997.

The ICRF is based on a catalogue of 608 compact radio sources (Ma et al., 1998) which are determined with an internal precision of 0.3 to 0.5 mas (milliarcsecond). It has been updated recently by the ICRF – Ext.1, which includes 59 new sources (IERS Annual report 1999).

The HIPPARCOS contains near 118 000 stars. They are brighter than magnitude 12 and mostly range between $V = 7$ and $V = 9$. It is far too restricting nowadays when searching reference stars for astrometric calibration. The mean density is less than 3 stars/square degree. It is not enough to insure a suitable astrometric reduction in the case of observations carried out in small fields with CCD detectors. Therefore it is necessary to produce large stellar catalogues with fainter sources (in the visible and in the infrared) and linked to the ICRF. The HIPPARCOS stars positions and proper motions are bases of the optical frame HCRF (Hipparcos Celestial Reference Frame). The HIPPARCOS Catalogue gives for each object: the position with an accuracy of the order of 1 mas at the epoch of the catalogue 1991.25, the proper

motions in $\mu_\alpha \cos\delta$ and μ_δ with a standard error of about 1 mas/yr, and very large number of other parameters.

There are various recent catalogues useful for the densification of the ICRF, at optical and other wavelengths (infrared, radio, X, etc.): the Tycho-2 Catalogue, the USNO CCD Astrograph Catalogue (UCAC), the 2MASS, DENIS (Deep Near Infrared Survey of the Southern Sky), etc. The 2MASS is the project of the near infrared sky which is based on two highly automated 1.3 m telescopes for both hemispheres, equipped with a three channel camera. The sky was observed simultaneously at J (1.25 microns), H (1.65 microns) and K_S (2.17 microns).

The 2MASS Second Incremental Data Release includes a Point Source Catalogue (PSC), with positions and photometry for 162 213 354 sources, an Extended Source Catalogue (XSC) with positions and photometry in the three survey band passes for 585 056 objects and an Atlas Images (1 897 017 FITS images in the three survey bands). The 2MASS catalogue was a joint project between the University of Massachusetts and the Infrared Processing and Analysis Center California Institute of Technology (Cutri et al., 2001), with observing facilities at Mt. Hopkins – AZ for the northern hemisphere and Cerro Tololo – Chile for the southern one. The 2MASS telescopes maped the sky by using a freeze – frame scanning technique, and operated by the Smithsonian Astrophysical Observatory (SAO) and the National Optical Astronomy Observatories (NOAO). The 2MASS was formed by the National Aeronautics and Space Administration (NASA) and the National Science Foundation (NSF).

The PSC of the 2MASS Second Incremental Data Release has been divided onto 49 right ascension segments, $0^h \leq \alpha < 24^h$, ordered by increasing declination within each segment. The data are covering 19 681 square degrees, which means about 47% of the sky. The relevant observations were carried out between 1997 June 7^{th} and 1999 February 20^{th} (329 northern and 239 southern nights with at least one photometric period). The magnitude limits are: 15.8 mag for J band, 15.1 mag for H one, and 14.3 mag for K_S one. The final 2MASS catalogues contain about 470 million stars and 1.6 million galaxies. The positions are accurate to $< 0.''2$, and α and δ done for J2000. Each star has got the epoch of observation. The positions of the 2MASS sources are correlated with the ACT or USNO-A optical catalogues, and are tied to the ICRS via the ACT Reference Catalogue. Some positional solution may have a random walk as much as $1.''0$ from the ICRS frame. About 77% of the PSC objects have $|b| < 20^o$ (the majority of point sources are concentrated towards the Galactic plane). Some data from the ACT (Urban et al., 1998) or USNO-A catalogues are included in the 2MASS PSC records, but these are not identifications between the infrared and optical sources. These are only associations, and the optical associations for the 2MASS sources are found using a simple closest positional algorithm. The astrometric accuracy of 2MASS PSC was reached via the comparison of the positions of stars in the PSC with those in the Tycho-2 and UCAC catalogues (which are not used in 2MASS position reconstruction). The accuracy of 2MASS positions is on line with the number and distribution of ACT astrometric reference stars in each tile.

As the example, the author did the cross – identification of HIPPARCOS – 2MASS PSC stars. The cross – identification results, based on the programme of 3σ criterion, are hopeful for similar jobs of the cross – identification of new big stellar catalogues.

2. THE CROSS – IDENTIFICATION PROGRAMME

The cross – identification programme is explained via the example HIPPARCOS – 2MASS. The rejection criterion was set to a 3σ value. The 2MASS PSC positions comparison was made with respect to the positions given by the HIPPARCOS Catalogue. The mean density of HIPPARCOS Catalogue is about 3 stars/sq.deg., while 2MASS one is near 8 242 stars/sq.deg. The cross – identification programme passed through each of 49 segments adopted for 2MASS, and made it only into 3^m long α respective segments (not across the all celestial HIPPARCOS sphere for each 2MASS star). It was made the matrix with the information about the 3^m segments locations for the HIPPARCOS Catalogue and that 3^m segments of α are changeable in the programme (can be longer or shorter in line with the information of errors of positions). In that way, for a suitable limited HIPPARCOS zone of the sky, each 2MASS star was compared with some numbers of HIPPARCOS ones. The identification was considered as effective when the HIPPAROCS star could be coupled to only one 2MASS star within a 3σ vicinity in both coordinates (α and δ).

The method was tested before the beginning of the cross – identification programme. It was done inside a very small part of the sky including just few HIPPARCOS known stars to check the quality of the results. After that, the programme was ran within the 49 mentioned 2MASS segments. Some stars were without enough data and these stars were removed before beginning the cross – identification programme. Therefore 18 122 stars, which represent about 0.01% of the 2MASS PSC were removed from this catalogue. In a similar way, 263 stars were removed from the HIPPARCOS Catalogue (about 0.22%), because of the absence of the proper motion data. Finally, there were 117 955 HIPPARCOS stars for the cross – identification.

For each star, the standard deviation σ was calculated, both in the α direction and in the δ one, respectively σ_α and σ_δ, by using HIPPARCOS and 2MASS data. There were enough data to do it. The calculated value of σ_α (and σ_δ) depends of few parts, $\sigma_\alpha^2 = \sigma_{\alpha 1}^2 + \sigma_{\alpha 2}^2 + \sigma_{\alpha 3}^2 + ...$ (and $\sigma_\delta^2 = \sigma_{\delta 1}^2 + \sigma_{\delta 2}^2 + \sigma_{\delta 3}^2 + ...$). The values $\sigma_{\alpha 1}$ and $\sigma_{\delta 1}$ are on line with the standard errors of the HIPPARCOS positions, and calculated by using the HIPPARCOS data. The values $\sigma_{\alpha 2}$ and $\sigma_{\delta 2}$ are on line with the observational epochs difference between HIPPARCOS and 2MASS (both catalogues data) and the errors of proper motions $\mu_\alpha \cos\delta$ and μ_δ (from HIPPARCOS data). The values $\sigma_{\alpha 3}$ and $\sigma_{\delta 3}$ are on line with the position error ellipse, and calculated by using the 2MASS data.

The epoch of HIPPARCOS observations is 1991.25, and each star of 2MASS PSC has its own epoch of observation. Because of it, it was necessary to take into account the standard error rate for the proper motions influence by using the values of $\mu_\alpha \cos\delta = \mu_{\alpha *}$, μ_δ and the epoch differences t (in years). Therefore, the positions in both catalogues are on line with J2000.0 epoch. Before carrying out the cross – identification programme by using $3\sigma_\alpha$ rejection threshold in the α direction and $3\sigma_\delta$ one in the δ one, the author took into account the changes of the HIPPARCOS coordinates α_H and δ_H due to the epoch differences t (in years) by using the HIPPARCOS proper motions $\mu_{\alpha *}$ and μ_δ: $\alpha_{Hipp} = \alpha_H + \mu_{\alpha *} t / \cos\delta$ and $\delta_{Hipp} = \delta_H + \mu_\delta t$, where α_{Hipp} and δ_{Hipp} are at the epoch of 2MASS observations. The cross – identification programme

identifies the common star if its position satisfies $\alpha_{Hipp} - \alpha_{2MASS} = \Delta\alpha < 3\sigma_\alpha$ and $\delta_{Hipp} - \delta_{2MASS} = \Delta\delta < 3\sigma_\delta$.

It was found 37 940 common stars, which represents about 32.2% of the 117 955 HIPPARCOS stars in our basic selection. Because of the fact that the 2MASS Second Incremental Data Release covers about 47% of the sky, this means that the cross – identification programme is near 70% successful. If the systematic error between HIPPARCOS and 2MASS coordinates is less than 0."1 (in line with the author preliminary investigations about the systematic discrepancies of HIPPARCOS-2MASS coordinates), and put it into the programme, it is possible to reach near 80 % of common stars.

Only two unsuccessful cross – identifications (of 37 940 common stars) have been found: each of the HIPPARCOS stars H16658 and H85045 can be associated with two 2MASS objects. In the HIPPARCOS Catalogue, the star H16658 is noted as a single star, but the star H85045 is noted as a double star (WDS17229+1628, J1248 AB). From the results presented here, both H16658 and H85045 are close double stars, or maybe the star H16658 is not double, but there is another one with close coordinates.

3. CONCLUSION

In this paper, only two unsuccessful cross – identifications of 37940 detected common stars have been found. These two cases are close double stars or just near each other on the sphere: H85045 is already marked as a double star (WDS17229+1628), H16658 is marked as the single star in the HIPPARCOS Catalogue. For these kinds of cases it is necessary to include the cross – identification part with photometric data into the programme.

The cross – identification of HIPPARCOS – 2MASS stars are presented by using the programme based on the 3σ criterion and the information of the positions of stars, the proper motions, etc. It is on line with the similar actions about the cross – identifications of new catalogues of millions stars.

Acknowledgements

This publication makes use of data products from the Two Micron All Sky Survey, which is a joint project of the University of Massachusetts and the Infrared Processing and Analysis Center/California Institute of Technology, funded by the National Aeronautics and Space Administration and the National Science Foundation. The author performed his work as a part of the Projects "Structure, Kinematics and Dynamics of the Milky Way" and "Investigation of Double and Multiple Stars" supported by the Ministry of Science and Technology od Serbia.

References

Cutri, R.M., Skrutskie, M.F., Van Dyk, S., Chester, T., Evans, T., Fowler, J., Gizis, J., Howard, E., Huchra, J., Jarrett, T., Kopan, E.L., Kirkpatrick, J.D., Light, R.M., Marsh, K.A., McCallon, H., Schneider, S., Stiening, R., Sykes, M., Weinberg, M., Wheaton, W.A., Wheelock, S.: 2001, Explanatory Supplement to the 2MASS Second Incremen-

tal Data Release, University of Massachusetts and the Infrared Processing and Analysis Center/California Institute of Technology, NASA and NSF.
ESA: 1997, The Hipparcos and Tycho Catalogues, ESA SP-1200.
International Earth Rotation Service (IERS): 1999, Annual Report 1999, Observatoire de Paris.
Ma, C. et al.: 1998, *Astron. J.*, **116**, 516.
Urban, S.E., Corbin, T.E., Wycoff, G.L.: 1998, *Astron. J.* **115**, 2161.

Proc. IV Serbian-Bulgarian Astronomical Conference,
Belgrade 21–24 April 2004,
eds. M. S. Dimitrijević, V. Golev, L. Č. Popović, M. Tsvetkov,
Publ. Astron. Soc. "Rudjer Bošković" No 5, 2005, 145 - 152 *Contributed paper*

KINEMATICS OF TWO ERUPTIVE PROMINENCES

M. DECHEV, P. DUCHLEV, K. KOLEVA, J. KOKOTANEKOVA and N. PETROV
Institute of Astronomy, 72, Tsarigradsko Shaussee Blvd., Sofia, Bulgaria
E–mail mdechev@astro.bas.bg

Abstract. In this paper we study the kinematics and evolution of two eruptive prominences (EPs), observed on May 8, 1979 and on May 5, 1980 in Astronomical Observatory of Wroclaw University, Poland. The EPs are typical representatives of two basic types of eruption (type I constant velocity and acceleration, type II acceleration, constant velocity and deceleration). Both velocity and acceleration are measured in all stages of the eruption. We show that there are essential differences between the final stages of these eruptive events. The kinematic differences between EPs are discussed in point of view of the temporal evolution of the topological by different parts in the erupting huge magnetic system. We suggest that the change of energy of twisting or untwisting of a helical magnetic structure may play important role in the observed eruptions.

1. INTRODUCTION

The quiescent prominences (QPs) as well as active region prominences (ARPs) some times undergo eruptions. A large part of the prominence material is usually lifted high into the corona during the prominence eruption and sometimes into the interplanetary space. In some eruptive events a part of the erupted matter falls back to the chromosphere (Rompolt, 1990). The time scale of the eruption is several hours and erupted matter reaches a height of several 10^5 km up to ten solar radii (Valnicek, 1968).

In the evolution of the prominence eruption the internal structure ot the prominence gradually transforms from intricate and chaotic to a simpler one, frequently characterized by helical-like patterns (Vršnak et al., 1991). These patterns indicate that the prominence could be described in cylindrical geometry as a twisted magnetic flux tube, whose footpoints are anchored in the photosphere (Vršnak, 1998). There is theoretical support for the concept that helically twisted structures are responsible for the eruption of the prominences (Hood and Priest, 1979).

In this paper we consider the evolution and kinematics of two EPs that are classical examples of two basic types of EPs (Rompolt, 1990). Here we present the results of a detailed analysis of their evolution and kinematics, as well as their comparison. We show the differences in their horizontal motions as a criterion for classification and discuss the possible importance of helical-like structures in the observed eruptions.

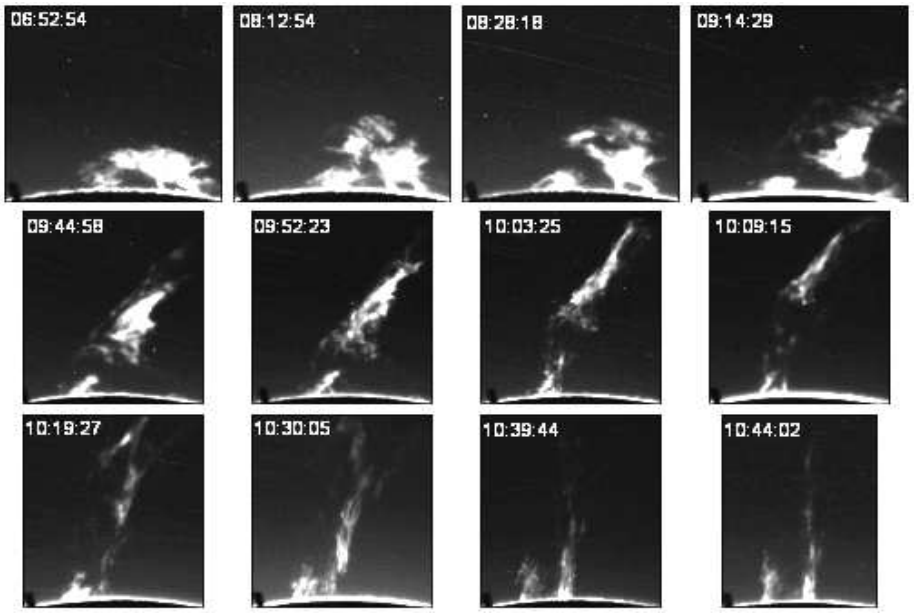

Figure 1: H_α filtergrams of EP on May 8, 1979.

2. OBSERVATIONAL MATERIAL

The eruptive prominences were observed in H_α on May 8, 1979 and on May 5, 1980, with a small coronograph at The Astronomical Observatory of Wroclaw University, Poland. All H_α plates were digitalized with the automatic Joyce-Loebl MDM6 microdensitometer at the National Astronomical Observatory Rozhen, Bulgaria.

The two-dimensional scans have a resolution of $20\mu m$ per pixel and a step of $20\mu m$ in both directions. The spatial resolution of the image (Fig. 1, Fig. 2) is a little more than 1 arcsec.

The first EP (May 8, 1979, CRN 1681) appeared on the western limb at a mean latitude of $S53°$. The prominence was observed between 06:53 UT and 11:09 UT. The prominence did not show eruption between 06:53 UT and 07:05 UT. Eruption started at 08:10 UT. In the first interval 08:10 ÷ 08:49 UT the prominence slowly rose and its morphology changed slightly. At 08:49 UT fast ascension began and EP reached maximal height, measured from the center of the solar disk, at 10:21 UT. Part of the erupted material fell back to the chromosphere after reaching maximal height.

The prominence eruption event on May 5, 1980 (CRN 1694) was observed on the western limb at a mean latitude of $N23°$. The observation had duration of 3.5 hours between 06:50UT and 10:35 UT (Fig. 2). In the interval 06:50 ÷ 09:27 UT the prominence arch slowly rose. The internal structure at that time also underwent slow variations. The start of the prominence eruption was at 10:02 UT. The prominence arch rose fist and after 10:35 UT it faded and disappeared.

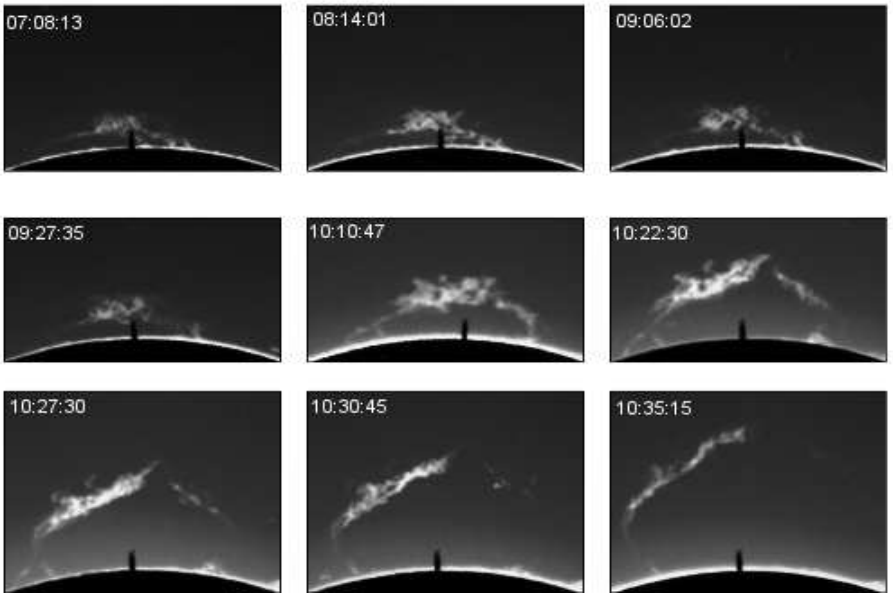

Figure 2: H_α filtergrams of EP on May 5, 1980.

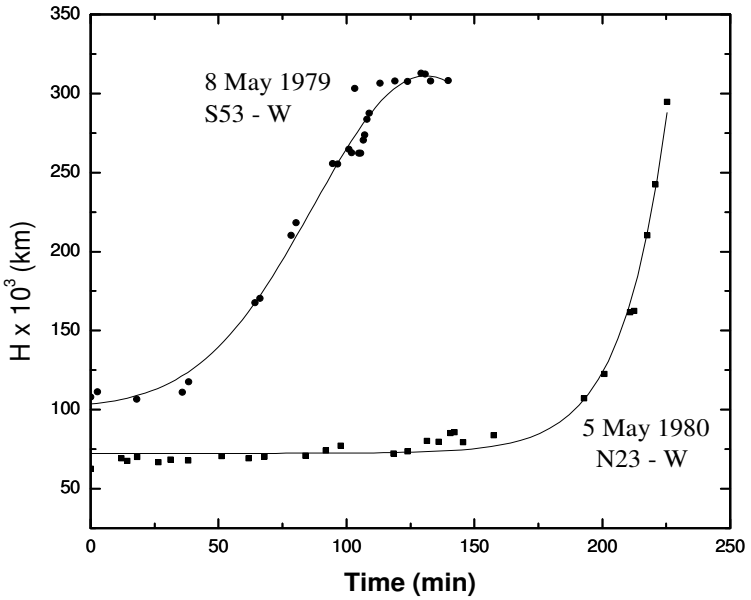

Figure 3: Prominence axis hight as a function of time for the two EPs.

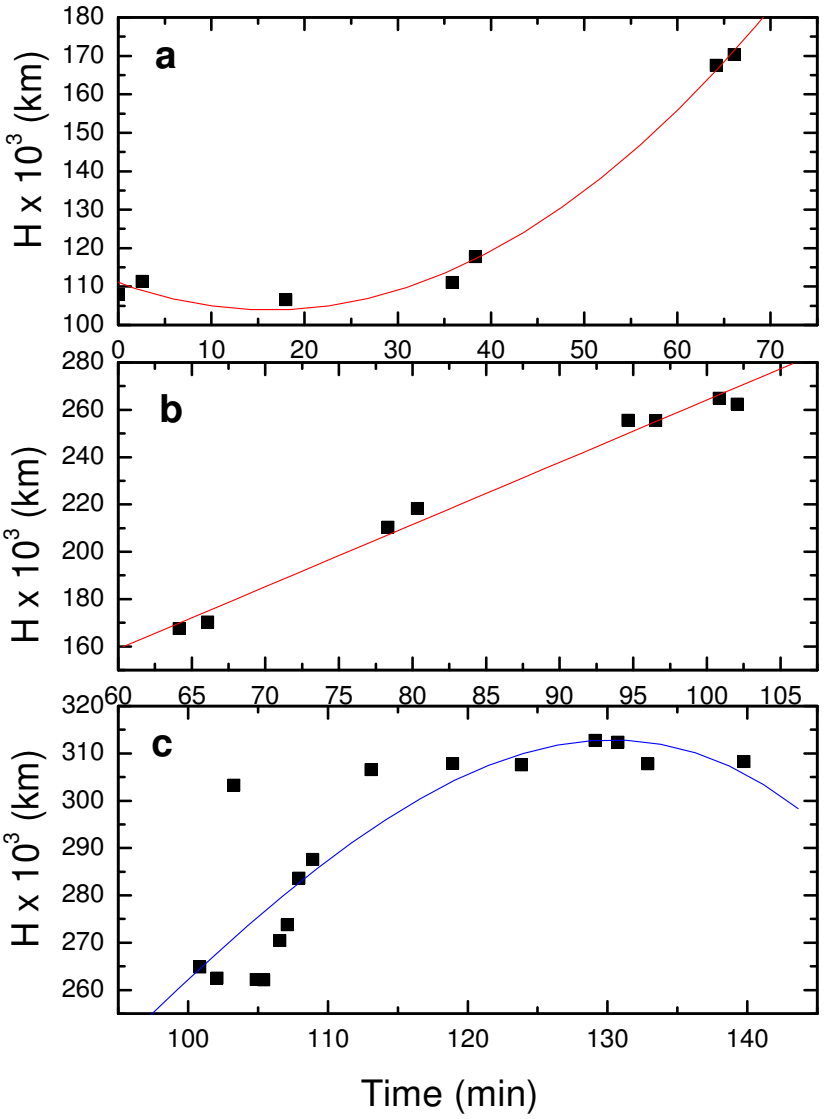

Figure 4: Height-time diagrams for three subphases of EP on May 8, 1979.

3. RESULTS AND DISCUSSION

In the Fig. 3 are presented "height-time" dependencies of the two EPs. One can see clearly the differences between the two types of EPs. EP (May 8, 1979) demonstrates three phases, which are shown in Fig. 4.

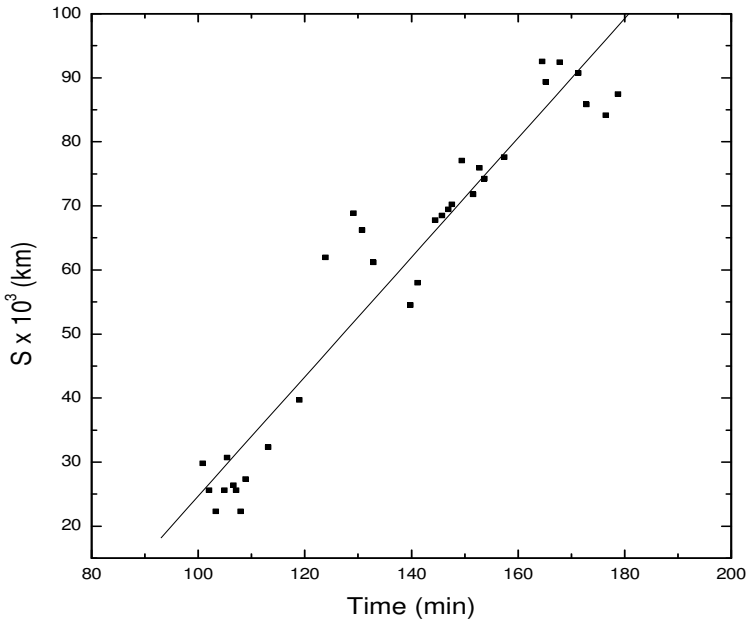

Figure 5: Horizontal expansion in EP on May 8, 1979.

The second-order polynomial fit (Fig. 4a) determines 15 m/s^2 acceleration in that phase of the eruption. In the interval 09:16 ÷ 09:56 UT EP rose with a constant velocity. To estimate the value of this velocity we use linear fit (Fig. 4b), which gives a value of 43.8 km/s. At 09:56 UT (height 106 550 km) one can observe the deceleration phase (Fig. 4c). The negative acceleration is determined by a third-order polynomial fit. The deceleration varies from -9.2 m/s^2 in the beginning of the phase to -35.5 m/s^2 just before the maximal height of 325750 km.

The H(t) of May 5, 1980 EP is shown in Fig. 3. One can see that time evolution of the eruptive event is composed of two distinctive characteristic phases: a pre-eruptive phase between 06:50 UT and 09:16 UT and an eruptive phase in the interval 09:27 ÷ 10:35 UT. The EP slowly increases its height from 65000 km to 85000 km with an average velocity of 1.8 m/s during the first phase. At 09:27 UT the prominence eruption entered in an acceleration phase. The prominence rose from 85000 km to approx. 300000 km in an interval of 70 min before disappearing and its velocity changed from 3.1 km/s to 228.8 km/s.

Beside the eruption in vertical direction the two EPs also exhibit expansion in a horizontal direction. Fig. 5 shows the horizontal expansion of the bundle feet of the EP body as a function of time. The expansion velocity, determined by a linear fit, is 15.5 km/s. It is clear that we cannot distinguish any eruption phases which are well seen in the vertical motion.

The horizontal expansion of eruptive event on May 5, 1980 is presented in the Fig. 6. The kinematic parameters are estimated by an exponential fit (95% confidential

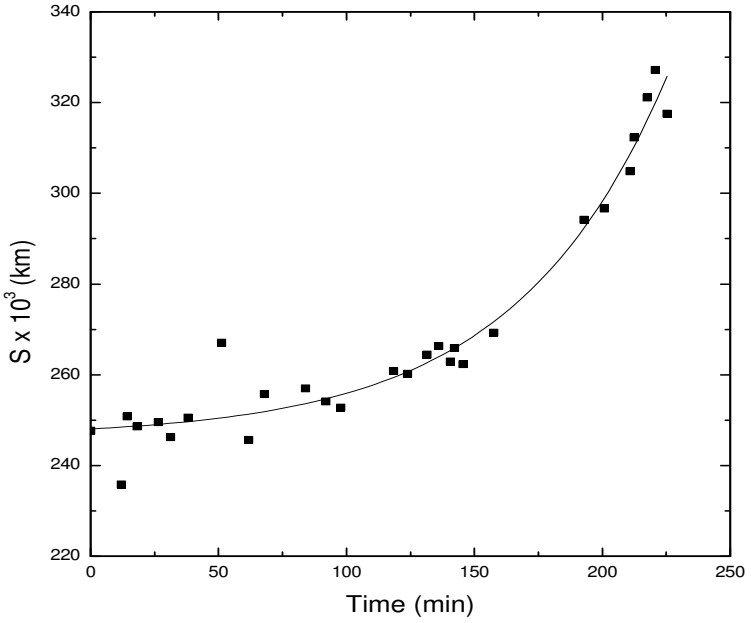

Figure 6: Horizontal expansion in EP on May 5, 1989.

probability). The results for the velocity and acceleration are presented in Fig. 7. Unlike EP type II (May 8, 1979) the eruption phases can be seen here clearly in the horizontal expansion behaviour. During the pre-eruptive phase the velocity slowly increased from 0.6 km/s to 5.8 km/s and acceleration changed from 0.2 m/s^2 to 1.6 m/s^2. In the eruptive phase velocity grew from 7.1 km/s to 22.3 km/s, respectively acceleration increased from 2 m/s^2 to 6.3 m/s^2.

We can measure dimension variations of the prominence legs during the eruption because EP type I does not undergo observable changes of inclination of the large magnetic tube. Fig. 8 represents that function. It is probable an anticorrelation between variations in the prominence legs to exist, but we cannot claim with a certitude because of the small number of points for correlation analysis.

Such changes in the dimensions of the prominence feet can be interpreted in terms of twisting and untwisting of the fine structure elements in the prominence body. Similar behaviour is discussed in Vršnak (1990) and Vršnak, Ruždjak and Rompolt (1991).

The two events show fundamentally different behaviour at the final stages of eruption. The matter of EP type I on May 5, 1980 disappeared while a part of the prominence material of May 8, 1979 event fell back. The estimated acceleration in that case is 66.1 m/s2 which is smaller than the solar free fall acceleration. Probably the changes in magnetic configuration do not allow such a free fall. Unfortunately we do not have enough time resolution to explore in details that last phase eruption.

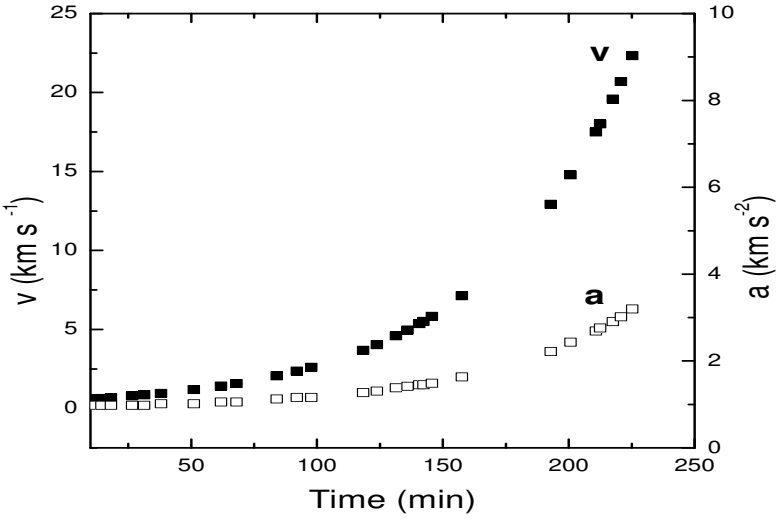

Figure 7: The velocity and acceleration of horizontal expansion for EP on May 5, 1980.

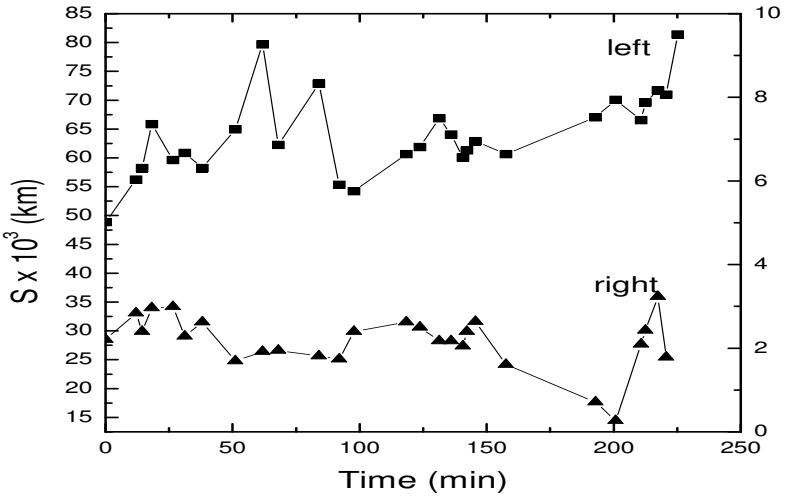

Figure 8: Dimension variations in the feet of EP on May 5, 1980.

4. CONCLUSION

The behaviour of both EPs during the pre-eruptive phase is similar, they rise slowly with a velocity of several km/s, but after the eruption onset their kinematics is radically different. The observed kinematics in vertical direction is as described in Rompolt (1990). One can see that there is a fundamental difference between the kinematics in horizontal direction, so we can classify these events by their horizontal motions.

The observations and measurements of the two events suggest presence of a helical fine structure with a specific twisting and untwisting motion during their eruption. More studies are needed on that point.

Acknowledgements

This work was supported by the National Scientific Foundation of Bulgaria under Grant F1004/2001.

References

Hood, A.W. and Priest, E.R.: 1979, *Solar Phys.*, **64**, 303.
Rompolt, B.: 1990, *Hvar. Obs. Bull.*, **14**, 37.
Valnicek, B.: 1968, in Structure and Development of Solar Active Region, ed. K. O. Kipenheuer, D. Reidel, Dordrecht, Holland, p. 282.
Vršnak, B.: 1990, *Solar Phys.*, **127**, 129.
Vršnak, B., Ruždjak, V. and Rompolt, B.: 1991, *Solar Phys.*, **136**, 151.
Vršnak, B.: 1998, in New Perspectives on Solar Prominences, eds. D. Webb, D. Rust and B. Schmieder, IAU Colloq. 167, ASP Conference Series, **150**, 302.

Proc. IV Serbian-Bulgarian Astronomical Conference,
Belgrade 21–24 April 2004,
eds. M. S. Dimitrijević, V. Golev, L. Č. Popović, M. Tsvetkov,
Publ. Astron. Soc. "Rudjer Bošković" No 5, 2005, 153 - 166 *Contributed paper*

INTERACTIVE COMPUTING OF THE EARTH ROTATION MATRIX ACCORDING TO IERS CONVENTIONS

S. FOTEV[1], N. GEORGIEV[1] and Y. CHAPANOV[2]

[1] *Space Research Institute – Bulgarian Academy of Sciences,*
6, Moskovska str., 1000 Sofia
E–mail sfotev@space.bas.bg
E–mail ngeorgiev@space.bas.bg

[2] *Central Laboratory for Geodesy - Bulgarian Academy of Sciences*
E–mail chapanov@clg.bas.bg

Abstract. The IAU 1976 Precession Model and the IAU 1980 Theory of Nutation are replaced by the precession-nutation model IAU 2000 A (MHB 2000), based on the transfer functions of (Mathews et al., 2002) at the beginning of 2003. In the proposed work the basic steps for computing of the rotation matrix of the Earth crust (the International Terrestrial Reference System) with respect to a geocentric set of axes tied to the quasars (the International Celestial Reference System) are described. IERS Conventions 1996 (July, 1996, `http://maia.usno.navy.mil/conventions.html` and IERS Conventions 2003 (November, 2003, `http://maia.usno.navy.mil/conv2000.html`) are used in the basic modules of the interactive program, written using IDL Version 6.0 Win32 (x86). It enables users to obtain the components of the coordinate transformation matrix – the transformation matrices arising from the motion of the celestial pole in the celestial system, from the rotation of the Earth around the axis of the pole, and from polar motion. The program allows taking into account the effect of:

1) The Earth Orientation Parameters (EOP), `http://hpiers.obspm.fr/eop-pc/`
• The celestial pole offsets ($\delta\psi,\ \delta\varepsilon$) or ($\delta X,\ \delta Y$);
• The rotation angle around the celestial intermediate pole, UT1-UTC;
• The polar motion of the celestial intermediate pole with respect to the terrestrial crust;
2) Tidal gravitational forcing;
3) Oceanic forcing;
4) Atmospheric forcing.

The results are compared with the interactive site of IERS EOP Product Center.

1. INTRODUCTION

The IERS Technical Note 21 (McCarthy, 1996) revises the most chapters of IERS Technical Note 13. The JPL DE 403 ephemeris (Standish et al., 1995) replaces the DE 200 model of IERS Technical Note 13. The NUVEL NNR-1A Model (DeMets et al., 1994) for plate motion has replaced the Nuvel NNR-1 Model of IERS Technical note 13. An empirical model, used to predict the difference in the celestial pole coordinates between those published by the IERS and those given by the IAU model is added.

The JGM3 model replaces the GEM-T3 and Love Numbers are revised. The subdaily and daily tidal variations in Earth orientation due to the effect of ocean tides are also added. The formulation has been modified to be consistent with IAU/IUGG resolutions.

The IERS Conventions 2003 were finalized in October, 2003, and the printed version will be available as IERS Technical Note 32. It is a continuation of the series of documents begun with the Project MERIT Standards (Melbourne et al., 1983) and continued with the IERS Standards (McCarthy, 1989; McCarthy, 1992) and IERS Conventions (McCarthy, 1996). The most significant changes from previous IERS standards and conventions are due to the incorporation of the recommendations of the 24^{th} IAU General Assembly held in 2000. These recommendations clarify and extend the concepts of the reference systems in use by the IERS and introduce a major revision of the procedures used to transform between them. A new theory of precession-nutation and new Terrestrial Reference Frame (ITRF2000) (Altamini et al., 2002) have been adopted.

In the proposed work are described the basic steps for calculation of the earth rotation matrix that transforms a coordinate **M** from the international terrestrial reference frame (ITRF) to the international celestial reference frame (ICRF). The matrix is composed according to IERS Conventions 1996/2003.

An interactive program module on the basis of the FORTRAN routines, provided from IERS web page is performed, using IDL Version 6.0 Win32 (x86). The program allows taking into consideration the effects of the celestial pole offsets, the rotation angle around the celestial intermediate pole, the polar motion of the celestial intermediate pole with respect to the terrestrial crust and the tidal gravitational forcing and the atmospheric forcing,

The results are compared with the matrix, on-line computed in the interactive web site of the IERS EOP Product Center, `http://hpiers.obspm.fr/eop-pc/`. The accuracy is $\sim 10^{-9}$ radians. The Cartesian or spherical point coordinates input/output are possible.

2. A COORDINATE TRANSFORMATION BETWEEN THE CELECTIAL AND TERRESTRIAL REFERENCE SYSTEM ACCORDING TO IERS CONVENTIONS

The matrix performing a transformation of the point coordinates from terrestrial to celestial reference system in the common case is

$$\Re_{ITRS \to ICRS} \;=\; Q(t) \cdot R(t) \cdot W(t) \tag{1}$$

where $Q(t)$ - transformation matrix arising from the motion of the celestial pole in the celestial system, $R(t)$ - transformation matrix arising from the rotation of the Earth around the axis of the pole, $W(t)$ - transformation matrix arising from the polar motion

Table 1. describes the basic steps for computation of the transformation matrix.

The parameters are described in more details in *Appendix A*.

Table 1: Computing the terrestrial to celestial transformation matrix – brief description.

$\Re_{ITRS\to ICRS} = Q(t)\cdot R(t)\cdot W(t)$	**The polar motion** $W(t)$	**The rotation of the Earth around the axis of the pole** $R(t)$	**The motion of the celestial pole in the celestial system** $Q(t)$
IERS Conventions 1996 *Coordinate transformation referred to the Equinox* *(McCarthy 1996, pp.20-33)* *http://maia.usno.navy.mil/conventions.html*	$W_{Eq1996}(t) = \Re_1(y_p)\cdot\Re_2(x_p)$	$R_{Eq1996}(t) = \Re_3(-GAST)$	$Q_{Eq1996}(t) = P_{Eq1996}(t)\cdot N_{Eq1996}(t)$ $N_{Eq1996}(t) = \Re_1(-\varepsilon_A)\cdot\Re_3(\Delta\psi)\cdot\Re_1(\varepsilon_A+\Delta\varepsilon)$ *IAU 1980 Theory of Nutation (Seidelmann 1982, Wahr 1981)* $P_{Eq1996}(t) = \Re_3(\xi_A)\cdot\Re_2(-\theta_A)\cdot\Re_3(z_A)$ *(Lieske et al. 1977)*
IERS Conventions 1996 *Coordinate transformation referred to the Nonrotating Origin* *(McCarthy 1996, pp.34-37)* *http://maia.usno.navy.mil/conventions.html*	$W_{NRO1996}(t) = \Re_3(-s')\cdot\Re_1(y_p)\cdot\Re_2(x_p)$	$R_{NRO1996}(t) = \Re_3(-\theta)$	$Q_{NRO1996}(t) = \Re_3(-E)\cdot\Re_2(-d)\cdot\Re_3(E)\cdot\Re_3(s)$ $Q_{NRO1996}(t) = Q_{XY}\cdot\Re_3(s)$ *IERS 1996 Theory of Precession/Nutation, ICRS (IERS Conventions 2003, Chapter 5., p.4)*
IERS Conventions 2003 *CEO-based coordinate transformation* *http://maia.usno.navy.mil/conv2000.html*	$W_{CEO2003}(t) = \Re_3(-s')\cdot\Re_1(y_p)\cdot\Re_2(x_p)$	$R_{CEO1996}(t) = \Re_3(-\theta)$	$Q_{CEO2003}(t) = \Re_3(-E)\cdot\Re_2(-d)\cdot\Re_3(E)\cdot\Re_3(s)$ *CEO-based bias-precession-nutation matrix consistent with IAU 2000A precession-nutation*
IERS Conventions 2003 *Equinox-based coordinate transformation,* *http://maia.usno.navy.mil/conv2000.html*	$W_{Eq2003}(t) = \Re_3(-s')\cdot\Re_1(y_p)\cdot\Re_2(x_p)$	$R_{Eq2003}(t) = \Re_3(-GAST)$	$Q_{Eq2003}(t) = B_{Eq2003}(t)\cdot P_{Eq2003}(t)\cdot N_{Eq2003}(t)$ $N_{Eq2003}(t) = \Re_1(-\varepsilon_A)\cdot\Re_3(\Delta\psi)\cdot\Re_1(\varepsilon_A+\Delta\varepsilon)$ $P_{Eq2003}(t) = \Re_1(-\varepsilon_0)\cdot\Re_3(\psi_A)\cdot\Re_1(\omega_A)\cdot\Re_3(\chi_A)$ $B_{Eq2003}(t) = \Re_3(-\delta\alpha_0)\cdot\Re_2(-\delta\psi_0\cdot\sin\varepsilon_0)\cdot\Re_1(\delta\varepsilon$ *Classical bias-precession-nutation matrix using IAU 2000A precession-nutation*

The parameter t, used in the expressions below, is defined to be consistent with IAU Resolution C7 (1994), which recommends that the epoch J2000.0 be defined at the geocenter and at the date 2000 January 1.5 TT = Julian Date 2451545.0TT, by

$$t = \frac{JD(TT) - JD(2000,\, January,\, 1,\, 12^h\ TT)}{36525} \tag{2}$$

$\Re_{1,2,3}$ means a rotation around axis OX, OY and OZ respectively.

3. COMPUTATION – BASIC STEPS

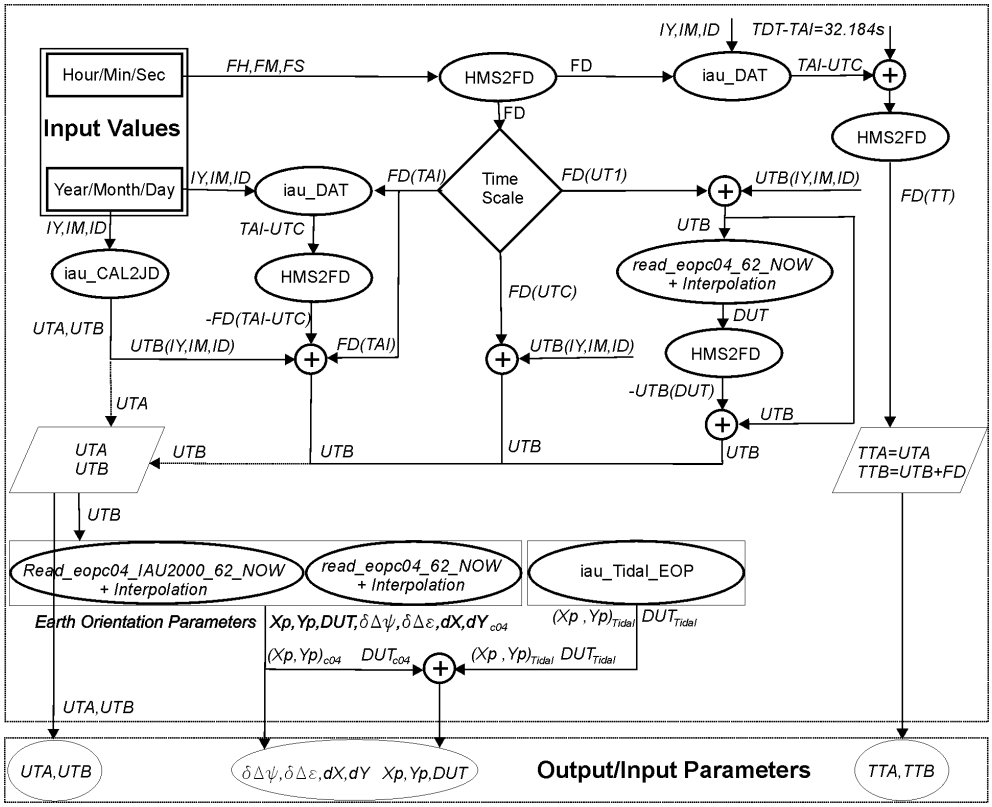

Figure 1: The basic steps of time scales calculation and obtaining Earth Orientation Parameters.

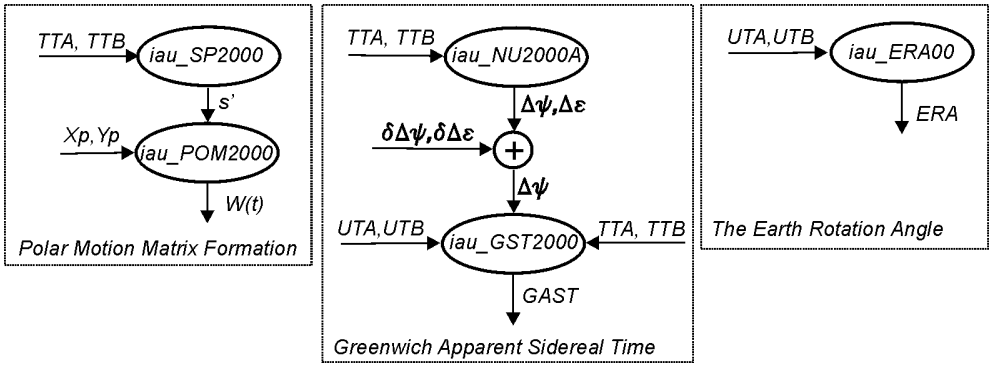

Figure 2: Illustration of the obtaining the transformation matrices, arising from the polar motion $W(t)$ and the rotation of the Earth around the axis of the pole $R(t)$.

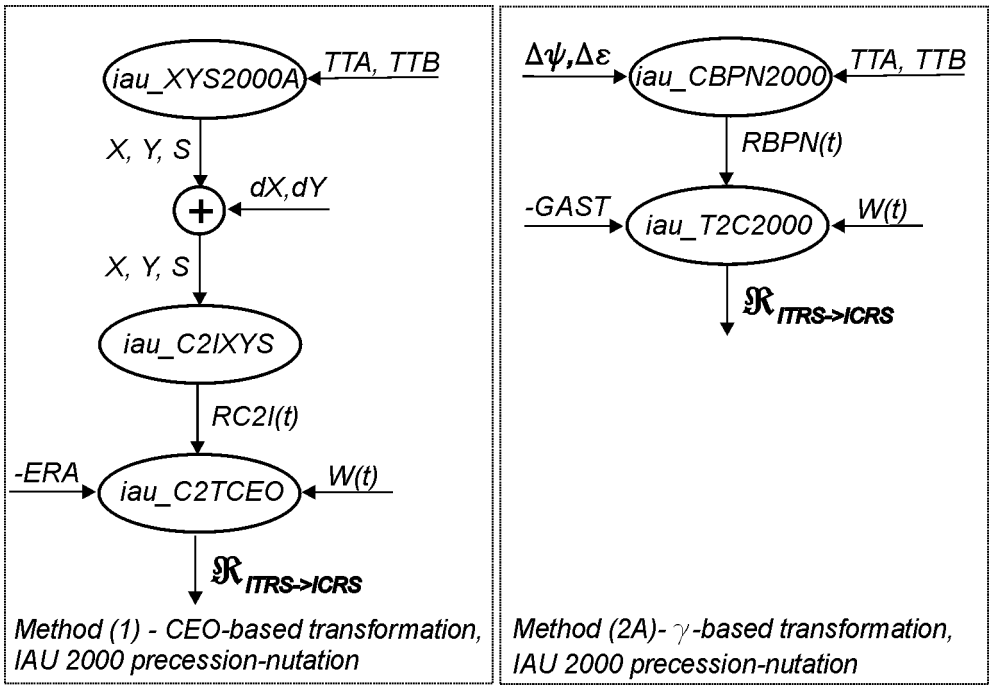

Figure 3: Computing transformation matrix $\Re_{ITRS \to ICRS}$ according to IERS Conventions 2003 – basic steps for Method (1) and Method (2A).

4. PROGRAM MODULE FOR COMPUTING THE EARTH ROTATION MATRIX

The software begins by displaying the following main menu screen:

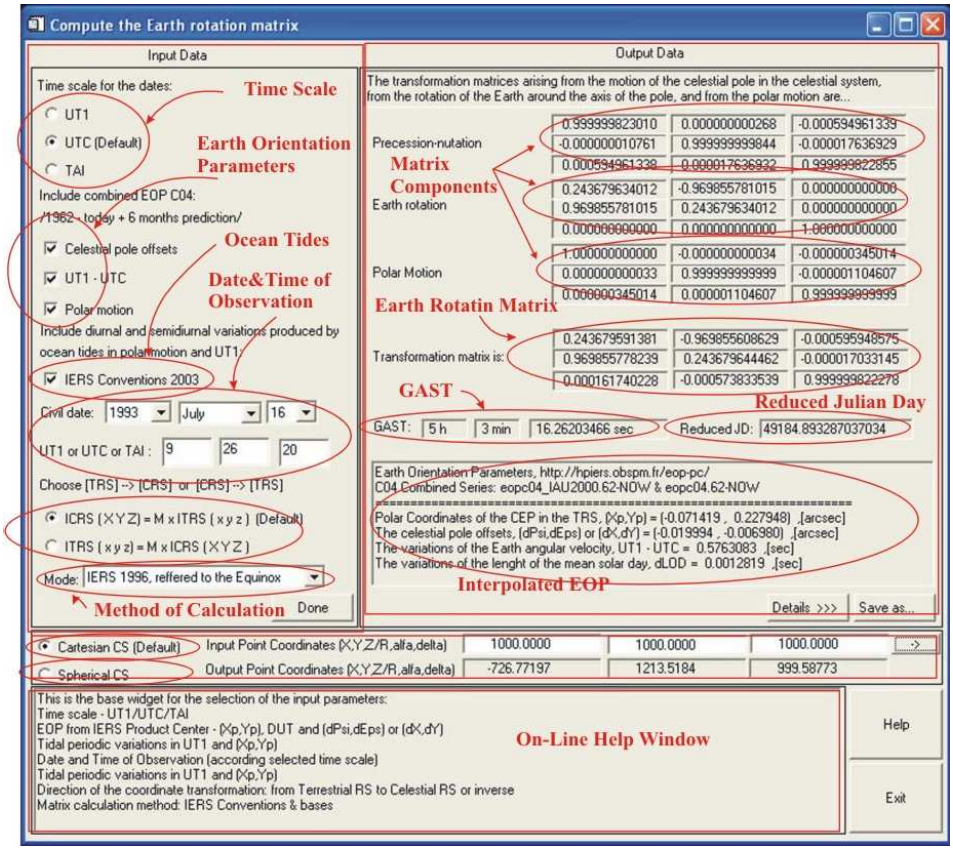

The main screen consists from four windows – Input Window, Output Window, Point Coordinate Transformation Window and On-line Help Window.

This input window allows the user to select such things as

- input time scale (UT1/UTC/TAI);

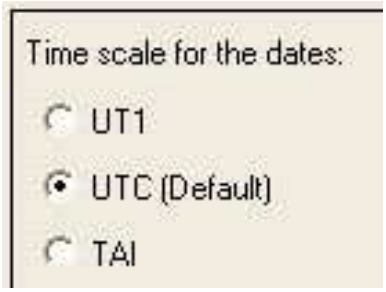

- including EOP series (celestial pole offset $(\delta\Delta\psi, \delta\Delta\varepsilon)$ / (dX, dY), $UT1 - UTC$ and polar coordinates (Xp, Yp));

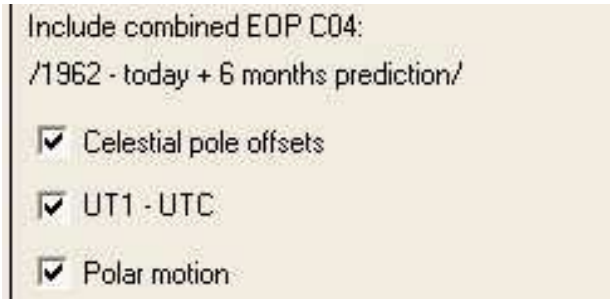

- including diurnal and semidiurnal variations, produced by ocean tides;

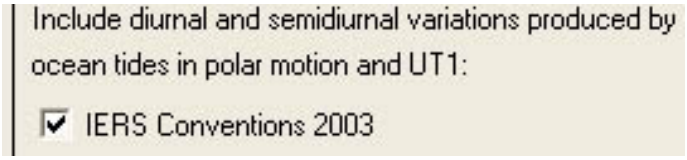

The user can enter the input date and time of observation in selected above time scale.

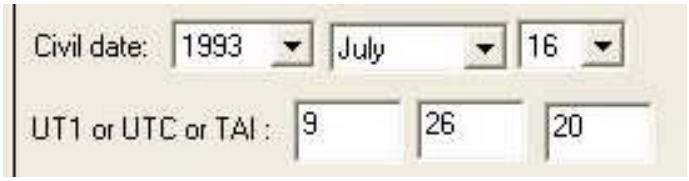

The "radio buttons" allows user to select the "direction" of the coordinate transformation – from terrestrial reference system to celestial reference system (default option) or inverse.

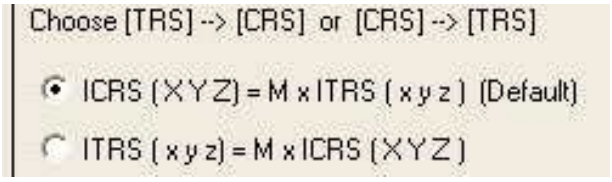

Four methods for computing the transformation matrix are available – computation according to

- *IERS Conventions 1996* – referred to the Equinox (Option 1) and referred to the Nonrotating origin (Option 2)

- *IERS Conventions 2003* – CEO based transformation consistent with IAU 2000A precession-nutation (default option) and Equinox –based transformation, using IAU 2000A precession-nutation.

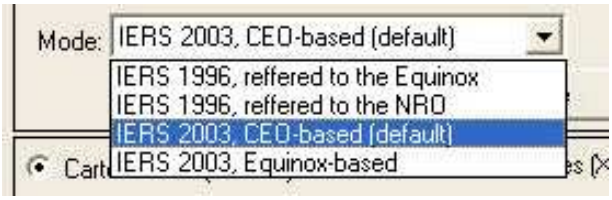

Output Window consists of:

- A window that displays transformation matrix and its parts – Polar motion matrix, Earth rotation matrix and Precession-Nutation matrix;

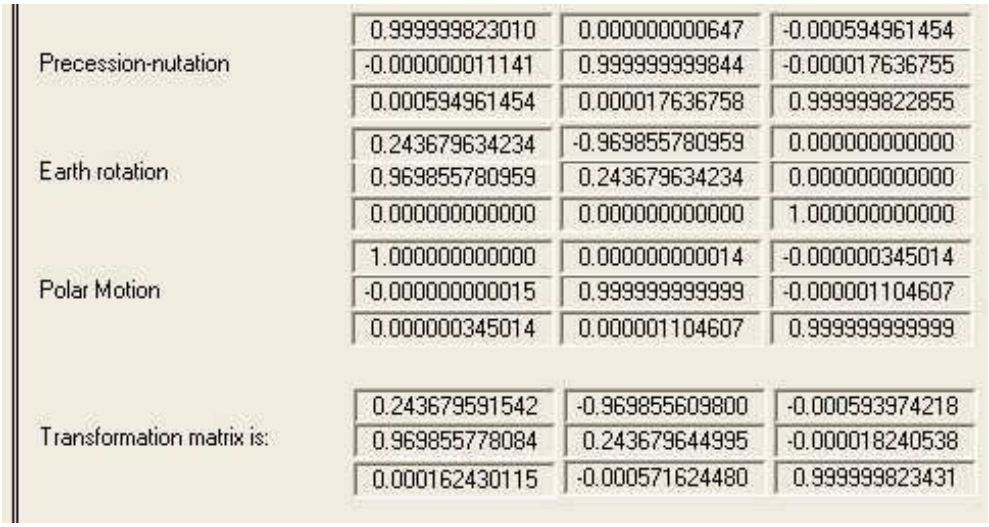

- Window that displays the interpolated EOP at the time of observation;

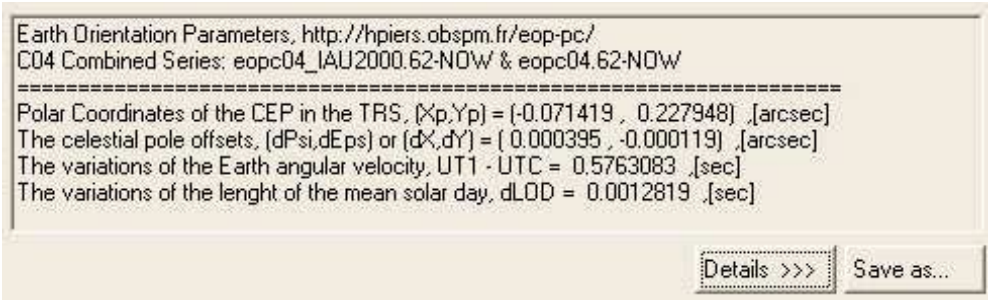

- The Greenwich Apparent Sidereal Time and Reduced Julian Date are displayed also

The software makes it possible to calculate point coordinate from terrestrial reference system to celestial reference system or inverse in Cartesian or Spherical coordinate system.

In on-line help window moving the mouse across windows and fields we can have instant information that supports our work.

5. CONCLUSION

The software, described above, is written in the Interactive Data Language (IDL), Version 5.6 Win 32 (x86). The basic modules are translated from the FORTRAN routines, provided from `ftp://maia.usno.navy.mil/conv2000/chapter5` Fortran Code and some routines from the IAU Standards of Fundamental Astronomy software collection.

The accuracy, achieved at calculating the transformation matrix is assessed in comparison to the on-line calculated transformation matrix on `http://hpiers.obspm.fr/eop-pc/`. An accuracy of less than 10-9 radians was achieved.

The sources of the software described are available on `ftp://aquila.skyarchive.org`.

References

Aoki, S. et al.: 1982, *Astron. Astrophys.*, **105**, 359.
Capitaine, N., Guinot, B., Souchay, J.: 1986, *Celest. Mech.*, **39**, 283.
Capitaine, N., Chapront, J., Lambert, S., Wallace, P.T.: 2003, *Astron. Astrophys.*, **400**, 1145.
Chapront, J., Chapront-Touze, M.: 2002, *Astron. Astrophys.*, **387**, 700.
McCarthy, D.D.: 1996, *IERS Conventions*, IERS Technical Note, **21**, Observatoire de Paris, Paris.
McCarthy, D.D., Petit, J.: 2003, *IERS Conventions*, `http://maia.usno.navy.mil/conv2000.html`.
Lieske, L.H., Lederle, T., Fricke, W., Morando, B.: 1977, *Astron. Astrophys.*, **58**, 1.
Mathews, P.M., Herring, T.A., Buffett, B.A.: 2002, *Geophys. Res.*, **107**, B4.

Appendix A: Description and expressions for transformation matrix quantities.

Parameter	Description	Expression
x_p, y_p	The "pole coordinates" of the CEP in ITRS, Earth Orientation Parameters	IERS value: ftp://hpiers.obspm.fr/eop-pc/eopc04.62-NOW or ftp://hpiers.obspm.fr/eop-pc/eopc04_IAU2000.62-NOW
s'	The accumulated displacement of the terrestrial origin on the equator due to polar motion.	$s' = -47\,\mu as \cdot t$
$GAST$	Greenwich Apparent Sidereal Time at date t, including both the effect of Earth rotation and precession and nutation in right ascension.	$GAST = GMST + \Delta\psi \cdot \cos\varepsilon_A + 0''.00264 \cdot \sin\Omega + 0''.000063 \cdot \sin 2\Omega$ $GMST = GMST_{0hUT1} + r \cdot [(UT1 - UTC) + UTC]$ $GMST_{0hUT1} = 6^h 41^m 50^s.54841 + 8640184^s.812866 \cdot T_u$ $+ 0^s.093104 \cdot T_u^{\,2} - 6^s.2 \cdot 10^{-6} \cdot T_u^{\,3}$ $r = 1.002737909350795 + 5.9006 \cdot 10^{-11} \cdot T_u + 5.9 \cdot 10^{-15} \cdot T_u^{\,2}$ *(Aoki et al. 1982)*
$DUT = UT1 - UTC$	Earth Orientation Parameter	IERS value: ftp://hpiers.obspm.fr/eop-pc/eopc04.62-NOW or ftp://hpiers.obspm.fr/eop-pc/eopc04_IAU2000.62-NOW
θ	Earth Rotation Angle - the stellar angle at date t due to the Earth angle of rotation (Capitain et al. 1986)	$\theta(T_u) = 2\pi \cdot (0.779057273264 + 1.00273781191135448 \cdot T_u \; x\,36525)$
ξ_A, θ_A, z_A	The precession quantities as functions of two parameters (t, T). When the arbitrary epoch is chosen to be J2000.0, *T=0* (Lieske *et al.* 1977).	$\xi_A = 2306''.2181 \cdot t + 0''.30188 \cdot t^2 + 0''.017998 \cdot t^3$ $\theta_A = 2004''.3109 \cdot t - 0''.42665 \cdot t^2 - 0''.041833 \cdot t^3$ $z_A = 2306''.2181 \cdot t + 1''.09468 \cdot t^2 + 0''.018203 \cdot t^3$
$\Delta\psi$	The nutation in longitude	$\Delta\psi = \Delta\psi(IAU1980) + \delta\Delta\psi$ $\Delta\psi(IAU1980) = \sum_{i=1}^{106} (A_i + A'_i \cdot t) \cdot \sin(ARG)$ $IAU1980$ - *IAU 1980 Theory of Nutation in longitude and obliquity* $\Delta\psi(IERS1996) = \sum_{i=1}^{112} A_i \cdot \sin(ARG) + A'_i \cdot \cos(ARG)$ $IERS1996$ - *IERS 1996 Theory of Precession/Nutation*

$\Delta\varepsilon$	The nutation in obliquity	$\Delta\varepsilon = \Delta\varepsilon(IAU1980) + \delta\Delta\varepsilon$ $\Delta\varepsilon(IAU1980) = \sum_{i=1}^{106}(B_i + B'_i \cdot t)\cdot\cos(ARG)$ *IAU*1980 - *IAU 1980 Theory of Nutation in longitude and obliquity* $\Delta\varepsilon = \sum_{i=1}^{112} B_i \cdot \sin(ARG) + B'_i \cdot \cos(ARG)$ *IERS*1996 - *IERS 1996 Theory of Precession/Nutation*
E, d IERS Conventions 1996	The coordinates (X, Y, Z) of the CEP in ICRS (McCarthy 1996, p. 34)	$E = arctg(Y / X)$ $d = arctg(\sqrt{\frac{X^2+Y^2}{1-(X^2+Y^2)}})$
X IERS Conventions 1996	The coordinate X of the CEP in ICRS (McCarthy 1996, p. 36)	$X = X(IAU\ 2000) + \delta X$ $X = PolynomialPart + NonPolynomialPart$ $X(PolynomialPart) = 2004''.3109\cdot t - 0''.442665\cdot t^2 - 0''.198656\cdot t^3$ $+ 0''.0000140\cdot t^4 + 0''.00006\cdot t^2\cdot\cos\Omega$ $+ 0''.00204\cdot t^2\cdot\sin\Omega + 0''.00016\cdot t^2\cdot\sin 2\cdot(F - D + \Omega)$ $X(NonPolynomialPart) = \sin\varepsilon_o\cdot\{\sum[(A_i + A'_i\cdot t)\cdot\sin(ARG) + A''_i\cdot t\cdot\cos(ARG)]\}$
Y IERS Conventions 1996	The coordinate Y of the CEP in ICRS (McCarthy 1996, p. 36)	$Y = Y(IAU\ 2000) + \delta Y$ $Y = PolynomialPart + NonPolynomialPart$ $Y(PolynomialPart) = -0''.00013 - 22''.40992\cdot t^2 + 0''.001836\cdot t^3 + 0''.000014\cdot t^4$ $- 0''.00231\cdot t^2\cdot\cos\Omega - 0''.00014\cdot t^2\cdot\cos[2\cdot(F - D + \Omega)]$ $Y(NonPolynomialPart) = \{\sum[(B_i + B'_i\cdot t)\cdot\cos(ARG) + B''_i\cdot t\cdot\sin(ARG)]\}$
s IERS Conventions 1996	The accumulated rotation of the celestial CEO on the true equator due to the celestial motion of the CEP, IAU 1980 Theory of Nutation (Lieske *et al.* 1977)	$s = -XY/2 + 0''.00385\cdot t - 0''.07259\cdot t^3 - 0''.00264\cdot sin\Omega + 0''.00006\cdot sin 2\Omega$ $+ 0''.00074\cdot t^2\cdot sin\Omega + 0''.00006\cdot t^2\cdot sin 2\cdot(F - D + \Omega)$

E, d IAU 2000A Precession-Nutation Model	The coordinates (X, Y, Z) of the CEP in ICRS (IERS Conventions 2003, Chapter 5., p.4)	$E = arctg(Y/X)$ $d = arctg(\sqrt{\frac{X^2+Y^2}{1-(X^2+Y^2)}})$
X IAU 2000A Precession-Nutation Model	The coordinate X of the CEP in ICRS (IERS Conventions 2003, Chapter 5., p.7)	$X = X(IAU\ 2000) + \delta X$
$X(IAU\ 2000)$ IAU 2000A Precession-Nutation Model	The coordinate X of the CEP in ICRS (IERS Conventions 2003, Chapter 5., p.7)	$X(IAU\ 2000) = X(PolynomialPart) + X(NonPolynomialPart)$ $X(NonPolynomialPart) = -0''.01661699 + 2004''.19174288 \cdot t$ $- 0''.42721905 \cdot t^2 - 0''.19862054 \cdot t^3$ $- 0''.00004605 \cdot t^4 + 0''.00000598 \cdot t^5$ $X(PolynomialPart) = \sum_{i=1}^{1306}[(a_{s,0})_i \cdot \sin(ARG) + (a_{c,0})_i \cdot \cos(ARG)]$ $+ \sum_{i=1}^{353}[(a_{s,1})_i \cdot t \cdot \sin(ARG) + (a_{c,1})_i \cdot t \cdot \cos(ARG)]$ $+ \sum_{i=1}^{36}[(a_{s,2})_i \cdot t^2 \cdot \sin(ARG) + (a_{c,2})_i \cdot t^2 \cdot \cos(ARG)]$
Y IAU 2000A Precession-Nutation Model	The coordinate Y of the CEP in ICRS (IERS Conventions 2003, Chapter 5., p.7)	$Y = Y(IAU\ 2000) + \delta Y$
$Y(IAU\ 2000)$ IAU 2000A Precession-Nutation Model	The coordinate Y of the CEP in ICRS (IERS Conventions 2003, Chapter 5., p.7)	$Y(IAU\ 2000) = Y(PolynomialPart) + Y(NonPolynomialPart)$ $Y(PolynomialPart) = -0''.00695078 - 0''.02538199 \cdot t$ $- 22''.40725099 \cdot t^2 + 0''.00184228 \cdot t^3$ $- 0''.00111306 \cdot t^4 + 0''.00000099 \cdot t^5$

		$Y(NonPolynomialPart) = \sum_{i=1}^{962}[(b_{c,0})_i \cdot \cos(ARG) + (b_{s,0})_i \cdot \sin(ARG)]$ $+ \sum_{i=1}^{277}[(b_{c,1})_i \cdot t \cdot \cos(ARG) + (b_{s,1})_i \cdot t \cdot \sin(ARG)]$ $+ \sum_{i=1}^{30}[(b_{c,2})_i \cdot t^2 \cdot \cos(ARG) + (b_{s,2})_i \cdot t^2 \cdot \sin(ARG$
s IAU 2000A Precession- Nutation Model	The accumulated rotation (between the epoch J2000.0 and the date t) of the celestial CEO on the true equator due to the celestial motion of the CEP, IAU 2000 Precession-Nutation Model (Capitaine *et al.* 2003)	$s(t) = -(XY/2) + PolynomialPart + NonPolynomialPart$ $PolynomialPart = +94.0 + 3808.35 \cdot t - 119.94 \cdot t^2$ $- 72574.09 \cdot t^3 + 27.70 \cdot t^4 + 15.61 \cdot t^5$ $NonPolynomialPart = \sum_{i=1}^{33}[(c_{s,0})_i \cdot \sin(ARG) + (c_{c,0})_i \cdot \cos(ARG)]$ $+ \sum_{i=1}^{3}[(c_{s,1})_i \cdot t \cdot \sin(ARG) + (c_{c,1})_i \cdot \cos(ARG)]$ $+ \sum_{i=1}^{25}[(c_{s,2})_i \cdot t^2 \cdot \sin(ARG) + (c_{c,2})_i \cdot \cos(ARG)]$ $+ \sum_{i=1}^{4}[(c_{s,3})_i \cdot t^3 \cdot \sin(ARG) + (c_{c,3})_i \cdot \cos(ARG)]$ $+ \sum_{i=1}^{1}[(c_{s,4})_i \cdot t^4 \cdot \sin(ARG) + (c_{c,4})_i \cdot \cos(ARG)]$
$\Delta\psi$ The IAU 2000 Nutation Model	The nutation in longitude	$\Delta\psi = \Delta\psi(IAU2000) + \delta\Delta\psi$ $\Delta\psi(IAU2000) = \sum_{i=1}^{106}(A_i + A'_i \cdot t) \cdot \sin(ARG) + (A''_i + A'''_i \cdot t) \cdot \cos(ARG)$
$\Delta\varepsilon$ The IAU 2000 Nutation Model	The nutation in obliquity	$\Delta\varepsilon = \Delta\varepsilon(IAU1980) + \delta\Delta\varepsilon$ $\Delta\varepsilon(IAU2000) = \sum_{i=1}^{106}(B_i + B'_i \cdot t) \cdot \cos(ARG) + (B''_i + B'''_i \cdot t) \cdot \sin(ARG)$

ψ_A, ω_A, χ_A	The precession quantities, compatible with the IAU 2000 Precession-Nutation Model (Lieske *et al.* 1977).	$\psi_A = \varepsilon_0 + 0''.05127 \cdot t^2 - 0''.007726 \cdot t^3$ $\omega_A = \varepsilon_0 - 46''.8150 \cdot t - 0''.00059 \cdot t^2 - 0''.001813 \cdot t^3$ $\chi_A = 10''.5526 \cdot t - 2''.38064 \cdot t^2 + 0''.018203 \cdot t^3$
ε_A	The mean obliquity at epoch t (Lieske *et al.* 1977).	$\varepsilon_A = \varepsilon_0 - 46''.8150 \cdot t - 0''.00059 \cdot t^2 + 0''.001813 \cdot t^3$
ε_0	The J2000 obliquity (Lieske et al. 1977)	$\varepsilon_0 = 84381.448''$
$\delta\alpha_0$	The ICRS RA of the J2000 equinox (Chapront *et al.*2002)	$\delta\alpha_0 = -0''.0146$
$\delta\psi_0$	The frame bias corrections in longitude	$\delta\psi_0 = -0''.0417750$
$\delta\varepsilon_0$	The frame bias corrections in obliquity	$\delta\varepsilon_0 = -0''.0068192$
$\delta\Delta\psi$, $\delta\Delta\varepsilon$	Earth Orientation Parameters	IERS values: ftp://hpiers.obspm.fr/eop-pc/eopc04.62-NOW
δX, δY	Earth Orientation Parameters	IERS values: ftp://hpiers.obspm.fr/eop-pc/eopc04_IAU2000.62-NOW

Proc. IV Serbian-Bulgarian Astronomical Conference,
Belgrade 21–24 April 2004,
eds. M. S. Dimitrijević, V. Golev, L. Č. Popović, M. Tsvetkov,
Publ. Astron. Soc. "Rudjer Bošković" No 5, 2005, 167 - 173 *Contributed paper*

BVR PHOTOMETRY OF THE OUTER REGIONS OF THE STARBURST GALAXY M 82

I. GEORGIEV[1,2], T. VELTCHEV[1], P. NEDIALKOV[1],
E. OVCHAROV[1], I. STANEV[1], Ch. DYULGEROV[1] and O. STANCHEV[2]

[1] *Department of Astronomy, University of Sofia,*
5 James Bourchier Blvd. Sofia 1164, Bulgaria
E–mail eirene@phys.uni-sofia.bg

[2] *Institute of Astronomy, Bulgarian Academy of Sciences,*
72 Tsarigradsko Shosse Blvd. Sofia 1784, Bulgaria
E–mail iskren@libra.astro.bas.bg

Abstract. We present BVR CCD photometry of stellar and non-stellar objects in the outer regions of the starburst galaxy M 82 carried out with IRAF software package. The CCD images were obtained with the 2m NAO-Rozhen telescope in May 2003 and cover a field of $\sim 15' \times 7'$, centered on M 82. Combining theoretical predictions and observational data for typical magnitudes and colors of globular clusters (GC), several GC candidates were selected on the color-magnitude diagrams (CMD). They form two distinctive groups most probably due to age differences.

1. INTRODUCTION

The prototype starburst galaxy M 82 is one of the most attractive objects for observers ever since Lynds and Sandage (1963) found evidence for energetic events in its central region, now known as a site of a huge starbursts. This starbursts is thought to have been triggered by interaction that happened $\sim 10^8$ yrs ago, (Achtermann and Lacy, 1995) between M 82 and the more massive galaxy M 81, host of the M 81 group of galaxies. Several bright knots in the central region (O'Connell and Mangano, 1978) have been resolved into numerous luminous ($L \sim 4 \times 10^6 L_\odot$), young ($\sim 50 Myr$), massive ($\sim 10^5 M_\odot$) stellar clusters, called "super star clusters" (SSC). In terms of age, SSC resemble the open clusters while they are as massive as globular clusters (GCs) (O' Connell et al., 1995; de Grijs and O'Connell, 2001). Most probably only the most massive and compact of these young systems (if they survive dynamically for a long time-scale) are going to evolve into old Milky Way like globular clusters (de Grijs, Bastian and Lamers, 2003). Therefore it is worth to investigate the older GC system in the outer parts of a galaxy with both very young SSCs and older GCs; it would contribute to a more full understanding of the starburst and its propagation. The abundance and spatial distribution of GCs can serve to test merger and accretion

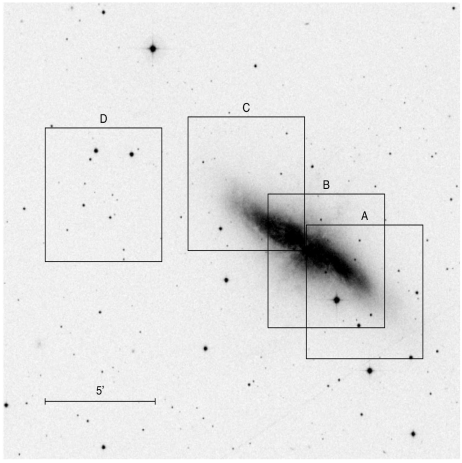

Figure 1: Digitized sky survey image of M 82. The footprints indicates the regions of the 2m NAO-Rozhen telescope observations.

theories (Brodie, 1993). Collisions and mergers of galaxies trigger bursts of "second-generation" star and cluster populations (Schweizer, 2002). Generally, there are three proposed scenarios of GCs formation depending on whether GCs formed before, simultaneously with or after the host galaxy (Fall and Rees, 1988; Schweizer, 1997, 2004).

Supposing a presence of possible intermediate-age GCs population, it is worthwhile to carry out investigation for GCs around M 82. In addition, the proximity of M 82 makes this galaxy an ideal target to study the relationship between galaxy interactions and GCs formation. The small size of globular clusters, $r \leq 40\,pc$, limits the distance range of their visual identification with ground based telescopes. At $3.9\,Mpc$ (Sakai and Madore, 1999) M 82 GCs with similar sizes are expected to has apparent angular diameter of $\sim 2''$. In comparison with the seeing mean value (see Table 1) of $\sim 1.4''$ for our observations, it is very difficult easily to resolve the GCs in virtue of their visual size. More promising is to use color criteria in order to establish the object's affiliation. Recently, Saito et al. (2003) performed a search for possible GC population in the central $6'$ ($6.8\,Kpc$) of M 82. The main goal of our photometry survey is to select GCs candidates on the base of their colors in two outer regions of M 82 (fields A and C in Fig. 1).

2. OBSERVATIONS, REDUCTIONS AND PHOTOMETRY

2.1. OBSERVATIONS

The CCD BVR images of the galaxy M 82 has been observed with the 2m telescope of the Rozhen National Astronomical Observatory between 01-05 May 2003. The observational conditions and the positions of the fields, covering the M 82 and the field with standards (Fig. 1) are summarized in Table 1. The 1024×1024 pixel

Table 1: Log of observations

Date	Field	Field's center $\alpha\,(2000.0)$ $\delta\,(2000.0)$	Filter	Exposure $[sec]$	Seeing $[arcsec]$ (FWHM)	Airmass X
05.05.2003	A	09:55:20.72	B	1200	1.2	1.390
		+69:39:21.19	V	400	1.1	1.517
			R	160	1.0	1.424
03.05.2003	B	09:55:41.83	B	1800	1.9	1.518
		+69:40:26.26	V	400	1.5	1.516
			R	160	1.3	1.559
03.05.2003	C	09:56:26.51	B	1200	1.8	1.308
		+69:43:11.10	V	400	1.4	1.383
			R	160	1.3	1.319
03.05.2003	D	09:57:40.64	B	300	1.3	1.183
	photometric	+69:42:11.07	V	75	1.2	1.186
	standards		R	50	1.3	1.188

CCD camera, with scale $12.8\,''/mm$, provide a field of $5,3' \times 5,3'$ with scale of $0.31 \times 0.31\,''/pixel$. The readout noise is 4.93.

2.2. REDUCTIONS AND PHOTOMETRY

The routine preliminary image processing (including subtraction of bias level, flat fielding and cosmic rays filtering), was performed using the Rozhen software (Georgiev, 1995). The images in each filter were aligned and combined using the centers of the bright stars as reference points. All requirements (for flux conserve, read noise, exposure time etc.) in the image combining procedures for correct subsequent photometry were fulfilled.

All the photometry procedures were done with DAOPHOT under IRAF. The objects in all frames were selected using the automatic star finding procedure DAOFIND. After visual inspection of the images a few faint objects omitted by DOAOFIND and suspected as a potential GCs candidates were added to the lists of objects for photometry. Then we have performed PSF photometry with the DAOPHOT procedure ALLSTAR. The output photometry lists were matched to leave only those objects simultaneously detected in the three filters.

The calibration of instrumental magnitudes was done using ~ 20 local standards (Afanasiev et al., 1990) found nearby M 82 (see Fig. 1). The aperture photometry for these standards was performed using PHOT found in DAOPHOT package. The resulting transformation equations are:

$$B = b - 1.23_{\pm 0.21} - 1.50\,X - 0.01_{\pm 0.24}\,(b - v)$$

$$V = v - 0.71_{\pm 0.18} - 0.80\,X - 0.07_{\pm 0.18}\,(b - v)$$

$$R = r - 0.87_{\pm 0.41} - 0.81\,X - 0.07_{\pm 0.38}\,(v - r)$$

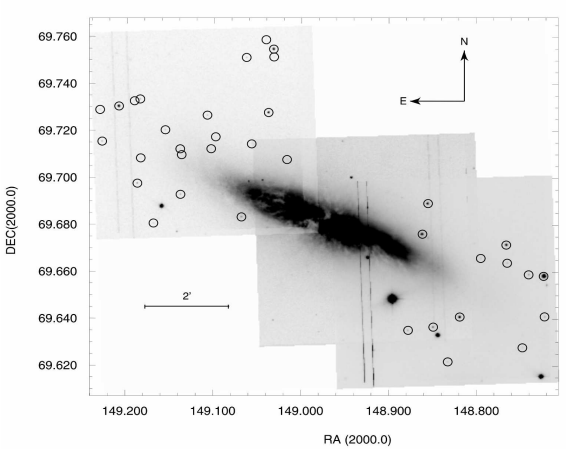

Figure 2: Mosaic view of M 82. With empty circles are indicated all objects placed in the CM diagrams.

where the $b,\ v,\ r$ and $B,\ V,\ R$ are the instrumental and standard magnitudes, respectively, in the B, V and R filters. X is the air mass.

Thorough investigations have been done of the core starbursts regions (de Grijs et al., 2003; Lipscy and Plavchan, 2004) and near the galaxy plane (Notni et al., 1996; Saito et al., 2003). Our images are not as much deep and doesn't possess the required resolution to carry out trustworthy photometry of common objects in the same regions. That is why comparison between our and early made photometry was not performed.

The colors were de-reddened and the magnitudes extinction-corrected using online data available at NED (`http://nedwww.ipac.caltech.edu/`) based on Schlegel (1998) maps. For the foreground extinction in the line of site toward M 82 we adopt $E(B-V) = 0.159,\ E(V-R) = 0.102,\ A_B = 0.685,\ A_V = 0.526,\ A_R = 0.424$.

An estimate for the Galactic foreground star contamination have been obtained using stellar population synthesis model of the Galaxy provided by Robin et al. (2003). The model predicts 5 and 11 foreground stars in 1.873 arcminutes^2 field falling in the GCs candidates magnitude and color range V_0 vs. $(B-V)_0$ and $(V-R)_0$, respectively (see Sect. 3).

3. PRELIMINARY SEARCH FOR GLOBULAR CLUSTERS CANDIDATES

We performed a preliminary inspection for GCs candidates outside the disk of M 82 (Fig. 2) on the basis of their colors and magnitudes. The CM diagrams of objects in fields A and C are plotted in Fig. 3. (The objects in field B need additional photometry and were not taken into consideration. Their analysis will be complemented with data from the Rozhen data archive in a forthcoming paper.)

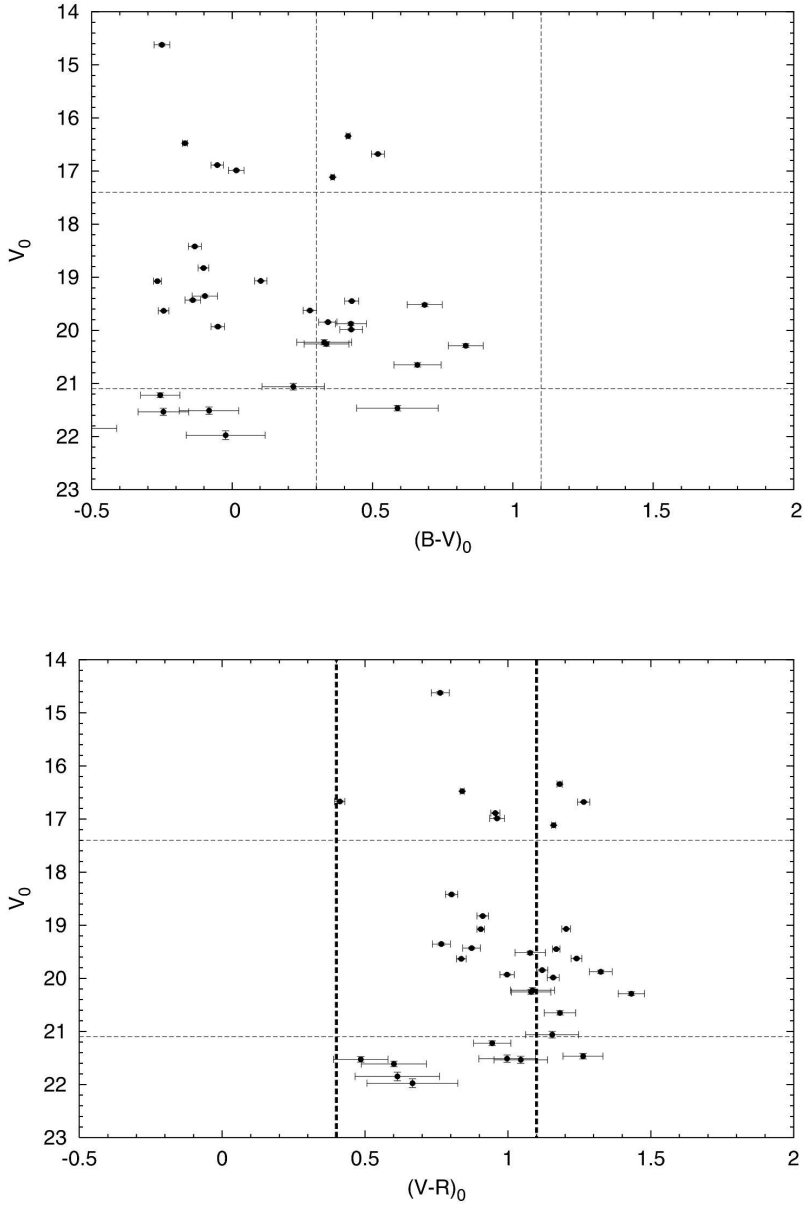

Figure 3: TOP: The V_0 vs. $(B-V)_0$ color magnitude diagram for fields A and C (Fig. 2). Dashed horizontal and vertical lines define the range of the colors and magnitudes values for GCs given by theoretical predictions for different ages and metallicities (cf. text). **BOTTOM:** The same like TOP panel but for V_0 vs. $(V-R)_0$. The $(V-R)_0$ range is marked with different line because it is defined by observational predictions (cf. text).

The expected loci of GCs candidates on diagrams V_0 vs. $(B-V)_0$ and V_0 vs. $(V-R)_0$ are delineated in Fig. 3. The theoretical range of magnitudes and colors is adopted from the models of Fritze (2004) that cover ages from 0.3 to 12 Gyr and metallicities $[Fe/H] = -1.7\ -0.4$ and $+0.4$. We have used the extreme values of above quantities to extract the limiting theoretical colors and magnitudes used in the CM diagrams. Unfortunately, the Fritze models do not provide synthetic $(V-R)_0$ color. For that color we impose observational limits, based on the McMaster catalog for Galactic globulars (Harris, 1996).

There are ~ 20 objects that fall within the range $0.3 \leq (B-V)_0 \leq 1.1$, respectively $0.4 \leq (V-R)_0 \leq 1.1$, for $17.4 \leq V_0 \leq 21.1$, typical for GCs (Fig. 3). Their magnitudes are comparable with the median values for globular cluster systems in galaxies outside the Local group ($-6.1 \leq M_V \leq -10.1$; Harris, 1991). We have ~ 8 objects in each panel brighter than $17^m.4$. These are foreground stars since the distance modulus to M 82 is $(m-M)_0 = 27^m.9 \pm 0.16$ (Sakai and Madore, 1999). The theoretical predictions, based on the elaborated model of the Galaxy (Robin et al., 2003), also shows that the foreground contamination in the above mentioned color and magnitude ranges are of 5 and 11 foreground stars, respectively. This number of predicted objects is below the number of candidates and thus we expect that most of the selected objects in that color magnitude regions are GCs candidates.

It is worth to mention at this early stage of our GC population study in M 82 that separation of GCs candidates into two groups is observed. The first one, having a mean colors of $(B-V)_0 \approx 0.4$, $(V-R)_0 \approx 1.1$ and magnitudes $19 \leq V \leq 21.1$ are most presumably contain Milky Way type GCs. Some of the second one, with bluer colors and higher V_0 magnitudes are probably younger second generation GC population. The other possible classification for these objects are to be LBV, multiple star systems or most massive red supergiants.

Color distributions of GC systems around all type galaxies are found to be bimodal, as in our case. Their blue peaks seem to be fairly universal and very similar to that of the Milky Way halo GCs. Such a populations originates in the last encounter between interacting galaxies, namely between M 81 and M 82. More over the young GC time scales in M 82 are the same as those in M 81 and also bimodal color and age distribution are observed (Chandar et al., 2001). The metallicity also plays a key role in the GC colors and should be taken into account. It is very difficult solely on photometrical criteria to say whether the color of the corresponding sample is due to its age or metallicity.

For more trustworthy conclusions concerning the age and metallicity are needed additional investigations on the basis of their spectra and deep space imaging of these objects.

4. CONCLUSIONS

We present BVR CCD photometry of stellar and non-stellar objects in the outer regions of the starburst galaxy M 82 in order to select globular clusters candidates. The CCD images were obtained with the 2m NAO-Rozhen telescope and cover a field of $\sim 15' \times 7'$. Combining theoretical predictions and observational data for typical

magnitudes and colors of globular clusters, ~ 10 candidates for GC emerged on the CM diagrams. They form two distinctive groups probably due to age differences.

The next steps in our GCs populations study in M 82 are:

i) to complement the photometry with data from the Rozhen data archive (performing investigation for color dependence in the transformation equations) which will let us *ii*) to construct representative color-color diagrams. Thus the analysis of the globular cluster population will be more complete and accurate; *iii*) to perform cross-identification with objects from 2MASS catalog.

Acknowledgements

This research was partially supported by the grant F-1302/2003 with the National Science Foundation, Bulgaria.

References

Achtermann, J., Lacy, J.: 1995, *Astrophys. J.*, **439**, 163.
Afanasiev, V., Vlasyuk, V., Dodonov, J., Lorens, H., Terebbizh, V.: 1990, *Astrofiz. Issledovaniya SAO*, **32**, 31.
Chandar, R., Tsvetanov, Z., Ford, H.C.: 2001, *Astron. J.*, **122**, 1342.
de Grijs, R., O'Connell R.W., Gallagher J.S. III: 2001, *Astron. J.*, **121**, 768.
de Grijs, R., Bastian, N., Lamers, H.J.G.L.M.: 2003, *Astrophys. J.*, **583**, 17.
Fall, S.M., Rees, M.J.: 1988, *IAU Symp.*, **126**, 323.
Fritze-v. Alvensleben, U.: 2004, *Astron. Astrophys.*, **414**, 515.
Georgiev, T.: 1995, *IAU Comission 9, WGWFI Newsletter*, **8**, 29.
Harris, W.: 1991, *Ann. Rev. Astron. Astrophys.*, **29**, 543.
Harris, W. E.: 1996, *Astron. J.*, **112**, 1487.
Catalogue available at `http://physun.physics.mcmaster.ca/Globular.html`
O'Connell, R.W., Gallagher, J.S., Hunter, D.A., Colley, W.N.: 1995, *Astrophys. J.*, **446**, L1.
Lipscy, S.J., Plavchan, P.: 2004, *Astrophys. J.*, **603**, 82.
Lynds, C.R. and Sandage, A.R.: 1963, *Astrophys. J.*, **137**, 1005.
Notni, P., Karachentsev, I., Makarova, L.: 1996, *Astron. Nachricht.*, **317**, 225.
Robin, A., Reyle, C., Derriere, S., Picaud, S.: 2003, *Astron. Astrophys.*, **409**, 523.
Model available at `http://www.obs-besancon.fr/modele/modele__ang.html`
Saito, Y. et al.: 2003, *IAU JD*, **6E**, 19.
Sakai, S., Madore, B.F.: 1999, *Astrophys. J.*, **526**, 599.
Schlegel, D.J., Finkbeiner, D.P., Davis, M.: 1998, *Astrophys. J.*, **500**, 525.

Proc. IV Serbian-Bulgarian Astronomical Conference,
Belgrade 21–24 April 2004,
eds. M. S. Dimitrijević, V. Golev, L. Č. Popović, M. Tsvetkov,
Publ. Astron. Soc. "Rudjer Bošković" No 5, 2005, 175 - 181 *Contributed paper*

DECOMPOSITION OF PROFILES OF GALAXIES WITH CONVEX DISK SHAPES

Ts. B. GEORGIEV and O. I. STANCHEV

Institute of Astronomy, Bulgarian Academy of Sciences,
72 Tsarigradsko Shosse, 1784 Sofia, Bulgaria
E–mail tsgeorg@astro.bas.bg
E–mail stanchev@astro.bas.bg

Abstract. An improved one-dimensional decomposition technique for galactic profiles is presented. Both bulge and disk shapes are modeled by the Sersic (1968) formula and for the disk shape a second order term is included. The optimal free parameters - central brightness, scale length and exponential number, are derived by iterative procedure in the spirit of Kormendy (1977). The method is applied on published profiles of some nearby galaxies. Earlier (Georgiev, 2004; Georgiev and Stanchev, 2004) have found that the disk shapes of the early type galaxies are more convex, with central depression, while the disk shapes of the later type galaxies are close to exponential form of Freeman (1970). In the present work we show that the use of a second order term in the Sersic formula occurs an useful tool for detection of disks with ring-like shapes. Such disks are shown here in the cases of the galaxies IC 4871 and ESO 416-G25, that have edge-on orientation, as well as in the cases of the galaxies 7 Zw 793 and M 51, with almost face-on orientation.

1. INTRODUCTION

Freeman (1970) has introduced the exponential model of the radial disk profiles as a first approximation, known till now as the "Freeman's law". It is considered that the exponential shape could be understood from theoretical point of view (Freeman, 1970; Mo et al., 1998; Reshetnikov, 2000). However, the deep CCD profiles of the galactic disks show convex or truncated shapes and the Freeman's law is a very rough approximation. Generally, the truncation of the surface brightness in the outer part of the disk could be explained by decreasing of the star forming rate, due to insufficient matter concentration or/and lack of reasons for disk instabilities (Bottema, 1993; Geressen et al., 1997; Bizyaev and Zasov, 2002).This phenomenon is not studied completely yet, but the convex disk shapes should be modeled for the studies of the galaxies. The model of the truncated shape of the disk profile is introduced by van der Kruit and Searle (1981) and applied widely by Barteldrees and Dettmar (1994) by means of a special parameter – a cut-off radius. However, when the deepness of the observation increases, the cut-off radius increases too. By this reason Pohlen et al. (2000) have introduced a presentation of the disk shape with two exponents: inner, corresponding to the Freeman's law, and outer, more steeper. The deep observations

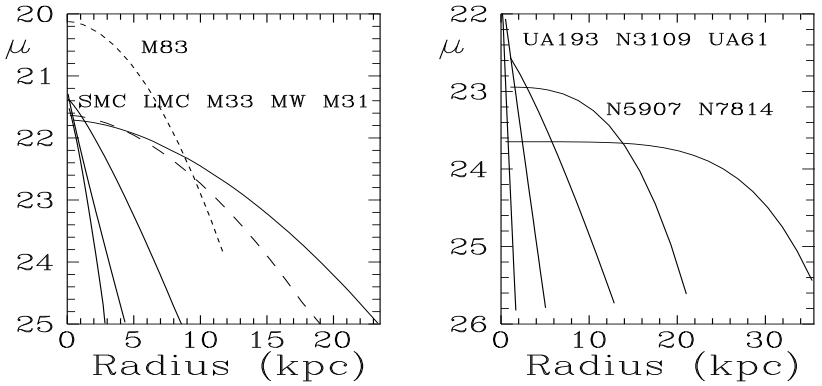

Figure 1: The disk shapes of nearby galaxies, modeled by the Sersic (1968) formula: **Left panel**: B-band radial disk profiles of the nearby galaxies (from the left to the right) SNC, LMC, M 33, and M 31, (solid curves), as well as the mass profile of the Milky Way with arbitrary ordinate shift, (long dashed curve) and B-band profile of the barred galaxy M 83 (short dashed curve) (Gerogiev, 2004); **Right panel**: B-band major axis profiles of five edge-on galaxies (from the left to the right) UGCA 193, NGC 3109, UGCA 61, NGC 5907 and NGC 7814, given with solid curves (Georgiev and Stanchev, 2004).

of 3 face-on galaxies, up to 29 mag/arcsec^2 in the R band of Pohlen et al. (2002) supported this "double exponent model".

Generally, the shape of the bulge changes smoothly with the Hubble type of the galaxy (Andredakis et al., 1995; Bagget et al., 1988; Chiotti and Bertin, 1999; Graham, 2001; Simard et al., 2002; Balcels et al., 2003). However, the changes of the disk shape with the Hubble type or with the mass of the disk are investigated poorly (van der Kruit, 2002) and what could be the reason is the lack of an adequate model of the observing profile of the disk. Another possibility for description of the disk shapes is the applying of a smooth model of the convex shape of the disk. In our previous papers (Georgiev, 2004; Georgiev and Stanchev, 2004) we have shown that the disk profiles could be modeled by means of the Sersic (1968) formula. It is applied in an iterative decomposition procedure in the spirit of Kormendy (1977), where both bulge and disk shapes are modeled by the Sersic equation. The number of the iteration is usually from 2 to 7.

Examples of nearby galaxies and edge-on galaxies are presented in Fig. 1.

The disk shapes are presented after correction to galactic extinction and reduction to absolute dimensions. It is found that in both cases the shape of the profile depends on the size or luminosity, i.e. on the mass of the disk. When the mass increases (toward the early spirals) the curvature of the radial disk profiles increases and the central peak of the disk brightness decreases. When the mass decreases (toward the late spirals and irregulars) the profile tends to be exponential with well prominent central peak.

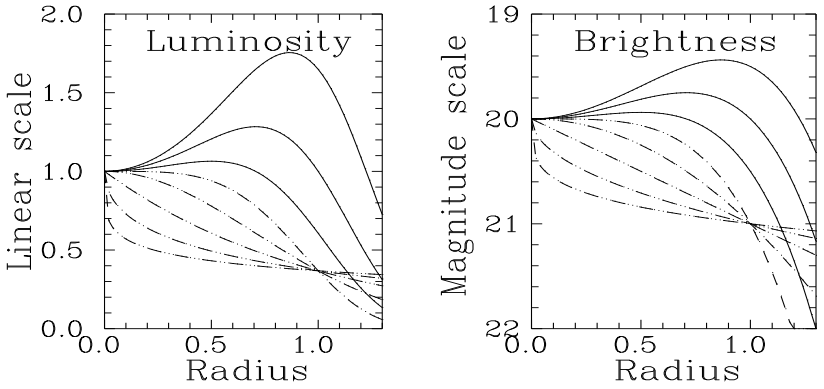

Figure 2: Shapes of radial profiles of bulges or disks, modeled by means of the Sersic formula of 1^{st} order for 5 values of n: 0.25, 0.5, 1, 2 and 4 (dashed curves, from left to the right, respectivelly) and 3 examples of 2^{nd} order Sersic formula (solid curves): **Left panel**: in the linear scale of the intensities; **Right panel**: in the magnitude scale of the brightness with arbitrary zero point.

However, the nature of the galactic disks seems more complicated: some of the disks of the early spirals seem to be rings (Kormendy, 1977). By this reason we have introduced more flexible modeling of the convex disk profiles, using "second order Sersic formula". In the present paper we give examples of this approach.

2. GENERALIZATION OF THE SERSIC FORMULA

In our previous papers (Georgiev, 2004; Georgiev and Stanchev, 2004) we have generalized the Sersic formula adding 2^{nd} and 3^{rd} order terms, calling the results "second order" and "third order" Sersic formulas. The full (3^{rd} order) formula could be written in two forms: in the linear scale, i.e. in intensities I_r, or in the magnitude scale, i.e. in surface brightness, μ_r:

$$\begin{aligned} I_r &= I_0\, exp\left[-\left(\frac{r}{h_1}\right)^n - \left(\frac{r}{h_2}\right)^{2n} - \left(\frac{r}{h_3}\right)^{3n}\right] \\ \mu_r &= \mu_0 + C_1 r^n + C_2 r^{2n} + C_3 r^{3n} \end{aligned} \qquad (1)$$

The usual 1^{st} order Sersic formula is a particular case of Eq. 1. It contains only the first term and it has 3 free parameters - the central intensity I_0 (or the central surface brightness $\mu_0 = -2.5 \log I_0$), the scale length $h_1 = (1.0857/C_1)^{1/n}$ and the exponential number n, which describes the curvature of the profile. Notice that usually the exponential number n is noted as $1/n$, but following Lauberts and Valentijn (1989) we prefer the notation, which has more simple interpretation. The 1^{st} order Sersic formula could represent various shapes of profiles. The case $n = 1/4$, which is known as "1/4 law" of de Vaucouleurs (1959), describes the profiles of the

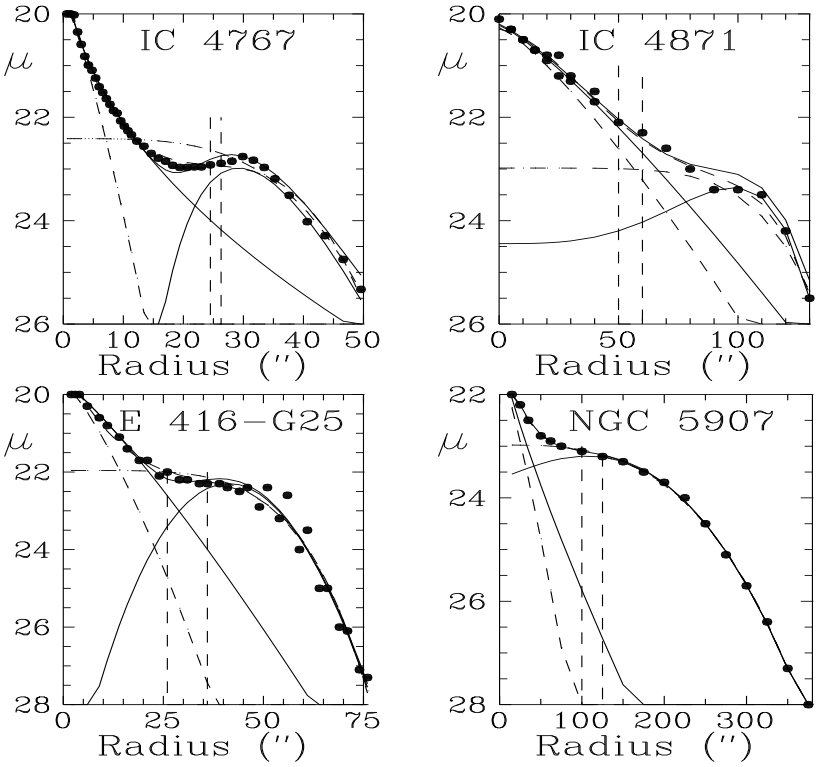

Figure 3: Decompositions of major axis profiles of edge-on galaxies. The solid curves represent the final shapes of the bulge, the disk and the restored profile, obtained by the use of the 2^{nd} order Sersic formula. The dashed curves represent the whole profile, modeled previously by means of 3^{rd} order Sersic formula, as well as the final shapes, obtained by means of the 1^{st} order Sersic formula. The vertical dashed lines show the last used point for the bulge model and the first used point for the disk model. The points between the vertical dashed lines are not used in the models of the bulge and the disk.

giant ellipticals. Exponential number $n \approx 1/2$ corresponds to the profiles of the big ellipticals and bulges of the early type spirals. if $n = 1$ (just the Freeman's law) this corresponds to the small ellipticals and the bulges of the late type galaxies, whereas $n = 2$ (just the Gaussian formula) seems correspond to some dwarf ellipticals and some small bulges of the late type galaxies. Examples are shown in Fig. 2 with dashed lines.

The 2^{nd} order Sersic formula has two scale length parameters. It could describe various shapes of the disks with external and internal truncation, i.e. the ring-like disks. Examples are presented in Fig. 2 with solid lines. In principle the 2^{nd} order formula comprehends the possibilities of the formula of Kormendy (1977), where,

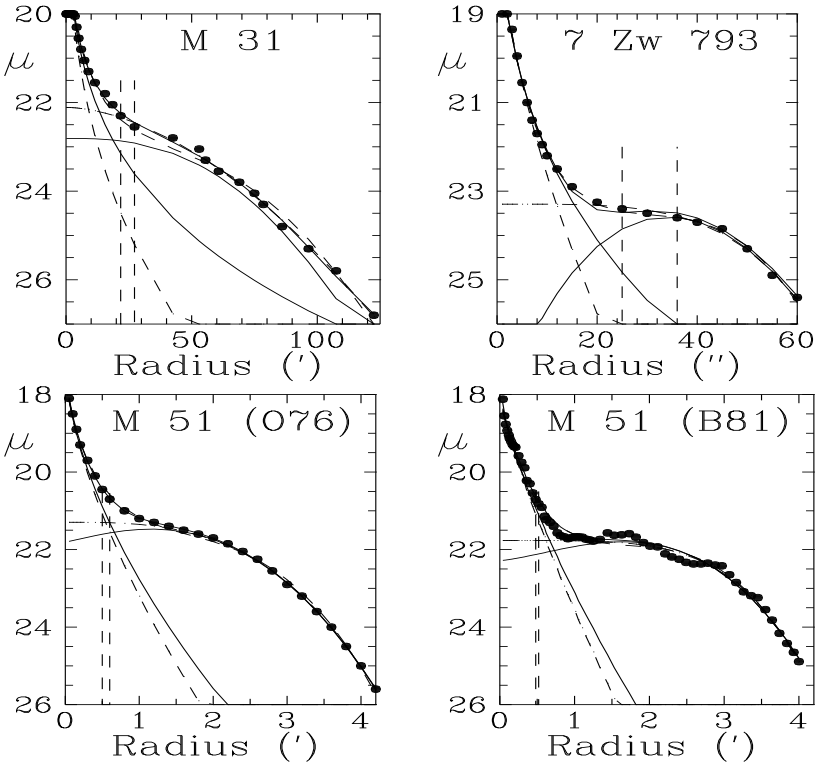

Figure 4: Decompositions of radial profiles of arbitrary oriented nearby galaxies (see the caption under Fig. 3.)

however, the exponential numbers of the first and second terms in Eq. 1. are equal to 1 and 3, respectively, and it describes a disk with exponential outer part and short internal truncation. Examples of the applying of 2^{nd} order formula are given in Figs. 3. and 4.

The 3^{rd} order Sersic formula (Eq. 1.) has three scale length parameters – $h_k = (1.0857/C_k)^{k/n}$; $k = 1, 2, 3$. The 3^{rd} order formula occur very useful before decomposition, because its inflex point is the natural dividing point between the bulge and the disk components, which is needed for the automatic beginning of the decomposition. In this case all 4 free parameters in Eq. 1. are derived from the whole observing profile by the MLS, with an application of the nonlinear numerical technique. We note that the inflex point, derived by means of the usual 3^{rd} order MLS polynomial, which is a particular case of Eq. 1. with $n = 1$, lies usually too far from the bulge.

In the present work we show the possibilities of our improved decomposition method for clarifcation of the cases in which the disks have strong central depressions or ring-like shapes. The possible presence of galactic bar is not accounted in this paper.

3. EXAMPLES OF DETECTION OF RING-LIKE DISKS

When a spiral galaxy is oriented edge-on, the integration of the light sources along the line of sight in the disk plane causes amplifying of the curvature of the major axis profile. Our analysis of about 120 published deep profiles shows that this phenomenon is obviously prominent in about 80% of all cases (Stanchev et al., 2002). In the rest cases some problems with the quality and the deepness of the profiles could be suspected. In our previous works we modeled the disk by means of the usual 1^{st} order Sersic formula. We have considered that in some cases this approximation is not sufficiently.

In the present work we show examples with 2^{nd} order formula, which represent the cases with ring-like disks. Examples are given in Figs. 3 and 4.

In Fig. 3 we show the decompositions of the published major axis profiles of 4 edge on galaxies: the "X-like" galaxy with polar ring IC 4767 (Whitemore and Bell, 1988), in B-band), IC 4871 and ESO 416-G25 (Barteldrees and Dettmar, 1994, in R-band), as well as NGC 5907 (van der Kruit and Searle, 1981, in B-band). The disk models, implemented by means of the 1^{st} order Sersic formula (dashed curves), show strong curvatures and almost flat central part. The exponential numbers of the models are 1,2,3,4, respectively. The use of 2^{nd} order Sersic formula (solid curves) underlines the presence of ring-like components. In the first case the profile is a photometry section along the edge-on polar ring of the galaxy IC 4767 and the ring-like shape of the "disk" component is not a surprise. In the second and third cases the edge-on galaxies IC 4871 and ESO 416-G25 show ring-like disks too. In the last example such structure, but not so strongly prominent, is found in the nearby edge-on galaxy NGC 5907.

In Fig. 4 we show the decompositions of the published deep radial profiles in the B-band of 4 galaxies: M 31 (de Vaucouleurs, 1958), 7 Zw 793 (Kormendy, 1977), M 51 (Okamura et al., 1976), M 51 (Boroson, 1981). When the orientation of the galaxy is not edge-on, the ring-like disk structure is less prominent. Though, in the given examples the 1^{st} order formula shows well prominent depressions of the central brightness of the disks (dashed curves) and the 2^{st} order formula elucidates the cases of true ring-like disks. The first example in Fig. 4 is the equivalent profile of the Sb galaxy M 31. The ring-like structures of the gas and the star forming regions of M 31 are well known, but the B-band profile of the disk does not show clearly the ring-like structure. The same result is derived for the B-band profile of M 83 and the Milky Way mass profile (from Freeman, 1970, not shown here). The S0 galaxy 7 Zw 793 in Fig. 4. shows strongly pronounced ring-like disk (see also Kormendy, 1977), well detected by our method. A surprise in the bottom of Fig. 4 is the face-on Sc galaxy M 51 with an active star-forming process. The 1^{st} order formula fits a flat central part of the disk, but the 2^{nd} order formula detects a central depression of about 0.5 mag. This result is derived from two independent photometry data: from Okamura et al. (1976) - equivalent profiles, and from Boroson (1981) - azimutaly averaged profiles of the southern part of the galaxy.

4. CONCLUSION

The application of the 2^{nd} order Sersic formula instead of the 1^{st} order has the advantage to give a flexible model of the disk – smooth and convex. The obvious disadvantage is the increasing of the free parameters, which makes the task of the profile restoration more uncertain. In the present paper we pay attention only on the explanation of ring-like disks and show that the 2^{nd} order Sersic formula is a useful tool for detection of such disks.

References

Andredakis, Y.C. Peletier, R.F. Balcells, M.: 1995, *Mon. Not. R. Astron. Soc.*, **275**, 874.
Bagget, W.E., Bagget, S.M., Anderson K.S.J.: 1998, *Astron. J.*, **116**, 1626.
Balcells, M., Graham, A.W., Dominguez-Palmero, L., Peletier R.F.: 2003, *Astrophys. J.*, **582**, L79.
Barteldrees, A., Dettmar R.J.: 1994, *Astrophys. J. Suppl. Series*, **103**, 475.
Bottema, R.: 1993, *Astron. Astrophys.*, **275**, 16.
Bizyaev, D.V., Zasov, A.V.: 2002, *Astron. Reports*, **46**, 721.
Boroson, T.: 1981, *Astrophys. J. Suppl. Series*, **46**, 177.
Chiotti, L., Bertin, G.: 1999, *Astron. Astrophys.*, **352**, 447.
de Vaucouleurs G.: 1958, *Astrophys. J.*, **128**, 465.
de Vaucouleurs, G.: 1959, Handbuch der Physik LIII, ed. Flugge, S., Springer-Verlag Berlin, **311**, 275.
Freeman, K.C.: 1970 *Astrophys. J.*, **160**, 811.
Geressen, J., Kuijken, K., Merrifield, M.: 1997, *Mon. Not. R. Astron. Soc.*, **288**, 618.
Gerogiev, T.B. : 2004, *Aerospace Researches in Bulgaria*, in print.
Gerogiev, T.B. and Stanchev, O.I.: 2004, *Bulgarian Journal of Physics*, in print.
Graham, A.W.: 2001, *Astron. J.*, **121**, 820.
Kormendy, J.: 1977, *Astrophys. J.*, **217**, 406.
Lauberts, A. Valentijn, E.A. : 1989, The surface photometry catalogue of the ESO-Uppsala, galaxies, Garching bei Munchen, ESO.
Mo, H.J., Mao, S., White, S.D.M.: 1998, *Mon. Not. R. Astron. Soc.*, **295**, 317.
Okamura, S., Kanazava, T., Kodaira, K.: 1976, *Publ. Astron. Soc. Japan*, **28**, 329.
Pohlen, M., Dettmar, R.J., Lutticke, R., Schwarzkopf, U.: 2000, *Astron. Astrophys. Suppl. Series*, **144**, 405.
Pohlen, M., Dettmar, R.J., Lutticke, R., Aronica, G.: 2002, *Astron. Astrophys. Suppl. Series*, **392**, 807.
Reshetnikov, V.P.: 2000, *Astron. Letters*, **26**, 485.
Sersic, J.L.: 1968, Atlas de Galaxies Australes (Cordoba: Obs. Astron. Univ. Nat.C ordoba).
Simard, L., Willmer, C.N.A., Vogt, N.P. et al. (10 coauthors): 2002, *Astrophys. J. Suppl. Series*, **142**, 1.
Stanchev, O.I. Groanova, Yu.B. and Georgiev, Ts.B.: 2002, *Publ. Astron. Obs. Belgrade*, **73**, 231.
van der Kruit, P.C. and Searle, L.: 1981, *Astron. Astrophys.*, **95**, 105.
van der Kruit, P.: 2002, in eds. G. S. Da Costa and E., M., Saadler, The Dynamics, Sructure and History of Galaxies, ASP Conference Serries.
Whitemore, B.C., Bell,M. : 1988, *Astrophys. J.*, **324**, 741.

Proc. IV Serbian-Bulgarian Astronomical Conference,
Belgrade 21–24 April 2004,
eds. M. S. Dimitrijević, V. Golev, L. Č. Popović, M. Tsvetkov,
Publ. Astron. Soc. "Rudjer Bošković" No 5, 2005, 183 - 186 *Contributed paper*

SPECTROPHOTOMETRIC OBSERVATIONS OF Mrk 817: PRELIMINARY RESULTS

D. ILIĆ[1], K. STAVREV[2], K. TSVETKOVA[2], M. TSVETKOV[2] and L. Č. POPOVIĆ[3]

[1]*Department of Astronomy, Faculty of Mathematics, University of Belgrade, Studentski trg 16, 11000 Belgrade, Serbia*
E–mail dilic@matf.bg.ac.yu

[2]*Institute of Astronomy, Bulgarian Academy of Sciencies, 72 Tsarigradsko Shosse Blvd., 1784 Sofia, Bulgaria*
E–mail kstavrev@skyarchive.org
E–mail katya@skyarchive.org
E–mail tsvetkov@skyarchive.org

[3]*Astronomical Observatory, Volgina 7, 11160 Belgrade 74, Serbia*
E–mail lpopovic@aob.bg.ac.yu

Abstract. The preliminary results of the image analysis of Mrk 817 observed with narrow-band filters is presented. The observations were made with the 2 m telescope at the National Astronomical Observatory Rozhen. The extensive structure in the continuum, He II and [OIII] lines was investigated in order to see the sign of the outflow in the extended region.

1. INRODUCTION

The galaxy Mrk 817, a Seyfert 1.5 galaxy, has been observed spectroscopically several times. One of the special features of its lines is that narrow [OIII] lines show very extensive blue part as shown in the Fig. 1. (Popović and Mediavlilla, 1997; Popović et al., 2004). This indicates an outflow in the narrow-line region, that is, in principal, large enough to be resolved in near AGNs. The aim of this work is to explore the extensive structure in different narrow spectral bands in order to see a sign of the outflow in the extensive region of this active galaxy.

2. OBSERVATIONS AND DATA REDUCTION

The presented observations are a part of the program for observing four Active Galactic Nuclei in narrow and broad-band filters at the National Astronomical Observatory Rozhen, Bulgaria (see Popović et al. in this proceedings). They were made in January 2004 with the 2 m Ritchey-Chrétien-Coudé telescope. In the Ritchey-Chrétien focus of the telescope, the equivalent focal length is 16 m and the field-of-view is one square degree with a scale $12.89''$/mm. The telescope is equipped with a

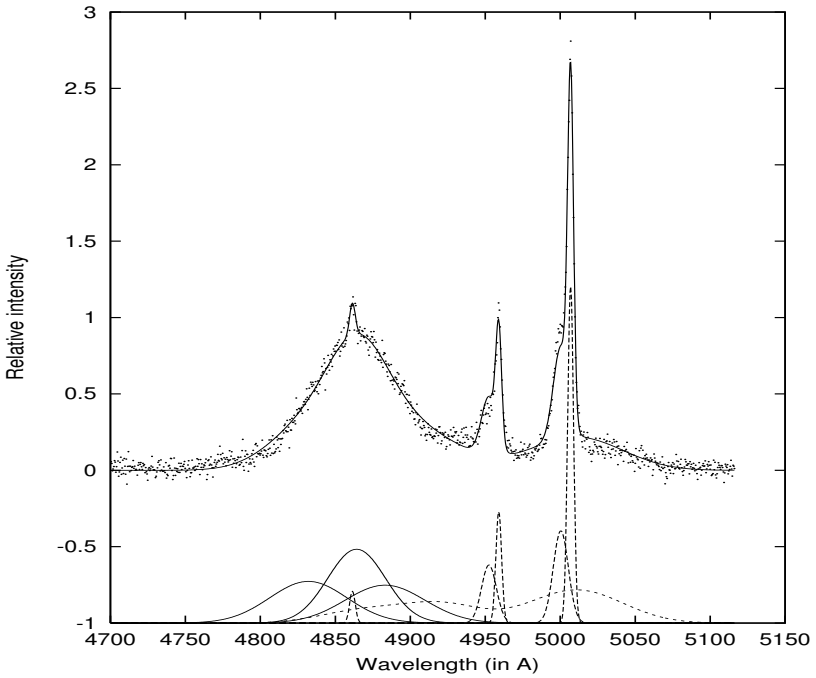

Figure 1: Decomposition of Hβ line of Mrk 817. The dots represent the observation and solid line is the best fit. The Gaussian components are shown at the bottom. The dashed lines at the bottom represent the Fe II template, [OIII] and Hβ narrow lines.

Photometrics AT200 CCD camera with 1024×1024 px array, with 1 px $= 0.32''$ and field $5.45' \times 5.45'$. The set of narrow-band filters in Rozhen Observatory (diameter 45 mm) used in these observations is given in Table 1.

Table 1: Narrow-Band Filters

λ_c [nm]	τ_{max} [%]	FWHM [nm]	Emission
468.1	0.607	18.8	HeII, 4686
500.9	0.726	22.3	[OIII], 4959,5007
575.5	0.644	23.5	Continuum
653.0	0.685	20.8	H_α, 6563
673.2	0.672	21.0	[SII], 6717, 6734

The galaxy was observed in the narrow bands [OIII] ($\lambda = 4959/5007$ Å), He II ($\lambda = 4686$ Å), and the continuum (see Table 2). Observations in other bands are planned for the near future.

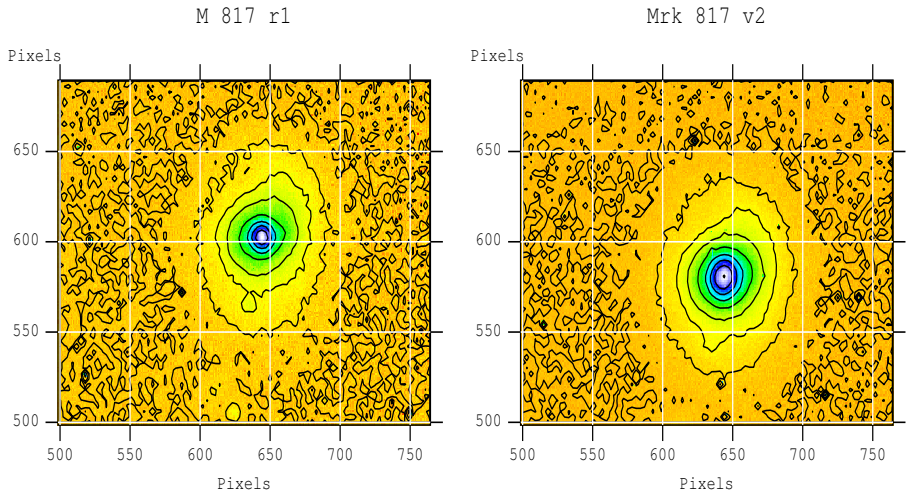

Figure 2: Seyfert galaxy Mrk 817 observed in the continuum (left) and the [OIII] (right) filter.

Table 2: Observations of Mrk 817

RA DEC	Redshift	Date of observation	Spectral line	Number of images	Exposure time [s]
$14^h36^m20^s.5$	0.031455	16-Jan-04	HeII	2	1200
$+58°48'14''.6$		16-Jan-04	[OIII]	2	1200, 1500
		16-Jan-04	Continuum	2	600

Standard reduction procedures including bias subtraction, trimming and flat-fielding were performed with the help of the IRAF software package.

3. PRELIMINARY RESULTS

We observed the galaxy Mrk 817 with 2 m telescope in order to resolve the outer regions of this active galaxy. With a combination of narrow-band filters we tried to confirm the existence of the outflow in the narrow-line region, detected previously with spectral analysis.

On all images the presence of the spiral arms is obvious and it is clear that the observed galaxy is vertically extended (see Figs. 2 and 3). We should also notice that the size of the galaxy varies in different spectral bands, being the biggest in the [OIII] line and the smallest in He II line.

The images taken in [OIII] filter show more intensive and wider central region of the galaxy. This can be in correlation with the previous spectral results (see the extended [OIII] lines in Fig. 1). More detail analysis should be applied and will be discussed elsewhere.

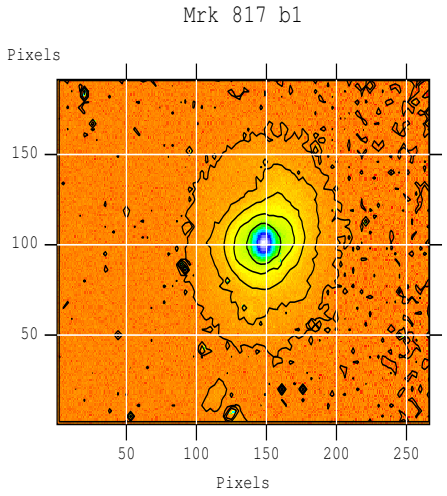

Figure 3: Seyfert galaxy Mrk 817 observed in the HeII filter.

Acknowledgements

This work was supported by the Ministry of Science, Technologies and Development of Serbia through the project P1196 "Astrophysical Spectroscopy of Extragalactic Objects", the Bulgarian National Science Fund project # I- 1103 and contract 436-BUL110-120 between Deutsche Forschungsgemeinschaft and the Bulgarian Academy of Sciences. L. Č. P. is supported by Alexander von Humboldt Foundation through the program for foreign scholars.

References

Osterbrock, D.E.: 1989, Astrophysics of Gaseous Nebulae and Active Galactic Nuclei, Mill Valle, University Science Press.
Popović, L.Č. and Mediavlilla, E.G.: 1997, *Publ. Astron. Obs. Belgrade*, **57**, 95.
Popović, L.Č., Mediavilla, E.G., Bon, E. and Ilić, D.: 2004, *Astron. Astrophys.*, accepted.

Proc. IV Serbian-Bulgarian Astronomical Conference,
Belgrade 21–24 April 2004,
eds. M. S. Dimitrijević, V. Golev, L. Č. Popović, M. Tsvetkov,
Publ. Astron. Soc. "Rudjer Bošković" No 5, 2005, 187 - 193 *Contributed paper*

SOLAR ACTIVITY INFLUENCE TO PRECIPITATIONS, VIII

B. D. JOVANOVIĆ

Faculty of Agriculture, Waterarranging Institute, Novi Sad, Serbia
E–mail jvbzd@polj.ns.ac.yu

Abstract. As in previous papers, by the same author, the Spectral decomposition theorem has been applied to find the eventual influences of the solar activity, known as the Total sunspot area, to the precipitations, on a spot in Serbia. By means of the cross periodograms, cospectral density, quadrature density, cross amplitude, the correlation has been studied. The cross correlation function proved that there may be a time lag of three years, for maximal precipitations, and a nine year lag for minimal precipitations, following the Solar activity.

1. ORIGINS

It is well known that the water is a sine qua non condition of living. So, one of the primary occupations of the spatial probes is the search after this matter, at the earlier times wrongly considered as an element. The main concern of scientists and specialists, on Earth, is the knowledge of the quantities and spots where it may be found, neverthless of that, will this be a still or a flowing one. The same problem is connected to precipitations which should fill the "reservoirs" on the surface.

Therefore it would be of a special benefit if we could be able to predict the maximal or the minimal rainfall, snowfall, etc. To our great sorrow we are, at the times, unable to forecast all conditions which are regulating these phenomena.

Some observed data are of a PERIODICAL nature, if they repeat themselves after the same time, and have the same intensity. But, other seem periodic, having neither the same time interval nor the same intensity. These are known as QUASIPERIODICAL PHENOMENA. To the latter ones we may list the activity of our sun, as well as the precipitations on our planet.

As told, we can not know all the sources of these changes. So, we are forced to use some mathematical methods, such as statistical or probabilistic ones, and look for the best fitting to our observations.

As in previous papers (Jovanović, 2001a-c; 2002ab; 2003; 2004) the spectral decomposition theorem has been applied to find the eventual influences of the solar activity, known as the Total sunspot area, to the precipations, on a spot in Serbia.

2. DATA AND DATA PROCESSING

Our attention has been narrowed to the single one spot, a station, in Serbia. Just from the beginning of these kinds of research, I thought, and J.-C. Pecker confirmed my opinion, in Pecker (1987), that the simultaneous use of data, observed at numerous stations on the Earth's surface, in the case of the solar-terrestrial influence study, may lead to distortions instead of correlation improvement.

Following data notations have been used:

Time series for SOLAR ACTIVITY (yearly means)::

X, Var 9 - TOTAL SUNSPOT AREAS, expressed in millionth parts of the visible solar hemisphere, corrected for sphericity, published by the Data center in Boulder, Colorado, USA.

Time series for PRECIPITATIONS (yearly means)::

Y, VAR 10 - PADAVINE, in mm/m^2, measured on a spot in Serbia, published by the Republic Hydrometeorological Institute in Beograd.

Both series are beginning by the year 1947 and are ending by the year 1996.

For obtaining the corresponding periodograms, of both seriers, we used the SPECTRAL DECOMPOSITION THEOREM which states that: the energy, or variance, of any time series, can be broken down into the contribution of statistical independent oscillations of different periods (frequencies). The peaks, in the spectral periodicity function graph (periodogram), stand for so-called independent harmonics. The most outstanding one is the MAJOR PERIOD (FREQUENCY), and the next ones mark the HIGHER HARMONICS or OVERTONES. My task was to pick up the pairs of vibrations with the same period (frequency) in both periodograms.

Following, we supposed that we have to do with two stationary time series, X, and Y, and that we wish to asses the extent to which we can use the past of X to predict Y. As a criterion of evaluation we used the CROSS CORRELATIONS. They gave the time lag of Y following the X.

More proves gave us the: CROSS PERIODOGRAM, COSPECTRAL DENSITY, QUADRATURE DENSITY and the CROSS AMPLITUDE.

3. RESULTS

The PERIODOGRAM for TOTAL SUNSPOT AREAS has eight peaks (Fig. 1). In other words, this series is a superposition of eight independent vibrations. The *major period* is of 12.5 years (87.86% of the whole). The first overtone is of 5.55 years (4.01%), the second is of 3.85 years (1.56%), the third is of 2.27 years (1.50%), the fourth is of 2.o8 years (1.44%), the fifth is of 2.50 years (1.27%), the sixth is of 3.13 years (1.22%), and the seventh overtone is of 2.77 years (1.04% of the whole variance of the Total sunspot areas).

The PERIODOGRAM for PRECIPITATIONS has seven independent oscillations – seven peaks (Fig. 2).The *major period* is of 12.5 years (24.50% of the whole). The first overtone has 3.57 years (22.15%), the second is of 4.55 years (19.54%), the third is of 2.94 years (11.40%), the fourth is of 2.38 years (10.29%), the fifth is of 2.17 years (6.66%), and the sixth overtone is of 25.00 years (5.45% of the whole variance of precipitations).

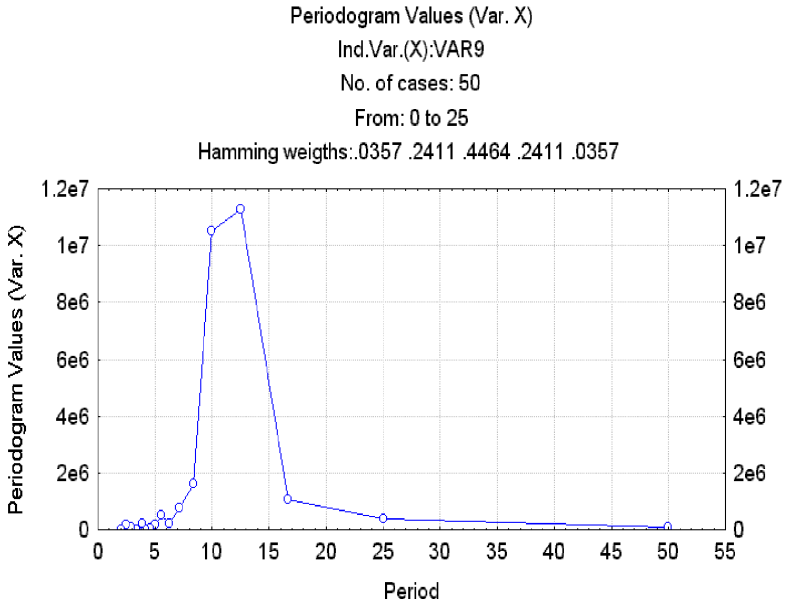

Figure 1:

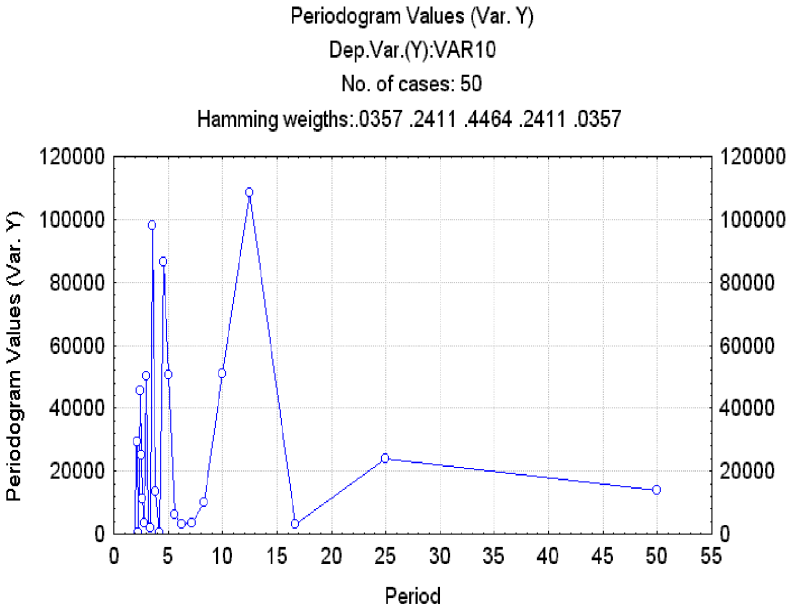

Figure 2:

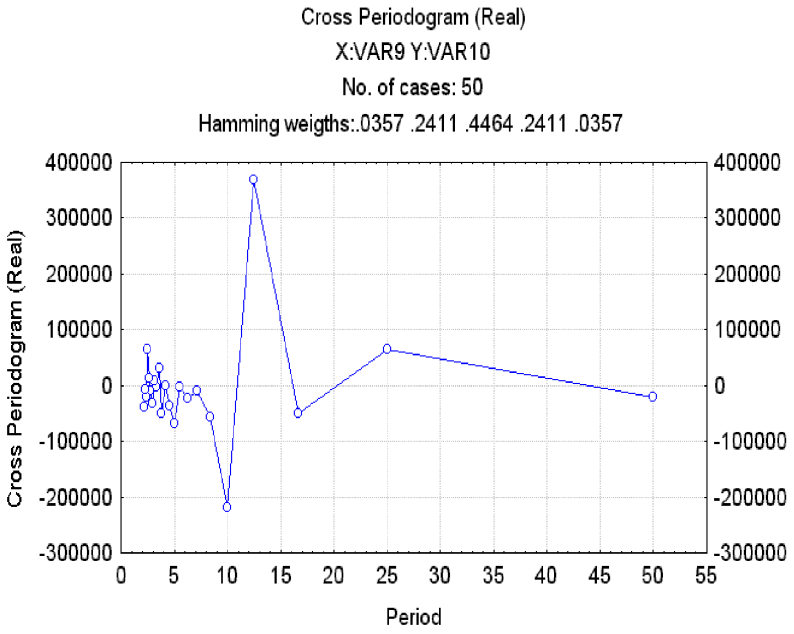

Figure 3:

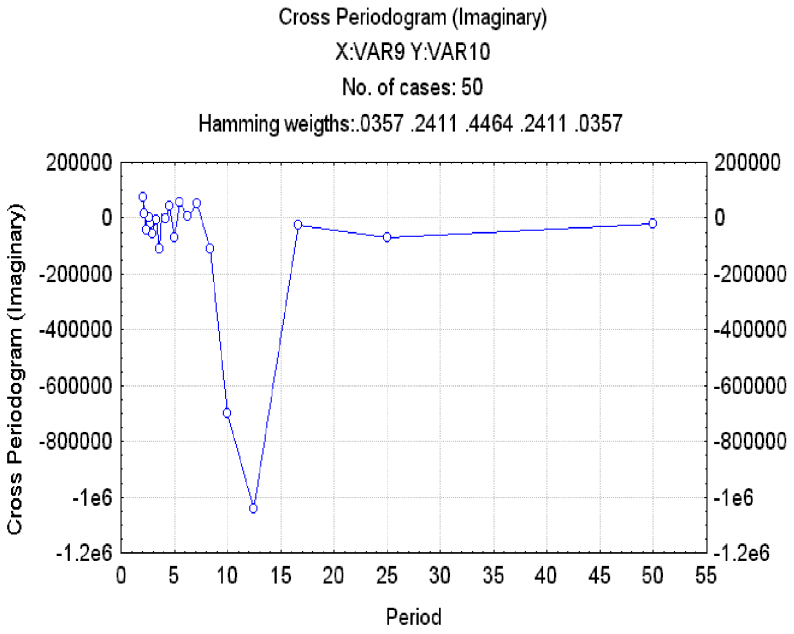

Figure 4:

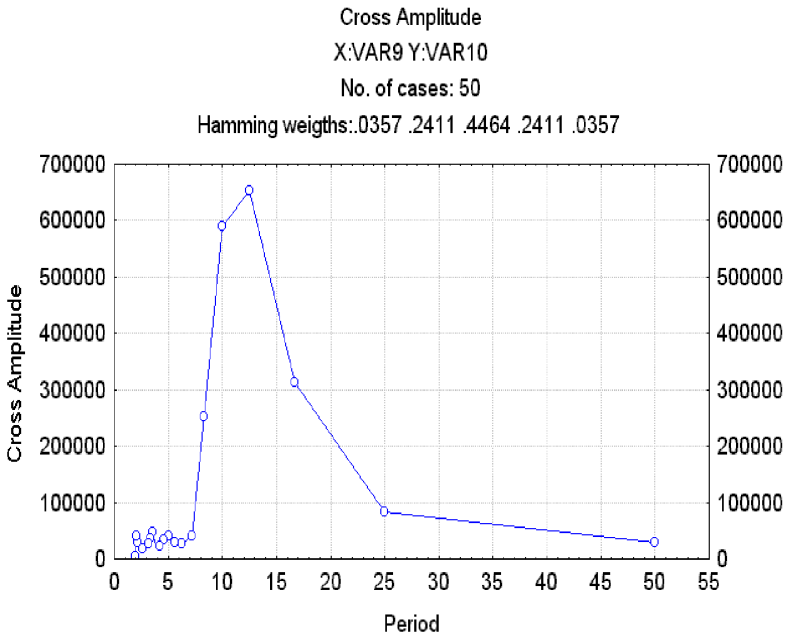

Figure 5:

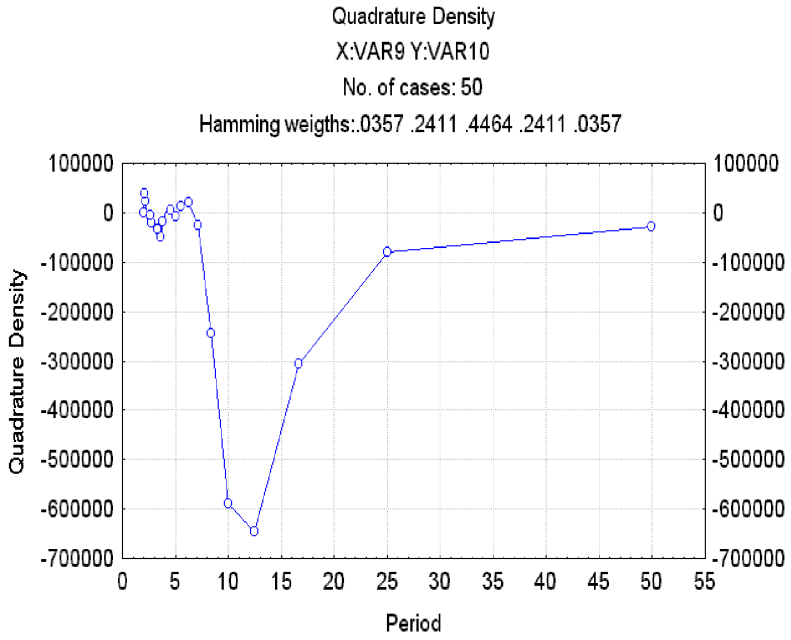

Figure 6:

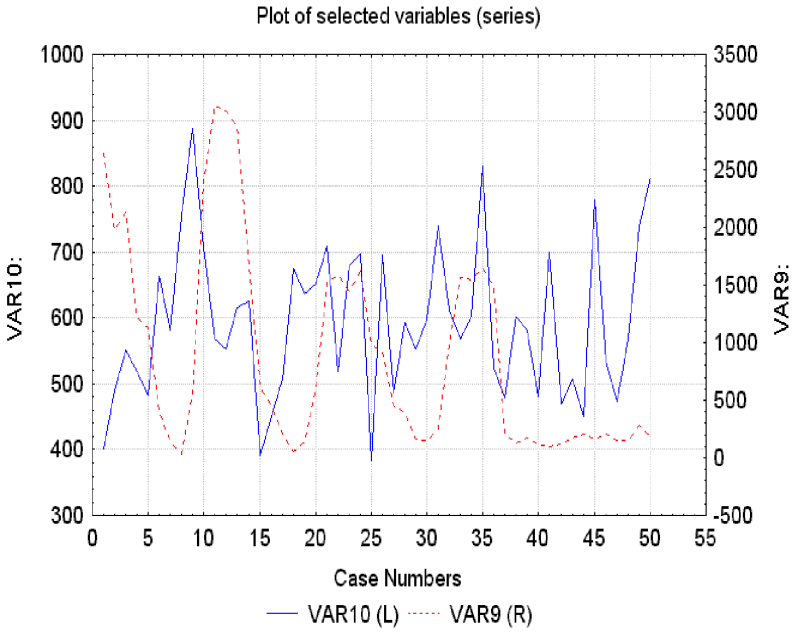

Figure 7:

If we compare, now, these two periodograms and their independent oscillations, we conclude that they have only *one pair of corresponding periods* 12.50 years long. Both of these are major periods.

The same correlation may be proved by means of their CROSS PERIODOGRAMS (Fig. 3 and Fig. 4), CROSS AMPLITUDE (Fig. 5), and QUADRATURE DENSITY (Fig. 6).

Now we turn to CROSS CORRELATIONS. The positive *maximum* of this graph stands for the *time lag of three years*, and the negative *minimums*tands for the *time lag of nine years.*

Let us show both time series in one Fig. 7 to see the obvious time lag.

4. CONCLUSION

According to constructed periodograms, following the Spectral decomposition theorem, and for calculated cross periodograms, cross amplitude and quadrature density, as well as for corresponding cross correlations, for the index of solar activity, known as the TOTAL SUNSPOT AREAS, expressed in millionth parts of the visible solar hemisphere, corrected for sphericity, X, VAR 9 time series, from the one side, and PRECIPITATIONS, expressed in mm/m^2, measured on a station in Serbia, X, VAR 10 time series, from the other side, we are entitled to announce that, in the statistical sense, *the solar activity may influence*, with accuracy given, *maximal precipitations with a lag of three years, and the minimal precipitations with a lag of nine years.*

References

Jovanović, B.D.: 2001a, Suša i poljoprivreda, Zbornik, Novi Sad, 33.
Jovanović, B.D.: 2001b, Eko-konferencija '01, Zbornik, Novi Sad, 375.
Jovanović, B.D.: 2001c, I medjunarodni simpozijum "Hrana u 21.veku", Subotica, in press.
Jovanović, B.D.: 2002a, Eko-konferencija '02, Zbornik, Novi Sad, 87.
Jovanović, B.D.: 2002b, Melioracije i poljoprivreda, Zbornik, Novi Sad, 19.
Jovanović, B.D.: 2003, Medjunarodna Eko konferencija 2003, Zbornik, Novi Sad, 217.
Jovanović, B.D.: 2004, Poljoprivreda izmedju suša i poplava, Zbornik, Novi Sad, 13.
Pecker, J.-C.: 1987, Compendium in Astronomy, D. Reidel, Dordrecht, 156.

Proc. IV Serbian-Bulgarian Astronomical Conference,
Belgrade 21–24 April 2004,
eds. M. S. Dimitrijević, V. Golev, L. Č. Popović, M. Tsvetkov,
Publ. Astron. Soc. "Rudjer Bošković" No 5, 2005, 195 - 200 *Contributed paper*

HOW MICROLENSING CAN CONTRIBUTE TO QSO VARIABILITY?

P. JOVANOVIĆ and L. Č. POPOVIĆ
Astronomical Observatory, Volgina 7, 11160 Belgrade 74, Serbia
E–mail pjovanovic@aob.bg.ac.yu

Abstract. We study the infuence of gravitational microlensing on the AGNs X-ray radiation in order to explain the recently observed shape variations of X-ray continuum and Fe Kα line in the high-redshifted lensed quasars MG J0414+0534, QSO 2237+0305 and H1413+117. Assuming that the X-ray radiation is originating in accretion disc, we used the ray tracing method considering both geometries, Schwarzschild and Kerr, to analyze the amplifications of X-ray continuum and the Fe Kα line flux due to microlensing by a caustic microlens. Different sizes of emission regions, as well as different emissivity laws and different microlens parameters are used in our study. Our results show that the observed Fe Kα amplification without corresponding amplification of X-ray continuum can be expected when their emitting regions have different dimensions. Moreover, here we will discuss the optical depth for microlensing of QSO X-ray emitting region by cosmologically distributed gravitational microlenses which could be localized in galaxies (or even in bulge or halo of gravitational macrolenses) or could be distributed in a uniform way.

1. INTRODUCTION

Recent observational and theoretical studies suggest that gravitational microlensing can induce variability in the X-ray emission of lensed QSOs. Microlensing of the Fe Kα line has been reported in at least three macrolensed QSOs: QSO J0414+0534 (Chartas et al, 2002), QSO 2237+0305 (Dai et al, 2003), and H1413+117 (Oshima et al, 2001). The influence of microlensing in the Fe Kα spectral line shape was discussed in Popović et al. (2001); Chartas et al. (2002) and Popović et al. (2003). Popović et al. (2003) show that objects in a foreground galaxy with even relatively small masses can bring observable changes in the Fe Kα line flux. Such effects could be caused by stellar mass objects located in a bulge or/and in a halo of foreground galaxy as well as by cosmologically distributed objects. Thus, the observations of the X-ray continuum and the Fe Kα line in multi-imaged AGNs open new possibilities to study the unresolved X-ray emitting structure in QSOs.

Here we present our investigations regarding the continuum and Fe Kα line variability due to microlensing. Also, we discuss the optical depth of high-redshifted QSOs.

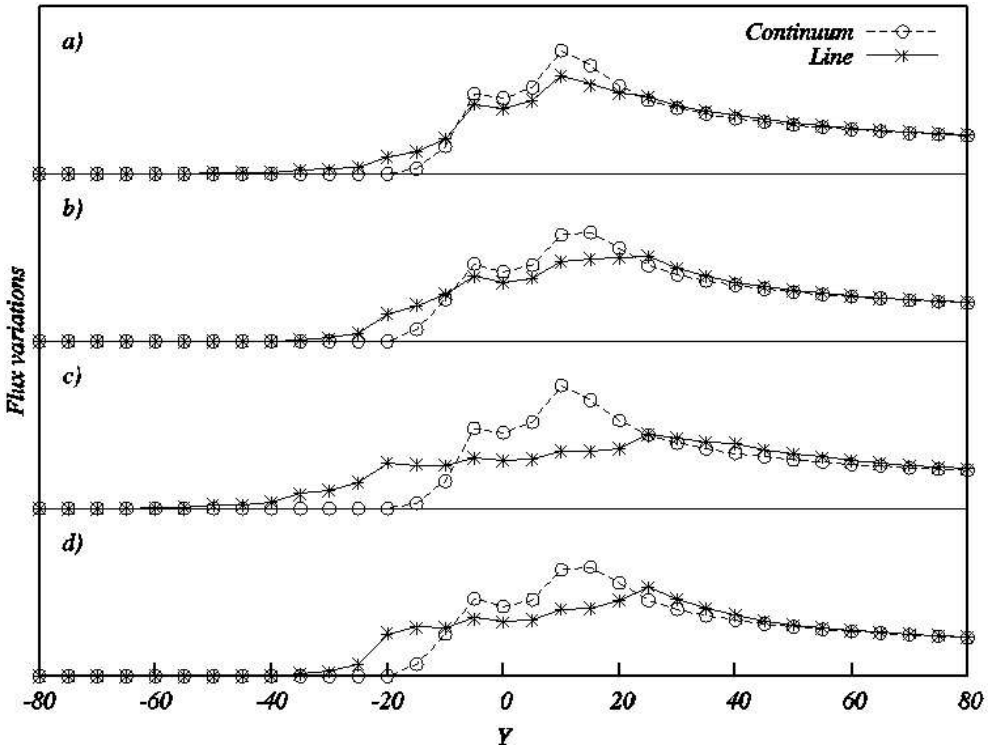

Figure 1: The variations of normalized total line and continuum flux in interval from 0.1 to 10 KeV due to caustic crossing (ERR=$50R_g$) parallel to the rotation axis for different Y positions in Schwarzschild metric. Figures correspond to: a) black body radiation in the case (II), b) modified black body in the case (II), c) black body radiation in the case (III), d) modified black body in the case (III). Flux variations are presented in the range from 1 to 1.7.

2. MICROLENSING OF A COMPACT ACCRETION DISC

Taking into account the previous results, we modeled the behavior of X-ray continuum and Fe Kα line during a microlensing event for different sizes of the continuum and the Fe Kα line emission regions. We assumed that X-ray continuum and Fe Kα line originated in an accretion disc with black body emission (Planck function) and that the microlensing event could be described by a caustic crossing. However, in the innermost part of the accretion disc the Planck function cannot be used properly and, therefore, we also used the standard Shakura-Sunyaev approach, where the disc emission was described by a "modified" black body radiation law (Shakura and Sunyaev, 1973).

For the disc inclination we adopted the averaged values given by Nandra et al. (1997) from the study of the Fe Kα line profiles of 18 Seyfert 1 galaxies: i= 35^o and for caustic parameters we addopted ERR=50 Rg, A_0=1 and β=1. The inner radius,

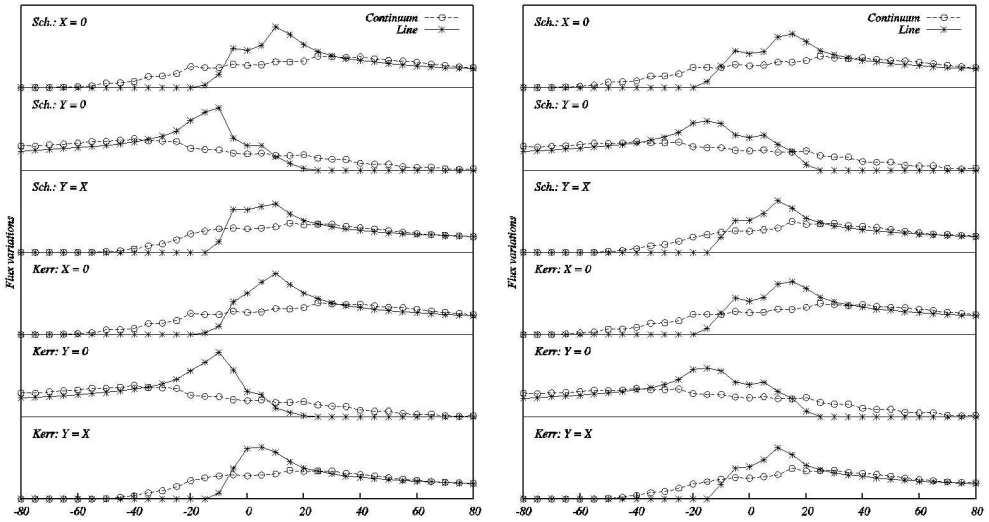

Figure 2: The variations of normalized total line and continuum flux in interval from 0.1 to 10 KeV for the case (IV) due to caustic crossing (ERR=$50R_g$) in three different directions. On the left are presented results for black body radiation and on the right for modified black body radiation. First three figures on each side correspond to Schwarzschild and last three to Kerr metric. Flux variations are presented in the range from 1 to 1.7.

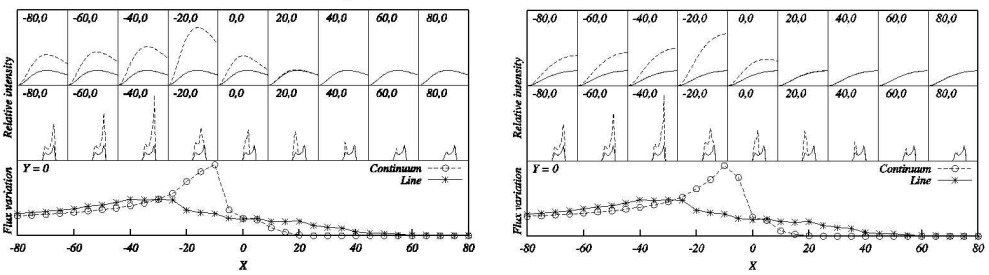

Figure 3: The variations of X-ray continuum and Fe Kα line for an highly inclined disc ($i = 75^o$) and ERR=2000 R_g in the case of black body radiation (left) and modified black body radiation (right). The other disc characteristics correspond to the case (III).

R_{in}, cannot be smaller than the radius of the marginal stability orbit, R_{ms}, that corresponds to $R_{ms} = 6\ R_g$ in the Schwarzschild metric and to $R_{ms} = 1.23\ R_g$ in the case of the Kerr metric with angular momentum parameter $a = 0.998$.

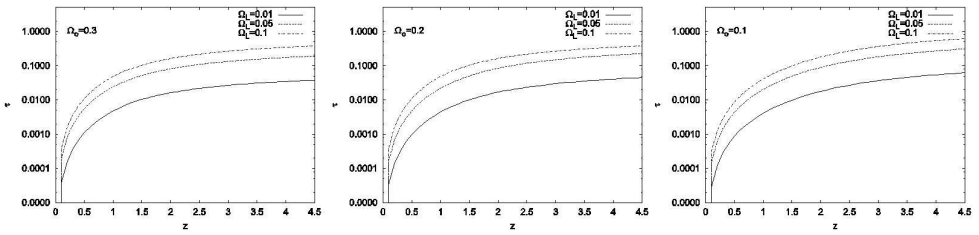

Figure 4: The calculated optical depth as a function of red-shift for different values of cosmological parameters Ω_L and Ω_0.

To explain the lack of the X-ray continuum response to the microlensing events detected in the Fe Kα line, we considered four cases of disc sizes for both continuum and line emitters:

- the inner and outer radii of both emission regions are the same, $R_{in} = R_{ms}$ and $R_{out} = 20\ R_g$
- the inner radii are the same, $R_{in} = R_{ms}$, but the outer radius of the X-ray continuum disc is smaller, $R_{out} = 20\ R_g$, than the radius of the line emission disc, $R_{out} = 80\ R_g$
- the continuum emission disc has radii $R_{in} = R_{ms}$, $R_{out} = 20\ R_g$ and the line emission disc $R_{in} = 20\ R_g$ and $R_{out} = 80\ R_g$
- the continuum emission disc has radii $R_{in} = 20R_g$, $R_{out} = 80\ R_g$ and the line emission disc $R_{in} = R_{ms}$ and $R_{out} = 20\ R_g$.

The corresponding results are presented in Fig. 1. and Fig. 2.

The observed BAL QSOs have highly inclined discs ($i > 60^o$), and the corresponding variations of X-ray continuum and Fe Kα line due to microlensing by solar mass deflectors are presented in Fig. 3. for both radiation laws.

In order to discuss the contribution of microlensing to X-ray variability of high-redshifted QSOs, we calculated optical depth (probability that at any instant of time the source is covered by a deflector) for microlensing caused by stellar mass objects. We considered the deflectors in the halo and bulge of host galaxy, as well as at the cosmological distances between observer and source. According to the cosmological SN (Supernovae) Ia data and CMB anisotropy one could take for the parameters of standard cosmological model $\Omega_\Lambda \sim 0.7$ and $\Omega_0 \sim 0.2$ (Zakharov et al. 2004). Optical depth is calculated using three different values for the matter fraction in compact lenses, Ω_L= 0.01, Ω_L= 0.05 and Ω_L= 0.1 (see Fig. 4). The first value could be adopted if we assume that 20% of baryon matter could form microlenses, the second one if almost all baryon matter could form microlenses and the last one if about 30% of non-baryonic dark matter forms objects with stellar masses (Zakharov et al. 2004).

3. RESULTS

From our calculations we can conclude:

1. Not only the Fe Kα line could experience significant amplification by a microlensing event, but also the continuum (even for very small mass microlenses). Thus, the absence of continuum amplification in the observed Fe Kα microlensed QSOs should be related to the structure of the accretion disk and/or the geometry of the event.

2. Segregation of the emitters allows us to reproduce the observed flux variability. If the Fe Kα emitters were distributed in a structure inner to the continuum disc the simulations reproduce satisfactorily the observed Fe Kα enhancement without continuum amplification.

3. In the case of observed BAL QSOs where inclination is greater than 60^o, microlensing by solar mass deflectors, having ERR$\sim$2000 R_g, can explain observed flux variations.

4. The optical depth in the bulge and halo of host galaxy is $\sim 10^{-4}$, so microlensing by the deflectors from host galaxy halo and bulge have minor contribution in X-ray variability of QSOs.

5. The optical depth for cosmologically distributed deflectors could be $\sim 10^{-2}$–0.1 and can significantly contribute to the X-ray variability of high-redshifted QSOs. The value 0.1 corresponds to the case when compact dark matter forms cosmologically distributed microlenses.

6. The optical depth for cosmologically distributed deflectors is higher for $z > 2$ and after $z > 2$ slowly increases. It indicates that the contribution of microlensing into X-ray variability of QSOs with redshift $z > 2$ may be significant as well as that this contribution could be nearly constant for high-redshifted QSOs. It is in good agreement with the fact that the AGNs of the same X-ray luminosity are more variable at $z > 2$ (Manners, et al, 2002).

References

Chartas, G., Agol, E., Eracleous, M., Garmire, G., Bautz, M.W., Morgan, N.D.: 2002, *Astrophys J.*, **568**, 509.

Dai, X., Chartas, G., Agol, E., Bautz, M.W., Garmire, G.P.: 2003, *Astrophys J.*, **589**, 100.

Manners, J., Almaini, O., Lawrence, A.: 2002, *Mon. Not. R. Astron. Soc.*, **330**, 390.

Nandra K., George I.M., Mushotzky R.F., Turner T.J., Yaqoob T.: 1997, *Astrophys J.*, **477**, 602.

Oshima, T., Mitsuda, K., Ota, N., Yonehara, A., Hattori, M., Mihara, T., Sekimoto, Y.: 2001, *Astrophys J.*, **551**, 929.

Popović, L.,Č., Mediavilla, E.G., Muñoz J., Dimitrijević, M.S., Jovanović, P.: 2001, *Serb. Aston. J.*, **164**, 73 (also, presented on GLITP Workshop on Gravitational Lens Monitoring, 4-6 June 2001, La Laguna, Tenerife, Spain).

Popović, L.Č., Mediavilla, E.G., Jovanović, P., Muñoz, J.A.: 2003, *Astron. Astrophys.*, **398**, 975.
Shakura, N.I., Sunyaev, R.A.: 1973, *Astron. Astrophys.*, **24**, 337.
Zakharov, A.F., Popović, L.Č., Jovanović, P.: 2004, *Astron. Astrophys.*, accepted.

Proc. IV Serbian-Bulgarian Astronomical Conference,
Belgrade 21–24 April 2004,
eds. M. S. Dimitrijević, V. Golev, L. Č. Popović, M. Tsvetkov,
Publ. Astron. Soc. "Rudjer Bošković" No 5, 2005, 201 - 207 *Contributed paper*

COSMOLOGICAL CONSTRAINTS ON NEUTRINO OSCILLATIONS FOR INITIALLY NON-ZERO STERILE STATE

D. KIRILOVA[1,2] and M. PANAYOTOVA[1]
[1] *Institute of Astronomy, Sofia, Bulgaria*

[2] *Abdus Salam ICTP, Trieste, Italy*
E–mail dani@libra.astro.bas.bg
E–mail mariana@libra.astro.bas.bg

Abstract. We discuss cosmological constraints on neutrino active-sterile oscillations for the specific case when the sterile neurino is partially- filled initially. We provide numerical analysis of the BBN production of He-4, Y_p, in the presence of electron-to-sterile neutrino oscillations, effective after neutrino decoupling. We account for all known oscillations effects on cosmological nucleosyntesis. We obtain isohelium contours corresponding to different levels of He-4 overproduction, $\delta Y_p/Y_p$, for non-zero initial population of the sterile state δN_s. We present the cosmological constraints on oscillation parameters corresponding to $\delta N_s = 0.0$ and 0.5 and $\delta Y_p/Y_p = 3\%$ and 5%. The cosmological constraints for the cases $\delta N_s \leq 0.5$ are slightly strengthened in comparison to $\delta N_s = 0$ case.

1. INTRODUCTION

There are many different experiments indicating and/or confirming the existence of neutrino oscillations:

solar neutrino oscillations experiments: Homestake, Kamiokande, SuperKamioKa, Gallex, SAGE, SNO;

atmospheric neutrino oscillations experiments: SuperKamioKa, Makro, Soudan 2, IMB;

terrestrial neutrino oscillations experiments: LSND, KamLAND, K2K.

In the case of non-zero neutrino masses the mass eigenstates ν_i are distinct from the flavour ones ν_f:

$$\nu_i = U_{if}\nu_f, \qquad f = e, \mu, \tau \tag{1}$$

and transitions between neutrinos of different types, known as neutrino oscillations, take place.

Neutrino oscillations may influence the physical processes in the early Universe evolution, such as baryogenesis, leptogenesis, nucleosynthesis, etc. Vice versa, Big Bang Nucleosynthesis (BBN) explains successfully the data on the primordial abundances

of D, He-3, He-4 and Li-7 and that is why it could be used as a probe for the physics of the early Universe and the neutrino oscillations, in particular.

The most stringent constraints on neutrino oscillations parameters were obtained from BBN considerations. In particular, LMA and LOW active-sterile solar oscillation solutions and atmospheric active-sterile solutions were excluded many years before the global analysis of experimental neutrino data pointed to the preference of flavour oscillations for solving these neutrino anomalies (for a review on these issues see Kirilova 2004). However, these constraints were obtained assuming zero sterile neutrino state population before neutrino oscillations epoch.

Here we discuss BBN constraints on neutrino oscillations parameters obtained in the more general case of sterile neutrino state initially partially occupied. This issue is interesting because sterile neutrinos ν_s may be present at the onset of BBN epoch — they may be produced in GUT models, in models with large extra dimensions, Manyfold Universe models, mirror matter models, or in $\nu_{\mu,\tau} \leftrightarrow \nu_s$ oscillations in 4-neutrino mixing schemes. Hence, the degree of population of ν_s may be different depending on the ν_s production model.

The general case of non-zero sterile neutrino population was discussed in ref. (see Kirilova, 2004b). The kinetic effect of oscillations was shown to be sensitive to the initial population of ν_s. Hence, it is desirable to generalize the cosmological constraints on neutrino oscillation parameters, as well.

2. PODUCTION OF PRIMORDIAL HELIUM-4 AND NEUTRINO OSCILLATIONS

2.1. PRIMORDIAL HE-4 - THEORY AND OBSERVATIONS

Y_p, predicted by BBN, is calculated with great precision (see e.g. Lopez and Turner, 1999; Esposito et al., 2000; Cyburt et al., 2003; Cuoco et al., 2003). The theoretical uncertainty is less than 0.1% ($|\delta Y_p| < 0.0002$) within a wide range of values of the baryon-to-photon ratio η. The predicted He-4 value is in relatively good agreement with the observational data for He-4 and is consistent with the abundances of the other light elements. Contemporary helium values, inferred from astrophysical observational data, are 0.238–0.245 (see Olive et al., 1997; Izotov and Thuan, 1998). Using η indicated either by D measurements or by CMB, taking the central Helium value of the 2 measurements 0.238 and assuming the systematic error of 0.005 the agreement between different helium measurements is at 2σ level and the uncertainty is only around 2%.

Measurements of primordial helium from CMB data are possible. Hopefully, future Planck CMB measurements will be capable of determining the helium mass fraction within $\delta Y \sim 0.01$ in a completely independent way (see Trotta and Hansen, 2003).

Thus ^{4}He is the most abundantly produced, most precisely measured and calculated element among the primordially formed elements, and therefore, it is the preferred one for obtaining limits on nonstandard physics.

Its primordial yield essentially depends on the freezing of the weak reactions governing the neutron to proton transitions. Their freeze-out occurs when in the process

of expansion the weak processes rates become comparable to the expansion rate:

$$\Gamma_w \sim G_F^2 E_\nu^2 N_\nu \leq H(t) \sim \sqrt{g_{eff}}\, T^2 \tag{2}$$

So, the primordially produced mass fraction of He-4 $Y_p \sim 2(n/p)_f/(1+n/p)_f$ is a strong function of relativistic degrees of freedom at BBN epoch, which enter through H, and also depends on the electron neutrino characteristics, namely its energy spectrum, number densities and the neutrino-antineutrino asymmetry, entering through Γ_w.

2.2. OSCILLATIONS EFFECTS

Flavor neutrino oscillations effect BBN negligibly because the energy spectrum distributions of different flavor neutrinos are almost equal (see g.e. Dolgov, 1981).

Active-sterile oscillations effect (a) expansion rate through exciting additional neutrino types, and (b) the weak interactions rate due to shifting neutrino densities and energy spectrum from BBN equilibrium values, thus directly influencing the kinetics of nucleons during the weak freeze-out and correspondingly the primordial production of helium-4.

(a) Due to its strong dependence on g_{eff}, He-4 is known as the best speedometer and its abundance is used to constrain the number of the relativistic particles during BBN (see Shvartsman, 1969; Steigman et al., 1986), usually parameterized by δN_ν. As far as oscillations between active and sterile neutrinos can bring the initially empty (or partially filled) sterile state into equilibrium, they lead to an increase of the number of neutrino species in equilibrium N_ν during BBN. This speeds up the expansion of the universe, $H(t) \sim g_{eff}^{1/2}$, and causes earlier n/p-freezing, $T_f \sim (g_{eff})^{1/6}$, at times when neutrons were more abundant (see e.g. Dolgov, 1981) and an overproduction of helium-4. This effect gives up to 5% ^{4}He overproduction (if one additional neutrino type is brought into equilibrium by oscillations, $\delta N_s = 1$).

(b)The effect of oscillations may be much stronger than $\delta N_s = 1$ in case of oscillations effective after ν decoupling, proceeding between partially populated sterile neutrino state $0 \leq \delta N_s < 1$ and electron neutrino (see e.g. Kirilova, 1988; Kirilova and Chizhov, 1996; Chizhov and Kirilova, 1997; Kirilova, 2002). The non-equilibrium initial condition, for most of the oscillations parameters of the model, leads to considerable and continuous deviations from the equilibrium ν_e spectrum (spectrum distortion) because the oscillation rate depends on energy according to $\Gamma \sim \delta m^2/E$.

The distortion leads to both a depletion of the active neutrino number density and a decrease of the Γ_w. Thus it influences the nucleon kinetics, causing an earlier n/p-freezing and an overproduction of ^{4}He yield.

The spectrum distortion is the greatest, if the sterile state is empty at the start of oscillations, $\delta N_s = 0$. It decreases with the increase of the degree of population of the sterile state at the onset of oscillations (see Kirilova, 2004b) as illustrated in the following figures.

Besides this leading kinetic effect of oscillations there is known an additional subdominant effect, namely the production of neutrino-antineutrino asymmetry: Neutrino-antineutrino asymmetry may be generated during the resonant transfer of neu-

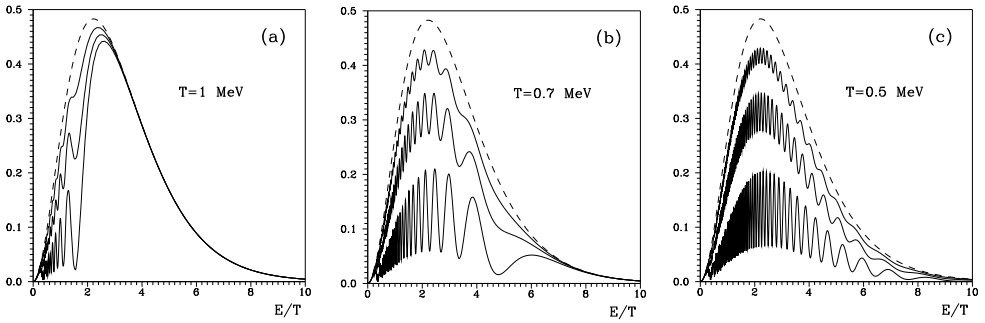

Figure 1: The figures illustrate the spectrum distortion at different degrees of population of the steriles, namely $\delta N_s = 0$ (lower curve), $\delta N_s = 0.5$ and $\delta N_s = 0.8$ (upper curve). The dashed curve gives the equilibrium spectrum for comparison. It is obvious that the distortion of the spectrum is considerable and with time, involves the whole neutrino ensemble.

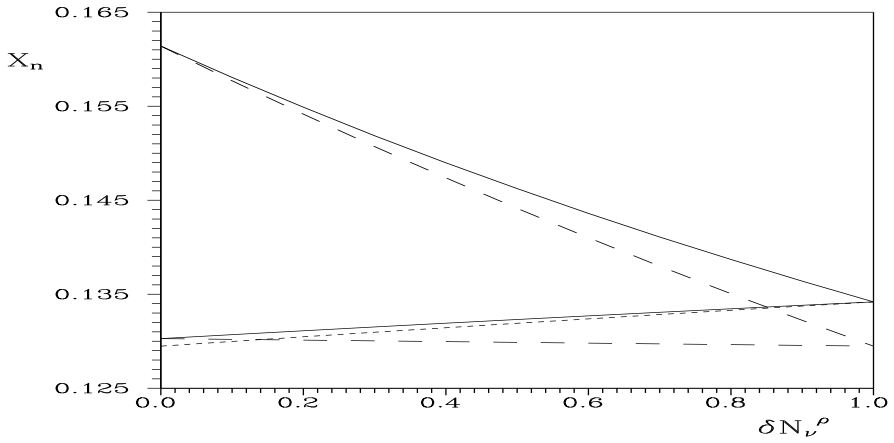

Figure 2: The solid curves show frozen neutron number density relative to nucleons $X_n^f = N_n^f/N_{nuc}$ as a function of the sterile neutrino initial population, at $\delta m = \pm 10^{-7}$ eV^2, $\sin^2 2\theta = 10^{-1}$. The dashed curves represent the kinetic effect, while the dotted curve shows the effect of energy density increase. The upper curves correspond to the resonant case and the lower the non-resonant one.

trinos (see e.g. Kirilova and Chizhov, 1996; Foot et al., 1996). This dynamically produced asymmetry suppresses oscillations at small mixing angles, leading to less overproduction of He-4 compared to the case without the account of asymmetry growth, and hence alleviating BBN constraints on oscillation parameters.

Non-zero initial sterile neutrino population influences neutrino effects on BBN -(i) it increases the expansion rate, (ii) in the $\nu_e \leftrightarrow \nu_s$ oscillations case, the presence of ν_s at the onset of oscillations influences the kinetic effects of $\nu_e \leftrightarrow \nu_s$ on BBN. Larger δN_s decreases the kinetic effects, because the element of initial non-equilibrium between the active and the sterile states is less expressed (see e.g. Kirilova, 2004). The dependence of the dynamical, kinetic and the total effect of on δN_s value is presented at Fig. 2.

Neutrino spectrum distortion effect is very strong even when there is a considerable population of the sterile neutrino state before the beginning of the electron–sterile oscillations. The kinetic effects are the strongest for $\delta N_s = 0$, they disappear for $\delta N_s = 1$, when ν_e and ν_s states are in equilibrium, and the total effect reduces to the SBBN with an additional neutrino

The cosmological constraints on oscillations parameters for the case of $\delta N_s \neq 0$ are changed.

3. COSMOLOGICAL CONSTRAINTS ON OSCILLATION PARMETERS

3.1. COSMOLOGICAL CONSTRAINTS ON OSCILLATION PARMETERS – $\delta N_S = 0$ CASE

Observational data on primordial ^{4}He abundance put stringent limits on the allowed oscillation parameters (see e.g. Barbieri and Dolgov, 1990; 1991).

In the discussed electron-sterile oscillation case the combined iso-helium contours for the nonresonant and the resonant case, for different levels of helium overproduction were calculated (see e.g. Chizhov and Kirilova, 1998; 2000; Kirilova and Chizhov; 2001), accounting for all oscillations effects on BBN. The dashed curves on the last figure present $\delta Y_p = (Y_{osc} - Y_p)/Y_p = 3\%, 5\%$ isohelium contours.

The analytical fits to the exact constraints are:

$$\delta m^2 (\sin^2 2\vartheta)^4 \leq 1.5 \times 10^{-9} \mathrm{eV}^2 \quad \delta m^2 > 0 \tag{3}$$

$$|\delta m^2| < 8.2 \times 10^{-10} \mathrm{eV}^2 \quad \delta m^2 < 0, \quad large \quad \vartheta, \tag{4}$$

The cosmological constraints exclude almost completely LOW solution to the solar neutrino problem, besides the LMA solution and sterile atmospheric solution, excluded in previous works. This result is consistent with the global analysis of the neutrino experiments data, which do not favour $\nu_e \leftrightarrow \nu_s$ solutions as dominant solutions.

3.2. COSMOLOGICAL CONSTRAINTS ON OSCILLATION PARMETERS – $\delta N_S \neq 0$ CASE

$\delta N_s \neq 0$ present before $\nu_{\mu,\tau} \leftrightarrow \nu_s$ just leads to an increase of the total energy density of the Universe, and it is straightforward to re-scale the existing constraints.

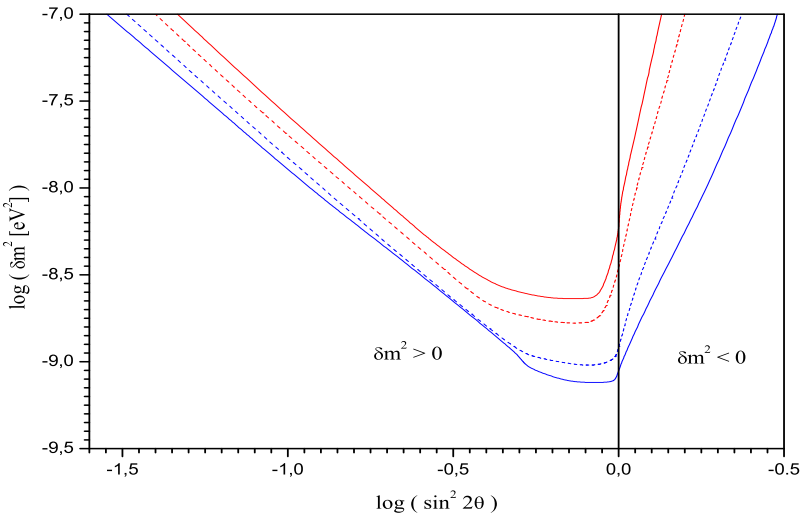

Figure 3: The dashed contours present BBN constraints for $\delta N_s = 0$, the solid — $\delta N_s = 0.5$ corresponding to $\delta Y_p/Y_p = 3\%$ (lower curves) and 5% (upper curves).

In the $\nu_e \leftrightarrow \nu_s$ oscillations case, however, the presence of ν_s at the onset of oscillations influences in addition the kinetic effects of $\nu_e \leftrightarrow \nu_s$ on BBN. Hence a precise study of the cosmological constraints for that case is needed.

We have calculated cosmological constraints corresponding to $\delta N_s = 0.5$ initial population of the sterile neutrino and for different levels of helium overproduction. As far as contemporary accuracy of helium observations allows at most 5% deviation from the standard BBN predicted value, we present the 5% isohelium contour as the maximum allowed one (see Kirilova and Panayotova, 2004).

Our numerical analysis has shown that up to $\delta N_s = 0.5$ the cosmological constraints corresponding to 3% and 5% He overproduction are slightly changed and remain stringent, as before (see e.g. Kirilova, 2004; Kirilova and Panayotova, 2004). Hence, even for partially filled sterile state the cosmological constraints give the most stringent limit on oscillation parameters.

The cosmological constraints in the case of non-empty initially sterile state exclude almost completely LOW solution to the solar neutrino problem as well as the LMA solution and sterile atmospheric solution. They are in agreement with the analysis of the experimental data from the solar and terrestrial neutrino oscillation experiments. However, the cosmological constraints are more restrictive by several orders of magnitude concerning the neutrino squared mass differences.

4. CONCLUSIONS

We have studied BBN constraints on neutrino active-sterile oscillations for the specific case when the sterile neurino is partially filled initially.

We have provided numerical analysis of the BBN production of He-4, Y_p, in the presence of electron-to-sterile neutrino oscillations, effective after neutrino decoupling, accounting for all known oscillations effects on cosmological nucleosyntesis.

We have obtained isohelium contours corresponding to different levels of He-4 overproduction, $\delta Y_p/Y_p$, for non-zero initial population of the sterile state δN_s.

We have calculated the cosmological constraints on oscillation parameters corresponding to $\delta N_s = 0.0$ and 0.5 and $\delta Y_p/Y_p = 3\%$ and 5%.

The cosmological constraints for the cases $\delta N_s \leq 0.5$ are slightly changed in comparison to $\delta N_s = 0$ case. I.e. even in case the sterile state was initially non-empty the cosmological constraints on oscillation parameters remain the most stringent ones.

The results are important for reveiling neutrino properties, and in particular, for defining the role of the sterile neutrino in resolving the solar and atmospheric neutrino anomalies.

Acknowledgements

M. Panayotova thanks the organizers for the financial support for her participation into the Conference. D. Kirilova appreciates the Regular Associateship of the Abdus Salam ICTP, Trieste. This work was supported in part by Belgian Federal Government (office for scientific affairs grant and IAP 5/27).

References

Barbieri, R. and Dolgov, A.: 1990, *Phys. Lett.*, **B 237**, 440.
Barbieri, R. and Dolgov, A.: 1991, *Nucl. Phys.*, **B 349**, 743.
Cuoco, A. et al.: 2003, astro-ph/0307213.
Cyburt, R., Fields, B. and Olive, K.: 2003, *Phys. Lett.*, **B 567**, 227.
Dolgov, A.D.: 1981, *Sov. J. Nucl. Phys.,* **33**, 700.
Enqvist, K., Kainulainen, K. and Thomson, M.: 1992, *Nucl. Phys.*, **B 373**, 498.
Esposito, S. et al. : 2000, *Nucl. Phys.*, **B 568**, 421.
Foot, R., Thomson, M. and Volkas, R.: 1996, *Phys. Rev.*, **D 53**, R5349.
Izotov, Yu.I. and Thuan, T.X.: 1998, *Astrophys. J.*, **500**, 188.
Kirilova, D.: 1988, JINR E2-88-301.
Kirilova, D.: 2003, *Astropart. Phys.*, **19**, 409.
Kirilova, D.: 2004, *Central European Journal of Physics*, in press, astro-ph/0312569.
Kirilova, D.: 2004, *Int. J. Mod. Phys. D*, in press, hep-ph/0209104 v.3.
Kirilova, D. and Chizhov, M.: 1996, *Neutrino96*, Helsinki, 1996, 478.
Kirilova, D. and Chizhov, M.: 1997, *Phys. Lett.*, **B 393**, 375.
Kirilova, D. and Chizhov, M.: 1998, *Phys. Rev.*, **D 58**, 073004.
Kirilova, D. and Chizhov, M. : 2000, *Nucl. Phys.*, **B 591**, 457.
Kirilova, D. and Chizhov, M.: 2001, *Nucl. Phys. Suppl.*, volB 100, 360.
Kirilova, D. and Panayotova, M.: 2004, in preparation.
Lopez, R.E. and Turner, M.S.: 1999, *Phys. Rev.*, **D 59**,103502.
Olive, K., Steigman, G. and Skillman, E.: 1997, *Astrophys. J.*, **483**, 788.
Shvartsman, V.: 1969, *Pisma Zh. Eksp. Teor. Fiz.*, **9**, 315; *J. Exp. Theor. Phys. Lett.*, **9**, 184.
Steigman, G. et al.: 1986, *Phys. Lett.*, **B 176**, 33.
Trotta, R. and Hansen, S.: 2004, *Phys. Rev.*, **D 69**, 023509.

Proc. IV Serbian-Bulgarian Astronomical Conference,
Belgrade 21–24 April 2004,
eds. M. S. Dimitrijević, V. Golev, L. Č. Popović, M. Tsvetkov,
Publ. Astron. Soc. "Rudjer Bošković" No 5, 2005, 209 - 214 *Contributed paper*

EARLY UNIVERSE BARYOGENESIS

D. P. KIRILOVA[1,2] and T. V. VALCHANOV[1]

[1] *Institute of Astronomy, Bulgarian Academy of Sciences, Sofia*
E–mail dani@astro.bas.bg
E–mail tony@astro.bas.bg

[2] *ICTP, Trieste, Italy*

Abstract. We discuss the scalar field condensate baryogenesis model, which is among the preferred today baryogenesis scenarios, compatible with inflation. According to that model the baryon excess in the Universe results from the decay of a scalar condensate, carrying a baryon charge, at later stages of Universe evolution ($T << 10^{15}$ GeV). The condensate itself is generated at the inflationary stage.

We update the parameters of the model and analyze numerically the post inflationary evolution of the scalar condensate. We determine the value of the generated baryon asymmetry, after the decay of the condensate.

The numerical analysis confirms the main result of the analytical and numerical estimations, obtained in previous studies, that the observed value of the baryon asymmetry can be obtained in the discussed model of baryogenesis. The dependence of the generated baryon density on the model's parameters is obtained.

1. INTRODUCTION

The generation of the observed baryon asymmetry β is one of the yet unsolved problems of cosmology. There exist numerous baryogenesis scenarios, the most famous among them being GUT, electroweak and scalar field condensate scenarios.

The most natural versions of GUT and electroweak baryogenesis scenarios were already ruled out by experimental data. Therefore, we discuss the scalar field condensate baryogenesis model, which is among the preferred today baryogenesis scenarios, compatible with inflation.

Attractive features of the model are: The model is compatible with inflation, there is no problem of insufficient reheating, there is no washing out of the baryon excess at EW phase transition, the model provides natural generation of a small β.

2. BARYON ASYMMETRY OF THE UNIVERSE

There exist strong predominance of matter over antimatter in our Galaxy indicated from the Cosmic Ray and Gamma Ray experiments.

Cosmic Ray search for $\bar{p}$ and antinuclei on baloons and spacecraft found: $\bar{p}/p \sim 10^{-5}$ at $E < 2$ GeV, and $\bar{p}/p \sim 10^{-4}$ at $E > 2$ GeV. So, antiprotons detected

in primary cosmic radiation can be totally due to interactions of the primary CR particles with the interstellar medium.

Antinuclei have not been detected, only the folowing upper limit was obtained (see e.g. Saeki et al., 1998).: $\bar{H}e/He < 1.7.10^{-6}$.

Thus cosmic ray data indicate that there are no antimatter objects within a radius of 1 Mpc.

Gamma Ray data, namely the absence of the annihilation feature expected from the borders between matter and antimatter regions, points that antimatter objects, eventually present in our cluster of galaxies, should be negligible.

Hence, in our near vicinity the baryon asymmetry reads:

$$\beta = (N_B - N_{\bar{B}})/N_\gamma \sim N_B/N_\gamma = \eta,$$

where N_B is the number density of baryons, N_γ is the number density of photons.

The observaional value of the baryon-antibaryon asymmetry in our neigbourhood is:

$$\beta \sim \eta \sim 6.10^{-10}$$

There are different ways to determine the baryonic density, also denoted as $\Omega_b h^2 = 3.65.10^7 \eta$. The most popular and precise among them are:

BBN precision determinations ($z \sim 10^9$): The concordance b/n predicted and extracted from observations of primordial abundances of D, He-3, He-4, Li-7 measures the baryon content of the Universe (see e.g. Cyburt et al., 2003; Cuocco et al., 2003). The extreme range of it being: $0.016 \leq \Omega_b h^2 \leq 0.025$.

D measurements towards low Z QAS (Lyman limit systems - LLS) ($z \sim 3$) + BBN (see e.g. Burles et al., 2001; Kirkman et al., 2003):

$$\Omega_b h^2 = 0.0216^{+0.0020}_{-0.0021}$$

for $D/H = (2.78^{+0.44}_{-0.38}) \times 10^{-5}$.

CMB determinations($z \sim 1000$):
The CMB anisotropy measurements after WMAP are providing the most precise value for the baryon density, namely (see e.g. Spergel et al., 2003):

$$\Omega_b h^2 = 0.0224 \pm 0.0009.$$

The explanation of the generation of the observed baryon density value and its sign is the main aim of the contemporary baryogenesis scenarios.

3. SCALAR FIELD CONDENSATE BARYOGENESIS MODEL

The model has been first proposed by Dolgov and Kirilova (see e.g. Dolgov and Kirilova, 1991) and discussed in detail in (see e.g. Kirilova and Chizhov, 2000). The model was based on the Affleck and Dine baryogenesis scenario. Essential characteristics of the model:

* Complex scalar field ϕ, carying baryon charge $B \neq 0$, is present at inflation.
The condensate of the baryon carrying scalar field $< \phi > \neq 0$ is formed as a result

of the enhancement of quantum fluctuations of the field (see e.g. Vilenkin and Ford, 1982; Linde, 1982; Bunch and Davies, 1978):

$$< \phi^2 >= H^3 t/4\pi^2$$

In the case when the length of the fluctuations exceeds the horizont, they cannot be distinguished from a homogeneous classical field with amplitude $< \phi^2 >^{1/2}$.

* Baryon charge violation at micro distances at the inflationary stage:
As a result of the baryon charge violation (BV) at large ϕ due to BV self-interaction terms in the potential $U(\phi)$ a condensate of a baryon charge (stored in $< \phi >$) is produced during the inflationary stage $B \sim H_I^3$.

$$U(\phi) = m^2\phi^2 + \frac{\lambda_1}{2}|\phi|^4 + \frac{\lambda_2}{4}(\phi^4 + \phi^{*4}), \tag{1}$$

where $m \ll H_I$, $\lambda_i \sim \alpha$, $m \sim 10^2 \div 10^4$ GeV. The initial values: $\phi_o^{max} \sim H_I \lambda^{-1/4}$ and $\dot{\phi}_o = 0$ are obtained from the natural assumption that the energy density of ϕ at inflation is $\sim H_I^4$.

3.1. EVOLUTION OF ϕ AND B AFTER INFLATION

At the end of inflation there exist 2 scalar fields: the inflanton ψ and ϕ, which begin to oscillate about their global minima, when $H \leq m$. As far as $m_\psi > m_\phi$, the inflanton oscillations start first:
$\psi = m_{PL}(3\pi)^{-1/2}\sin(m_\psi t)$, $H = 2/(3t)$; $\rho_\psi > \rho_\phi$.
It further diminishes with expansion according to $\rho = m_\psi^2 M_{Pl}^2[(R_{os}/R]^3$ Therefore we make the natural assumption that the inflanton energy density dominates the Universe.

Then in the expanding Universe ϕ satisfies the equation:

$$\ddot{\phi} - a^{-2}\partial_i^2\phi + 3H\dot{\phi} + \Gamma\dot{\phi} + U'_\phi = 0, \tag{2}$$

At $\phi >> m$ ϕ oscillates with a decreasing amplitude, as (see e.g. Dolgov and Kirilova, 1990; Kirilova and Chizhov, 1996) due to:
(a) Universe expansion
(b) particle production by the oscillating with frequency ω scalar field, coupled to fermions $g\phi\bar{f}_1 f_2$: Hence, ϕ is damped: $\phi \to \phi\exp(-\Gamma t)$, where $\Gamma = \alpha.\omega$, $g^2/4\pi = \alpha$, $\omega \sim \lambda^{1/2}\phi_i(x)$.

In this toy model we have accounted for the damping due to particle creation adiabatically. B is damped correspondingly, as well, since $B = -i\lambda_2(\phi^4 - \phi^{*4})$.

If ω is a decreasing function of time there is slow damping, and therefore B could survive until B-conservation epoch t_b, corresponding to $\phi \sim m$.

At $\phi \sim m$ ϕ decays. The amplitude of ϕ decreases due to particle creation till t_b epoch. $\phi \sim m$ marks the beginning of the B-conservation epoch t_b during which ϕ decays with nonzero average baryon charge into quarks and leptons $\phi \to q\bar{q}l\gamma$. This baryon charge transfered to quarks dictates the observed today baryon asymmetry.

In fact the baryon charge transfered to quarks at the baryon conservation epoch should be diminished by the entropy resulting from the reheating of the Universe due to the inflanton decay.

4. THE NUMERICAL ANALYSIS - DESCRIPTION AND RESULTS

We have provided a numerical analysis of the scalar field evolution after the inflationary stage till the field's decay. We have used Runge-Kutta 4th order scheme with step $h = 10^{-7} - 10^{-8}$. The following range of the model's parameters was analyzed: $10^{-2} \leq \lambda \leq 5 \times 10^{-2}$, $10^{-3} \leq \alpha \leq 10^{-2}$, $10^{6} \leq H \leq 10^{13}$, $100 \leq m \leq 2000$.

In Fig. 1, the baryon charge carrying scalar field is presented. The upper part gives the evolution of the field without particle creation account, the lower one – with the account of the particle creation processes. Depending on the value of $\Gamma \sim \phi \sim \alpha H$ the damping of the field may be more or less strongly expressed.

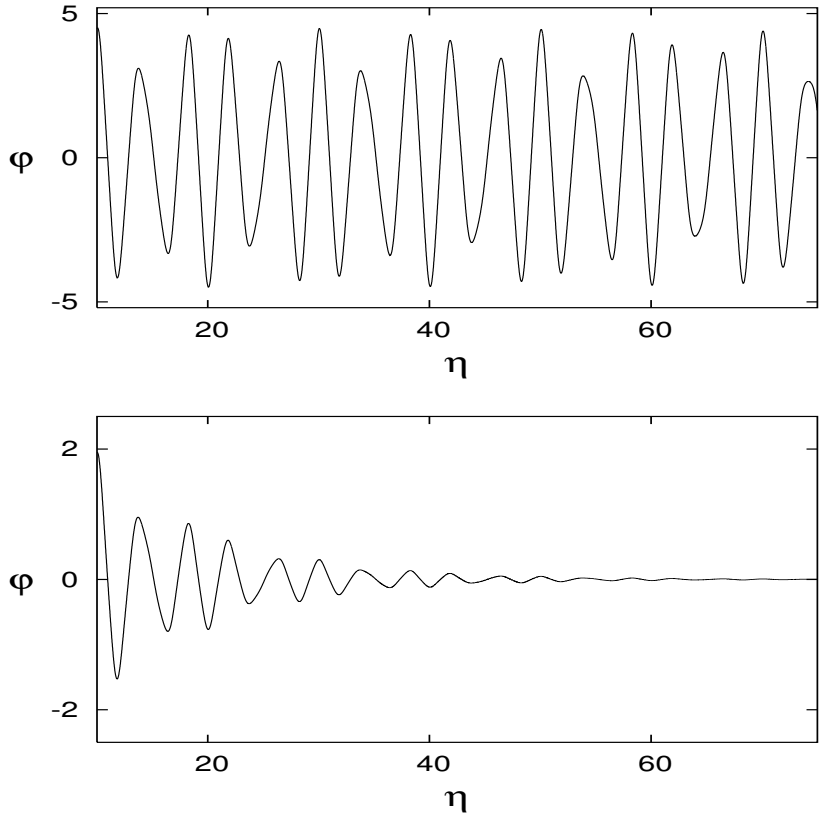

Figure 1: The evolution of the field $\phi_1(\eta)$ for $\lambda_1 = \alpha = 10^{-2}$, $\lambda_2 = 10^{-3}$, $m =$ 350 GeV, $H_I = 10^{12}$ GeV $\phi_o = H_I \lambda^{-1/4}$, and $\dot{\phi}_o = H_I^2$.

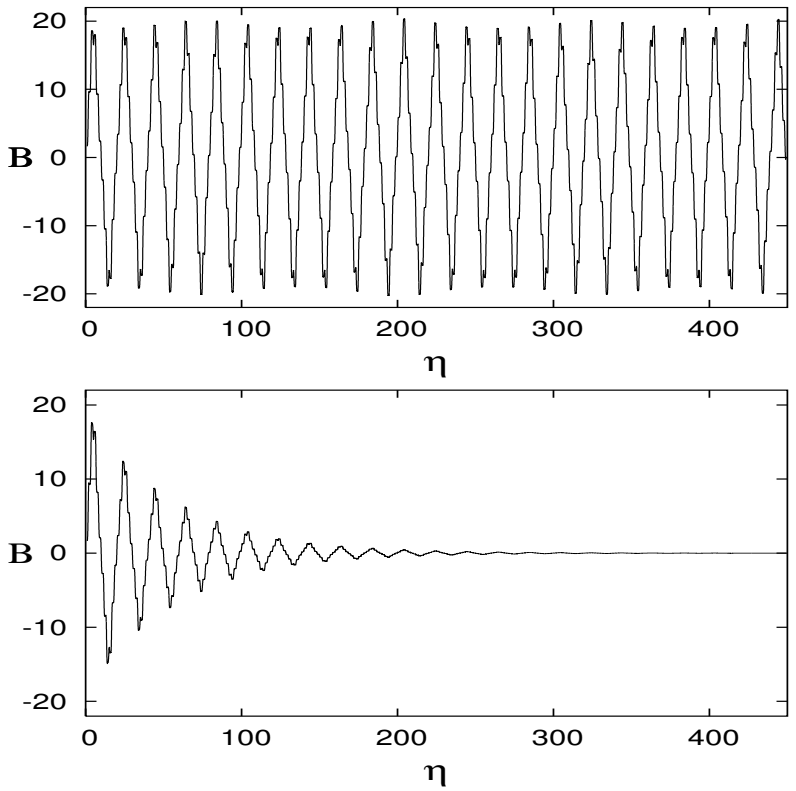

Figure 2: The evolution of the baryon charge $B(\eta)$ contained in the condensate $<\phi>$ for $\lambda_1 = 10^{-2}$, $\lambda_2 = \alpha = 10^{-3}$, $m = 350$ GeV, $H_I = 10^{12}$ GeV $\phi_o = H_I \lambda^{-1/4}$, and $\dot{\phi}_o = H_I^2$.

As illustared, particle creation may lead to a considerable decrease of the field's amplitude for large α or/and large H values, which reflects finally into the decrease of the baryon charge carried by the condensate. This is easy to understand having in mind that, $\Gamma \sim \alpha H$.

The evoluition of the baryon charge contained in the condensate and the field are shown in the Fig. 2. The upper curve presents the evolution of the baryon charge of the condensate in the case when particle creation is negligible, the second one presents the more realistic situation, when the particle creation processes are accounted for.

Due to the oscillatory character of B, the value of the generated asymmetry is very sensitive to the parameters of the model, as well as to the numerical methods used, and therefore, the problem requires further precise numerical studies. On the first place, due to the extreme sensitivity of the generated baryon value to Γ, it is necessary to account more accurately for the damping due to particle creation. Here we have used the analytical estimation, obtained e.g. in Dolgov and Kirilova (1991) for the frequency of the field.

Future more realistic models of baryogenesis should obtain selfconsistently the frequency and correspondingly Γ from the exact numerical analysis of the fields evolution. Our preliminary results concerning this show that the numerically calculated oscillation frequency of the field may be quite different from the assumed, analytically estimated one, used in the adiabatical approximation of the particle creation.

5. RESULTS AND CONCLUSIONS

We have provided more precise numerical analysis of the scalar field condensate baryogenesis model.

The range of parameters H, m, T_R, was updated according to the current observational cosmological constraints.

We have numerically analyzed the evolution of the baryon charge carrying scalar field using the exact kinetic equations. In previous studies it was studied semi-analytically.

We confirm the most essential result of the original studies that the model can serve as a successful baryogenesis model, compatible with inflation. We have determined the values of model's parameters required for generating the observed B value. The analysis has shown that for a natural range of the model's parameters the observed value of the baryon asymmetry can be obtained.

This toy model can be further improved by providing more precise account for the particle creation processes, which play essential role for the determination of the final baryon value.

Acknowledgements

T. Valchanov thanks the organizers for the financial support for his participation at the Conference. D. Kirilova appreciates the Regular Associateship of the Abdus Salam ICTP, Trieste. This work was supported in part by Belgian Federal Government (office for scientific affairs grant and IAP 5/27).

References

Affleck, I. and Dine, M.: 1985, *Nucl. Phys.*, **B249**, 361.
Bunch, T. and Davies, P.: 1978, *Proc. Roy. Soc.*, **A360**, 117.
Burles, Nollet and Turner, M.: 2003, *Astrophys. J. Lett.*, **552**, L1.
Cuoco, A. et al.: 2003, astro-ph/0307213.
Cyburt, R., Fields, B. and Olive, K.: 2003, *Phys. Lett.*, **B567**, 227.
Dolgov, A. and Kirilova, D.: 1990, *Yad. Fiz.*, **51**, 273.
Dolgov, A. and Kirilova, D.: 1991, *Journal of Moscow Phys. Soc.*, **1**, 217.
Kirilova, D. and Chizhov, M.: 1996, *Astron. Astropys. Transactions*, **10**, 69.
Kirilova, D. and Chizhov, M.: 2000, *Mon. Not. R. Astron. Soc.*, **314**, 256.
Kirkman, D. et al.: 2003, *Astrophys. J. Suppl.*, **149**, 1.
Linde, A.: 1982, *Phys. Lett. B*, **116**, 335.
Saeki et al. (BESS Collaboration): 1998, *Phys. Lett. B*, **422**, 319.
Spergel, D. et al. : 2003, *Astrophys. J. Suppl.*, **148**, 175.
Vilenkin, A. and Ford, L.: 1982, *Phys. Rev. D*, **26**, 1231.

Proc. IV Serbian-Bulgarian Astronomical Conference,
Belgrade 21–24 April 2004,
eds. M. S. Dimitrijević, V. Golev, L. Č. Popović, M. Tsvetkov,
Publ. Astron. Soc. "Rudjer Bošković" No 5, 2005, 215 - 220 *Contributed paper*

OB ASSOCIATIONS IN SEXTANS A DWARF IRREGULAR GALAXY

R. KURTEV[1], L. GEORGIEV[2], Ch. DYULGEROV[1], J. BORISSOVA[3] and M. ROSADO[2]

[1] *Department of Astronomy, Sofia University and Isaac Newton Institute of Chile Bulgarian Branch, James Bourchier Ave. 5, BG – 1164 Sofia, Bulgaria*
E–mail kurtev@phys.uni-sofia.bg
E–mail dyulgerov@phys.uni-sofia.bg

[2] *Instituto de Astronomía, Universidad Nacional Autónoma de México, México*
E–mail georgiev@astroscu.unam.mx
E–mail margarit@astroscu.unam.mx

[3] *Pontificia Universidad Catolica de Chile, Departamento de Astronomia y Astrofica, Av. Vicuna Mackenna 4860, 782-0436 Macul, Santiago, Chile*
E–mail jborisso@astro.puc.cl

Abstract. The galaxies of the Local Group serve as our laboratories for understanding star formation and stellar evolution in differing environments. Irregular galaxies provide unique opportunities for studies of star formations triggered by the combined effect of stellar winds and supernova explosions in rich stellar groupings. Sextans A is a dwarf irregular galaxy located just beyond the Local Group. Using the public data from the new wide-field mosaic camera attached to the 4-m KPNO telescope we are producing a catalogue of UBVRI photometry of roughly 100 thousand stars in area around Sextans A. Using an automatic and objective method (Battinelli's technique) 36 groups of young objects (OB associations) were found. The mean size of these stellar groups is about 50 pc. Some basic properties of the associations are defined.

1. INTRODUCTION

The stellar content investigations of the Local Group galaxies allow us to study in fine details the star formation history of these systems. They also provide important verification information for the stellar evolution theory. The youngest and the brightest stars of one galaxy are the OB stars. These massive stars are rare and short lived but are the most important agents in shaping the interstellar medium. They rapidly inject heavy elements and have a strong energy input into this medium. Thus they are playing a key role in regulating star formation for the next generation stars. The distribution of young and massive stars in space and by mass is very important for understanding the processes of star formation. The most of the youngest and massive stars are found in OB associations and star clusters but there are also runaways. Stellar association is "a single, unbound concentration of early-type luminous stars,

embedded in a very young starforming region" (Kontizas et al., 1999). The properties of the associations and the ionized gas clouds in which they are embedded allow tracing of the regions of most recent star formation in the galaxies.

Sextans A is an irregular galaxy located just beyond the Local Group, which is possible to resolve into stars from the ground. The young stellar content of Sextans A was investigated by van Dyk et al.(1998). They record that the galaxy shows the most recent burst of star formation (< 50 Myr). It is very interesting for us to investigate OB associations in the galaxy and to define their parameters.

2. OBSERVATIONS AND REDUCTIONS

A set of $UBVRIH\alpha$ frames of the area around Sextans A galaxy were obtained with new, wide-field Mosaic cameras attached to the 4-m KPNO telescope. The exposure time of each image is from 60 to 600 sec. The observing area is $36' \times 36'$. The seeing during these observations was good: $1.0 - 1.2''$. The standard transformation equations for this camera were used to calibrate the data and transform the instrumental magnitudes in Johnson $UBVRI$ system. Transformation equations ere given in `http://www.lowell.edu/users/massey/phot.html`.

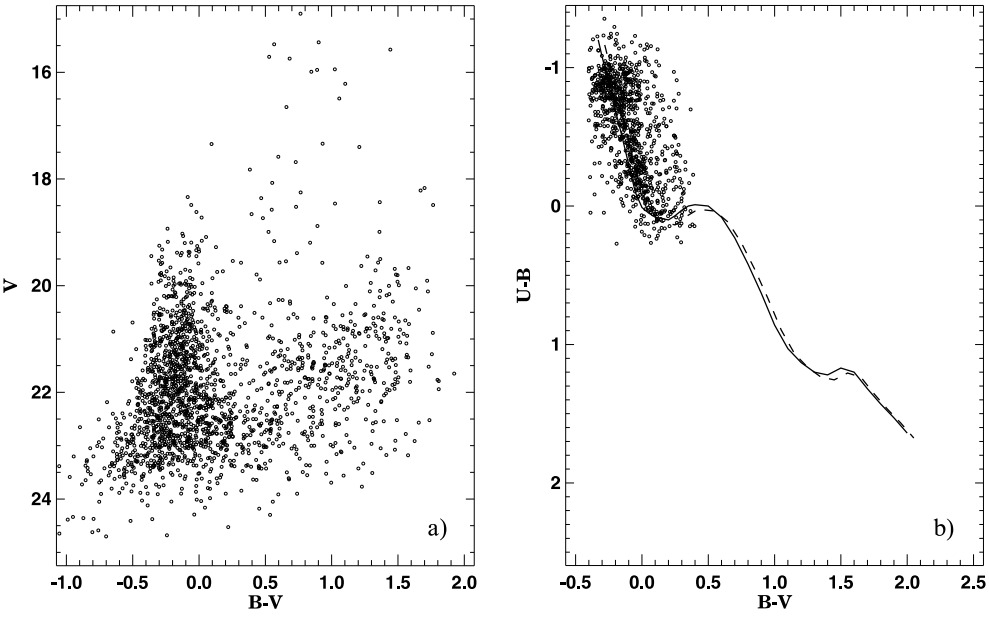

Figure 1: a) $(B-V, V)$ color-magnitude diagram of Sextans A galaxy. Only stars with photometric errors not larger than 0.15 in both filters are plotted. **b)** $(B-V, U-B)$ color-color diagram (CCD) of the bluest stars in the Sex A galaxy. Only stars with photometric errors not larger than 0.15 in all filters are plotted. The fiducial loci of stars (luminosity class V) without reddening (solid line) and reddened with $E(B-V) = 0.05$ (dashed line) are superimposed.

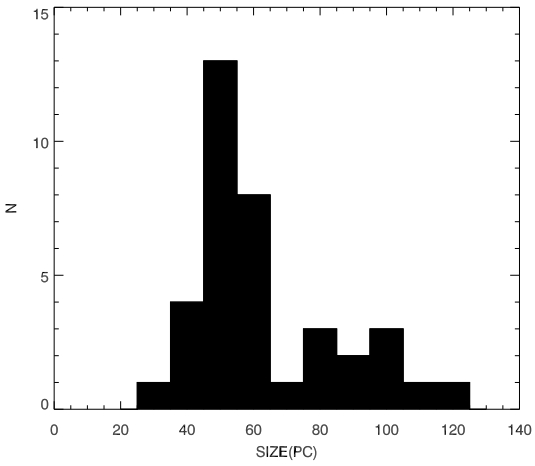

Figure 2: Size distribution of the associations in Sextans A.

The stellar photometry of the frames was performed with the point-spread function fitting routine ALLSTAR available in DAOPHOT (Stetson, 1993). Complete details of the data reduction and analysis may be found in Georgiev et al. (1999). The stars with values of DAOPHOT CHI > 2 and those with formal errors from the PSF fitting greater than 0.15 mag are rejected so the final photometry list contains about 8000 Sextans A stars with photometry in two filters at least.

3. RESULTS

3.1. COLOR-MAGNITUDE AND COLOR-COLOR DIAGRAMS

Fig. 1a represents the $(B-V), V$ color-magnitude diagram (CMD). To construct this CMD only the stars with photometric errors not larger than 0.15 in both filters have been selected. The mean feature is distinctive plume of luminous blue stars in the Sextans A galaxy mixed with the foreground stars of the Milky Way mostly with $B-V > 0.3$

The "unshifted" $(B-V, U-B)$ color-color diagram (CCD) of the 960 bluest (OB) stars from the galaxy is given in Fig. 1b. We used Q-parameter technique to measure the reddening. Our final estimation is $E(B-V) = 0.04$. This is also the most frequent value used from different authors.

3.2. OB ASSOCIATIONS

The automatized search for OB associations was carried out using the method of Battinelli (1991) (so called friend-of-friends algorithm). The bright blue stars from the Main sequence in Sex A were selected by strong photometric criterion by absolute magnitude $M_V < -2.0$ and color $(B-V)_0 < 0$. In the most cases friend-of-friends

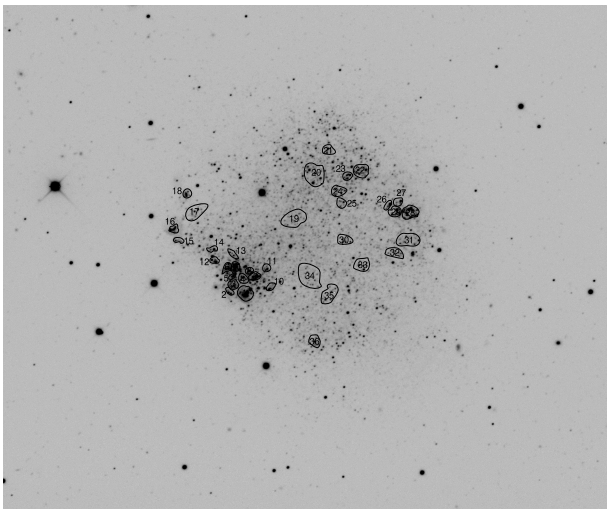

Figure 3: The boundaries of the OB associations superimposed on U image of Sex A.

algorithm selects the minimum number of 4 OB stars in some clump in order to have a "real" association. We put in our case the same minimum number of stars.

The friend-of-friends algorithm selects 36 associations with sizes between 30 and 120 pc (with accepted true distance modulus of $\mu_0 = 25.61$). The mean size is about 50 pc. The distribution of the associations' sizes is given in Fig. 2.

The spatial distribution of the OB associations around the galaxy is given in Fig. 3. The youngest associations occupy NW and SE parts of Sextans A. There is a clear connection between these young, compact and bright associations and ionized medium in the galaxy seen in the Hα image.

The X, Y coordinates in pixels, the mean size of the associations in pc, the V magnitude of the brightest member, the number of OB members, and the mean absolute magnitude ($M_V < 3 >$) of the three brightest members are given in Table 1.

Comparing Sextans A with the Magellanic Clouds, M 33 and NGC 6822 (Bresolin et al., 1998; Ivanov, 1996) we can see that the distribution of the OB associations in size is similar with peak between 40 and 80 pc. Those in M 31 are slightly larger – 90 pc. Bresolin et al. (1998) obtain for LMC – 60 pc, SMC – 70 pc and M33 – 60 pc, confirming in this way the idea that the size of the associations do not depends on the morphological type of the galaxy. The mean size of the OB associations in Sex A, obtained in this work, is very near to the value for SMC associations, obtained in a very recent paper of Oey et al. (2004) – 34 pc. These much smaller values are consistent with a greater completeness in the data, yielding a higher density of OB stars, and therefore smaller clustering distance.

Table 1: Properties of the OB associations in Sextans A

No	X	Y	size(pc)	Vmax	Nmem	Mv< 3 >
1	1890.5	3433.5	83.2	17.345	20	-6.501
2	1832	3405.5	40.6	19.971	4	-4.882
3	1845.5	3427	52.8	20.213	7	-4.614
4	1881.5	3451.5	51.7	20.167	8	-5.236
5	1835	3425	29.7	21.528	4	-3.269
6	1819	3449	51.9	20.125	8	-5.789
7	1858	3464.5	55.2	18.620	15	-6.546
8	1907.5	3481.5	45.3	19.574	8	-5.485
9	1931.5	3486	50.8	20.199	8	-5.966
10	1990	3493	48.9	20.006	8	-5.089
11	1970.5	3519	38.9	20.193	4	-4.963
12	1771.5	3438	40.3	19.969	3	-5.383
13	1845	3484	63.8	20.375	9	-4.681
14	1764	3457.5	48.3	19.193	4	-4.809
15	1637	3410	46.5	21.351	4	-4.652
16	1615	3419.5	51.0	20.530	5	-5.395
17	1701.5	3489.5	85.6	19.854	8	-4.765
18	1667.5	3510	47.4	20.913	7	-4.629
19	2077	3672.5	96.0	20.567	18	-5.203
20	2149.5	3785.5	106.8	19.278	15	-6.521
21	2208	3865.5	54.5	21.900	6	-3.983
22	2330	3886.5	75.9	20.990	16	-4.941
23	2279	3846	50.2	19.387	9	-5.804
24	2248	3807.5	68.1	19.953	10	-5.750
25	2255.5	3785	56.7	19.983	6	-4.899
26	2436.5	3869.5	45.5	18.932	4	-4.982
27	2474	3896.5	40.4	19.596	5	-4.586
28	2518	3902.5	86.2	19.324	19	-6.017
29	2462	3872	60.1	18.339	11	-6.276
30	2275.5	3731	55.9	20.218	5	-4.853
31	2515.5	3854	97.9	20.625	9	-4.893
32	2461	3801.5	77.8	21.603	10	-4.313
33	2336.5	3708	63.6	19.365	7	-5.740
34	2139.5	3574	122.9	21.265	17	-4.465
35	2205.5	3587	103.3	19.964	11	-5.394
36	2159	3473.5	58.0	20.156	5	-5.315

4. A BRIGHT FUTURE

- We are going to refine our analysis about the OB associations.
- We are going to select candidates for red supegiant stars and are going to define their physical parameters. We are going to look for connection between the associations' parameters, distribution of the OB associations and other young objects like LBVs, WRs, HII regions, etc.
- Sextans A is the first of ten Local group galaxies in which we plan to investigate OB associations. We would like to carry out a qualitative and quantitative comparative analysis of the OB associations in the Local Group - the major purpose of the project. This has been made only in part until now.

Acknowledgements

This material is based upon work supported by the National Science Foundation under Grant No. 0093060. Any opinions, findings, and conclusions or recommendations expressed in this material are those of the author(s) and do not necessarily reflect the views of that National Science Foundation.

References

Battinelli, P.: 1991, *Astron. Astrophys.*, **244**, 69.
Bresolin, F., Kennicutt, Jr., Ferrareze, L., Gibson, B., Graham, J. et al.: 1998, *Astron. J.*, **116**, 119.
Georgiev, L., Borissova, J., Rosado, M., Kurtev, R., Ivanov, G. et al.: 1999, *Astron. Astrophys. Supp.*, **134**, 21.
Kontizas, E., Kontizas, M., Gouliermis, D., Dapergolas, A., Korakitis, R. and Morgan, D.: 1999, in IAU Symp. 190, New view of the Magelanic Clouds, ed. Y.-H., Chu, N. Suntzeff, J. Hesser and D. Bohlender, San Francisco:ASP, 410.
Ivanov, G.: 1996, *Astron. Astrophys.*, **305**, 708.
Oey, S., King, N., Parker, J.: 2004, *Astron. J.*, **127**, 1632.
Stetson, P.: 1993, "DAOPHOT II: The Next Generation", MIDAS Users' Manual, ESO, Garching.
van Dyk, S., Puche, D., Wong, T.: 1998, *Astron. J.*, **116**, 2341.

Proc. IV Serbian-Bulgarian Astronomical Conference,
Belgrade 21–24 April 2004,
eds. M. S. Dimitrijević, V. Golev, L. Č. Popović, M. Tsvetkov,
Publ. Astron. Soc. "Rudjer Bošković" No 5, 2005, 221 - 226 *Contributed paper*

DEVELOPMENT AND PERFORMANCE OF DSP BASED 16-BIT HIGH-RESOLUTION CCD CONTROLLER

H. LUKARSKI and S. FOTEV

Space Research Institute – Bulgarian Academy of Sciences,
6, Moskovska str., 1000 Sofia, Bulgaria
E–mail hristo@skyarchive.org
E–mail sfotev@space.bas.bg

Abstract. Hyperspectral imaging systems are becoming more and more important concerning a great variety of systems with commercial and military purposes. The valuable fact about hyperspectral sensor of a given spatial resolution or pixel size is that it will give data on the scene that is not obtainable by single band or multi-spectral sensors. Several approaches have been applied to use a single higher spatial resolution band to improve the spatial resolution of the hyperspectral data.

The following items are described in the proposed research work:

- the electronic block of the video-spectrometric system;
- the used elements' base and scheme solutions;
- its alignment with the optic system.

Thanks to the usage of digital signal processors (DSP) and high-speed, high resolution ADC an extra flexibility and speed of processing is achieved. According to the task, the number of received channels may be reduced in the spectrometer itself.

Schemes of the optic part and of the electronic block are presented.

1. INTRODUCTION

During the last decade, the remote sensing sciences have progressively moved towards the development of the spaceborne and airborne based hyperspectral devices, making use of the hyperspectral sensors (Birk, 1994; Kramer, 1996; Kunkel, 1997; Gekov 2000). Part of this development has been spurred on by systems capable of acquiring and fusing accurate globally referenced data in fully digital form with short turn-around-time in a cost-effective fashion. Therefore, it raises the requirements to the input-output controllers (precision timing generators) and digitalization devices of the spectral video signal. It necessitates higher request to:

- the readout speed of the information,
- the resolution of the ADC,
- the digital signal processing, and
- the compression and transmission of the data.

The proposed work gives a description of the hardware configuration of the input-output controller, worked out in the Onboard Section, for remote sensing hyperspec-

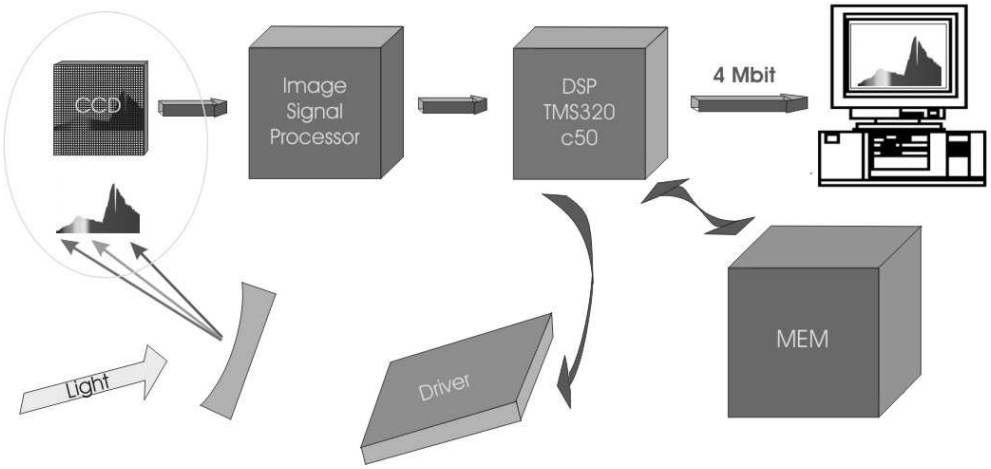

Figure 1: Workflow of the video spectrometric signal processing – hardware configuration.

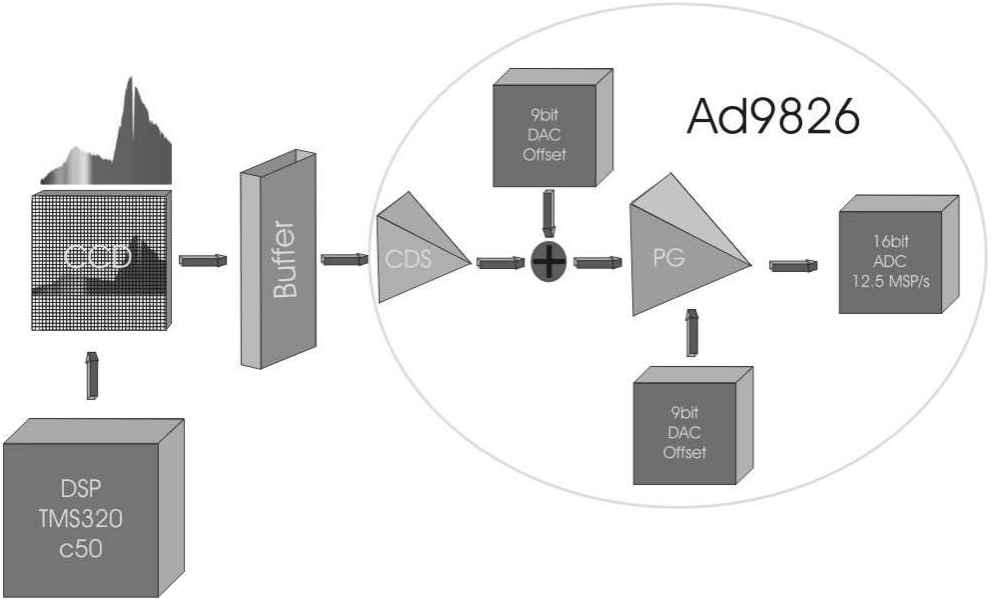

Figure 2: Workflow of the video spectrometric signal processing – image signal processing.

tral applications. The newest devices for CDS and ADC of "Analog Device" and DSP of "Texas Instrument" are used. The RMS output noise histogram is presented. The prototype level of the videospectrometric system is designed in spectral range 530 – 680 nm. The radiometric and geometric calibration is accomplished with using monochromator.

2. HIGH-RESOLUTION CCD CONTROLLER

High-resolution CCD controller includes (Fig. 1):
- CCD area image sensor
- Compete analog signal processor
- Digital signal processor (TMS320C50), with memory (MEM),
- Drivers for vertical and horizontal transfer,
- IBM-PC.

2.1. CCD AREA IMAGE SENSOR

There is a suggested possibility for the worked out controller to switch on two types of matrixes: Texas Instruments' "TC217" and *"CCD 02-06"* of the E2V Company. TC217 is a high-resolution matrix with small pixels and big dynamic diapason. It can be used for scanning the Earth in one spectral channel. The second type of matrixes "CCD 02-06" of the E2V Company is proposed for spectrometers in the diapason 420-1060 nm. Its major advantage to other similar matrixes is the big pixel size – 22 22 μm. This adds both a higher sensibility on one side and on the other for bigger coverage of the spectral diapason. Additionally it has very small noise of reading the elements and big dynamic diapason. It is recommended in systems with cooling which will be necessary in our case. The CCD receiver is a standard three- phase matrix of the type "frame transfer" with dimensions of the sensitive part 12.7 x 8.5 mm. The quantum efficiency is 45% at 700 nm and the dynamic range is 25000:1.

2.2. COMPETE ANALOG SIGNAL PROCESSOR (Fig. 2)

The video signal of the CCD receiver is amplified by a buffer and is transmitted to the analog-digital video processor AD9826, worked out by the "Analog Device" company, operating in a mode of double correlated sampling (Correlated Double Sampling, CDS). A 9bit DAC (OFFSET) runs the shift of the DC part of the signal. The amplification of the signal is regulated by a 6-byte DAC programmable gain amplifier (PG). Each mode is selected by programming the configuration registers through the serial interface. The analog-digital converter has a operating frequency up to 12.5 MSP/s.

2.3. DIGITAL SIGNAL PROCESSOR (TMS320C50), WITH MEMORY (MEM),

The received 16-byte digital signal is transmitted to the signal processor TMS320C50. It supports the time diagram of the CCD, the analog video processor and it does the transfer to the PC. Apart from this, a local processing of the data is possible as a correction of the image, compression or other. With suitable software the standard filters of SPOT, LANDSAT and other satellites can be realized.

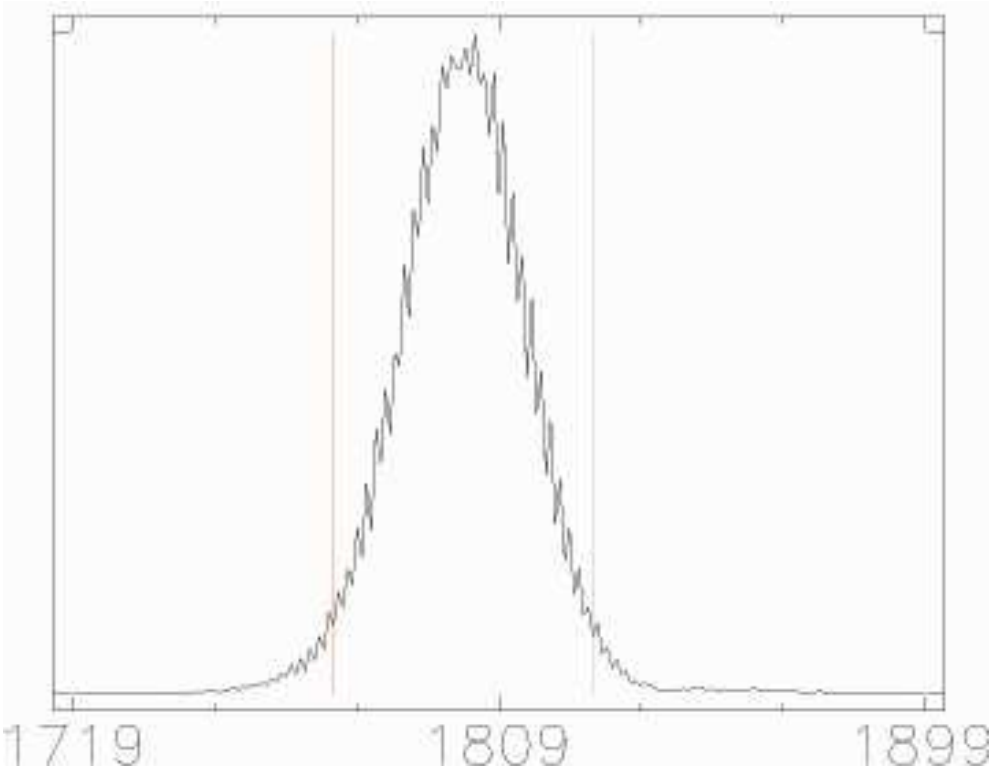

Figure 3: RMS output noise histogram of the precision timing generator.

2.4. IBM-PC

The memorizing of the received information is done on a PC. The requirements to it are not very big only to have the ability to store the vast data source. Experiment – 1-3 hours with a speed of 500kB/sec.

3. RESULTS

Fig. 3. shows the results of dark current research of matrix TC217. Experiments at different values of offset and power gate amplifier were conducted. The histogram graphic of the best result is shown. RMS of dark current 12.01 is received at maximum level of saturation 15 000. Obviously the S/N ratio is better than 1000.

Figs. 4, 5 and 6 illustrate the first experiments with grating monochromator. The graphic represents that there is background and low level of input signal. But definitely the results are very promising. The spectral lines at 560, 530 and 680 mm are steep and the resolution at wavelength is 8 – 10 nm at 0.5 levels. There is still work to be done for the precise calibration of optical part and of the electronic block.

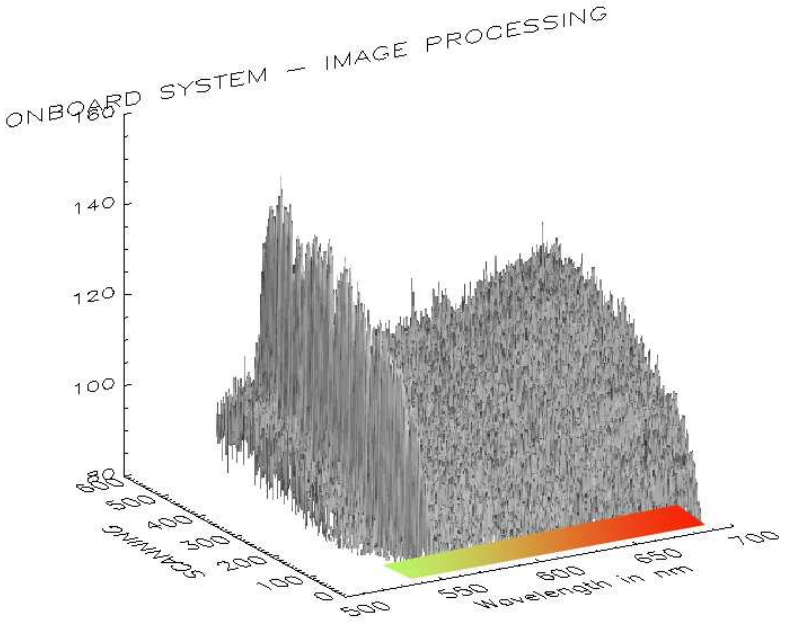

Figure 4: 2D Spectrum, Wavelength = 560 nm.

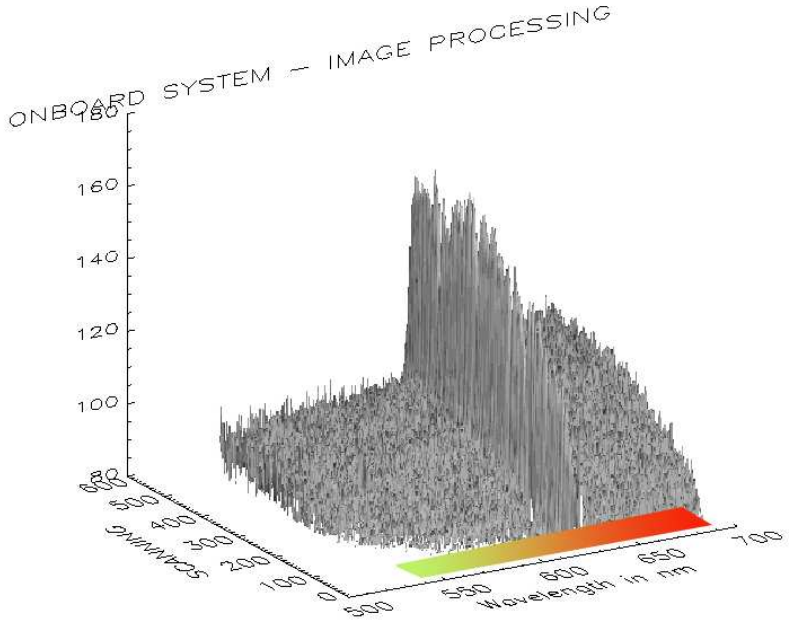

Figure 5: 2D spectrum, Wavelength = 630 nm.

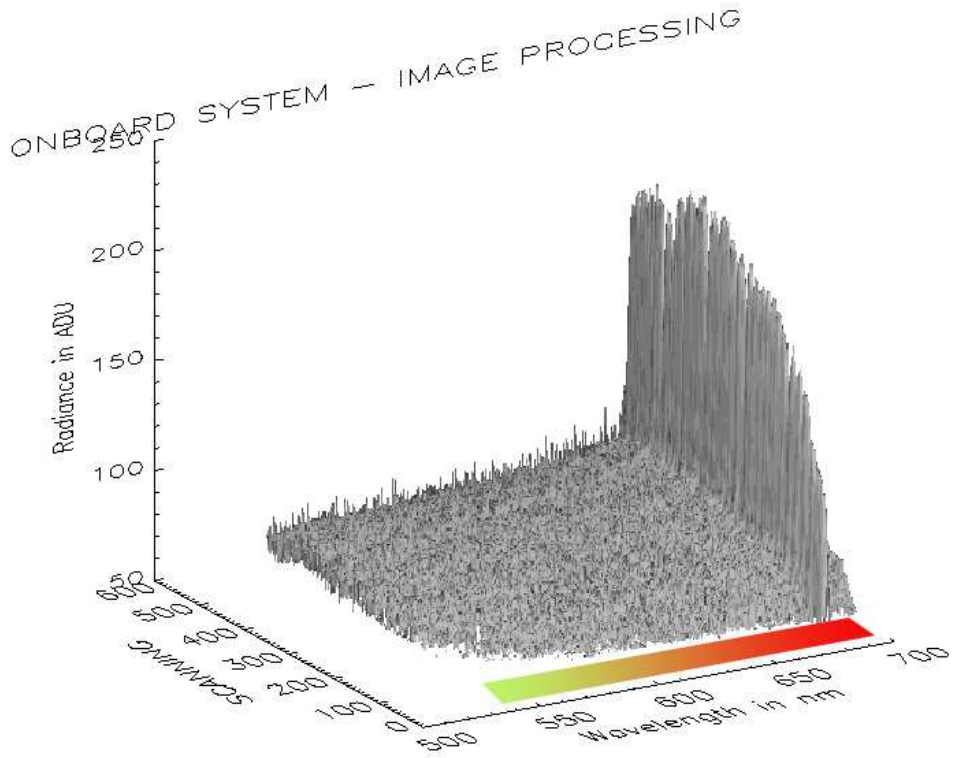

Figure 6: 2D Spectrum, Wavelength = 680 nm.

4. CONCLUSION

The worked out input-output controller is a part of an airborne-based video spectrometric system at the prototype level for remote sensing investigation of the land cover. The used newest technologies in the last years allow development of the portable devices with high-speed signal processing and low consumption. It is, therefore, recommended to design an industrial computer system that can accommodate the necessary boards for simultaneous navigation and image data acquisition. This would greatly improve system portability and cost

References

Birk, R.J., McCord, T.B.: 1994, *IEEE Aerospace and Electronics Systems Magazine*, **9**, 10.
Kramer, H.J.: 1996, Observation of the Earth and its Environment - Survey of Missions and Sensors, Third Enlarged Edition, Springer Verlag, 1-960.
Kunkel, B.P., Schmidt, E., Del Bello, U., Harnisch, B., Meynart, R.: 1997, EUROPTO European Symposium on Environmental Sensing III.
Gekov, G. et al.: 2000, 30 Years of Organized Space Research in Bulgaria – Reports Collection, Space Research Institute – BAS, 321.

Proc. IV Serbian-Bulgarian Astronomical Conference,
Belgrade 21–24 April 2004,
eds. M. S. Dimitrijević, V. Golev, L. Č. Popović, M. Tsvetkov,
Publ. Astron. Soc. "Rudjer Bošković" No 5, 2005, 227 - 230 *Contributed paper*

ION-ATOM COLLISIONS AT INTERMEDIATE IMPACT VELOCITIES AS A NEW SOURCE OF UV AND VUV RADIATION

A. A. MIHAJLOV and Lj. M. IGNJATOVIĆ
Institute of Physics, P. O. Box 57, 11001 Belgrade, Serbia
E–mail mihajlov@phy.bg.ac.yu

Abstract. The processes of the radiative charge exchange in $H^+ + H(1s)$ collisions at the intermediate ion-atom impact velocities are treated as a source of continuous EM emission in the far UV range. The spectral intensity of this emission is determined, within the semiclassical method developed in previous works, for the ion-atom impact energies (in the center of mass reference frame) from 0.5 keV to 12.5 keV. The results obtained show that the spectral intensity of the examined EM emission increases for several orders of magnitude when passing from the visible to the VUV range of wavelength, and that the position of the maximum of this spectral intensity drifts with increase of collision energy from $\lambda \simeq 51$ nm to $\lambda \simeq 18$ nm. These results imply that considered radiation processes may be of interest from astrophysical aspect as a new sources of continuous UV and VUV emission.

1. INTRODUCTION

There are some astrophysical object where the relative movement of their plasma greatly exceeds the thermal velocities. The most significant example are the giant streams of the hydrogen plasma (jets), ejected from the central parts of active galaxies. The typical velocities of such jets can be 1000-2500 km/s, as in the case of Akn 120 galaxy (Popović et al., 2001). Another characteristic example are streams of weakly ionized hydrogen plasma (outflows), produced during the creation of young stars (Eisloffel et al., 2000). The velocity of these streams can be greater than 200 km/s. Also, some stars can release the outer layers of their atmospheres. Typical example is the yellow hyper giant ρ-Cassiopeiae, with velocity of weakly ionized layers around 100 km/s (Lobel et al., 2003). Another very interesting case is the formation of two nearly spherically symmetrical layers of hydrogen plasma, an outer (slow wind) and inner (fast wind), moving from the central star with velocities of 20 km/s and 2000 km/s, respectively (Icke, 2003; Kwok, 1982). A great difference in velocities results in strong interaction of these layers, which manifests in non-thermal atom-ion collisions with typical impact velocities at 100 - 1000 km/s.

With regard to all these examples, our primary objective is to show the influence of ion-atom collisions at impact velocities 100-2000 km/s in corresponding astrophysical plasmas. These processes are sources of the UV and VUV electromagnetic emission and are of interest in various diagnostics.

We will consider the following ion-atom collision processes:

$$H^+ + H \rightarrow \varepsilon_\lambda + \begin{cases} H + H^+ \\ H^+ + H \end{cases} \tag{1}$$

in the middle range of impact velocities. Here $H = H(1s)$ denotes a hydrogen atom in its ground state, and ε_λ is the energy of the photon with the wavelength λ. The theory of processes (1) has been developed in two previous papers (Drukarev and Mihajlov, 1974; Ermolaev and Mihajlov, 1991). In the first, a dynamical semiclassical theory of the process (2) was evolved, and in the second, a method (based on this theory) was worked out for calculating spectral characteristics of a group of processes of that type in the range of intermediate collision energies. In Ermolaev and Mihajlov (1991) this method was tested just in the example of the process (1) at impact energies of 10 keV, in the infra-red and visible region. However, the results of later estimations (Mihajlov and Ermolaev, 1998) showed that the intensity of the examined EM emission at these impact energies should increase for several orders of magnitude at transition from the visible into the VUV region. In view of the fact that a proof of such results would imply that the process (1) in the case of the intermediate $H^+ + H$ impact energies may also be interesting in astrophysical aspect, we have performed corresponding calculations of spectral intensity of the EM emission generated in this process. Here we present the results of the calculations of this spectral intensity for wavelengths from visible up to the soft X-ray region, which refer to the $H^+ + H$ impact energies in the center of mass reference frame from 0.5 keV to 12.5 keV.

2. RESULTS AND DISCUSSION

The results of our calculation are presented in Figs. 1, 2 and 3.

One may conclude on the base of the presented results that the radiative process (1) for intermediate impact energies could be of interest from astrophysical point of view, as a new source of EM emission in the UV region and up to the X-rays region, with a conspicuous maximum in the VUV region. First of all, we would like to emphasize the necessity of taking into account the process (1), in situation of two weakly ionized hydrogen plasma layers penetrating one into each other and moving with respect to the other with macroscopic velocity $\approx 10^6 m/s$, since this process can very strongly affect the shape of the considered continuous emission spectra in the UV, and especially in the VUV region. It is clear that all presented here could be applied to the interaction of weakly ionized hydrogen plasma layers with beams of intermediate energy hydrogen ions.

Presented results could be directly used when the relative velocity of the radiation source with respect to the observer, v_r, is much smaller than the speed of light. Namely, our estimations show that in the range $0 \leq v_r \leq 0.01c$ the spectral intensity changes for less than 1% due to Doppler effect. If the source velocity increases up to $0.1c$, the values of $S(\lambda, v)$ might change 10% - 15%. This is due to the fact that the spectrum of EM emission generated in the processes [1] at intermediate impact energies is broad and does not contain sharp maxima and minima. On the other hand, if the velocity of the source increases up to $0.1c$, the values of spectral intensity

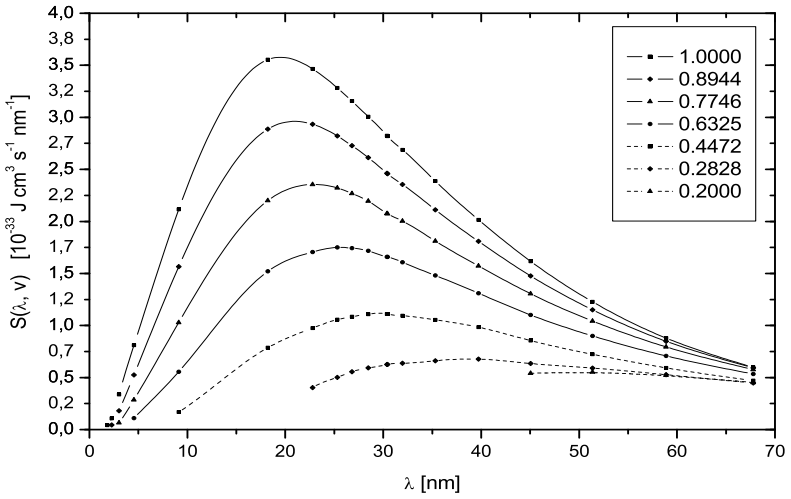

Figure 1: Spectral intensity $S(\lambda, v)$ as a function of wavelength λ, in the region $\lambda \leq 67.79$ nm, for impact velocities v in the range $0.2v_0 \leq v \leq 1.0v_0$.

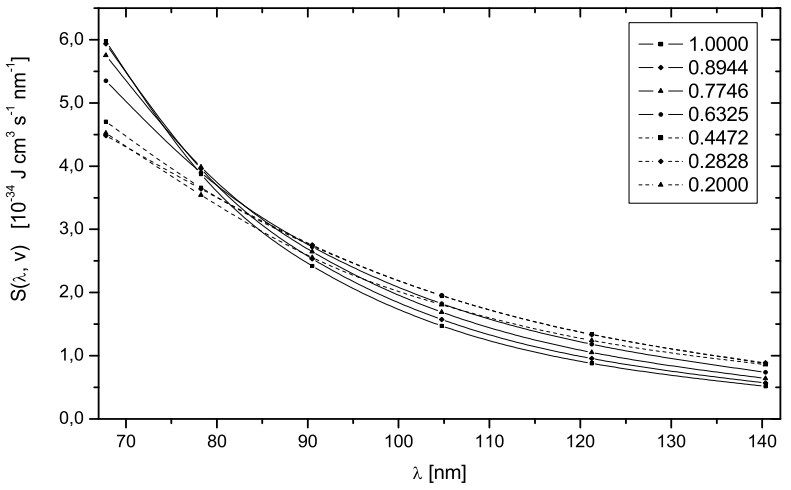

Figure 2: Same as on the Fig. 1, but in the wavelength range 67.79nm $\leq \lambda \leq$ 140.363 nm.

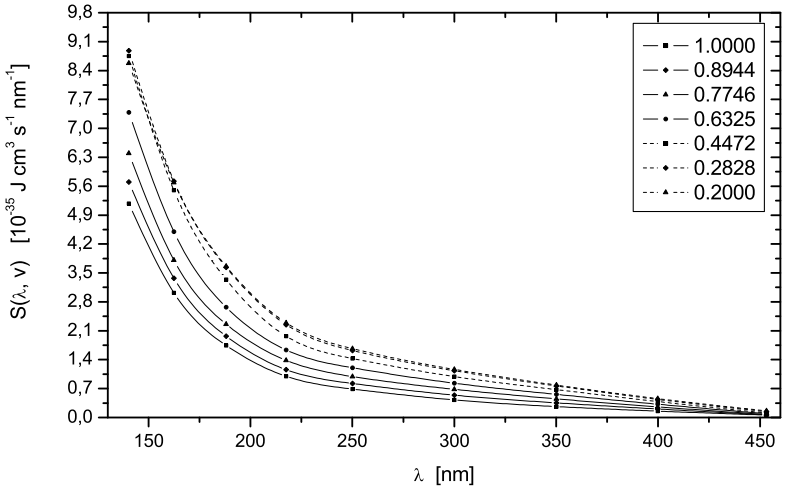

Figure 3: Same as on the Fig. 1, but in the wavelength range $\lambda \geq 140.363$ nm.

would change for 10% to 15% from the ones presented here, which would in general require additional elaboration. However, one should keep in mind that for practical purposes such an accuracy of determination of the spectral intensity of EM emission is often quite acceptable.

References

Drukarev, G.P. and Mihajlov, A.A.: 1974, *Opt. Spektrosk.*, **37**, 384.
Eisloffel, J., Smith, M.D., and Davis, C.J.: 2003 *Astron. Astrophys.*, **359**, 1147.
Ermolaev, A.M. and Mihajlov, A.A.: 1991, *J. Phys. B: At. Mol. Opt. Phys.*, **24**, 155.
Icke, V.: 2003, *Europhysicsnews*, **34/1**, 12.
Kwok, S.: 1982, *Astrophys. J.*, **258**, 280.
Lobel, A., Dupree, A.K., Stefanik, R.P., and Torres, G.: 2003, *Astrophys. J.*, **583**, 923.
Mihajlov. A.A. and Ermolaev, A.M.: 1998, *IV S'EZD ASTRONOMICHESKOGO OBSCESTVA, Trudy*, 41, Moskva.
Popović, L.Č., Stanić, N., Kubičela, A., and Bon, E.: 2001, *Astron. Astrophys.*, **367**, 780.

Proc. IV Serbian-Bulgarian Astronomical Conference,
Belgrade 21–24 April 2004,
eds. M. S. Dimitrijević, V. Golev, L. Č. Popović, M. Tsvetkov,
Publ. Astron. Soc. "Rudjer Bošković" No 5, 2005, 231 - 235 *Contributed paper*

EXPERIMENTAL TOTAL STARK SHIFTS IN THE Ar I SPECTRUM

V. MILOSAVLJEVIĆ and S. DJENIŽE

Faculty of Physics, University of Belgrade, P.O.B. 368, Belgrade, Serbia

Abstract. The Stark shifts (d) in the 4s'–5p' transitions of neutral argon (Ar I) have been studied in a linear, low–pressure, optically thin pulsed arc discharge. The line shapes are measured in three different plasmas at about 16 000 K electron temperature (T) and about 7.0x10^{22} m^{-3} electron density (N). The separate electron and ion contributions to the total Stark shift ($d_{\rm t}$), i.e. $d_{\rm e}$ and $d_{\rm i}$ have also been obtained and represent new experimental data in this field.

On the basis of the observed asymmetry of the Stark broadened line profile we have deduced the ion broadening parameters which describe the influence of the ion–static (A) and the ion–dynamical effect (E) to the Stark shift.

1. INTRODUCTION

The presence of the neutral argon (Ar I) spectral lines has been discovered in various cosmic light sources in the last few years. Recently, Weaver et al. (2002) have referred the presence of (Ar I) lines in the spectra of long-period comets. The Ar I absorption lines have been detected in the spectra of the quasar Q0347-3819 and PG 1259 + 593. In the study by Friedman et al. (2000) the absorptions in the Ar I lines were presented. Argon is detected in the spectrum of the damped Ly$_\alpha$ system of IZw 18. Mallouris et al. (2001) refer the presence of Ar I lines in the spectrum of the Wolf–Rayet binary SK 108. Thus, the Ar I spectral line shapes represent important sources of information about the physical conditions in the place of birth of the radiation, especially since the launch of the Hubble space telescope.

In this work we applied the line deconvolution procedure (Milosavljević and Poparić, 2001) to precisely recorded Ar I lines profile. The spectral lines are measured using the step–by–step technique (Milosavljević et al., 2000) for three different plasmas created in a linear, low–pressure, pulsed arc discharge in argon–helium and argon–hydrogen mixtures.

The basic plasma parameters, i.e. electron temperature (T) and electron density (N) have been obtained using well–known, experimental diagnostical techniques, but also using the line deconvolution procedure (Milosavljević and Poparić, 2001).

In this paper we are presenting the measured Stark shift of the 415.86, 416.42 and 426.63 nm Ar I spectral lines (in 4s'–5p' transition, multiplet [3/2]^o-[3/2]) at about 16 000 K electron temperature and at about 7.0x10^{22} m^{-3} electron density. The used T values are typical for many cosmic light sources and laboratory plasmas.

On the basis of the observed Ar I line profile asymmetry, the characteristics of the ion contribution to the total Stark shift (d_t), has been obtained in function of the ion contribution parameter (A) and ion–dynamical effect (E). Our d_t, d_e and d_i quasi–static values have been compared to theoretical and experimental values.

2. EXPERIMENT

The modified version of the linear low pressure pulsed arc (Milosavljević et al., 2000; Djeniže and Bukvić, 2001; Djeniže et al., 2002abc; 2003) has been used as an optically thin plasma source. A pulsed discharge was driven in a quartz discharge tube of 5 mm inner diameter and plasma length of 7.2 cm. The tube has end-on quartz window. Experimental set-up system, line profile recording technique and plasma diagnostical procedures are described in Milosavljević et al. (2000) and in Djeniže et al. (2003).

3. THEORETICAL BACKGROUND AND DECONVOLUTION PROCEDURE

The total line Stark shift (d_t) with the corresponding electron (d_e) and ion (d_i) contributions is given as:

$$d_\mathrm{t} = d_\mathrm{e} + d_\mathrm{i} \tag{1}$$

For a non–hydrogenic, isolated neutral atom line the ion broadening is not negligible and the line profiles are described by an asymmetric K function (see Eq. (5)). The d_t may be calculated from the equation:

$$d_\mathrm{t} \approx W_\mathrm{e}[d_\mathrm{e}/W_\mathrm{e} \pm 2AE(1 - 0.75R)] \tag{2}$$

where W_e is electron Stark FWHM and R is the Debye shielding parameter. A is the quasi–static ion broadening parameter, E is a coefficient of the ion–dynamical contribution to the shift, with the established criterion:

$$E = \frac{2.35 \cdot B^{-1/3} - 3A^{1/3} \cdot R}{2 \cdot (1 - 0.75 \cdot R)} \qquad \text{for} \qquad B < 1;$$

or

$$E = 1 \qquad \text{for} \qquad B \geq 1, \tag{3}$$

where

$$B = A^{1/3} \cdot \frac{4.03 \cdot 10^{-7} \cdot W_e[\mathrm{nm}]}{(\lambda[\mathrm{nm}])^2} \cdot (N[\mathrm{m}^{-3}])^{2/3} \cdot \sqrt{\frac{\mu}{T_\mathrm{g}[\mathrm{K}]}} < 1; \tag{4}$$

is the factor with atom–ion perturber reduced mass μ (in amu) and gas temperature T_g. When $E = 1$ the influence of the ion–dynamic is negligible to the width and shift respectively, and the line shape is treated using the quasi–static ion approximation, described by Milosavljević and Poparić (2001) and references therein:

Table 1: The Stark shift characteristics for Ar I lines. Measured: $d_{\rm t}^{\rm exp}$, $d_{\rm e}^{\rm exp}$ and $d_{\rm i}^{\rm exp}$ (in pm) within 12% accuracy at measured electron temperature ($T^{\rm exp}$ in 10^3K) and electron density ($N^{\rm exp}$ in $10^{22}{\rm m}^{-3}$). Ref. represents sources of experimental data. Tw denotes our data. Other notations: Bu, Bues et al. (1969); Po, Powell (1969); Mo, Morris and Morris (1970); Ge, Gericke (1961); Gr, Griem (1962); Ch, Chapelle et al. (1967). $A^{\rm exp}$ denotes our quasi–static ion broadening parameters.

Multiplet	λ (nm)	$T^{\rm exp}$	$N^{\rm exp}$	$A^{\rm exp}$	$E^{\rm exp}$	$d_{\rm t}^{\rm exp}$	$d_{\rm e}^{\rm exp}$	$d_{\rm i}^{\rm exp}$	Ref.
$[3/2]_2^o$-$[3/2]_2$	415.86	15.6	6.7	0.143	1.46	57	41	16	Tw
		16.0	7.0	0.146	1.93	68	46	22	Tw
		16.2	7.1	0.147	1.91	71	48	23	Tw
		9.75–12.7	1.2–9.4			13–94			Bu
		14.0	1.0			9.9			Po
		13.5	12.8			142			Mo
		11.4	4.6			50			Ge
		9.72–14.83	1.7–18.0			16–172			Gr
$[3/2]_2^o$-$[3/2]_1$	416.42	15.6	6.7	0.140	1.51	55	40	15	Tw
		16.0	7.0	0.142	1.97	65	44	21	Tw
		16.2	7.1	0.142	1.97	68	47	21	Tw
		9.75–12.7	1.2–9.4			11–79			Bu
		14.0	1.0			10			Po
		11.4	4.6			42			Ge
		13.8	14.5			75			Ch
$[3/2]_1^o$-$[3/2]_2$	426.63	15.6	6.7	0.132	1.55	60	45	15	Tw
		16.0	7.0	0.132	2.06	71	51	20	Tw
		16.2	7.1	0.134	2.02	72	51	21	Tw
		14.0	1.0			9			Po
		13.5	12.8			129			Mo
		11.4	4.6			50			Ge

$$K(\lambda) = K_{\rm o} + K_{\rm max} \int_{-\infty}^{\infty} exp(-t^2) \cdot [\int_0^{\infty} \frac{{\rm H_R}(\beta)}{1 + (2\frac{\lambda-\lambda_{\rm o}-\frac{{\rm W_G}}{2\sqrt{\ln 2}}\cdot {\rm t}}{{\rm W_e}} - \alpha \cdot \beta^2)^2} \cdot d\beta] \cdot dt. \quad (5)$$

Here $K_{\rm o}$ is the baseline (offset) and $K_{\rm max}$ is the maximum intensity (for λ=$\lambda_{\rm o}$) (Milosavljević and Poparić, 2001). $H_{\rm R}(\beta)$ is an electric microfield strength distribution function of normalized field strength β=$F/F_{\rm o}$, where $F_{\rm o}$ is the Holtsmark field strength. A (α=$A^{4/3}$) is the static ion broadening parameter and represents the measure of the relative importance of ion and electron broadenings. R is the Debye shielding parameter and $W_{\rm e}$ is the electron width (FWHM) in the $j_{\rm A,R}$ plasma broadened spectral line profile (Griem, 1974). The $W_{\rm G}$ is the Gaussian FWHM width (Eq.(2.3) in Milosavljević and Poparić (2001)).

More details, about deconvolution procedure, it can be find in Milosavljević and Poparić (2001).

On the end it is important to point out that, taking into account the uncertainties of the line profile measurements and mentioned in Milosavljević and Poparić (2001), we estimate errors as ±12% for the d_e and d_i, ±15% for the A parameter and ±20% for E.

4. RESULTS AND DISCUSSION

The plasma broadening parameters (d_t^{exp}, d_e^{exp}, d_i^{exp}, A^{exp}, E^{exp}) obtained using our deconvolution procedure of the recorded line profiles at measured N^{exp} and T^{exp} values are presented in Table 1 together with those of the other authors.

In order to facilitate the comparison among the measured total (electron + ion) Stark shift (d_t^{exp}) values and the well-known theoretical one (d_t^G), due to Griem (1974), the dependence of the ratio d_t^{exp} / d_t^G on the electron temperature is presented graphically in Fig. 1.

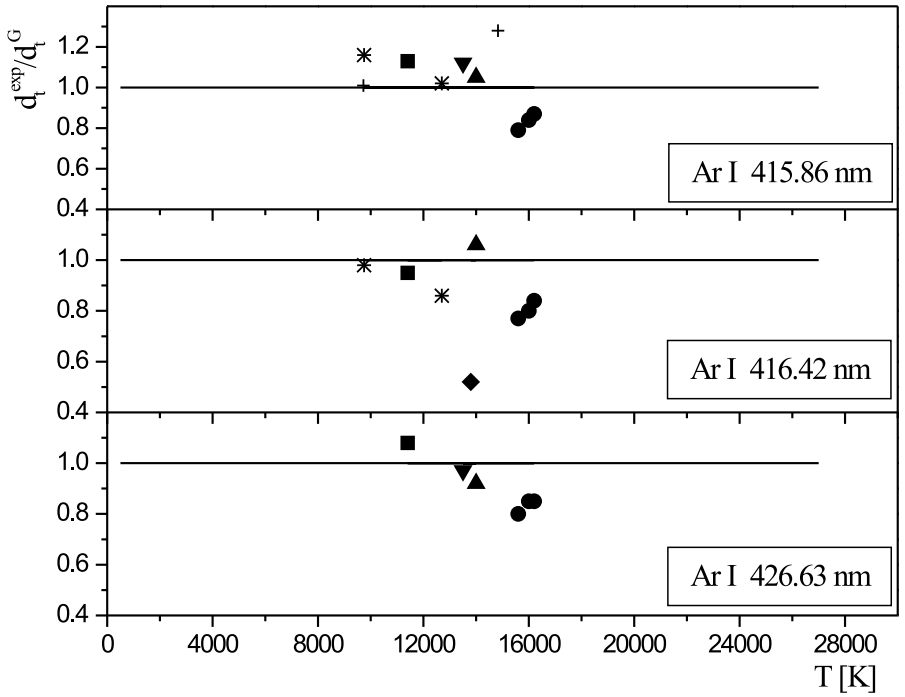

Figure 1: Ratios of the experimental total Stark shift (d_t^{exp}) to the theoretical (d_t^G) predictions (Griem, 1974) vs. electron temperature for three Ar I spectral lines. ∘, our experimental results and those of other authors: ∗, Bues et al. (1969); □, Gericke (1961); △, Powell (1969); ∇, Morris and Morris (1970); +, Griem (1962) and ♢, Chapelle et al. (1967).

5. CONCLUSION

Our d_t values lie below Griem's (1974) at about 20%. We have found that the ions contribute about 30% to the investigated Ar I Stark shifts at our plasma conditions.

Acknowledgements

This work is a part of the project "Determination of the atomic parameters on the basis of the spectral line profiles" (OI1228) supported by the Ministry of Science and Environment Protection of the Republic of Serbia.

References

Bues, L., Haag, T. and Richter, J.: 1969, *Astron. Astrophys.*, **2**, 249.
Chapelle, J., Cabonne, Sy.A., Cabannes, F. and Blandin, J.: 1967, *JQSRT*, **8**, 1201; 1967, C.R.H. *Acad. Sci. Ser. B*, **264**, 853.
Djeniže, S. and Bukvić, S.: 2001, *Astron. Astrophys.*, **365**, 252.
Djeniže, S., Milosavljević, V. and Dimitrijević, M.S.: 2002a, *Astron. Astrophys.*, **382**, 359.
Djeniže, S., Srećković, A. and Bukvić, S.: 2002b, *Eur. Phys. J. D*, **20**, 11.
Djeniže, S., Dimitrijević, M.S., Srećković, A. and Bukvić, S.: 2002c, *Astron. Astrophys.*, **396**, 331.
Djeniže, S., Milosavljević, V. and Dimitrijević, M.S.: 2003, *Eur. Phys. J. D*, **27**, 209.
Friedman, S.D., Howk, J.C., Andersson, B–G, et al.: 2000, *Astrophys. J. Lett.*, **538**, L39.
Gericke, W.E.: 1961, *Z. Astrophys.*, **53**, 68.
Griem H. R.: 1962, *Phys. Rev.*, **128**, 515.
Griem, H.R.: 1974, Spectral Line Broadening by Plasmas, New York: Acad. Press.
Mallouris, C., Welty, D.E., York, D.G. et al.: 2001, *Astrophys. J.*, **558**, 133.
Milosavljević, V., Djeniže, S., Dimitrijević, M.S. and Popović, L.Č.: 2000, *Phys. Rev. E*, **62**, 4137.
Milosavljević, V. and Poparić, G.: 2001, *Phys. Rev. E*, **63**, 036404.
Morris, J.C. and Morris, R.U.: 1970, *Aerospace Research Laboratories Report*, **No. ARL 70-0038**.
Powell, W.R.: 1969, *Diss. Abstr.*, **B29**, 3030.
Weaver, H.A., Feldman, P.D., Combi, M.R. et al.: 2002, *Astrophys. J.*, **576**, L95

Proc. IV Serbian-Bulgarian Astronomical Conference,
Belgrade 21–24 April 2004,
eds. M. S. Dimitrijević, V. Golev, L. Č. Popović, M. Tsvetkov,
Publ. Astron. Soc. "Rudjer Bošković" No 5, 2005, 237 - 240 *Contributed paper*

IMPROVED KOVAL'SKIJ METHOD AND ITS NEW POSSIBILITIES

D. OLEVIĆ and Z. CVETKOVIĆ
Astronomical Observatory, Volgina 7, 11160 Belgrade 74, Serbia
E–mail dolevic@aob.bg.ac.yu
E–mail zcvetkovic@aob.bg.ac.yu

Abstract. We improved the Koval'skij analytical method for binary star orbital elements determination, in order to enlarge its possibilities. The improved method is applicable to the determination of orbital elements for all cases of observation distributions on the apparent arc of the orbit, and always gives the elliptical solution.

1. INTRODUCTION

The duplicity of star Zeta UMa-Misara was noticed by Ricciolli as early as in 1650. Afterwards the duplicity was discovered for a constantly enlarging number of stars more or less accidentally. By 1775 the number of discovered binaries attained a few tens. In the late XVIII century H. Meier published a list containing 89 pairs for which he wrote that he had noticed the motion of a satellite around the parent star. These "observations" made by him were derided by his contemporaries. With regard to the equipment he used and large measuring errors this claim was bold. The year 1803 is considered as the year when binaries were discovered. In that year Herschel published a paper on the changes of mutual positions for binaries where he explained the causes of these changes. The action of the gravitation law was through this obviously noticed also beyond the Solar System confirming thus its universal validity.

At that time the campaign of discovering binaries was initiated: their equatorial coordinates were determined, micrometric measurements of the separations and position angles were done. V. Ya. Struve formulated this as his main task.

When a sufficiently large observational material became available, the first methods for the calculation of the orbital elements were proposed. The first orbital elements for visual binaries were determined by using the graphical method (Zwiers, 1896). The first analytical method was proposed by Koval'skij (see Subbotin, 1968), to be a little bit later improved by Glazenap. Further on many new methods for the purpose of solving some concrete problems were proposed: how to calculate orbital elements on the basis of a low number of measurements, how to obtain qualitative results in the presence of large observational errors and how to avoid a too long calculation. The tables for some analytic expressions were formed (Thiele-Innes (TI), TI- van den Boss (TIvdB) etc).

Table 1: Observations and residuals for WDS 07143-2621 = FIN 323

t	θ°	ρ''	$\Delta\theta^\circ_{KO}$	$\Delta\rho''_{KO}$	$\Delta\theta^\circ_{K}$	$\Delta\rho''_{K}$
1955.2600	136.6	.100	3.4	.000	61.9	−.221
1955.3100	135.5	.102	1.7	.002	60.2	−.217
1956.2100	135.5	.105	0.2	.004	57.0	−.178
1958.2400	139.6	.102	1.1	−.001	49.6	−.093
1959.2500	140.8	.101	0.7	−.003	40.0	−.051
1960.2400	137.8	.098	−3.8	−.006	19.1	−.019
1961.2900	141.8	.098	−1.4	−.006	−7.0	.000
1962.2700	142.7	.100	−2.1	−.003	−36.1	−.010
1963.2460	145.9	.102	−0.4	.000	−53.3	−.039
1964.2830	148.4	.098	0.4	−.002	−63.5	−.087
1965.2730	145.8	.098	−3.9	.000	−73.5	−.131
1966.2780	150.5	.099	−1.0	.004	−73.8	−.175
1967.2820	151.0	.099	−2.4	.008	−77.0	−.219
1968.3210	157.6	.098	2.0	.012	−73.2	−.263
1989.3083	141.6	.129	1.1	.010	65.3	−.314
1989.9336	142.0	.129	1.1	.010	64.7	−.296
1990.9137	142.6	.132	0.7	.006	63.5	−.265
1991.2500	144.0	.131	1.7	.002	64.2	−.256
1993.0953	144.6	.133	0.6	−.008	60.2	−.195
1996.1752	123.4	.150	−22.9	−.009	25.8	−.076

Table 2: Observations and residuals for WDS 13320-6519 = FIN 369

t	θ°	ρ''	$\Delta\theta^\circ_{KO}$	$\Delta\rho''_{KO}$	$\Delta\theta^\circ_{K}$	$\Delta\rho''_{K}$
1961.5600	117.3	.121	7.7	.020	−18.9	−.003
1962.5400	115.5	.126	−10.6	.023	−26.0	.001
1963.5590	143.5	.124	1.7	.013	−3.2	−.003
1964.5430	161.4	.130	7.0	.007	9.7	.001
1965.5630	164.2	.134	−0.7	−.004	7.6	.003
1966.5390	171.7	.140	−1.3	−.013	10.5	.007
1967.5800	185.5	.143	5.4	−.026	19.6	.007
1989.3036	344.5	.099	10.8	−.006	−3.1	−.008
1990.3437	355.2	.121	6.5	.005	0.9	.002
1991.2500	358.0	.131	−1.5	.004	−1.2	.003
1993.0984	8.2	.144	−8.5	−.003	0.8	−.002

With appearance of computers Koval'skij's method became more practical with regard that the "geometric" elements (first Kepler's law) are calculated by using the least-square method. A disadvantage of this method is that the dynamical elements P and T are calculated on the basis of these geometric elements without satisfying second Kepler's law (law of areas) simultaneously.

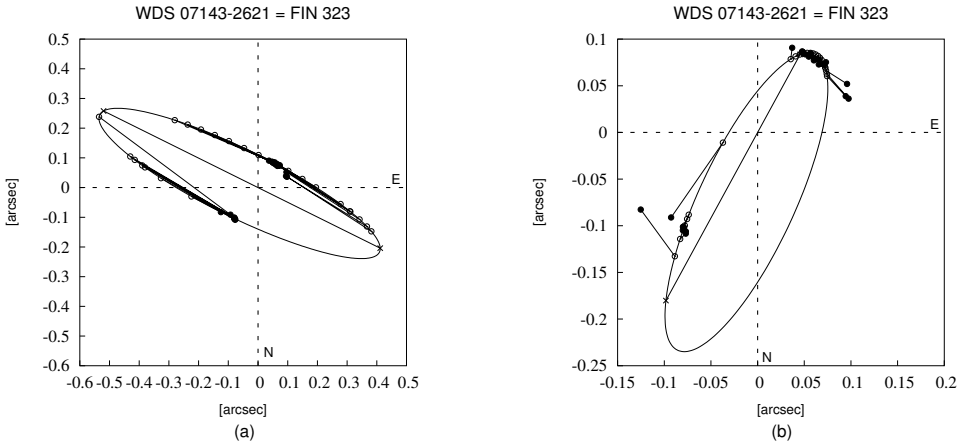

Figure 1: Orbits of FIN 323. (a) obtained by applying Koval'skij's method; (b) obtained by applying KOVOLE.

The TIvdB method uses among its input data the area constant determined through plots being a significantly crude and uncertain approach. This method, as most frequently used, has been improved by Docobo (1985). The main progress of Docobo's imrovement is that it became unnecessary to know the area constant.

Among other methods we shall also mention that proposed by Eichhorn (1985).

Koval'skij's method has been improved by one of us (Olević). In this way one obtains a new method (KOVOLE) usable for all cases. Unlike Koval'skij's method KOVOLE always yields an elliptical solution. Its more detailed description can be found in Olević and Cvetković (2004). By varying the amount for a number of fictive separations corresponding to given position angles the elements are calculated through an iterative procedure and the solution yielding the best fit to both first and second Kepler's laws is adopted.

The advantages of KOVOLE will be demonstrated through two examples.

2. EXAMPLES DEMONSTRATING THE SUCCESSFULNESS OF KOVOLE

In Fig. 1 one presents orbits of star WDS 07143-2621 = FIN 323: a) obtained by applying Koval'skij's method; b) obtained by applying KOVOLE.

In Fig. 2 one presents orbits of star WDS 13320-6519 = FIN 369: a) obtained by applying Koval'skij's method; b) obtained by applying KOVOLE.

The filled circles are for the measured positions, the empty ones are for the corresponding ephemeris values.

In Tables 1 and 2 one presents the observations and residuals. The designations are: t - observational epoch; θ and ρ - polar coordinates; $\Delta\theta_{KO}$ and $\Delta\rho_{KO}$ - residuals obtained by applying KOVOLE; $\Delta\theta_K$ and $\Delta\rho_K$ - residuals obtained by applying Koval'skij's method.

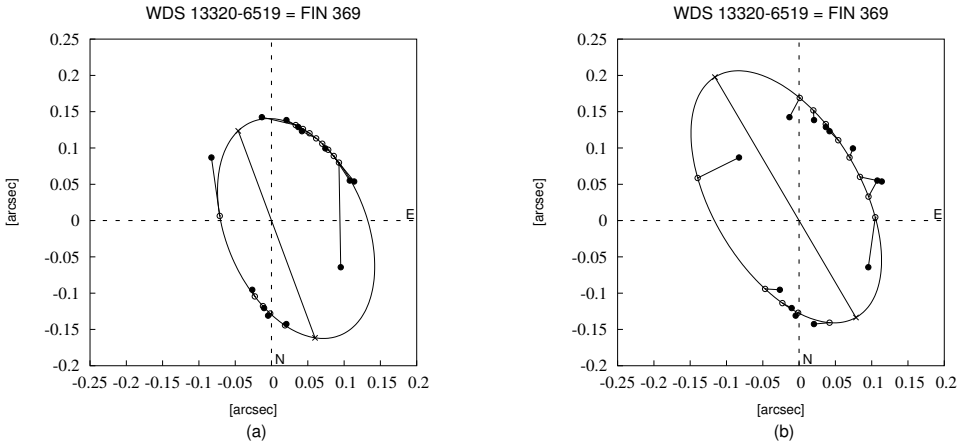

Figure 2: Orbits of FIN 369. (a) obtained by applying Koval'skij's method; (b) obtained by applying KOVOLE.

The $\Delta\theta_{KO}$ and $\Delta\rho_{KO}$ residuals are significantly smaller than the $\Delta\theta_K$ and $\Delta\rho_K$ ones. This is a clear confirmation of KOVOLE advantages. In favour are also the rms errors for the residuals of the observed values from the calculated ones.

The rms errors $(O-C)$ for star FIN 323 are: 0.2280 arc seconds, i.e. 0.0134 arc seconds, when one applies Koval'skij's method, i.e. KOVOLE, respectively. In the case of FIN 369 the rms errors $(O-C)$ are: 0.0174 arc seconds and 0.0138 arc seconds for the use of Koval'skij's method and KOVOLE, respectively.

References

Docobo, J.A.: 1985, *Cel. Mech.*, **46**, 143.
Eichhorn, K.H.: 1985, *Astrophys. Space Sci.*, **110**, 119.
Olević, D. and Cvetković, Z.: 2004, *Astron. Astrophys.*, **415**, 259.
Subbotin, M.F.: 1968, Vvedenie v teoreticheskuyu astronomiyu, Nauka, Moskva.
Zwiers, H.J.: 1896, *Astron. Nachr.*, **139**, 369.

Proc. IV Serbian-Bulgarian Astronomical Conference,
Belgrade 21–24 April 2004,
eds. M. S. Dimitrijević, V. Golev, L. Č. Popović, M. Tsvetkov,
Publ. Astron. Soc. "Rudjer Bošković" No 5, 2005, 241 - 246 *Contributed paper*

SURFACE PHOTOMETRY OF NGC 5610 – A BOX/PEANUT STRUCTURE IN AN INTERMEDIATELY INCLINED GALAXY

G. T. PETROV, L. S. SLAVCHEVA-MIHOVA and B. M. MIHOV
Institute of Astronomy, Bulgarian Academy of Sciences,
72 Tsarigradsko Chausse Blvd., 1784 Sofia, Bulgaria
E–mail petrov,lslav,bmihov@astro.bas.bg

Abstract. We report NGC 5610 as a new case of an intermediately inclined barred spiral galaxy with a box/peanut-shaped bulge. The ellipticity and the position angle of the galaxy measured at 25 B mag arcsec^{-2} isophote are 0.67 ± 0.02 and 99.7 ± 1.1 degree, respectively. The galaxian inclination estimated from the ellipticity is 70.7 ± 1.2 degree. The weight-averaged bar length, ellipticity and position angle are 17.3 ± 0.5 arcsec (or 5661.7 ± 162.3 pc), 0.83 ± 0.01 and 92.1 ± 0.6 degree, respectively.

1. INTRODUCTION

Recent statistics based on 734 disk galaxies selected from RC3 catalogue shows that $45.0 \pm 4.5\%$ of S0-Sd galaxies have box/peanut-shaped bulges (Lütticke et al., 2000a). Therefore, the research on these bulges is important to clarify the evolution of disk galaxies. However, the physical processes leading to box/peanut (hereafter b/p) bulges are not clear yet. According to the most popular scenario b/p bulges are explained by dynamical processes in bar potential (Combes and Sanders, 1981; Combes et al., 1990; Raha et al., 1991; Pfenniger and Friedli, 1991; Lütticke et al., 2000a; Lütticke et al., 2000b). This scenario is supported mainly by N-body simulations (e.g. Combes and Sanders, 1981). Additional support comes from spectroscopic observations (characteristic bar signatures in velocity fields are found, Kuijken and Merrifield, 1995) and from statistical studies (overall frequency of barred galaxies, about 55%, is able to explain the high fraction of b/p bulges, Lütticke et al., 2000a; Knapen et al., 2000). On the other hand, the connection between b/p bulges and the presence of a bar is difficult to be proved by surface photometry – b/p bulges are observable only in almost edge-on galaxies (inclination less then about 75 degree for an edge-on bar, Shaw et al., 1990; Combes et al., 1990; Lütticke et al., 2000b). However, there is photometric evidence in a few edge-on galaxies from cuts parallel to the major axis (de Carvalho and da Costa, 1987; Dettmar and Ferrara, 1996) and in two intermediately inclined galaxies (NGC 4442, Bettoni and Galletta, 1994 and NGC 7582, Quillen et al., 1997) pointing to bars. In particular, the observations of intermediately inclined galaxies is important in clarifying the nature of b/p bulges because in such cases both the bar and the b/p bulge can be observed simultaneously.

Table 1: Journal of observations for NGC 5610

Date [d.m.y]	Band	Exposure [second]	Seeing [arcsecond]	Number of frames
01.06.1997	V	300	1.82	1
01.06.1997	$R_{\rm C}$	80	1.89	1
03.03.1998	U	180	1.83	2
03.03.1998	B	120	1.66	2
03.03.1998	V	60	1.56	2
03.03.1998	$R_{\rm C}$	60	1.27	2
03.03.1998	$I_{\rm C}$	60	1.37	2

In this paper we report the observation of a new case of intermediately inclined galaxy with a b/p bulge, namely, the barred spiral galaxy NGC 5610.

2. OBSERVATIONS AND DATA REDUCTION

The galaxy NGC 5610 was observed with the Photometrics CCD camera attached to the 2-m telescope of Rozhen NAO in $UBVR_{\rm C}I_{\rm C}$ bands. The journal of observations is presented in Table 1.

The Photometrics CCD camera has 1024×1024 pixels, 0.24 μm each, a field of view 5.3×5.3 arcsec with the 2-m telescope and a non-binned scale of 0.309 arcsec px^{-1}. The possibility for 2×2 binning can be used for matching the seeing to the CCD pixel size. The CCD camera can be operated in two regimes of sensivity: (1) conversion factor 4.93 e$^-$ ADU^{-1} and readout noise 5.1 e$^-$ px^{-1} = 1.03 ADU px^{-1} and (2) conversion factor 1.21 e$^-$ ADU^{-1} and readout noise 3.3 e$^-$ px^{-1} = 2.73 ADU px^{-1}. We used the first regime and 2×2 binned camera during the observations.

The basic reduction steps for both dates are as follows: bias subtraction, flat fielding, defringing (applied to $I_{\rm C}$ frames only) and cosmic rays cleaning. All frames in each band were aligned and then averaged (applied to June, 1998 data only).

Adaptive filtering (Lorenz et al., 1993), multiple masking and sky background subtraction were made. Next, ellipse fitting was performed following Bender and Möllenhoff (1987) method. Finally, the images and the one-dimensional surface brightness profiles were transformed to the standard system. We used (1) NGC 7790 cluster for calibrating June, 1997 data (Odewahn et al., 1992; Petrov et al., 2001), and (2) NGC 4147 cluster (Davis, private comminication) for calibrating March, 1998 data.

3. RESULTS AND DISCUSSION

We present the isophotes of the V band image of NGC 5610 taken in June, 1997 in Fig. 1. The flattening of the bulge light distribution is clearly seen; one can recognize a peanut structure inside the boxy isophotes. This is an indication for a b/p shaped bulge (see Shaw, 1987)

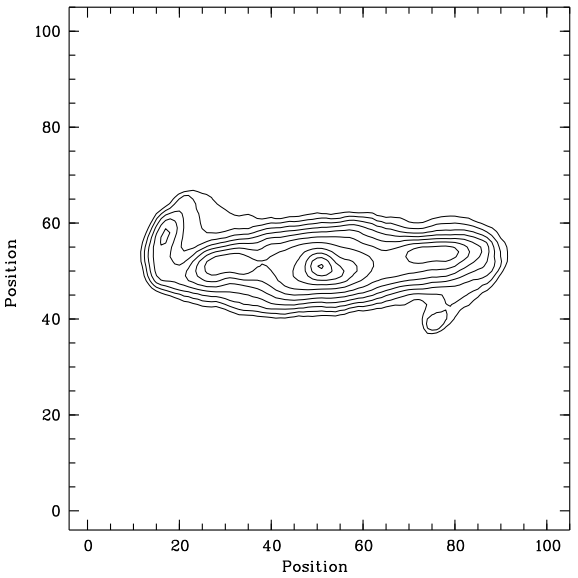

Figure 1: Isophotes of the V band image of NGC 5610 taken in June, 1997. Isophotes are drawn from 19.0 mag to 21.5 mag with a step of 0.25 mag. Axes labels are in units of pixels (1 pixel corresponds to 0.309 arcsec). A b/p structure could be identified in the central part of the galaxy. North is at the top, East is to the left.

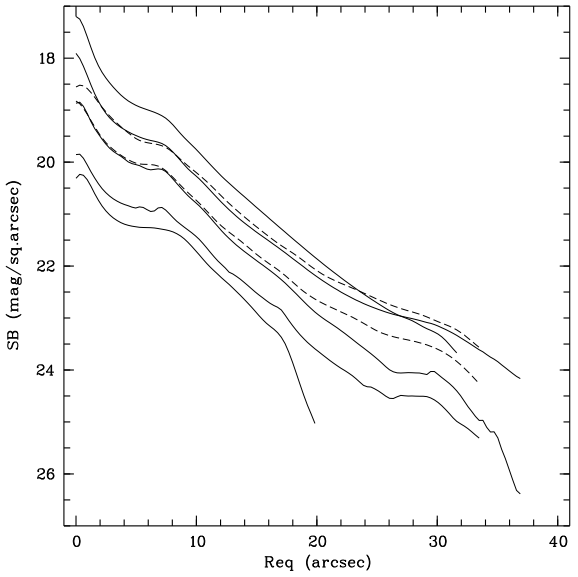

Figure 2: $UBVR_{\rm C}I_{\rm C}$ surface brightness profiles for NGC 5610: dashed lines – June, 1997, and solid lines – March, 1998. U band profile is the lower one, and $I_{\rm C}$ band profile is the upper one.

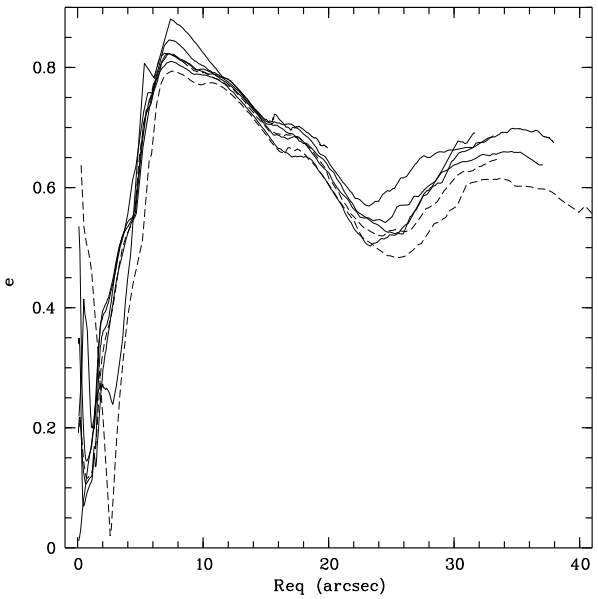

Figure 3: $UBVR_{\rm C}I_{\rm C}$ ellipticity profiles for NGC 5610: dashed lines – June, 1997, and solid lines – March, 1998.

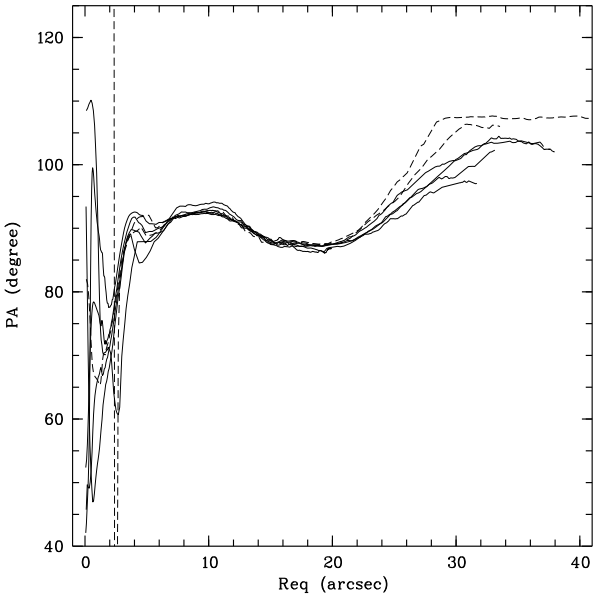

Figure 4: $UBVR_{\rm C}I_{\rm C}$ position angle profiles for NGC 5610: dashed lines – June, 1997, and solid lines – March, 1998.

Table 2: Estimated bar parameters for different epoches and bands

Date [d.m.y]	Band	Length [arcsec]	Length [parsec]	Ellipticity	Position angle [degree]
01.06.1997	V	16.5 ± 1.7	5388.5 ± 556.0	0.82 ± 0.04	91.5 ± 2.1
01.06.1997	$R_{\rm C}$	16.5 ± 1.2	5400.0 ± 384.6	0.79 ± 0.03	91.9 ± 1.8
03.03.1998	U	21.4 ± 2.1	7019.8 ± 697.3	0.88 ± 0.02	93.2 ± 1.3
03.03.1998	B	18.6 ± 6.4	6077.2 ± 2091	0.85 ± 0.11	92.0 ± 6.2
03.03.1998	V	17.4 ± 1.0	5688.7 ± 318.1	0.82 ± 0.02	91.5 ± 1.2
03.03.1998	$R_{\rm C}$	17.0 ± 1.6	5579.6 ± 517.7	0.82 ± 0.03	91.7 ± 1.9
03.03.1998	$I_{\rm C}$	17.2 ± 0.9	5645.6 ± 287.9	0.81 ± 0.02	92.0 ± 1.1

The ellipticity ($e = 1 - b/a$, where b and a are the minor and major semi-axes) and the position angle (PA, North through East) measured at $25\,B\,\mathrm{mag\,arcsec}^{-2}$ isophote are $e = 0.67 \pm 0.02$ and $PA = 99.7 \pm 1.1$ degree, respectively. According to HyperLeda database the ellipticity and the position angle of NGC 5610 are 0.65 and 108 degree, respectively, so, there is a good agreement between the catalogue values and ours. We plot the surface brightness, ellipticity and position angle profiles as a function of the equivalent radius ($R_{\rm eq} = \sqrt{ab}$) in Figs. 2-4, respectively. The correspondence between the surface brightness profiles observed in different epoches and between the ellipticity and the position angle profiles observed in different bands and in different epoches is satisfactory. This points to a good internal accuracy of our data.

The inclination ($i = \cos^{-1}(1-e)$) of NGC 5610 determined by us is 70.7 ± 1.2 degree compared to $i = 66.5$ degree for NGC 4442 and to $i = 64.1$ degree for NGC 7582 (the data about the intermediately inclined galaxies with b/p bulges NGC 4442 and NGC 7582 are taken from HyperLeda database).

The bar could be defined as a region of gradually rising ellipticity while position angle remains almost constant (e.g. Mulchaey et al., 1997). The bar length is then given by the major axis length of the ellipse at which the rising ellipticity reaches its maximal value. Our estimates of the bar length are presented in Table 2. We used heliocentric radial velocity of $5063 \pm 22\,\mathrm{km\,s}^{-1}$ taken from NED and Hubble parameter of $75\,\mathrm{km\,s}^{-1}\,\mathrm{Mpc}^{-1}$ to calculate the bar length in parsecs. One can see that within the errors there is a good correspondence between the bar parameters derived from observations obtained in different epoches and in different bands. The weight-averaged (over all epoches and all bands) bar length, ellipticity and position angle are 17.3 ± 0.5 arcsec (or 5661.7 ± 162.3 pc), 0.83 ± 0.01 and 92.1 ± 0.6 degree, respectively.

In conclusion, NGC 5610 could be considered as a new case of intermediately inclined galaxy that shows b/p bulge. Further study of this galaxy is useful.

The authors are thankfull to Drs A. Strigachev and E. Semkov for obtaining a part of the observational data. We used the HyperLeda database which is accessed at `http://www-obs.univ-lyon1.fr/hypercat/`. Part of this research has made use

of the NASA/IPAC Extragalactic Database (NED) which is operated by the Jet Propulsion Laboratory, California Institute of Technology, under contract with the National Aeronautics and Space Administration.

References

Bender, R., Möllenhoff, K.: 1987, *Astron. Astrophys.*, **177**, 71.
Bettoni, D., Galletta, G.: 1994, *Astron. Astrophys.*, **281**, 1.
Combes, F., Sanders, R.H.: 1981, *Astron. Astrophys.*, **96**, 164.
Combes, F., Debbasch, F., Friedli, D., Pfenniger, D.: 1990, *Astron. Astrophys.*, **233**, 82.
de Carvalho, R.R., da Costa, L.N.: 1987, *Astron. Astrophys.*, **171**, 66.
Dettmar, R.-J., Ferrara, A.: 1996, IAU Symp. 171, New Light on Galaxy Evolution, eds. R. Bender and R. Davis, Kluwer, p. 362.
Knapen, J.H., Shlosman, I., Peletier, R.F.: 2000, *Astrophys. J.*, **529**, 93.
Kuijken, K., Merrifield, M.R.: 1995, *Astrophys. J.*, **433**, L13.
Lorenz, H., Richter, G.M., Capaccioli, M., Longo, G.: 1993, *Astron. Astrophys.*, **277**, 321.
Lütticke, R., Dettmar, R.-J., Pohlen, M.: 2000a, *Astron. Astrophys. Suppl. Series*, **145**, 405.
Lütticke, R., Dettmar, R.-J., Pohlen, M.: 2000b, *Astron. Astrophys.*, **362**, 435.
Mulchaey, J. S., Regan, M.W., Kundu, A.: 1997, *Astrophys. J. Suppl. Series*, **110**, 299.
Odewahn, S.C., Bryja, C., Humphreys, R.M.: 1992, *Publ. Astron. Soc. Pacific*, **104**, 553.
Petrov, G., Seggewiss, W., Dieball, A., Kovachev, B.: 2001, *Astron. Astrophys.*, **376**, 745.
Pfenniger, D., Friedli, D.: 1991, *Astron. Astrophys.*, **252**, 75.
Quillen, A.C., Kuchinski, L.E., Frogel, J.A., Depoy, D.L., 1997, *Astrophys. J.*, **481**, 179.
Raha, N., Sellwood, J.A., James, R.A., Kahn, F.D. : 1991, *Nature*, **352**, 411.
Shaw, M., Dettmar, R.-J., Barteldrees, A.: 1990, *Astron. Astrophys.*, **240**, 36.
Shaw, M.A.: 1987, *Mon. Not. R. Astron. Soc.*, **229**, 691.

Proc. IV Serbian-Bulgarian Astronomical Conference,
Belgrade 21–24 April 2004,
eds. M. S. Dimitrijević, V. Golev, L. Č. Popović, M. Tsvetkov,
Publ. Astron. Soc. "Rudjer Bošković" No 5, 2005, 247 - 250 *Contributed paper*

THE FLUX RATIO OF [OIII]$\lambda\lambda$4959,5007 LINES IN Sy2: COMPARISON WITH THEORETICAL CALCULATIONS

L. Č. POPOVIĆ[1,2], M. S. DIMITRIJEVIĆ[1], E. BON[1] and M. DAČIĆ[1]
[1] *Astronomical Observatory, Volgina 7, 11160 Belgrade 74, Serbia*

[2] *Astrophysikalisches Institut Potsdam, An der Sternwarte 16, D-14482 Potsdam, Germany*

Abstract. Here we present the measurements of the [OIII]$\lambda\lambda$4959,5007 line flux ratios for a sample of 10 Sy 2 galaxies. Our measurements are compared with sophisticed calculation given by Storey and Zeippen (2000) and measurements given by Iye et al. (1987) and Leisy and Dennefeld (1996). We found that the ratio of the [OIII] line flux for Sy 2 is slightly smaller and in better agreement with theoretical one, than previous meausrement from emission nebulae.

1. INTRODUCTION

The forbidden [O III] 4958.911 Å ($2s^2 2p^2\ ^1D_2 - 2s^2 2p^2\ ^3P_1$) and 5006.843 Å ($2s^2 2p^2\ ^1D_2$ – $2s^2 2p^2\ ^3P_2$) spectral lines are among the most prominent not only in the spectra of photoionized nebulae but also in the spectra of photoionized gas around AGN's due to relatively high abundance of doubly charged oxygen ions in such objects. It should be underlined also their position in the centre of the visible spectral range. These two spectral lines are first of all the consequence of magnetic dipole transitions with a small contribution of electric quadrupole radiation. The elaborate theoretical work of Galavís et al. (1997) gives an 5006.843/4958.911 intensity ratio of 2.89. From astronomical spectra, Rosa (1985) deduced an intensity ratio of 3.03 ± 0.03, while measurements of Iye et al. (1987) provide a value of 3.17 ± 0.04, and of Leisy and Dennefeld (1996) 3.00 ± 0.08. Storey and Zeippen (2000) underline that in spite of the fact that the difference between experiment and theory is between 4 and 9 per cent, it must be considered as well-established because these lines can be observed with very high signal-to noise ratio in the spectra of gaseous nebulae. They demonstrated, taking into account relativistic corrections to the magnetic dipole operator introduced by Eissner and Zeippen in the context of a line-intensity ratio in [O III], that the probabilities for 5006.843 Å and 4958.911 Å transitions are affected by small relativistic corrections to the magnetic dipole operator. They obtained the A-value ratio of 3.01, implying a line intensity ratio of 2.98, which is only two percent or less different from the values of Rosa (1985) and Leisy and Dennefeld (1996) obtained from astronomical spectra, and the difference with the value of Iye et al. (1997) is 6 per cent.

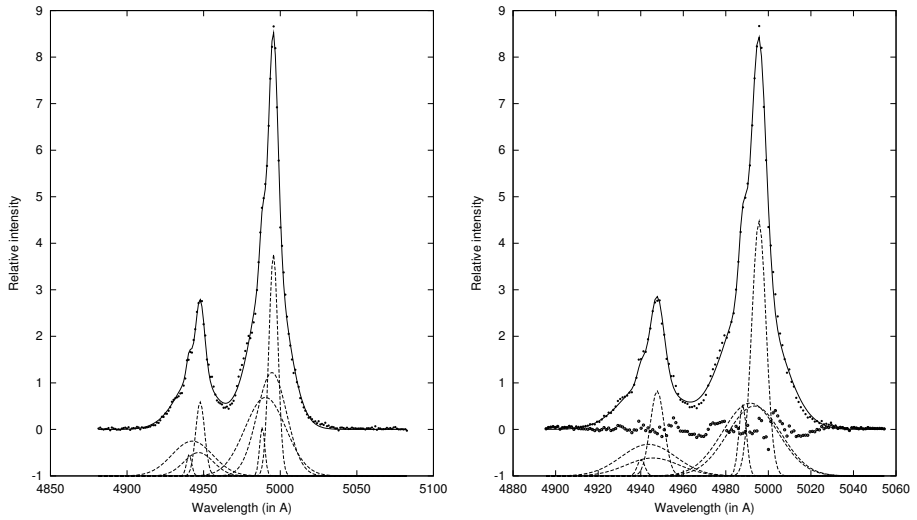

Figure 1: The [OIII] 4959, 5007 lines of NGC 1068 fitted with multi-Gaussian fit. The spectra of the slit position 1 is left and the slit postioin 2 is right (see Cecil et al., 2002).

On the other side, the measurements of the flux ratio of [OIII]4959,5007 lines for Sy 1 galaxies given in Popović et al. (2004) indicate that it can be significantly smaller than before measured values.

Up to now, all observational checks of [OIII] 5006.843/4958.911 intensity ratio have been made for planetary nebulae spectra. The aim of this paper is to measure the considered flux ratio in Sy 2 galaxies in order to see if they are also convenient for such cheks and to compare the obtained results with theoretical ones and with results obtained for planetary nebulae.

2. USED OBSERVATION AND MEASUREMENTS

In order to measure the flux ratio for [OIII]4959,5007 lines of Sy 2 galaxies, we use HST observations obtained with the Space Telescope Imaging Spectrograph (STIS) and Faint Object Spectrograph (FOS), covering the wavelength ranges 2900-5700 Å. From very large data base of AGN spectra at HST archive we selected the objects that have spectra with needed quality. For NGC 1068, we used several spectra made by HST with different slit positions (see Cecil et al., 2002).

The spectra were reduced by the HST team. We transformed the wavelength scale to zero red-shift taking into account the cosmological red-shift of the objects (Véron-Cetty and Véron, 2000). After that we estimated and subtracted the continuum. The fluxes of the lines were measured by using the DIPSO software. To estimate the error we measured several times the fluxes, where the procedure of subtracting of continuum has been three times repeated.

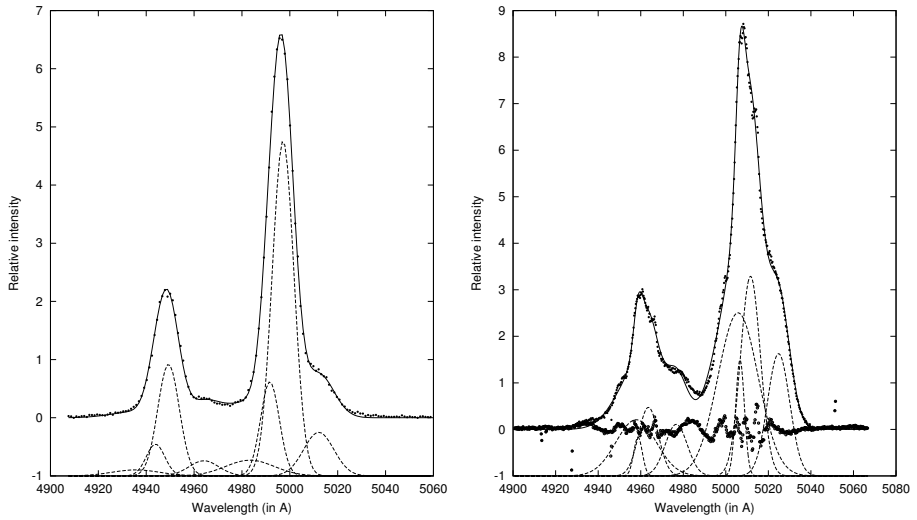

Figure 2: The same as in Fig. 1, but for the slit position 3 (left) and 4 (right).

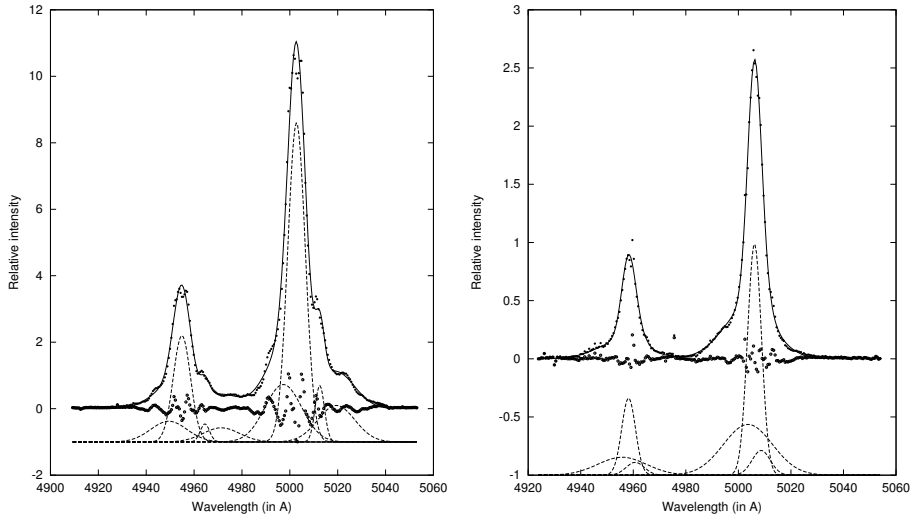

Figure 3: The same as in Fig. 1, but for the slit position 5 (left) and 6 (right).

In the case of NGC 1068, where the [OIII] lines show very complex profiles (in difference with slit orientation) we apply multi-gaussian method to determine the flux of both lines (see Figs. 1-4). The total flux in a line is obtained as a summ of Gaussians that represent the line.

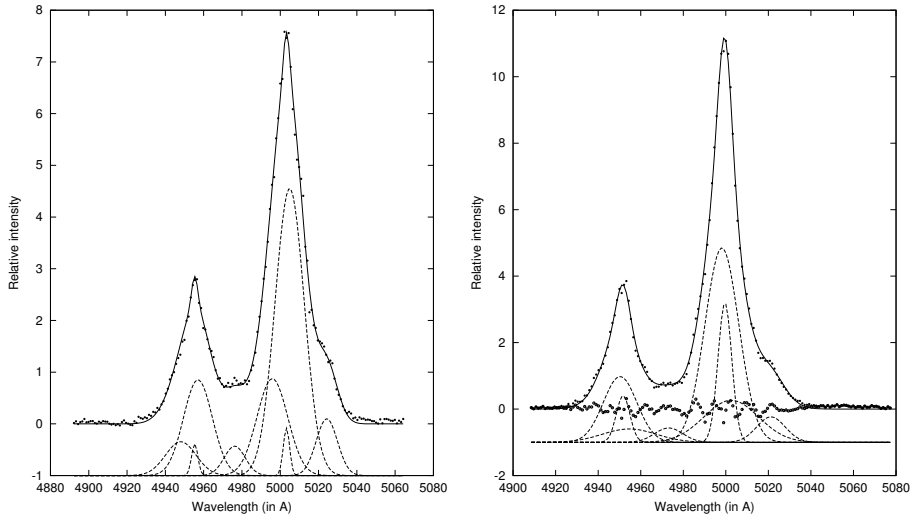

Figure 4: The same as in Fig. 1, but for the slit position 7 (left) and 8 (right).

3. PRELIMINARY RESULTS

We have analyzed the [O III] 4959,5007 intensity ratio in the spectra of 10 Sy 2 galaxies and our preliminary averaged value is 2.921 ± 0.084. which is in reasonable agreement with the theoretical value of 2.98 obtained by Storey and Zeippen (2000), better than some of the values within the 2.89-3.17 range obtained from planetary nebulae observations (Rosa, 1985 - 3.03; Iye et al., 1987 - 3.17; Leisy and Dennefeld, 1996 - 3.00; Galavías et al., 1997 - 2.89). Consequently, one can conclude that our results are in reasonable agreement with the sophysticated calculations of Storey and Zeippen (2000) and that the spectra of Sy 2 galaxies could be also used for checks of such theoretical calculations. More detailed discussion will be given elsewhere (Popović et al., 2004).

References

Cecil, G., Dopita, M.A., Groves, B., Wilson, A.S., Ferruit, P., Pcontal, E., Binette, L.: 2002, *Astrophys. J.*, **568**, 627.

Eissner, W., Zeippen, C.J.: 1981, *J. Phys. B*, **14**, 2125.

Galavís, M.E., Mendoza, C., Zeippen, C.J.: 1997, *Astron. Astrophys. Suppl. Series*, **123**, 159.

Iye, M., Ulrich, M.H., Peimbert, M.: 1987, *Astron. Astrophys.*, **186**, 84.

Leisy, P., Dennefeld, M.: 1996, *Astron. Astropphys. Suppl. Series*, **116**, 95.

Popović L.Č., Mediavilla, E., Bon, E., Ilić, D.: 2004, *Astron. Astrophys.*, accepted (astro-ph/0405447).

Popović L.Č., Dimitrijević M.S., Bon E., Dačić M.: 2004, in preparation.

Rosa, M.: 1985, *The Messenger*, **39**, 15.

Storey, P.J., Zeippen, C.J.: 2000, *Mon. Not. R. Astr. Soc.*, **312**, 813.

Véron-Cetty, M.-P., Véron, P.: 2000, A Catalogue of Quasars and Active Galactic Nuclei, Sci. Report, **19**.

Proc. IV Serbian-Bulgarian Astronomical Conference,
Belgrade 21–24 April 2004,
eds. M. S. Dimitrijević, V. Golev, L. Č. Popović, M. Tsvetkov,
Publ. Astron. Soc. "Rudjer Bošković" No 5, 2005, 251 - 257 *Contributed paper*

OBSERVATIONS OF AGNs WITH THE 2m TELESCOPE OF ROZHEN OBSERVATORY: AIMS AND PRELIMINARY RESULTS

L. Č. POPOVIĆ[1,2], K. STAVREV[3], K. TSVETKOVA[3], M. TSVETKOV[3],
D. ILIĆ[4], S. F. SANCHEZ[2], G. RICHTER[2] and P. BÖHM[2]

[1] *Astronomical Observatory, Volgina 7, 11160 Belgrade 74, Serbia*

[2] *Astrophysikalisches Institut Potsdam, An der Sternwarte 16, D-14482 Potsdam, Germany*

[3] *Institute of Astronomy, Bulgarian Academy of Sciences, 72 Tsarigradsko Shosse Blvd., BG-1784 Sofia, Bulgaria*

[4] *Department of Astronomy, Studentski trg 16, 11000 Belgrade, Serbia*

Abstract. Here we present an observational program for four Active Galactic Nuclei (AGNs) with the 2-meter telescope of Rozhen observatory (Bulgaria). The aims of the observations are given. Some of the preliminary results for Mrk 1040 are presented.

1. INTRODUCTION

Active Galactic Nuclei (AGNs) are one of the most interesting objects in astrophysics today (Osterbrock, 1989). First, by investigation of the processes in central part of these objects we can learn about the innermost part of other, 'normal', galaxies, i.e. the nucleus can be directly observed in multi- wavelength region, that can bring us information about the most central part of galaxies. Second, AGNs are located at different cosmological time-scales, consequently their investigations are cosmologically important. One of the characteristics of AGNs are emission lines. The lines can have very complex shapes (see e.g. Sulentic et al., 2000, and references therein), it depends where is their forming region. Using radiation in lines and continuum we are able to conclude about structure and kinematics of the emission region in AGNs as well as about the physics of the innermost part of these objects. One of interesting question is; what can generate the activity in these objects? To answer on the question, the investigation of connection between the nucleus and an extensive structure of AGNs are needed.

Here we will present our program for observations of four AGNs with 2 meter telescope of Rozhen observatory in order to investigate an extensive structure of AGNs.

Table 1: The selected objects

Object	Typ	red-shift	mag.
Akn 120	Sy1 with doub.-peaked lines	0.03230	14.1
Arp 102B	Sy1 with doub.-peaked lines	0.02417	15.12
Mrk 1040	Sy1 with comp.	0.01665	14.46
Mrk 817	Sy 1 with asymm. [OIII]	0.03145	14.50

2. ASTROPHYSICAL CONTEXT – AIMS

We intend to observe four objects in different narrow filter bands as well as in U and I filters. The idea is, for different astrophysical reasons (see below), using the images in different filters to explore an extensive structure of these AGNs. The selected objects are presented in Table 1.

2.1. Mrk 1040 AND COMPANION

LEDA 212995 is a small galaxy with emission lines that indicates star-forming region (H II lines, see Popović et al., 2004a). The dimension of galaxy is $0.20' \times 0.10'$ and magnitude >19. The galaxy is visually located near the Sy 1 galaxy Mrk 1040 (z=0.01665, Huchra et al., 1999).

Afanasiev and Fridman (1993) pointed out that an analysis of the (B-R) color distribution in the galactic disk and the presence of a distinct dust lane in the disk show that 'the northeast side of the galaxy is farther away, and the companion, which is bluer than the disk of Mrk1040, is closer to the observer'. The spectroscopical observations of Mrk1040 and LEDA 212995 were given in Amram et al. (1992), where the asymmetry in velocity field of companion is found and assumed that this asymmetry is due to interaction of these two galaxies. According to the red-shift of companion 0.0169 ± 0.00015 estimated by Popović et al. (2004b), it seems that objects are close each other and with the observations we would like to see any evidence for interaction between these galaxies.

2.2. AGNs WITH DOUBLE-PEAKED LINES

The double-peaked line shapes indicate that in these AGNs the emission of an accretion disk is present (Eraclous and Halpern, 1994; 2003). These galaxies not only have the similar (double-peaked) line profiles, but they show some similarity as (Eraclous and Halpern, 1994; 2003): i) an unusually large contribution of starlight to the optical continuum around Hα, ii) unusually large equivalent widths of low-ionization lines, iii) unusually large ratio of [OI]/[OIII]. With observations in different narrow filter bands of two AGNs (see Table 1) we would like to investigate an extensive structure of these objects, in order to see differences and similarities in AGNs with double-peaked lines.

2.3. Mrk 817 - AGN WITH ASYMMETRIC [OIII] LINES

Mrk 817 was observed spectroscopically several times. The narrow [OIII] lines show very extensive blue part (Popović et al., 2004b). This indicates an outflow in narrow

Table 2: Narrow-Band Filters

λ_c nm	τ_m %	$FWHM$ nm	Emission
468.1	0.607	18.8	HeII, 4686
500.9	0.726	22.3	[OIII], 4959,5007
575.5	0.644	23.5	Continuum
653.0	0.685	20.8	Hα, 6563
673.2	0.672	21.0	[SII], 6717, 6734

line region. In principle, narrow line region is enough large that can be resolved in near AGNs. We would like to explore an extensive structure in [OIII] lines, continuum, He II and Balmer lines in order to see sign of the outflow in the extensive region of the AGN.

3. OBSERVATIONS AND DATA REDUCTION

The observations have been made at Rozhen National Astronomical Observatory (longitude: 01h38m58s (E), latitude: $+41°41'35''$, altitude 1759 m) with the 2 m Ritchey-Chretien-Coude telescope. In Ritchey-Chretien focus the equivalent focal length is 16 m, the field is one square degree with a scale of 12.89 arcsec/mm. The telescope is equipped with a Photometrics AT200 CCD camera with 1024×1024 pixels array, with 1 pixel=0.32 arcsec and field $5.45'\times5.45'$.

The realization of the UBVRI broad-band system on the telescope is as follows – U: 2mm UG1 + 1mm BG39; B: 1mm BG14 + 1mm GG11 + 1mm BG23; V: 2mm GG495 + 1mm BG39; R: 2mm OG570 + 1mm KG3; I: 3mm RG9.

The set of narrow-band filters in Rozhen Observatory (diameter 45 mm) is given in Table 2.

All AGNs fro the Table 1, should be observed with filters noted in Table 2.

Additional observations of Mrk 1040 in the period 25-29 November 2003e, were performed with the two-channel focal reducer of the Max-Plank-Institute for Aeronomy (MPAe, Jockers et al., 2000). The blue channel was equipped with the Rozhen Photometrics AT200 CCD camera. A mask was used to remove the scattered light. This reduces the useful field to 512×512 pixels, where 1 pixel=$0.88''$ and field $7.5'\times7.5'$.

For the red channel the MPAe CCD camera was used. The field is also $7.5'\times7.5'$ with 1 pixel=$0.88''$. A color divider reflecting for λ <520 nm and transmitting for $\lambda > 580$ nm has been used. The filters used with the two-channel focal reducer during the observations in the period 25-29 November 2003 are given in Tables 4 and 5.

Standard reduction procedures including bias subtraction, trimming and flat-fielding have been performed with the help of the IRAF software package.

4. PRELIMINARY RESULTS

Till now, we have a complete set of observations only for Mrk 1040. The galaxy was observed in November 2003, and in January 2004. We observed narrow and broad-band images of the object Mkn1040 (described in previous section). Here we

Table 3: The MPAe Narrow-Band Filters

Filter	λ_c nm	τ_m %	$FWHM$ nm	Emission	Notes
IF 443	443	0.797	4.4	[OIII] 4363	No blocking filter is necessary
IF 501	500.2	0.701	4.1	[OIII] 4959	
IF 510	509.4	0.734	4.4	[OIII] 5007	
IF 667	666.2	0.910	5.5	Hα, 6563	

Table 4: The MPAe Broad-Band Filters

Filter	λ_c nm	τ_m %	$FWHM$ nm	Notes
DUG 11	338	0.832	75	Stronger cut-off than the cut-off of the filter because of absorption in the camera lens and the collimator
I	797	0.964	153	Up to 900 nm only

processed only the observations in the U- and I-band (broad band filters) and in the [HeII]4686 and [OIII]4959,5007 narrow filter bands. Also, we compare the narrow bands with continuum filter $\lambda = 5755$ Å.

Mrk 1040 is a Sy1 galaxy with different star-forming regions in stellar disk. LEDA 212995, a close companion, is also under star-formation (see Fig. 1). It is not clear if the companion is under interaction or not, and if the star-formation (in companion) and nuclei activity (in Mrk 1040) are caused by the interaction of these two galaxies.

In order to find any evidences about interaction we have processed the images applying the following techniques:

(1) A surface brightness analysis over the narrow-band images has been applied, assuming an elliptical isophotal model, and based on the technique given by Jedrzejewski (1987). We used own code (Sanchez) for the analysis, which provides us with a model (for Mrk 1040) of the smooth component in the images. This model has been subtracted from the images (in different narrow bands). After subtraction we obtained an image where can be seen the substructures in the objects as well as structure(s) that may indicate interaction between the objects (see Figs. 2 and 3, panel top-left).

(2) We have modeled Mrk 1040 galaxy using GALFIT (Peng et al., 2002). The galaxy model has been done including three components: The nuclear point-like source, a bulge and disk. This model has been subtracted to the images in order to detect the substructures (Figs. 2 and 3, panel down-left).

(3) We have scaled the continuum image to the narrow-band images, and subtracted from them. It provides us with images of the pure HeII and [OIII] emission lines (Fig. 4, bottom-right).[1]

[1]We should note that the continuum image is not as deep as the non-subtracted narrow-band images. It is due to the noise of the continuum image.

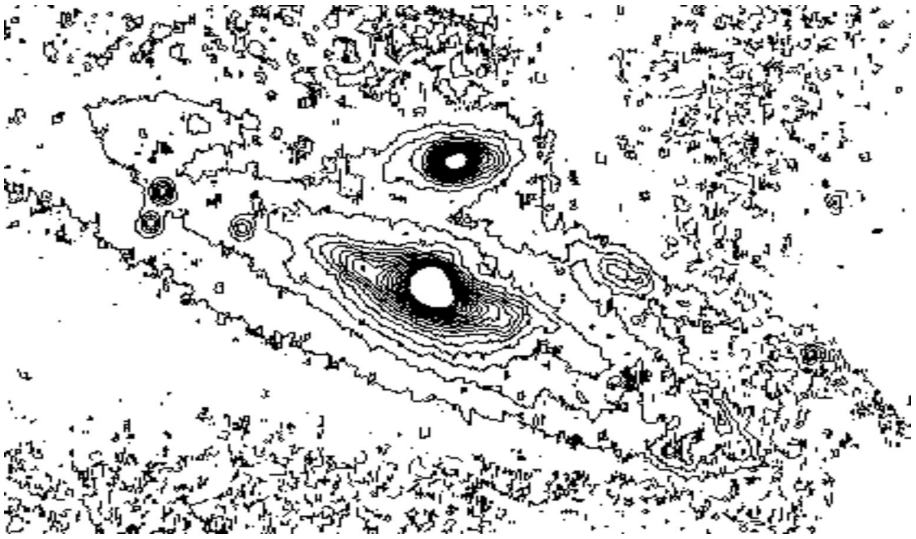

Figure 1: The brightness of Mrk 1040 and companion in the [OIII]4959,5007 lines.

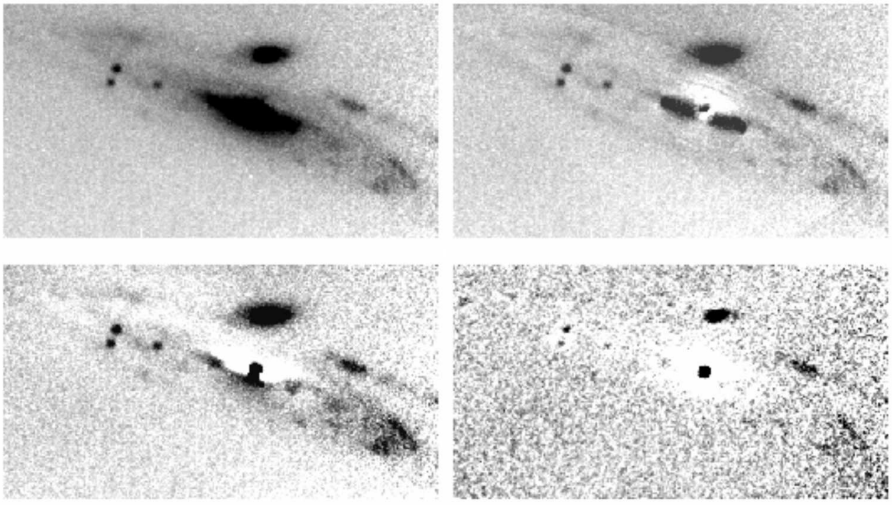

Figure 2: The image in [OIII] narrow band: Original Narrow-band image (top-left) Residual Image once subtracted the model obtained by the Surface Brightness analysis (top-right); Residual Image once subtracted the model obtained using GALFIT (bottom-left); Residual Image once subtracted the continuum scaled image (bottom-right).

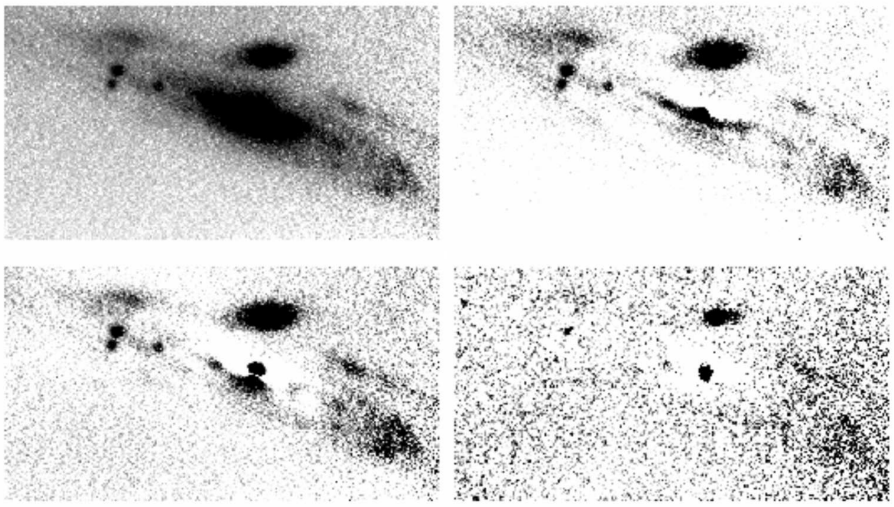

Figure 3: The same as in Fig. 1, but for the He II line.

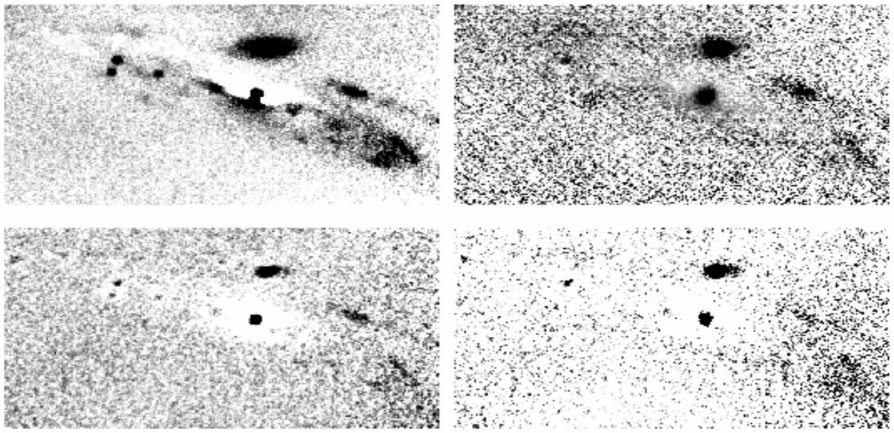

Figure 4: The original continuum narrow-band image (top-left); U-I color image (top-right); The [OIII] line regions after subtracting continuum (bottom-left); The HeII4686 line region after subtracting the continuum (bottom-right).

(4) We have divided the U-band image by the I-band image, in order to get a U- I color image (Fig. 4, top-right)

As one can see from Figs. 2-4, the substructures seen in all images are remarkably similar, indicating that: (i) There is very strong point-like innermost center of Mrk 1040, that is from AGN. The companion has un-regular structure that is expectable in the case of star-forming region; (ii) Different star-forming regions in the disk of Mrk 1040 galaxy, seen in west part of the arm; (iii) From our preliminary analysis we can conclude that there is no tidal tail of young stars in between Mrk 1040 and LEDA 212995.

In future work, we are going to apply the above described methods to the all observed narrow band filters of Mrk 1040 and companion, but first look in the data is in favour that there is no evidence for an interacting system.

Acknowledgements

This work was supported by the Serbian Ministry of Science and Environmental Protection through the project P1196 "Astrophysical Spectroscopy of Extragalactic Objects", the Bulgarian National Science Fund project # I-1103 and DFG/BAS contract: 436-BUL110-120. L. Č. P. is supported by Alexander von Humboldt Foundation through the program for foreign scholars.

References

Afanasiev, V.L. and Friedman, A.M.: 1993, *Astron. Lett.*, **19**, 319.

Amram, P., Marcelin, M., Bonnarel, F., Boulesteix, J., Afanasiev, V.L., Dodonov, S.N.: 1992, *Astron. Astrophys.*, **263** 69.

Eracleous, M., Halpern, J.P.: 1994, *Astropys. J. Suppl. Series*, **90**, 1.

Eracleous, M., Halpern, J.P.: 2003, *Astrophys. J.*, **599**, 886.

Huchra, J.P., Vogeley, M.S., Geller, M.: 1999, *Astrophys. J. Suppl. Series*, **121**, 287.

Jedrzejewski, R.I.: 1987, *Mon. Not. R. Astron. Soc.*, **226**, 747.

Jockers, K., Credner, T., Bonev, T., Kisele, V.N., Korsun, P., Kulyk, I., Rosenbush, V., Andrienko, A., Karpov, N., Sergeev, A., Tarady, V.: 2000, Kinematika i Fizika Nebesnykh Tel, Suppl, no. 3, 13.

Osterbrock, D.E.: 1989, Astrophysics of Gaseous Nebulae and Active Galactic Nuclei, (Mill Valle: University Science Press).

Peng, C.Y., Ho, L.C., Impey, C.D., Rix, H.-W.: 2002, *Astron. J.*, **124**, 266.

Popović, L.Č., Mediavilla, E., Bon, E., Ilić D., Richter, G.: 2004a, *Astron. Nachrichten*, accepted (astro-ph/0402010).

Popović, L.Č., Mediavlilla, Bon E., Ilić, D.: 2004b, *Astron. Astrophys.*, accepted.

Sulentic, J.W., Marziani, P. and Dultzin-Hacyan, D.: 2000, *Ann. Rev. Astron. Astrophys.*, **38**, 521.

Proc. IV Serbian-Bulgarian Astronomical Conference,
Belgrade 21–24 April 2004,
eds. M. S. Dimitrijević, V. Golev, L. Č. Popović, M. Tsvetkov,
Publ. Astron. Soc. "Rudjer Bošković" No 5, 2005, 259 - 262 *Contributed paper*

WATER IN ASTRONOMY AND PLASMA PHYSICS AND A PROJECT FOR RELATED RESEARCH

N. POPOVIĆ[1], M. SIMIČIĆ[1], Lj. NIKOLIĆ-BUJANOVIĆ[1], V. BORKA[1]
A. RADENKOVIĆ[1] and M. S. DIMITRIJEVIĆ[2]

[1] *Chemical Power Sources Institute (IHIS), 11080 Belgrade-Zemun, Serbia*
[2] *Astronomical Observatory, Volgina 7, 11160 Belgrade 74, Serbia*
E–mail ihis@eunet.yu
E–mail mdimitrijevic@aob.bg.ac.yu

Abstract. Importance of the investigations of water in astronomy, water-plasma interaction and discharges in water for the removal of organic pollutants and microorganisms from water, as well as the significance of discharges in water for medicine are briefly reviewed. It is also announced and briefly discussed our project for investigations of plasma-water interaction, plasma containing water molecules, or obtained in the presence of water molecules, of interest for astronomy, laboratory physics and technology.

1. WATER IN ASTRONOMY

The importance of water, the dissolvent without whom our kind of life would be impossible, is obvious and the research of all aspect of this compound is of great interest for many sciences. In astronomy, water is found in comets, Jovian satellites, on the Mars... The first molecule to be detected by radio astronomy methods, was the radical OH in 1963. Some OH sources in interstellar H II regions show strong H_2O emission as well. Their H_2O emission is variable, with intensity changes occuring in periods of months and days. In such regions temperature is around 10000 K and ion density around 5000 ions on m^3. Water molecules are found and in OH-IR stars, which are probably dust enshrouded Myras having period 600 - 2000 days, and are not visible optically. Recently, water molecules have been detected in the mid-infrared (11-12 microns) spectrum of Arcturus, a K1.5III giant star (Ryde, N., et al. 2003). In Brand et al. (2003) analysis of the properties of water maser emission in 14 star forming regions has been performed while Beck et al. (2003) have found and investigated water vapor emission from an elliptical ring of masers located near the protostar Cepheus A HW2.

2. PLASMA-WATER INTERACTION FOR WATER TREATMENT AND SOME APPLICATIONS IN MEDICINE

Plasma obtained from H_2O is of interest and for investigations of underwater discharges, some aspects of electrolysis research, and for various treatments of water. Namely, electrical discharges in water or close to water as pulsed corona discharge, electric barrier discharge and contact glow discharge electrolysis techniques are used e.g. for decomposition of organic pollutants (Sun et al, 1997, Joshi et al, 1995, Hoeben et al, 1999, Šunka et al, 1999, 2004, Arif Malik and Ghaffar, 2001, Sano et al. 2003, Šunka et al, 2004) and for the removal of microorganisms from water (Sun et al, 1999). Such investigations are of particular interest since there is a continuing need for the development of effective, cheap and environmentally friendly processes for the disinfection and degradation of such pollutants in water. An overview of such techniques and important developments that have taken place in this area are discussed in Arif Malik and Ghaffar (2001) and Šunka et al. (2004). In Serbia, coaxial dielectric barier discharge for potable and waste water treatment is studied in detail by Kuraica et al. (2004ab), which developed also an ozonized water reactor system. Sano et al. (2003) developed a cylindrical wetted-wall corona-discharge water purification reactor, which was used for the study of decomposition of phenol in water by corona discharge.

Laser induced breakdown plasma in water is of interest for pulsed cellar microsurgery and micromanipulation and microirradiation techniques. In Venugoplan et al. (2002) for example, the physical processes underlying pulsed cellular microsurgery and micromanipulation have been investigated using nanosecond 532 and 1064 nm laser pulses. Moreover, the implications of obtained results for biophysical microirradiation procedures are discussed. Underwater spark discharges are also of interest for the development of the so-called extra-corporeal shock wave lithotripsy, a noninvasive method for treatment of kidney stone desease (Burlion et al. (1994). Namely we have spark discharge between needle electrodes in water, providing a point-like source of strong shock waves. When the discharge is in the focus of a semi-ellipsoidal metallic cavity, the wave energy is concentrated in the secondary focus. If the kidney stones is positioned in the secondary focus the interaction with the shock wave results in crushing the stone into small particles that naturally leave the body (Šunka et al. 2004). The success of this method stimulated also the study of the focused shock waves applications in other branches of medecine (Coleman and Sounders, 1993).

3. PLANS

We are beginning our research work concerning plasma generation in water. Investigations will be undertaken from aspects of laboratory, technological and astrophysical plasmas, experimentally and theoretically. We have started to construct two devices with corona discharge, one reactor with wire cathodes out of water and plate anode submerged in water. A gas corona discharge is directly contacted with a treated water surface. The second one is a wetted-wall corona-discharge reactor. Our first task will be directed to investigations of plasma-water interactions and plasma induced water characteristics (disinfection and degradation of organic pollutants in water). We are

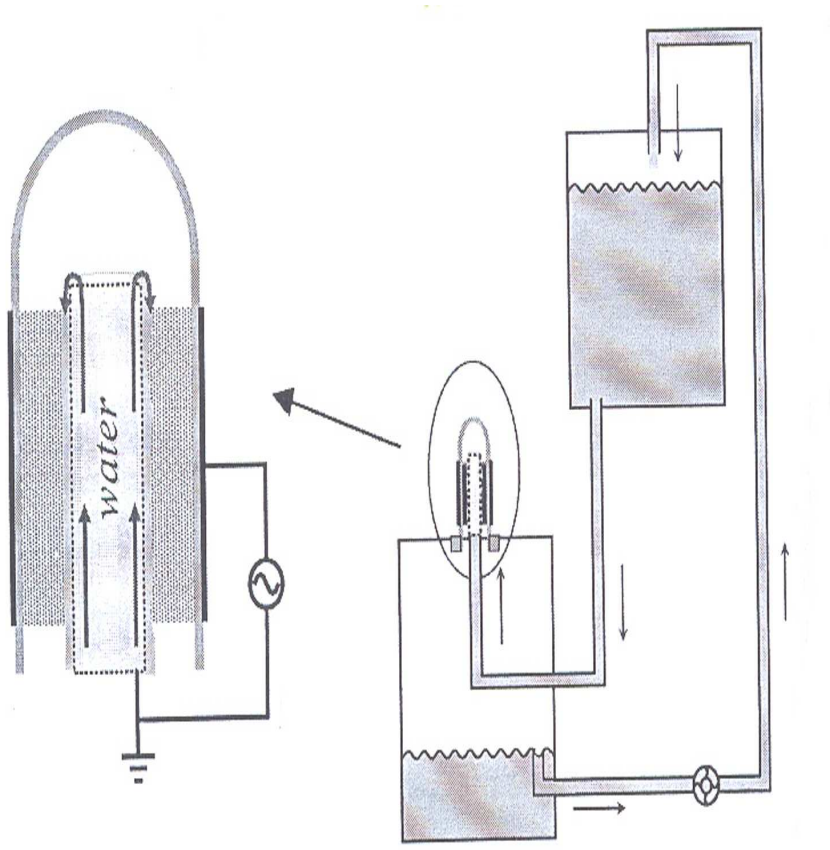

Figure 1: (From Kuraica et al, 2004a.) Schematic diagram of the ozonized water reaction system. Water flows up through a vertical hollow cylindrical electrode and flows down making thin dielectric film over the electrode. Filamentary discharge is generated in air within 4 mm gap between the dielectric and the water layer.

ready for collaboration with similar groups working in this domain in Bulgaria and Serbia.

References

Arif Malik, M., Ghaffar, A.: 2001, *Plasma Sources Science and Technology*, **10**, 82.
Beck, H., Wolfe, C., Gallimore, J., Thornley, M.:
Brand, J., Cesaroni, R., Comoretto, G., Felli, M., Palagi, F., Palla, F., Valdettaro, R.: 2003, *Astron. Astrophys.*, **407**, 573.
Burlion, M., Dancer, P., Lacoste, F.: 1994, *Rev. Sci. Instrum.*, **65**, 2356.
Coleman, A. J., Sounders, J.E.: 1993, *Ultrasonics*, **31**, 75.
Hoeben, W.F.L.M., van Veldhuizen, E.M., Rutgers, W.R., Koersen, G.M.W.: 1999, *J. Phys. D*, **32**, 133.
Joshi, A.A., Locke, B.R., Arce, P., Finney, W.C.: 1995, *J. Hazardous Materials*, **10**, 3.

Kuraica, M.M., Obradović, B.M., Manojlović, D., Ostojić, D.R., Purić, J.: 2004a, 22^{nd} Summer School and Int. Symp. Phys. Ioniz. Gases, ed. Lj. Hadžievski, Vinča Institute of Nuclear Sciences, Belgrade, 453.

Kuraica, M.M., Obradović, B.M., Manojlović, D., Ostojić, D.R., Purić, J.: 2004b, Proc. V Symp. of Belarus - Serbia and Montenegro on Physics and Diagnostics of Laboratory and Astrophysical Plasmas, eds. V. S. Burakov, A. F. Chernyavskii, Nat. Acad. Sci. Belarus, Inst. Mol. At. Physics, Minsk, 6.

Ryde, N., Lambert, D.L., Richter, M.J., Lacy, J.H.: 2002, *Astrophys. J.*, **580**, 447.

Sano, N., Yamamoto, D., Kanki, T.: 2003, *Ind. Eng. Chem. Res.*, **42**, 5423.

Sun, B., Sato, M., Clements, J.S.: 1997, *J. Electrost.*, **39**, 189.

Sun, B., Sato, M., Clements, J.S.: 1999, *J. Phys. D*, **32**, 1908.

Šunka, P., Babický, V., Člupek, M., Lukeš, P., Šimek, M., Schmidt, J., Černák, M.: 1999, *Plasma Sources Sci. Technol.*, **8**, 258.

Šunka, P., Babický, V., Člupek, M., Fuciman, M., Lukeš, P., Šimek, Beneš, J., Locke, B., Majcherová, Z.: 2004, *Acta Physica Slovaca*, **54**, 135.

Venugoplan, V., Guerra, A., Nahen, K., Vogel, A.: 2002, *Phys. Rev. Lett.*, **88**, 078103.

**Proc. IV Serbian-Bulgarian Astronomical Conference,
Belgrade 21–24 April 2004,
eds. M. S. Dimitrijević, V. Golev, L. Č. Popović, M. Tsvetkov,
Publ. Astron. Soc. "Rudjer Bošković" No 5, 2005, 263 - 265** *Contributed paper*

TEMPORAL VARIABILITY OF THE GRB LIGHT CURVE

S. SIMIĆ[1], L. Č. POPOVIĆ[2] and M. I. ANDERSEN[3]

[1] *Faculty of Science, University of Kragujevac,
Radoja Domanovića 12, 34000 Kragujevac, Serbia
E–mail ssimic@kg.ac.yu*

[2] *Astronomical Observatory, Volgina 7, 11160 Belgrade 74, Serbia
E–mail lpopovic@aob.aob.bg.ac.yu*

[3] *Astrophysikalisches Institut Potsdam,
An der Sternwarte 16, 14482 Potsdam, Germany*

Abstract. The variability of Gamma Ray Bursts (GRBs) light curves at the beginning of GRB event can bring us information about the nature of the hidden 'inner engines'. Here, we will present a numerical model which can synthesize light curves in the first phase of GRB. At the beginning we assume that an 'inner engine' creates a large number of small mass shock waves which are expanding isotropically and after short period of time (a couple of seconds) disappearing in the surrounding media. This process causes creation of a massive shock wave which interacts with surrounding media and produces the GRB afterglow. The peaks in the light curve arise in the moment of mutual shocks interaction. We have modeled light curves from a given dynamics, by assuming synchrotron radiation mechanism.

1. MODEL

In order to explain a temporal variability of the light curve we propose the following scenario. In the first phase of explosion, central engine creates a large number of small mass highly collimated shocks which are expanding isotropically. These shocks have high Lorentz factors with different magnitudes, so the faster shocks can catch the slower ones - this is known as the internal model (Kobayashi, Piran and Sari, 1997; Fenimore and Ramirez-Ruiz, 1999; Piran, 2000). When interaction happens a number of radiating particles for faster shock sharply increases, as well as the velocity of particles, creating a pulse in the GRB light curve. Duration of the pulse depends on the width of the shocks and on its Lorentz factor, with typical values of several tens of milliseconds. Since the masses of shocks are relatively low (few orders lower than mass of the afterglow shock), they have short live times and suddenly disappear in surrounding media. But the central engine makes them repeatedly in the initial phase. They accelerate particles of the inter-stellar medium (hereafter ISM) around the GRB center, and together create one bigger, more massive shock, which continues to spread. Then starts the second phase of GRB, with creation of the afterglow.

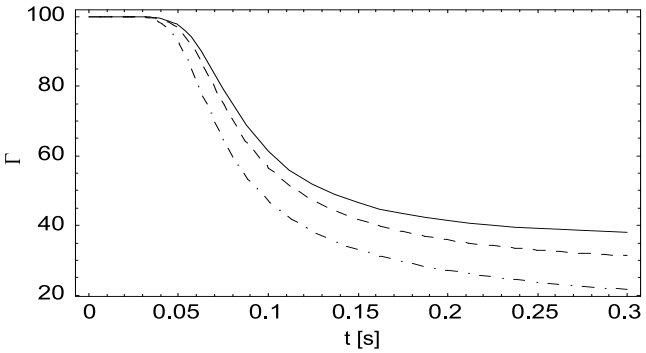

Figure 1: Evolution of Lorentz factor for a time of collision.

If the shock wave on his way, encounter another, the slower one, this event will increase the number of radiating particles. Mathematically, we may represent this density disturbance with a Gaussian function, where the width on the half maximum b represents the width of the slower shock, and intensity of the Gaussian a represents the slower shock number density. The equation we used have a following form:

$$n = n_0 \left(\frac{R_0}{R}\right)^s (4\Gamma + 3) \left(1 + a \cdot \exp\left[-\left(\frac{R - R_c}{b}\right)^2\right]\right) \tag{1}$$

where R_c and R_0 are the distance to the place of shock wave creation and the shock wave interaction, respectively. The n_0 is the density of the ISM (interstellar medium), and Γ is the Lorentz factor of the shock wave. The width of shock wave is given by Blandford and McKee (1976) and it is mainly in a range from $10^{12} - 10^{13}$ cm, depend on the relative velocity of the shock waves. This range may be broadened to higher values to include effect of grouping (superposition) of shock waves, then the maximal width of such composed shock is $\sim 10^{14}$ cm. Let us briefly describe the physical scenario of these processes. As we mentioned above, the number of small shocks is created by the central engine. They are colliding with each other and created pulses, but if some of shocks are not in collision, it will create a background radiation. If a collision is not enough intensive - low density shocks - pulses will be very small or will not be created at all. However, if collision include a broader and slower shocks with higher density, the produced pulse will be very intensive. This present main mechanism to explain high variability of the light curve.

That conformation of light curve is probably the result of specific distribution of ISM around the GRB center. It can be explained by the superposition of slower shock waves which have lost much of its energy, but stay in shock wave form. The presented model may simulate this situation with specific parameter values. In that case we were forced to change parameters a and b to acquire wider and low density barrier. Results of such analyze are not presented here in this paper and could be the subject of another research.

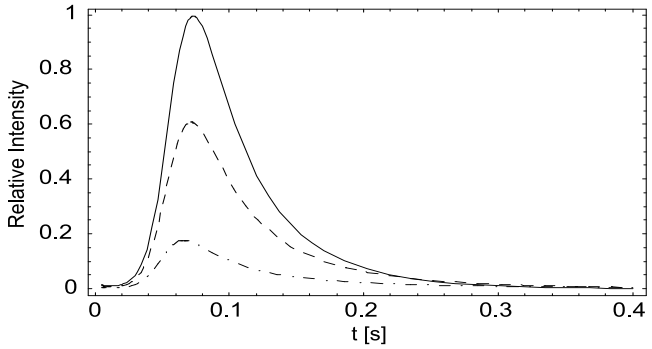

Figure 2: The shape of the typical GRB pulse given for three different values of ejected mass M_{ej}.

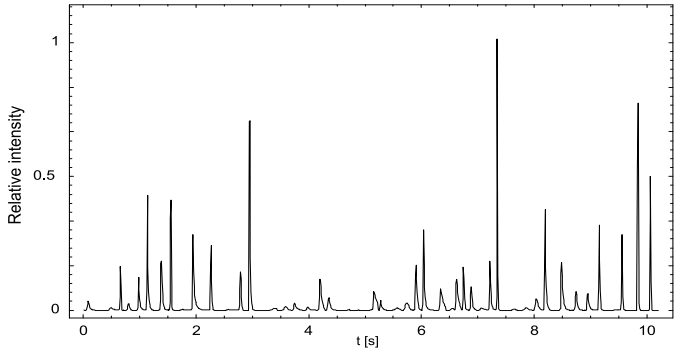

Figure 3: Synthesized temporal variability in the first 10 sec.

References

Blandford, R.D. and McKee, C.F.: 1976, *Physics of Fluids*, **19**, 1130.
Fenimore, E.E., Ramirez-Ruiz, E.: 1999, *Astron. Astrophys. Suppl. Series*, **138**, 521R.
Kobayashi, S., Piran, T., and Sari, R.: 1997, *Astrophys. J.*, **490**, 92.
Piran, T.: 2000, *Phys. Reports*, **333**, 529.

Proc. IV Serbian-Bulgarian Astronomical Conference,
Belgrade 21–24 April 2004,
eds. M. S. Dimitrijević, V. Golev, L. Č. Popović, M. Tsvetkov,
Publ. Astron. Soc. "Rudjer Bošković" No 5, 2005, 267 - 270 *Contributed paper*

ON THE STARK BROADENING OF F III SPECTRAL LINES

Z. SIMIĆ, M. S. DIMITRIJEVIĆ and L. Č. POPOVIĆ
Astronomical Observatory, Volgina 7, 11160 Belgrade 74, Serbia
E–mail zsimic@aob.aob.bg.ac.yu
E–mail mdimitrijevic@aob.aob.bg.ac.yu
E–mail lpopovic@aob.aob.bg.ac.yu

Abstract. We have modeled the F III atom and calculated Stark broadening parameters using two methods, semiclassical perturbation method for resonance transition and modified semiempirical method for additional ten multiplets.

1. INTRODUCTION

Importance of trace elements in stellar atmospheres increased with the development of space and satellite technology. Spectral lines of fluorine were observed in Solar (Moore et al., 1966), as well as in stellar spectra (Merrill, 1956). Also these spectral lines were founded in the ejecta of SN 1987A supernova (Trimble, 1991).

The first, qualitative, experimental investigation of the Stark broadening of F III spectral lines was made by Sarma (1961). Quantitative experimental data were obtained in 1988 by Purić et al. (1988). Since then, two additional experimental works on the F III Stark broadening have been published (Djeniže et al., 1991a; Blagojević, et al, 2000). The first quantitative theoretical determination was made by Dimitrijević and Konjević (1981), by using four different theoretical methods: the semiempirical method (Griem, 1968), the modified semiempirical method (Dimitrijević and Konjević, 1980), the simplified semiclassical method (Griem, 1974) and its modification (Dimitrijević and Konjević, 1981).

In order to provide new Stark broadening parameters for F III spectral lines, we adopted first of all a model of F III ion, with simplified energy level structure, facilitating and optimizing our further considerations. Using such a model, Stark broadening data for the resonance transition and additional 10 F III multiplets, have been determined. These multiplets belong to the 3s-3p, 3s-4p, 3p-4s and 4s-4p transition arrays (quartets).

2. RESULTS AND DISCUSSION

We applied full semiclassical perturbation method (Sahal-Bréchot, 1969ab) only to the astrophysically most important, resonance line, since for other lines there is no enough complete set of atomic data for such calculations. Consequently, for additional

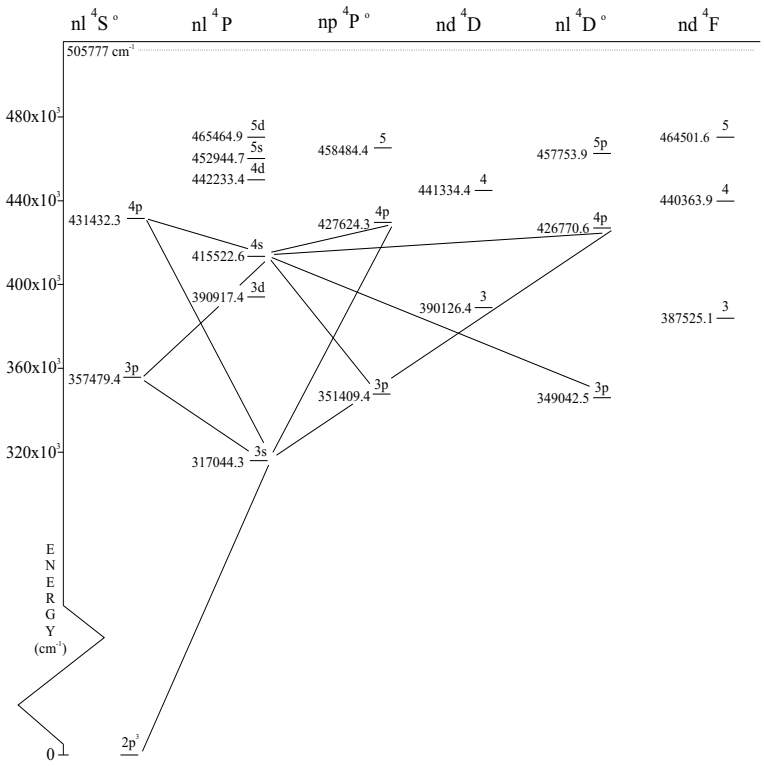

Figure 1: F III ion model adopted for Stark broadening parameters calculation. The resonance line $2p^3\ {}^4S^o$ - $3s\ {}^4P$ has been calculated by using this model within the semiclassicl approach (Sahal- Bréchot, 1969ab) and other lines within the modified semiempirical approach (Dimitrijević and Konjević, 1980). The ionization potential is presented by a dotted line at 505777 cm^{-1}.

Table 1: Stark broadening parameters for electron impact broadening for the resonance F III spectral line (Full width at half maximum and shift) determined within the semiclassical theory, for a perturber density of 10^{17} cm^{-3} and the temperature range from 10000 K up to 300000 K.

Transition	T(K)	W(0.1 nm)	d(0.1 nm)
$2p^3\ {}^4S^o$ - $3s\ {}^4P$ 31.54 nm	10000	0.123E-02	0.143E-03
	20000	0.771E-03	0.648E-04
	50000	0.465E-03	0.635E-04
	100000	0.341E-03	0.681E-04
	150000	0.291E-03	0.669E-04
	300000	0.230E-03	0.615E-04

Table 2: Stark widths (Full width at half maximum) for F III spectral lines obtained by using the modified semiempirical approach for a perturber density of 10^{17} cm^{-3} and the temperature range from 10000 K up to 300000 K.

Transition	T(K)	W(0.1 nm)	Transition	T(K)	W(0.1 nm)
	10000	0.886E-01		10000	0.348E-01
3s ^{4}P - 3p ^{4}S^o	20000	0.627E-01	3s ^{4}P - 4p ^{4}S^o	20000	0.246E-01
247.3 nm	50000	0.396E-01	87.4 nm	50000	0.178E-01
	100000	0.298E-01		100000	0.159E-01
	200000	0.253E-01		200000	0.148E-01
	300000	0.242E-01		300000	0.141E-01
	10000	0.399E-01		10000	0.343E-01
3s ^{4}P - 4p ^{4}P^o	20000	0.240E-01	3s ^{4}P - 3p ^{4}D^o	20000	0.242E-01
90.4 nm	50000	0.172E-01	91.1 nm	50000	0.147e-01
	100000	0.151E-01		100000	0.154E-01
	200000	0.139E-01		200000	0.142E-01
	300000	0.134E-01		300000	0.136E-01
	10000	0.113		10000	0.905E-01
4s ^{4}P - 3p ^{4}S^o	20000	0.795E-01	4s ^{4}P - 3p ^{4}P^o	20000	0.640E-01
172.3 nm	50000	0.576E-01	156.0 nm	50000	0.465E-01
	100000	0.507E-01		100000	0.409E-01
	200000	0.462E-01		200000	0.374E-01
	300000	0.438E-01		300000	0.354E-01
	10000	0.838E-01		10000	0.272E+01
4s ^{4}P - 3p ^{4}D^o	20000	0.593E-01	4s ^{4}P - 4p ^{4}S^o	20000	0.193E+01
150.4 nm	50000	0.431E-01	628.6 nm	50000	0.143E+01
	100000	0.380E-01		100000	0.131E+01
	200000	0.347E-01		200000	0.122E+01
	300000	0.329E-01		300000	0.116E+01
	10000	0.443E+01		10000	0.511E+01
4s ^{4}P - 4p ^{4}P^o	20000	0.313E+01	4s ^{4}P - 4p ^{4}D^o	20000	0.361E+01
826.3 nm	50000	0.232E+01	889.0 nm	50000	0.268E+01
	100000	0.209E+01		100000	0.243E+01
	200000	0.194E+01		200000	0.226E+01
	300000	0.186E+01		300000	0.215E+01

ten multiplets, the modified semiempirical method (Dimitrijević and Konjević, 1980) has been applied, and only Stark widths have been calculated.

Energy levels for F III transitions have been taken from Baskin and Stoner (1975). Oscillator strenghts have been calculated by using the method of Bates and Damgaard (1949) and the tables of Oertel and Shomo (1968). For higher levels, the method described by Van Regermorter et al. (1979) has been used.

Our calculations have been performed by using a model of F III atom, see Fig. 1.

In Tables 1. and 2. are shown Stark broadening parameters for F III spectral lines.

Acknowledgements

This work is a part of the project GA-1195 "Influence of collision processes on astrophysical plasma line shapes", supported by Ministry of Science and Environmental Protection of Serbia.

References

Bashkin, S., Stoner, J.O.: 1975, Atomic Energy Levels and Grotrian Diagrams, **I**, American Elsevier Publishing Company, Inc-New York.
Bates, D.R., Damgaard, A.: 1949, *Phyl. Trans. Roy. Soc.*, **A242**, 101.
Blagojević, B., Popović, M.V., Konjević, N.: 2000, *J. Quant. Spestrosc. Radiat. Transfer*, **67**, 9.
Dimitrijević, M.S., Konjević, N.: 1980, *J. Quant. Spestrosc. Radiat. Transfer*, **24**, 451.
Dimitrijević, M.S., Konjević, N.: 1981, in Spectral Line Shapes, Vol. **1**, ed. B. Wende, Walter de Gruyter & Co., New York, 211.
Djeniže, S., Labat, J., Srećković, A., Labat, O., Platiša, M., Purić, J.: 1991, *Physica Scripta*, **44**, 148.
Griem, H. R.: 1968, *Phys. Rev.*, **165**, 258.
Griem, H. R.: 1974, Spectral Line Broadening by Plasmas, Academic Press, New York.
Merrill, P.W.: 1956, Lines of the Chemical Elements in: Astronomical Spectra, Carnegie Inst. of Washington Publication, **610**, Washington D.C.
Moore, C.E., Minnaert, M.G.J., Houtgast, J.: 1966, The Solar Spectrum 2935Å to 8770Å, NBS Monographs, **61**, U.S. Department of Commerce, NBS, Washington D.C.
Oertel, G.K., Shomo, L.P.: 1968, *Astrophys. J. Suppl. Series*, **16**, 175.
Purić, J., Srećković, A., Djeniže, S., Platiša, M.: 1988, *Phys. Rev.*, A **37**, 4380.
Sahal-Bréchot, S.: 1969a, *Astron. Astrophys.*, **1**, 91.
Sahal-Bréchot, S.: 1969b, *Astron. Astrophys.*, **2**, 322.
Sarma, M.B.K.: 1961, *Proc. Phys. Soc.*, London, **77**, 665.
Trimble, V.: 1991, The Origin and Abudance of the Chemical Elements Revisited, *Astron. Astrophys. Review*, **3**, 1.
Van Regemorter, H., Hoang Binh Dy., Prud′homme, M.: 1979, *J. Phys.*, **B12**, 1053.

Proc. IV Serbian-Bulgarian Astronomical Conference,
Belgrade 21–24 April 2004,
eds. M. S. Dimitrijević, V. Golev, L. Č. Popović, M. Tsvetkov,
Publ. Astron. Soc. "Rudjer Bošković" No 5, 2005, 271 - 274 *Contributed paper*

ON THE STARK BROADENING OF Cd I LINES

Z. SIMIĆ[1], M. S. DIMITRIJEVIĆ[1] and S. SAHAL-BRÉCHOT[2]

[1] *Astronomical Observatory, Volgina 7, 11160 Belgrade 74, Serbia*
E–mail zsimic@aob.aob.bg.ac.yu
E–mail mdimitrijevic@aob.aob.bg.ac.yu

[2] *Observatoire de Paris-Meudon, 92190 Meudon, Cedex, France*
E–mail Sylvie.Sahal-Brechot@obspm.fr

Abstract. We have calculated within the semiclassical perturbation theory Stark broadening parameters (width and shift) for 13 Cd I multiplets in UV and V, and for 24 multiplets in infrared spectral ranges, for temperatures between 2500 K and 50000 K, of interest for stellar plasma investigations.

1. INTRODUCTION

Investigation of Stark broadening parameters of neutral cadmium spectral lines is of interest for a number of problems as e.g. for the determination of chemical composition and plasma diagnostic of stellar atmospheres, as well as for radiative transfer, plasma modelling and stellar spectra interpretation and synthesis. The electron-impact broadening mechanism is the main pressure broadening mechanism in hot star atmospheres, and it is of interest especially for A type stars and some white dwarfs, or pre dwarfs like PG-1195 type ones.

Stark broadening parameters of cadmium lines are also of interest for the consideration of regularities and systematic trends, which are useful for interpolation of new data and critical evaluation of existing ones.

The first experimental investigations of the influence of the Stark broadening mechanism on cadmium lines have been performed by Nagibina (1958), and by Gorodnichyute and Gorodnichyus (1961). In our case will be of interest experimental results obtained by Kusch and Oberschelp (1967).

Here, we have calculated within semiclassical approach, Stark broadening parameters of 13 Cd I multiplets in UV and V, and 24 multiplets in infrared spectral ranges, for temperatures between 2500 K and 50000 K.

2. RESULTS AND DISCUSSION

Stark broadening parameters (the full line width at half maximum and the line shift) of neutral cadmium have been determined by using the semiclassical perturba-

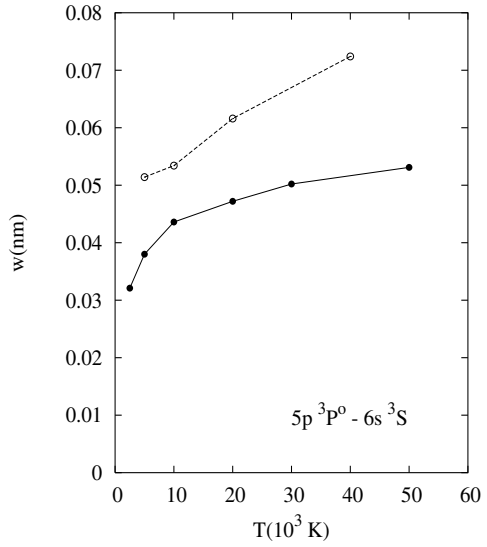

Figure 1: Stark widths due to electron impacts for Cd I 5p $^3P^o$ - 6s ^3S (494.13 nm) spectral multiplet as a function of temperature. Values of Dimitrijević and Konjević (1983) are presented by white points, and values of Simić, Dimitrijević and Sahal-Bréchot (present results) by black points.

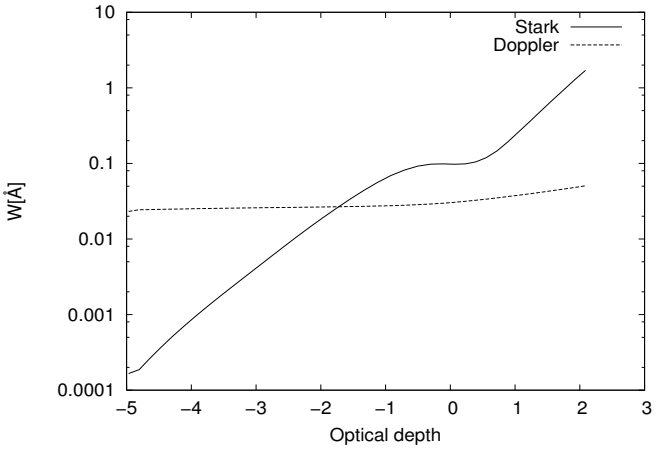

Figure 2: Stark and Doppler widths for Cd I 6s $^3S^o$ - 7p $^3P^o$ (740.09 nm) spectral line as a function of optical depth.

Table 1: Experimental (w_{KO} - Kusch and Oberschelp, 1967) and theoretical values of Stark widths (w_{DK} - Dimitrijević and Konjević, 1983; w_{SDS} - present work) for Cd I 5p $^3P^o$ - 6s ^3S spectral lines. The electron density is 10^{17} cm^{-3} and temperature 11100 K.

Wavelength (nm)	w_{KO}/w_{DK}	w_{KO}/w_{SDS}
508.58	6.34	6.41
479.99	6.63	7.53
467.82	3.00	3.59

tion formalism (Sahal-Bréchot, 1969ab). The discussion of updatings and validity criteria has been briefly reviewed e.g. in Dimitrijević (1996).

Energy levels for Cd I lines have been taken from Moore (1971). Oscillator strenghts have been calculated by using the method of Bates and Damgaard (1949). For higher levels, the method of Van Regermorter et al. (1979) has been used.

In Table 1, we present comparison between existing experimental results of Kusch and Oberschelp (1967), with theoretical results of Dimitrijević and Konjević (1983) and our results for Cd I 5p $^3P^o$ - 6s ^3S. With w_{KO} are denoted experimental full width at half maximum of Kusch and Oberschelp (1967), with w_{DK} - theoretical ones determined in Dimitrijević and Konjević (1983) by GBKO (Griem et al., 1962) theory, and with w_{SDS} - our results for the mentioned multiplet of Cd I. The first column represents wavelenghts for this multiplet of neutral cadmium in [nm] for perturber density of 10^{17} cm^{-3} and temperature 11100K.

Both theoretical results are in a disagreement with experimental ones, and self absorption is indicated as a possible reason in Konjević et al. (1984).

In Fig. 1 are shown both theoretical results for Cd I 5p $^3P^o$ - 6s ^3S (494.13 nm). In our calculations have been included symmetrization of perturber velocity before and after impact, in distinction from calculations of Dimitrijević and Konjević (1983), as well as a different treatement of elastic collisions and impact parameter cut-offs. In future new experimental results will be of help for a detailed analysis.

In order to see the influence of Stark broadening mechanism for neutral cadmium spectral lines in stellar plasma conditions, we have calculated the Stark widths for Cd I (740.09 nm) spectral line for a Kurucz's (1979) A type star atmosphere model with T_{eff}=10000 K and log g=4.0. From Fig. 2. one can see the existence of atmospheric layers where Stark width is dominant and that Stark broadening effect should be taken into account in abundance determination, spectra synthesis and modeling of stellar plasmas.

Acknowledgements

This work is a part of the project GA-1195 "Influence of collision processes on astrophysical plasma line shapes", supported by Ministry of Science and Environmental Protection of Serbia.

References

Bates, D.R., Damgaard, A.: 1949, *Phyl. Trans. Roy. Soc.*, **A242**, 101.
Dimitrijević, M.S.: 1996, *Zh. Prikl. Spektrosk.*, **63**, 810.
Dimitrijević, M.S., Konjević, N.: 1983, *J. Quant. Spectrosc. Radiat. Transfer*, **30**, 45.
Gorodnichyute, M.G., Gorodnichyus, G.A.: 1961, *Litov. Fiz. Sb.*, **1**, 163.
Griem, H.R., Baranger, M., Kolb, A.C., Oertel, G.K.: 1962, *Phys. Rev.*, **125**, 177.
Konjević, N., Dimitrijević, M.S., Wiese, W.L.: 1984, *J. Phys. Chem. Ref. Data*, **13**, 619.
Kurucz, R.L.: 1979, *Astrophys. J. Suppl. Series*, **40**, 1.
Kusch, H.J., Oberschelp, E.: 1967, *Z. Astrophys.*, **67**, 77.
Moore, C.E.: 1971, *Atomic Energy Levels*, Vol. III, NSRDS-NBS, **35**, 55.
Nagibina: 1958, *Opt. Spek.*, **4**, 430.
Sahal-Bréchot, S.: 1969a, *Astron. Astrophys.*, **1**, 91.
Sahal-Bréchot, S.: 1969b, *Astron. Astrophys.*, **2**, 322.
Van Regemorter, H., Hoang Binh D., Prud′homme, M.: 1979, *J. Phys.*, **B12**, 1053.

**Proc. IV Serbian-Bulgarian Astronomical Conference,
Belgrade 21–24 April 2004,
eds. M. S. Dimitrijević, V. Golev, L. Č. Popović, M. Tsvetkov,
Publ. Astron. Soc. "Rudjer Bošković" No 5, 2005, 275 - 279** *Contributed paper*

ON THE EXPERIMENTAL AND THEORETICAL INVESTIGATIONS OF F II STARK BROADENING

A. SREĆKOVIĆ[1], S. BUKVIĆ[1], S. DJENIŽE[1] and M. S. DIMITRIJEVIĆ[2]

[1] *Faculty of Physics, University of Belgrade,
Studentski trg 14, 11000 Belgrade, P.O.B. 368, Serbia
E–mail ebukvic@ff.bg.ac.yu.yu
E–mail steva@ff.bg.ac.yu*

[2] *Astronomical Observatory, Volgina 7, 11160 Belgrade 74, Serbia
E–mail mdimitrijevic@aob.bg.ac.yu*

Abstract. Stark widths (W) and shifts (d) of 5 singly ionized fluorine (F II) spectral lines within the $3s-3p, 3s'-3p'$ and $3d-4f$ transitions have been measured in a linear, low-pressure, pulsed arc discharge created in SF_6 plasma at $30400-33600$ K electron temperatures and at $(2.75-2.80)\times10^{23}$ m^{-3} electron densities. The widths and shifts have also been calculated using the semiclassical perturbation formalism (SCPF) (taking into account the impurity of energy levels, i.e. that the atomic energy levels are expressed as a mix of different configurations due to the configuration interaction). Calculations have been performed for temperatures between 5 000 K and 100 000 K for the for electrons, protons and helium ions as perturbers. Our measured and theoretical Stark parameters are compared with existing experimental and theoretical data. Tolerable agreement was found among them.

1. INTRODUCTION

In the last five years fluorine spectral lines have become important for abundance investigations in various astrophysical plasmas (Lodders, 2003; Zhu et al., 2002; Highberger et al., 2001). Only two experiments (Platiša et al., 1977 and Djeniže et al., 1991), deal with investigations of Stark broadening parameters (W, d) of singly ionized fluorine spectral lines.

The aim of this work is to present measured Stark FWHM (full-width at half intensity maximum, W) and shift (d) values at $(30400-33600)$ K electron temperatures and at $(2.75-2.80)\times10^{23}$ m^{-3} electron densities for 5 F II spectral lines belonging to the $3s-3p,\ 3s'-3p'$, and $3d-4f$ transitions, together with their calculated values using the semiclassical perturbation formalism (SCPF) updated several times (Sahal-Bréchot, 1969ab, see also a review in Dimitrijević, 1996). A unique exception is the transition $3p-3d$ from the F II spectrum (multiplet No. 3) for which only calculated values are presented. Our measured and calculated Stark parameters are compared with the existing experimental and theoretical data (Griem, 1974; Platiša et al., 1977; Djeniže et al., 1991) elsewhere (Srećković et al., 2004).

Table 1: Measured F II Stark FWHM (W_m in pm) and shift (d_m in pm) at a given T (in 10^4 K) and N (in 10^{23} m^{-3}). Transitions and wavelengths (λ in nm) are taken from NIST (2003). Negative shift is toward the blue.

Ion	Transition Multiplet	λ	T	N	W_m	d_m
FII	$2p^3 3s - 2p^3\ (^4S^o)3p$	385.167	3.36	2.80	64.8	-3.4
	$^5S - {}^5P$					
	(1)					
	$2p^3 3s' - 2p^3\ (^2D^o)3p'$	410.916	3.04	2.75	61.0	-1.8
	$^3D^o - {}^3D$		3.36	2.80	54.8	
	(5)					
	$^1D^o - {}^1F$	429.916	3.04	2.75	74.4	
	(7)		3.36	2.80	71.8	-0.6
	$^1D^o - {}^1D$	320.276	3.04	2.75	61.0	
	(8)		3.36	2.80	57.8	-5.0
	$2p^3 3d - 2p^3\ (^4S^o)4f$	424.666	3.04	2.75	381	-1.8
	$^5D^o - {}^5F$		3.36	2.80	355	4
	(9)					

2. EXPERIMENT

A linear pulsed arc has been used as plasma source. The working gas was SF_6 at 130 Pa filling pressure in a flowing regime (10 ml/min). The complete experimental procedure, plasma diagnostic techniques and set-up of the system used are described in Djeniže et al. (2002).

The measured profiles were of the Voigt type due to the convolutions of the Lorentzian Stark and Gaussian profiles caused by Doppler and instrumental broadening. For the electron density and temperature presented in our experiment, the Lorentzian fraction was dominant.

The standard deconvolution procedure has been applied using the least squares algorithm. The Stark widths were measured with $\pm 12\%$ error at a given N and T. Our measured Stark FWHM (W_m) values are presented in Table 1.

The Stark shifts were measured relative to the unshifted spectral lines emitted by the same plasma using a method established and applied first by Purić and Konjević (1972). Stark shift data are determined with ± 0.8 pm error at a given N and T. Measured (d_m) Stark shifts are presented in Table 1.

3. METHOD OF CALCULATION

The semiclassical perturbation formalism used here (Sahal-Bréchot, 1969a,b), has been briefly reviewed e.g. in Dimitrijević (1996).

Table 2: Calculated F II Stark FWHM (W in pm) and shift (d in pm) values for electrons (a), protons (b) and helium ions (c) as perturbers for various plasma temperatures (T in 10^3 K) and 10^{23} m^{-3} perturber density. $< \lambda >$ is the mean wavelength in the multiplet. The negative shift is toward the blue.

Transition Multiplet	$< \lambda >$ (nm)		T (10^3 K)											
			5		10		20		30		50		100	
			W	d	W	d	W	d	W	d	W	d	W	d
$3s\ ^5S - 3p\ ^5P$	385.01	a	38.5	-0.17	27.9	-0.34	20.4	-0.44	17.6	-0.43	15.3	-0.52	13.7	-0.46
(1)		b	0.64	-0.08	1.12	-0.16	1.58	-0.28	1.75	-0.34	1.92	-0.43	2.15	-0.52
		c	0.91	-0.08	1.14	-0.15	1.75	-0.24	1.89	-0.30	2.05	-0.36	2.22	-0.43
$3s'\ ^3D^o - 3p'\ ^3D$	411.48	a	44.7	0.08	32.3	-0.45	23.5	-0.62	20.2	-0.61	17.6	-0.74	15.7	-0.64
(5)		b	0.72	-0.11	1.27	-0.24	1.79	-0.39	1.99	-0.48	2.19	-0.60	2.45	-0.71
		c	1.02	-0.11	1.55	-0.22	1.98	-0.34	2.14	-0.42	2.32	-0.49	2.53	-0.59
$3s'\ ^3D^o - 3p'\ ^3P$	354.08	a	34.0	0.40	24.6	-0.07	18.0	-0.14	15.6	-0.13	13.7	-0.16	12.3	-0.16
(6)		b	0.64	-0.02	1.08	-0.05	1.51	-0.09	1.65	-0.12	1.81	-0.16	2.01	-0.20
		c	0.90	-0.02	1.33	-0.05	1.65	-0.08	1.78	-0.11	1.93	-0.14	2.08	-0.17
$3s'\ ^1D^o - 3p'\ ^1F$	430.54	a	49.5	-0.06	35.8	-0.56	26.3	-0.61	22.8	-0.66	20.2	-0.78	18.2	-0.73
(7)		b	0.87	-0.13	1.50	-0.26	2.10	-0.44	2.32	-0.53	2.55	-0.66	2.86	-0.79
		c	1.23	-0.12	1.84	-0.24	2.31	-0.38	2.50	-0.47	2.72	-0.54	2.94	-0.66
$3s'\ ^1D^o - 3p'\ ^1D$	320.65	a	29.8	0.62	21.6	0.43	16.1	0.25	14.1	0.35	12.7	0.40	11.7	0.32
(8)		b	0.70	0.08	1.14	0.17	1.55	0.27	1.68	0.33	1.84	0.41	2.04	0.49
		c	0.96	0.08	1.40	0.15	1.67	0.24	1.80	0.29	1.95	0.34	2.08	0.41
$3p\ ^5P - 3d\ ^5D^o$	350.54	a	41.4	0.96	30.9	1.00	23.4	0.96	20.6	1.07	18.4	1.14	16.8	1.01
(3)		b	1.50	0.22	2.26	0.42	2.84	0.64	3.07	0.76	3.34	0.88	3.63	1.06
		c	1.90	0.21	2.65	0.38	3.05	0.55	3.27	0.63	3.52	0.73	3.69	0.87
$3d\ ^5D^o - 4f\ ^5F$	424.70	a	990	-2.01	158	-3.88	129	-3.1	120	-2.75	110	-3.28	99.9	-3.02
(9)		b	11.5	-7.37	15.7	-10.7	19.6	-14.8	21.9	-16.5	24.8	-19.0	28.2	-21.5
		c	11.9	-5.98	15.0	-8.59	18.0	-12.2	19.4	-13.3	21.5	-15.4	23.3	-17.7

Atomic energy levels needed for the calculation have been taken from Bashkin and Stoner (1975). The calculations have been performed for electron temperatures between 5 000 K and 100 000 K.

Calculated W and d values are presented in Table 2.

4. RESULTS AND DISCUSSION

Our measured (W_m and d_m) and calculated (W and d) values at a given electron temperature (T) and density (N) are given in Tables 1 and 2, respectively. For each value given in Table 2, the collision volume multiplied by the perturber density is much less than one and the impact approximation is valid (Sahal-Bréchot, 1969a,b).

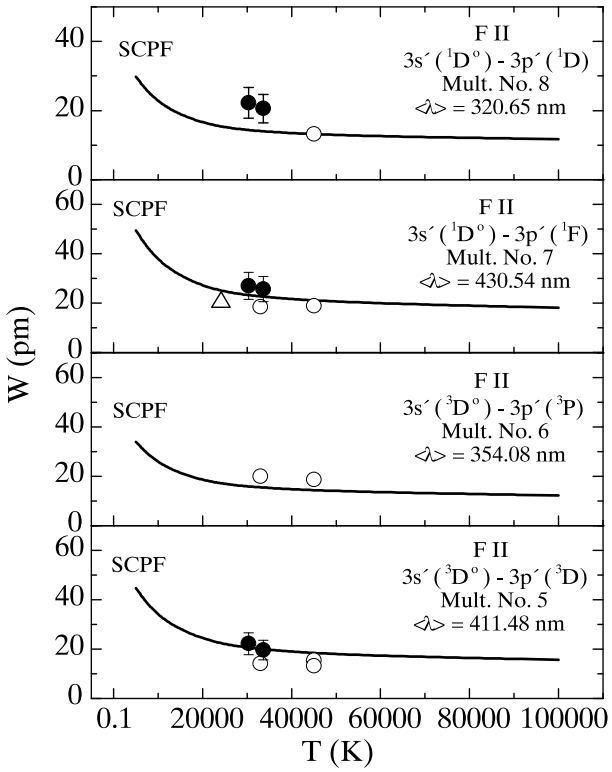

Figure 1: F II Stark widths (W in pm) as a function of the electron temperature (T) in the $3s - 3p$ transition at 10^{23} m^{-3} electron density. •, our experimental results, △, Platiša et al. (1977) and ∘, Djeniže et al., (1991). SCPF (full line) represents our calculations using the semiclassical perturbation formalism. Error bars include the uncertainties of the width and electron density measurements (±20%).

To compare the measured and calculated Stark FWHM values, we have presented in Figs. 3-8 an existing experimental data set including our results, together with our (SCPF) theoretical results and those from Griem (1974) (G).

The F II W values generated by protons and helium ions are up to 5-10 times smaller than the widths generated by electrons and show weak dependence on the temperature (see Table 2). The F II d values generated by electrons, protons and helium ions are very small, except for the multiplet No. 9, and are of the same magnitude.

Very good agreement has been found among our measured and calculated F II W and d values. Existing experimental W values (Djeniže et al., 1991; Platiša et al., 1977) also agree with our calculated values (see Fig. 1). Griem's (1974) W values lie below ours.

On the basis of the obtained W and d values we can conclude that a good agreement is found between our measured and calculated (SCPF) W values (within the

experimental accuracy and uncertainties of the calculations) in the case of the F II lines that belong to the $3s - 3p$, $3d - 4f$ and $3s' - 3p'$ transition.

We found that the Stark width generated by electrons is dominant and that the proton and helium ion contributions to the total Stark width can be neglected up to 150 000 K.

Our calculated Stark shift d values are generally very small (< 1 pm) with negative sign in the case of the F II lines belonging to the $3s - 3p$ and $3s' - 3p'$ transitions except for the muliplet No. 8 where the calculated d values have a positive sign. Small d values with positive sign are found for the $3p - 3d$ transition. In the case of the $3d - 4f$ transition the calculated d values are less than 4 pm with a negative sign.

We hope that the results presented in this paper, for Stark broadening parameters of the F II spectral lines, will be of interest for a number of problems in plasma physics and astrophysics.

Acknowledgements

This work is a part of the projects "Determination of the atomic parameters on the basis of the spectral line profiles" (OI 1228) and "Influence of collision processes on astrophysical plasma line shapes" (GA 1195) supported by the Ministry of Science and Environment Protection of the Republic of Serbia.

References

Bashkin, S., Stoner, Jr.J.J.: 1975, Atomic Energy Levels and Grotrian Diagrams, Vol. 1., North-Holland, Amsterdam.
Dimitrijević, M.S.: 1996, *Zh. Prikl. Spectrosk.*, **63**, 810.
Djeniže, S., Labat, J., Srećković, A., Labat, O., Platiša, M., Purić, J.: 1991, *Physica Scripta*, **44**, 148.
Djeniže, S., Srećković, A., Jelisavčić, M., Bukvić, S.: 2002, *Astron. Astrophys.*, **389**, 1086.
Griem, H.R.: 1974, Spectral Line Broadening by Plasmas, Academic Press, New York.
Highberger, J.L., Savage, C., Bieging, J.H. and Ziurys, L.M.: 2001, *Astrophys. J.*, **562**, 790.
NIST: 2003, Atomic Spectra Data Base Lines (Wavelengths ordered), `http://www.physics.nist.gov.`
Lodders, K.: 2003, *Astrophys. J.*, **591**, 1220.
Platiša, M., Dimitrijević, M.S., Popović, M.V., Konjević, N.: 1977, *Astron. Astrophys.*, **54**, 837.
Purić, J., Konjević, N.: 1972, *Z. Phys.*, **249**, 440.
Sahal-Bréchot, S.: 1969a, *Astron. Astrophys.*, **1**, 91.
Sahal-Bréchot, S.: 1969b, *Astron. Astrophys.*, **2**, 322.
Srećković, A., Bukvić, S., Djeniže, S., Dimitrijević, M.S.: 2004, *Astron. Astrophys.*, accepted.
Zhu, C., Krems, R., Dolgano, A. and Balakrishnan, N.: 2002, *Astrophys. J.*, **577**, 795.

Proc. IV Serbian-Bulgarian Astronomical Conference,
Belgrade 21–24 April 2004,
eds. M. S. Dimitrijević, V. Golev, L. Č. Popović, M. Tsvetkov,
Publ. Astron. Soc. "Rudjer Bošković" No 5, 2005, 281 - 288 *Contributed paper*

CALIBRATION OF DIAMETER-HI LINE WIDTH RELATION FOR EDGE-ON SPIRAL GALAXIES

O. I. STANCHEV[1], P. NEDIALKOV[2], Ts. GEORGIEV[1] and I. GEORGIEV[1]

[1] *Institute of Astronomy, Bulgarian Academy of Sciences,*
72 Tsarigradsko Shosse, 1784 Sofia, Bulgaria
E–mail stanchev@astro.bas.bg
E–mail tsgeorg@astro.bas.bg
E–mail iskren@astro.bas.bg

[2] *Department of Astronomy, University of Sofia,*
James Bourchier 5, Sofia 1164, Bulgaria
E–mail japet@phys.uni-sofia.bg

Abstract. Calibrated B and I-band diameter Tully-Fisher relations for edge-on spiral galaxies are derived from published data. In order to apply TF calibration for edge-on spiral galaxies, the diameters of the calibrators are corrected into edge-on view, before the TF constructions. Two versions of TF relations are compared showing the differences in the resulting ditance estimation from applying HI line width data and maximum rotational velocity data. The standart error (SE) of $(\log A_{edge-on} - \log W_{20})$ TF relation is 0.25 and 0.30 for B and I-band, respectively, corresponding to relative distance error of 12% and 14%, whereas the SE of the $(\log A_{edge-on} - \log V_{max})$ TF relation is 0.27 and 0.28 for both photometrical bands, respectively. This corresponds to larger relative distance error of 13% and 14% and means that the choise of the rotational parameters is important for the distance determination to the spiral galaxies. The diameter-HI line width TF relation appear to be better distance estimate than the diameter-rotation velocity TF relation.

1. INTRODUCTION

In recent years the analysis of the peculiar velocity field using redshift-independent galaxy distance indicators has significantly enhanced our underestanding of the formation and evolution of large scale structure. The most prevalent example of these indicators have been the Tully-Fisher (TF) relation. TF relation is one of the most popular extragalactic distance indicators. This is due to the large number, up of thousands of spiral galaxies, and wide distance range, $\rightarrow 100h^{-1}Mpc$, of the objects applicable for TF studies. The correlation between the absolute magnitude and the logarithm of the maximum rotational velocity of spiral galaxiy is known as TF relation after Tully and Fisher (1977).

Although, the most commonly used version of this relation is with the participation of the galaxy luminosity (or absolute magnitude) as dependent variable, there is other

version of the TF relation in which the dependent parameter is replaced by the galaxy linear size (absolute diameter). In these both cases the relation have the following analytical form:

$$M = a \log W_{20} + b$$

$$\log A = a \log W_{20} + b$$

Here a is the TF slope, b the zero point and $\log W_{20}$ is the logarithm of the rotational parameter - HI line width measured at the 20% level in km/s. It is a distance independent quantity, which often is replaced by the logarithm of the maximum rotational velocity of the galaxy $\log V_{max}$. Independence of distance means that $\log V_{max}$ or $\log W_{20}$ observations are not affected by any selection effects caused by limitations in detector sensitivity for distant, apparently dim objects. The other observables, the luminosity and linear diameter of a galaxy, suffer from such effects. This and the scatter of the derived distances around the true average, lead to systematic errors known as the Malmquist biases, which produce underestimation of the derived distance moduli.

But actually this is not the focus of this paper. Here we only present the B and I-band diameter TF relations with two rotational parameters for the spiral galaxies in the calibration sample published in Macri and Huchra (2000). The TF rlations are constructed with the edge-on magnitudes after applying internal extinction correction into edge-on view. Furthermore our aim is to find out how these both TF relations contribute to the final galaxy distance derivation.

The physical basis of the TF relation comes from the fact that both the rotational velocity and the luminosity (or linear diameter) are related to the mass of a galaxy when a constant mass to light ratio is assumed. This means that the mass plays an intermediary role between luminosity and rotation velocity. Keeping in mind the galaxy luminosity-size relation, this is true for the two variations of the TF relation – with magnitudes and the diameters, respectively.

The mean shape of the mass-luminosity and mass-rotation velocity relations, determine the slope of the observed TF relation, while the scatter of each of the two relations contributes to the dispersion in the luminosity at a fixed maximum rotation velocity (see Rhee and van Albada, 1996; see also Djorgovski, de Carvalho and Han, 1988).

$$V_{rot}^2 = \frac{G m_{gal}(R)}{R} \propto L(R)$$

where $V_{rot}(R)$ is the rotational velocity at R, $m_{gal}(R)$ is the mass, and $L(R)$ the integrated luminosity inside radius R from the center of a galaxy.

2. CALIBRATION OF THE DIAMETER TULLY-FISHER RELATION

The main task of the calibration is the determination of accurate distances to relatively close spiral galaxies of suitable type and inclination. Among all extragalactic

distance indicators currently only Cepheid-based distances are considered accurate enough (error less than 10%) and obtainable for a reasonable large sample of galaxies.

There is several important problems concerned with the calibration of the TF relation. Some of these problem are disscused here very shortly.

For the proper calibration of the TF relation we need a calibration sample containing spirals galaxies in all morphological types and accurate derived Cepheid distances. To have accurate distance determination to the target galaxies, the precise derivation of the Cepheid distances to the calibrator galaxies is important. The completeness of the calibrator sample is other crucial point concerned with the application of the calibration technique. The absence of galaxies from some morphological type in the calibration sample would be crucial for the distance derivation if the target sample is more complete in morphological types. This mean the calibrator sample must be representative for the whole target sample, otherwise there would arise selection bias. But the situation is more complex when we concern our attention to the problems about the Cepheid Period-Luminosity (PL) relation which is the basis for the derived calibrator distances. There are some problems about the Cepheid PL relation (see Allen and Shanks, 2004). The first one is the bias due to incompleteness in the PL relation at faint magnitudes. Usually the effect of the magnitude limited bias tends to make the slope of the PL relation shallower.

Other problem is the effect of the metallicity on the Cepheid PL relation. The dependence of the metallicity with the rms dispersion of this relation is discussed in details in Allen and Shanks, (2004).

There is increasing evidence that Cepheid distances require significant corrections for the effects of metallicity and incompleteness bias with important potential consequences for the distance scale, Hubble constant and cosmology. The better uderstanding on these effects is of importance for the accurate distance determination to the spiral galaxies calibrated on the Cepheid-based distances.

2.1. DIAMETER TRANSFORMATION INTO EDGE-ON VIEW

In order to calibrate the TF relation for distant sample of edge-on spiral galaxies, it is important to have homogeneity in the derived inclination dependent parameters for both calibration and target samples. Before the construction of the TF relations with both rotational parameter ($\log W_{20}$ or $\log V_{rot}$) we make correction of each calibrator diameter into edge-on view.

Let consider the following dependence between the galaxy diameter and galaxy axial ratio:

$$\log\left(\frac{A_o}{A}\right) = c_A \log\left(\frac{a}{b}\right) \tag{1}$$

Here A_o is the inclination corrected galaxy linear diameter in kpc, A - the linear diameter of a galaxy at arbitrary inclination angle, c_A - coefficient accounting for the diameter-inclination dependence, and (a/b) is the apparent axial ratio of the galaxy. From now on if we denote the inclination corrected diameters at 0° and 90° to the line of sight as "edge-on" and "face-on", respectively, then the linear size of each galaxy may be corrected in edge-on view in the following way:

$$\log A_{face-on} = \log A + c_A \log\left(\frac{a}{b}\right) \tag{2}$$

$$\log A_{edge-on} = \log A_{face-on} - c_A \log\left(\frac{1}{q_0}\right) \tag{3}$$

Here q_0 is the galaxy intrinsic axial ratio. This parameter is morphologically dependent and in this work we use the following values: q_0=0.13 for the late type spirals and q_0=0.20 for the early type galaxies (Sakai et al., 2000; Tully et al., 2000; Kannappan et al., 2002; Courteau, 1997). When the galaxy is corrected into edge-on view it is expected to increase its linear diameter, because of accumulation of more ligtht in the plan of the galaxy and the sharpening of the peripheral surface brightness gradients.

Finally for the galaxy edge-on linear diameter we obtain:

$$\log A_{edge-on} = \log A + c_A \log\left(\frac{a}{b}\, q_0\right) \tag{4}$$

We use this equation for the calculation of the edge-on diameters of the calibrator galaxies. The values for the coefficient $c_A = -0.21$ was taken from Nedialkov (1994) and the galaxy axial ratio (a/b) was determined using the Holmberg equation:

$$\cos^2 i = \frac{(b/a)^2 - q_0^2}{1 - q_0^2} \;\Rightarrow\; \left(\frac{a}{b}\right) = \frac{1}{\sqrt{\cos^2 i(1 - q_0^2) + q_0^2}}$$

Thus derived edge-on linear diameters we use for the B and I-band TF relations with the galaxies from the calibration sample. The calculated edge-on diameters as well as te used rotational parameters for the TF relations are shown in Table 1.

2.2. THE DIAMETER TF RELATION

The homogeneous data for 21 nearby spiral galaxies with accurate determined distances, collected in the paper of Macri and Huchra (2000), are used. The distances are based on observations of Cepheid variable stars. Most of the observations were made with the *Hubble Space Telescope* (Freedman et al., 1997; Sandage et al., 1996). The morphological types of the galaxies are Sb – Sd. With respect to the HI line-width, the linear diameter and inclination angles, the calibrator galaxies cover the following ranges:

- $238 < W < 553$ km/s
- $1.11 < \log A_{edge-on} < 1.89$ kpc
- $42 < i < 78$ deg

The data about the angular diameters at 25 mag/arcsec^2 surface brightness level in B-band are taken from LEDA, whereas the data in I-band are taken from Macri and Huchra (2000).

After applying extinction correction in our Galaxy and internal extinction correction into edge-on view, the linear diameters of the calibrators were obtained as:

Table 1: Calculated B and I-band edge-on diameters of the calibrator sample. The data about B-band diameters are taken from LEDA and they are within the isophote of 25 mag.arcsec^2 surface brightness level. The I- band diameters are taken from Macri and Huchra (2000). They are within the isophote of 23.5 mag.arcsec^2 surface brightness level.

Name	$\log A_{25}$ [kpc]	$\log A_{23.5}$ [kpc]	$\log W_{20}$ [km/s]	$\log V_{rot}$ [km/s]
NGC0925	1.55	1.46	2.420	2.058
NGC1365	1.91	1.79	2.682	2.356
NGC1425	1.67	1.63	2.621	2.251
NGC2090	1.54	1.45	2.501	2.187
NGC2541	1.40	1.31	2.370	1.988
NGC3198	1.56	1.49	2.531	2.183
NGC3319	1.49	1.39	2.405	2.031
NGC3351	1.43	1.44	2.586	2.168
NGC3368	1.53	1.50	2.674	2.321
NGC3621	1.41	1.34	2.499	2.167
NGC3627	1.55	1.54	2.626	2.266
NGC4414	1.57	1.51	2.743	2.342
NGC4535	1.69	1.65	2.586	2.311
NGC4536	1.64	1.60	2.562	2.207
NGC4548	1.56	1.54	2.617	2.291
NGC4725	1.71	1.26	2.671	2.382
NGC7331	1.72	1.16	2.746	2.409
NGC4603	1.76	1.73	2.575	2.367
NGC4639	1.40	1.35	2.519	2.256
NGC4651	1.63	1.68	2.584	2.358
NGC4654	1.51	1.44	2.487	2.201

$$A = \frac{a_o}{206265} 10^{\,[0.2(m-M)-10]} \tag{5}$$

where the last term is the distance expressed in kpc. Data for the used distance modulus are taken from Tully and Pierce, (2000).

The HI line width data are corrected for inclination and turbulence and taken from Tully and Pierce (2000). V_{rot} data are taken from LEDA (*Lyon-Meudon Extragalactic Database*).

Further we compare both TF relations depending on the rotational parameter used - $\log W_{20}$ and $\log V_{rot}$. This relations are shown in Fig. 1 and Fig. 2.

It is expected that the TF relation with $\log W_{20}$ must be more accurate than that with the participation of $\log V_{rot}$ parameter. This is due to the fact that the first parameter represents the rotation of the galactic disk as a whole. The HI line width come from the broadening of the 21 cm radio emission line in neutral hydrogen, due to the motions of atomic hydrogen to the observer's line of sight. The other rotational

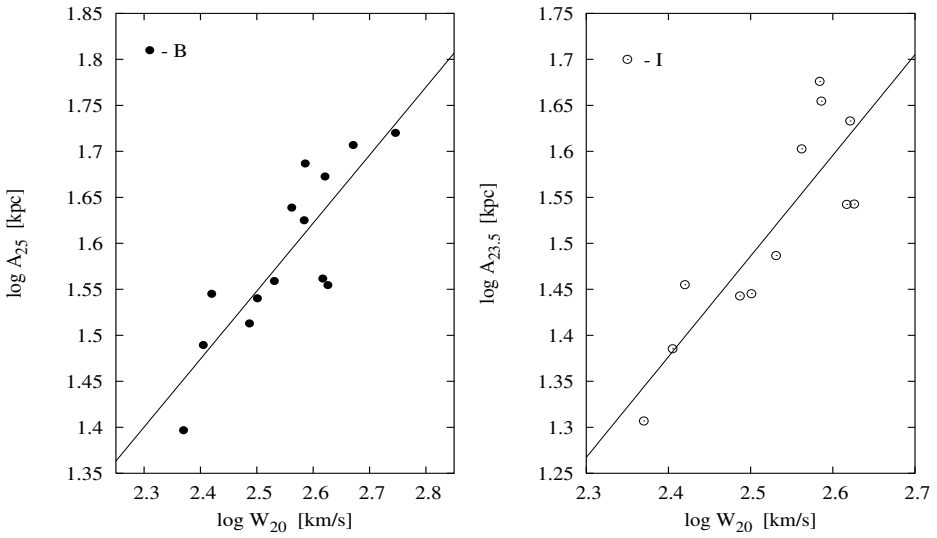

Figure 1: Diameter TF relation for the calibration sample. Both graphs present diameter TF relation with the logarithm of HI-line width $\log W_{20}$. The left panel shows B-band TF relation for 14 galaxies from the calibration sample. The right panel shows the I-band TF relation with 12 galaxies. The linear fits are made using standard least square technique.

parameter – maximum rotational velocity is parameter in some sense fixed at given distance from the center of the galaxy. Its value depends on the specific shape of the galaxy rotation curve. In general this produce some scatter on the TF relation because of the "intrinsic" properties of the galaxies.

In Fig. 1 is shown the diameter TF relation for the calibration sample with the HI line width rotational parameter. The data for B-band diameters are taken from LEDA, whereas these about I-band are taken from Macri and Huchra (2000). The diameters participating in the forthcoming TF relation in B and I-bands are corrected for Galactic extinction and recalculated into edge-on view through equation (4). The TF relation in B-band is constructed for 14 galaxies from 21 calibrators in the sample. The galaxies NGC 1365, NGC 3351, NGC 3368, NGC 3621, NGC 4414, NGC 4603 and NGC 4639 do not participate in the relation and they are excluded as outliers. Three of the above listed galaxies – NGC 3351, NGC 3368 and NGC 4639 are classified as galaxies with ring and all galaxies, with exception of NGC 4414, are barred. The relation in I-band is with the participation of 12 calibrators. In addition two calibrators are excluded as outliers - NGC 4725 and NGC 7331. The first calibrator is barred galaxy with ring and the second is classified just as Sb galaxy. The SE of the both B and I-band TF relations are $\sigma_\mu \sim 5\sigma_{\log A}$, which makes 0.25 mag. and 0.30 mag., respectively. That corresponds to relative distance error of 12% and 14%.

Fig. 2 presents B and I-band TF relation with maximum rotational velocity parameter. To make comparison the same galaxies are used in both TF relation as these

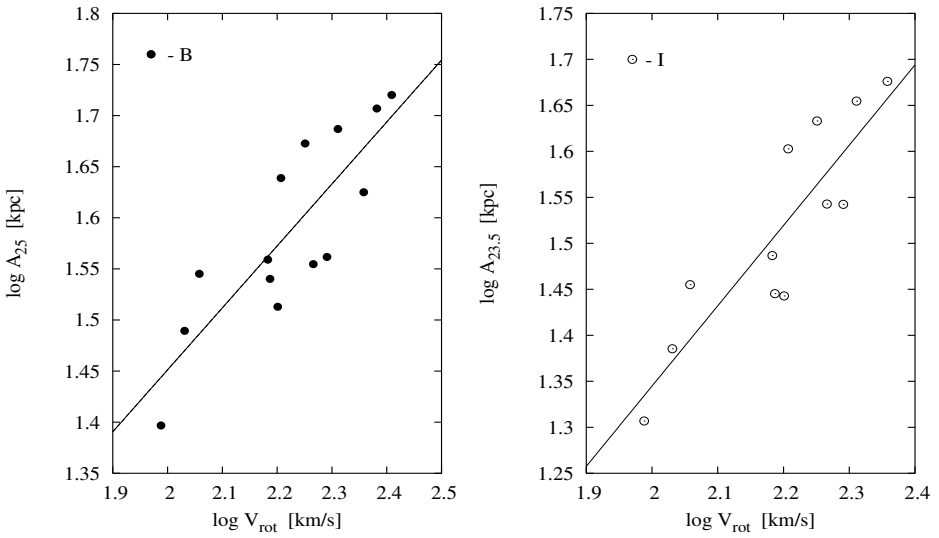

Figure 2: B and I-band diameter TF relations for the calibration sample with $\log V_{rot}$ rotation parameter. The notations are similar to these in Fig. 1.

in Fig. 1. Here the SE from the linear least square fits is 0.27 mag. and 0.28 mag. for B and I-band, respectively. With respect to the $\log A_{edge-on} - \log W_{20}$ relations this corresponds to larger relative distance error of 13% and 14%.

The diameter TF relations presented above show that as for the case with the magnitude TF relation here using the diameters, $\log W_{20}$ rotational parameter produces more accurate distance estimation in comparison with $\log V_{rot}$ parameter. Apparently the better distance determination could be produced when the HI line width is used as independent variable in TF relation.

3. CONCLUSIONS

In this paper we present calibration TF relation for diameters of the spiral galaxies. That is why we have used B and I-band data taken from LEDA and Macri and Huchra (2000). We recalculate the galaxy diameters into edge-on view in order to be used for calibration of the TF relation for target samples with highly inclined galaxies. TF relations are constructed with the participation of two rotational parameters: HI line width ($\log W_{20}$) and maximum rotational velocity ($\log V_{rot}$). The comparison between the relations with these both parameters shows that using $\log W_{20}$ parameter more accurate distance estimation can be reproduced. We obtain 12% and 14% relative distance error for B and I-band ($\log A_{edge-on} - \log W_{20}$) TF relation and 13% and 14% for ($\log A_{edge-on} - \log V_{max}$) relation. This mean that the first version of the diameter TF relation is better distance estimator and can be used for distance determination to edge-on spiral galaxies.

References

Allen, P.D. and Shanks, T.: 2004 *Mon. Not. R. Astron. Soc.*, **347**, 1011.
Courteau, S.: 1997, *Astron. J.*, **114**, 2402.
Djorgovski, S., de Carvalho, N. and Han, M.-S.: 1988, The Extragalactic Distance Scale, eds. S. van den Bergh and C. J. Pritchet, Astronomical Society of Pacific, Provo, 329.
Freedman, W.L., Mould, J.R., Kennicutt, R.C. and Madore, B.F.: 1997, Cosmological Parameters and the Evolution of the Universe, IAU Symp. **183**, 17.
Kannappan, S.J., Fabricant, D.G. and Franx, M.: 2002, *Astron. J.*, **123**, 2358.
Macri, L.M., Huchra, J.P.: 2000, *Astrophys. J. Suppl. Series*, **128**, 461.
Rhee, M.-H., van Albada, T.S.: 1996, A physical basis of the Tully-Fisher relation, PhD Thesis, Rijsk University Groningen.
Sakai, S., Mould, J.R. et al.: 2000, *Astrophys. J.*, **529**, 698.
Sandage, A., Saha, A., Tammann, G.A., Labhardt, L., Panagia, N. and Machetto, F.D.: 1996, *Astrophys. J.*, **460**, L15.
Tully, R.B., Fisher, J.R.: 1977, *Astron. Astrophys.*, **54**, 661.
Tully, R.B. and Pierce, J.M.: 2000, *Astron. Astrophys.*, **533**, 744.

Proc. IV Serbian-Bulgarian Astronomical Conference,
Belgrade 21–24 April 2004,
eds. M. S. Dimitrijević, V. Golev, L. Č. Popović, M. Tsvetkov,
Publ. Astron. Soc. "Rudjer Bošković" No 5, 2005, 289 - 294 *Contributed paper*

BARICENTRIC MOTION OF THE SUN

A. S. TOMIĆ[1] and Dj. KORUGA[2]
[1] *People's observatory, Kalemegdan, 11000 Belgrade, Serbia*
[2] *Faculty of Mechanical engineering, 27. marta 80, 11000 Belgrade, Serbia*
E–mail atomic@aob.bg.ac.yu

Abstract. The baricentric motion of the Sun is calculated for 51 years (1939-1990.). Obtained path presents spiraloid curve which a half of period opens, second part closes, with mean period of 11,86 years. This motion of the Sun can not be neglected in nano-gravity scale of influence, because its amplitude is up to 2,175 solar radius, and velocity 9 to 16 m/s. Authors propose name for the curve of baricenter orbit: pulsating spiral of Kepler.

1. INTRODUCTION

Solar system, in the first approximation can be treated as a system consisting of the Sun and big planets, with mass of the Sun 744 times bigger than the sum of planetary masses. Considering from the point of view of mass ratio it is usually to say that planetary orbits are ellipses with the Sun in one of the focal points (1st Kepler's law). 3rd Kepler's law has, for motion in two bodies system, the form containing mass of both bodies:

$$G(m_1 + m_2) = a^3\omega^2 \tag{1}$$

G – gravity constants, $\omega = 2\pi/T$ – angular velocity, a – big half-axis of the orbit, T – period. Planetary masses often were neglected even as the sum, because of big difference between planetary and solar mass: for biggest planet - Jupiter 1/1047, for smallest - Pluton, only 1/ 3 000 000. But, in solving of the problem of three bodies appears the third mass too (e. g. Vernic, 1953), what implies that for the description of the motion for all nine planets around the Sun must be included mass of each of nine planets. In other words, mass of the Sun and big planets must be taken, as equal to:

$$M = M_S(1 + \frac{1}{744}) = 1,001344 \cdot M_S \tag{2}$$

In this case it is useful to calculate the baricentric distance of Solar system to the Sun, what was made in the calculation of planetary efemerides (e. g. Grin, 1998). For our research of the celestial nano-gravity phenomena on the Earth's surface was important just the determination of the orbit and period of the Sun refered to the baricenter.

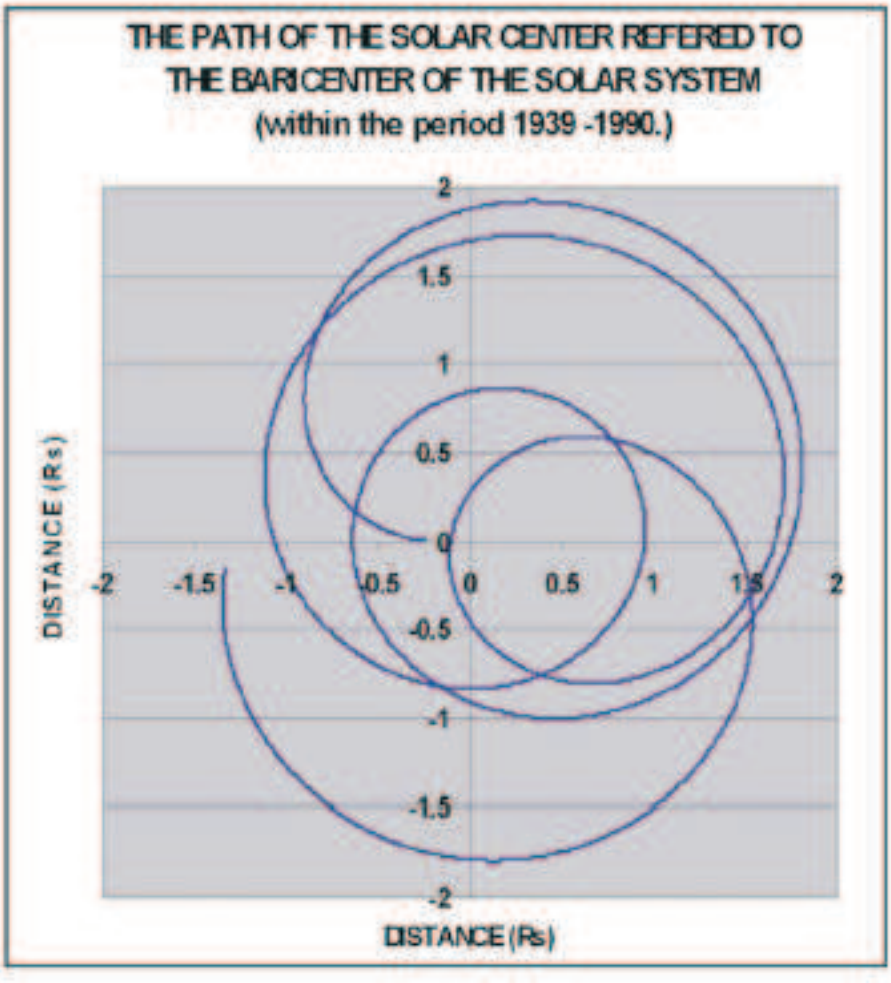

Figure 1: Motion of the baricenter of the Solar system between years 1939 - 1990. Starting position is on the left.

2. DETERMINATION OF SOLAR BARICENTRIC DISTANCE

Within a system of two bodies the baricentric position is determined by a classical formula:

$$r_B = (m_1 \cdot r_1 + m_2 \cdot r_2)/(m_1 + m_2) \tag{3}$$

where: m_1, m_2 – are masses, r_1, r_2 – are Solar and planetary distances in an arbitrary coordinate frame. For example, if the beginning of the frame is in the Solar center, and the second body is Jupiter, the formula gives the baricentric distance with the Solar radius as the unit (R_S):

$$r_B = [0 \cdot 1 + 5,2 \cdot 215 \cdot (1/1047,58)]/[1 + (1/1047,58)] = 1,066 \cdot R_S \qquad (4)$$

what refered to the mean Jupiter distance to the Sun, of 1118 R_S, can be neglected for many purposes. But, it can not be told a priori that it could be neglected in all cases. From heliocentric planetary motion we have calculated the position of the baricenter, as:

$$x_B = [\sum_{i=1}^{9} a_i \frac{m_i}{M} \cos(\omega_i \cdot t + \lambda_i)]/[1 + \sum_{i=1}^{9} \frac{m_i}{M}] \qquad (5)$$

$$y_B = [\sum_{i=1}^{9} a_i \frac{m_i}{M} \sin(\omega_i \cdot t + \lambda_i)]/[1 + \sum_{i=1}^{9} \frac{m_i}{M}] \qquad (6)$$

a_i, ω_i – big half-axis of the orbit, and angular velocity of each planet, λ_i – planetary longitude to the point in the beginning of the calculation, m_i, M – planetary masses and the mass of the Sun and planets. We calculated the path for 2000 days with the step of one day, begining with the year 1939, and we continued the obtained path up to 51 years. With the biggest - influence of Jupiter, and smal planetary orbits eccentricities, one obtains circular orbits as satisfactory. Unexpectedly nice picture is obtained. (Fig.1) Spatial motion of baricenter is often rectilinear, or negligible. Three resultantes of gravity forces of two bodies on the third, in system of three body, give cross-section into the same point - center of the attraction.

By the congruence the center of attraction with the baricenter resulting path is an ellipse (Milankovic, 1935). Here we present solar motion related to the baricenter, with a spiraloid orbit, which formula in polar coordinates is:

$$r^2 = \frac{\sum A_i^2}{A} + \frac{\sum A_i A_j \cos[(\omega_i - \omega_j) \cdot t + (\lambda_i - \lambda_j)]}{A} \qquad (7)$$

$$A = 1 + \sum \frac{m_i}{M}, \quad A_i = \frac{a_i \cdot m_i}{M}, \quad A_j = \frac{a_j \cdot m_j}{M}, \quad i, j = 1, 2, \ldots (9), \ldots \qquad (8)$$

what gives the amplitude of distance: $r_{MAX} = 2,175 \cdot R_S$. The corresponding velocity is variable, (9 – 16) m/s (Fig. 2). Our search just for the velocity appearing in gravity potential waves of Lunar tidal influence at the Earth's surface (Koruga et al., 2003) was argument for the calculation of baricentric motion, since other motion between Sun, Earth and Moon gives not an explanation of this velocity.

We examined variation of the "period" of solar baricentric motion, which can be determined on the few manner. The period we use here is the temporal interval between two successive approaches to the extreme distance. Mean value of that period is approximately equal to the Jupiter's revolution or to the period of the Solar activity.

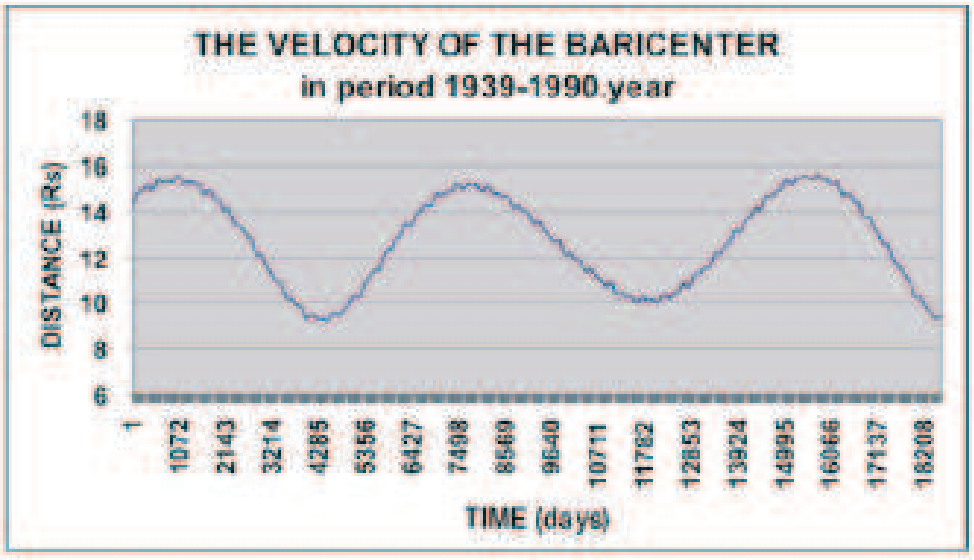

Figure 2: The velocity of the baricenter.

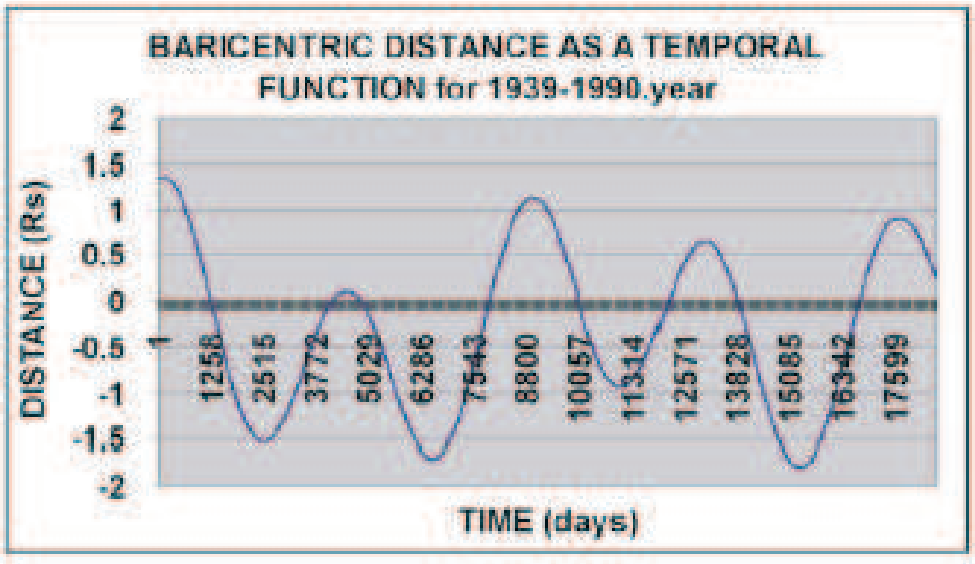

Figure 3: The baricentric distance as temporal function determines period.

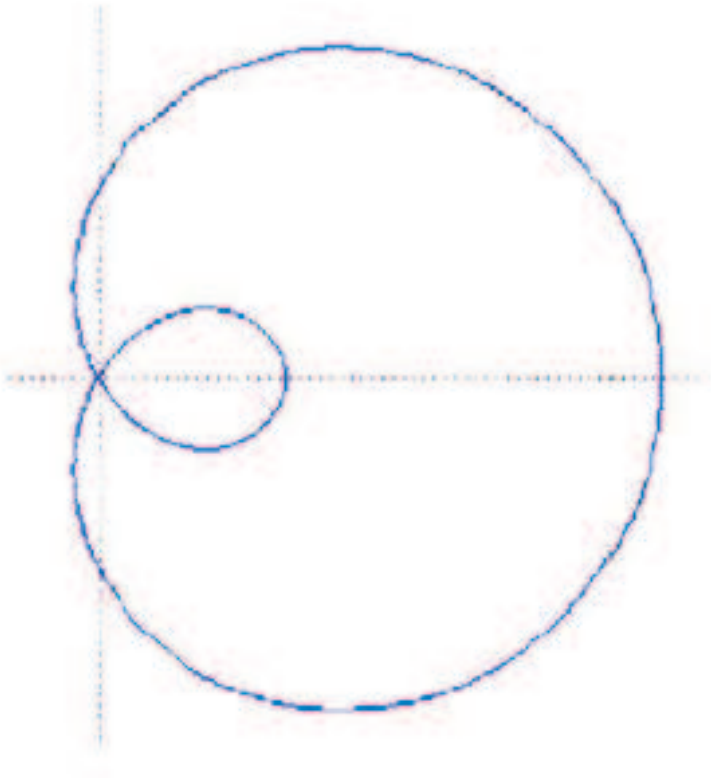

Figure 4: Limacon of Pascal.

3. A REMARK

The nearest curve by its form is known under the name of limacon of Pascal. It is a spiral form given by the formula:

$$r = b + 2a \cdot \cos(\omega \cdot t), \tag{9}$$

with exponent in amplitude for the unity smaller compared with our curve, in generalized form:

$$r^2 = b^2 + 2a^2 \cdot \cos(\omega \cdot t + \Delta), \tag{10}$$

Our curve is in form very similar to spiral of Archimedes, which half period opens and second half closes. We think that fact of mutually dependent parameters, connected by Kepler's law: $\omega_i^2 a_i^3 = GM/m_i = const$, caused the pulsating form of this curve. That is reason for our proposal that this curve would be denoted **as pulsating spiral of Kepler**.

4. CONCLUSIONS

The baricentric motion of the Sun with amplitude of 2.175 solar radius, and with period of 11.86 years have not remarkable influence to the orbital motion of planets. But, this motion is not negligible in some investigations, as it is nano-gravity at the Earth's surface. Effect of the baricentric motion of the Solar center can appear as a gravity potential wave in the Sun - Earth - Moon system, built-in into lunar tidal influence. (Koruga et all. 2003). Here we gave period, amplitude, velocity and form of orbit for this motion.

References

Grin, R.M.: 1998, ASTRONOMIJA – klasika u novom ruhu, Vesta Company, Beograd. (R. M. Green: Astronomy – classics in new form, textbook of practical astronomy).

Koruga, Dj., Tomić, A., Ratkaj, Ž.: 2003, Proceed. of 5th Congres of Balkan Phys. Union, Vrnjacka Banja, 24-28. VIII 2003, A-23, 2023.

Milanković, M.: 1935, Nebeska mehanika, textbook.

Vernic, R.: 1953, in Almanah Bošković za 1953. g, Hrv. Prirodosl. Društvo, Zagreb, 145.

Proc. IV Serbian-Bulgarian Astronomical Conference,
Belgrade 21–24 April 2004,
eds. M. S. Dimitrijević, V. Golev, L. Č. Popović, M. Tsvetkov,
Publ. Astron. Soc. "Rudjer Bošković" No 5, 2005, 295 - 301 *Contributed paper*

KONKOLY WIDE-FIELD PLATE ARCHIVE

M. TSVETKOV[1], L. G. BALÁZS[2], A. FRONTÓ[2], J. KELEMEN[2], A. HOLL[2], K. Y. STAVREV[1], K. TSVETKOVA[1], A. BORISOVA[1], D. KALAGLARSKY[3] and R. BOGDANOVSKI[3]

[1] *Institute of Astronomy, Bulgarian Academy of Sciences,*
72 Tsarigradsko Shosse blvd., 1784 Sofia, Bulgaria
E–mail tsvetkov@skyarchive.org

[2] *Konkoly Observatory, Hungarian Academy of Sciences,*
Konkoly Thege M. ut 15-17, 1121 Budapest, Hungary
E–mail balazs@konkoly.hu

[3] *Space Research Institute, Bulgarian Academy of Sciences,*
6 Moskovska str., 1000 Sofia, Bulgaria
E–mail damyan@skyarchive.org

Abstract. The wide-field photographic observations in Konkoly Observatory were performed in the period 1962 – 1997 with the 60/90/180 cm Schmidt telescope in Piszkéstető Mountain Station. The archive of the telescope contains more than 13 000 observations described in the Konkoly plate catalogue. After the preparation of an enlarged version of the catalogue it has been incorporated in the Wide-Field Plate Database installed in the Sofia Sky Archive Data Center with a possible on-line search at `http://www.skyarchive.org/search/`. Results from the analysis of the catalogue data characterizing the observational activity at Konkoly in the period 1962 – 1997 are presented.

1. THE KONKOLY SCHMIDT TELESCOPE

The main instrument for wide-field observations of Konkoly Observatory of the Hungarian Academy of Sciences is the 60/90/180 cm Schmidt telescope, manufactured by Carl Zeiss Jena and put in operation in 1962. The telescope (Fig. 1) is located in the Piszkéstető Mountain Station of the Konkoly Observatory at about 120 km North-East of Budapest, in the Matra Mountains (coordinates: $\lambda = 19°53'.7$ E, $\phi = +47°55'.1$) at 958 m altidude.

The main characteristics of the telescope are: clear aperture - 0.60 m, mirror diameter – 0.90 m, focal length – 1.80 m, scale – $115''$/mm, and field size – $5°$ (circular field with diameter 15 cm).

Up to the beginning of 1997 the telescope was used with photographic plates for direct observations or with $2°$ and $5°$ objective prisms. The following Kodak emulsions were used: 103aO, IIaO, OAO, 103aJ, IIIaJ, 103aG, 103aD, IIaD, OAD, 103aF, IIIaF,

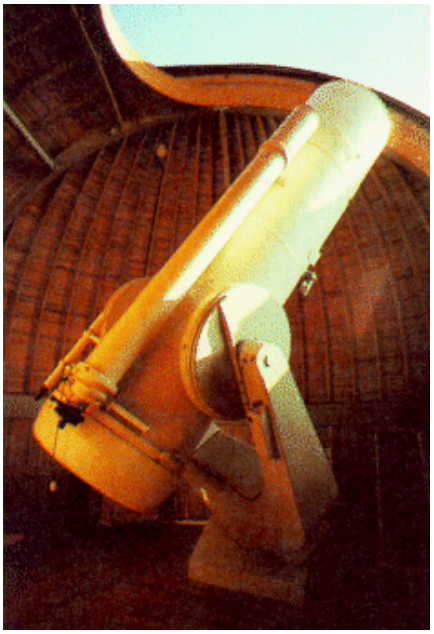

Figure 1: The 60/90/180 cm Schmidt telescope of Konkoly Observatory.

103aE, I-N and 09802, as well as some ORWO (ZP, ZU, RP, RO, ASTRO), AGFA, and Perutz emulsions. Standard *RGU* and Johnson (*UBVRI*) photographic filters were at disposal: UG1, UG2, BG12, GG5, GG13, GG14, RG1 and RG5.

Since 1996 the main light detector is a Photometrics liquid cooled CCD camera with a Kodak KAF1600 1534×1024 chip.

2. THE PLATE ARCHIVE

The plate archive was accumulated in the period 1962 – 1997. It comprises about 12 300 direct and about 800 objective prism plates. Usually plates with size of 16×16 cm were used. The limiting magnitude reached is about $19^{\rm m}$ (B). The astronomer in charge for the archive is L. G. Balázs (balazs@konkoly.hu). The plate archive is stored in the main building of the Konkoly Observatory.

The original plate catalogue made by the observatory team contains the following information: running plate number, equatorial coordinates of plate centre, emulsion type and hypersensibilization, objective prism, filter, observation date and time (usually UT), exposure duration, code for the observer, comments for quality and availability, object or field name, and method of observation.

The original plate catalogue was reduced to the format required by the WFPDB by the Sofia Sky Archive Data Center team. The description of the WFPDB format can be found through the VizieR catalogue browser in CDS – Strasbourg at `http://vizier.u-strasbg.fr/cats/VI.htx` – catalogue number VI/90.

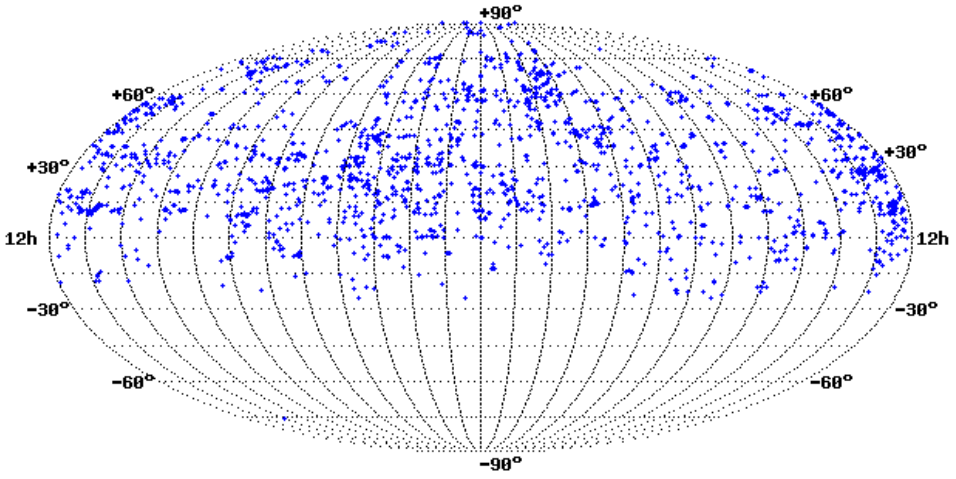

Figure 2: All-sky distribution of the Konkoly Schmidt telescope observations.

3. ANALYSIS OF THE KONKOLY PLATE CATALOGUE

The analysis of the Konkoly plate catalogue is based on data retrieval from the Wide-Field Plate Database (WFPDB, `http://www.skyarchive.org`). In the WFPDB the Konkoly plate catalogue can be found under the WFPDB Instrument Identifier KON060, which according to the accepted rule consists of a 3-letter abbreviation for the observatory name and the clear aperture of the telescope in cm.

The total number of direct and spectral plates in the plate catalogue is 12 707, obtained in the period 1962 – 1996.

The distribution of the plate centres on the celestial sphere in equatorial coordinates is presented in Fig. 2.

The time distribution of the number of plates is shown in Fig. 3. As it is seen the most productive period is 1967 – 1979 after which a decline in the number of photographic observations started. It deserves to mention the years 1967 – 1968, when there is a maximum of observational activity for the whole period of the telescope operation. Starting with the seventies the plate consumption was gradually decreasing due to the steadily increasing prices of the photographic plates and the economic troubles of Hungary. Those scientific topics received more emphasis where the information content of an observed plate was high. One has to mention the Hα survey of young stellar objects in star forming regions which is still the most powerful research topic of the institute.

The month distribution of the number of plates shows a maximum for October and a comparatively high observational activity during the winter months (January – March), which obviously is partly due to the length of the night and the meteorological conditions.

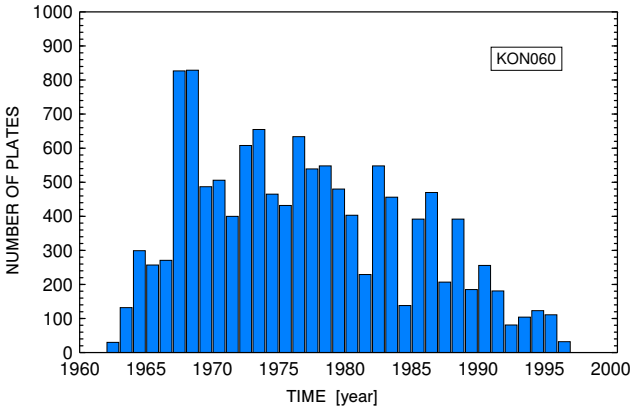

Figure 3: Time distribution of the number of Konkoly plates.

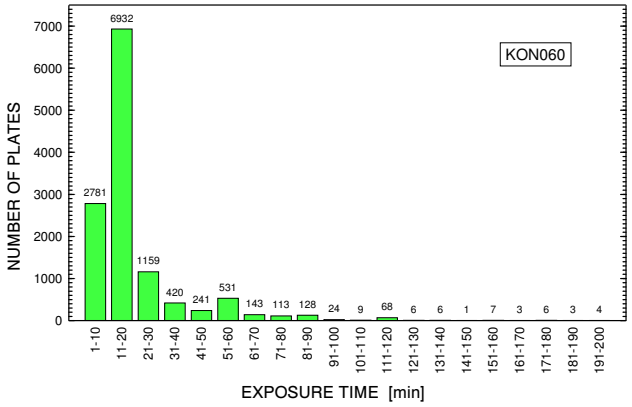

Figure 4: Distribution of Konkoly observations by exposure time.

Exposures mainly up to 30 min were used (Fig. 4). Exposures larger than 1 hour were rarely applied.

In Fig. 5 the distribution of the number of plates versus object type is given. The majority of plates in Konkoly Observatory is devoted to observations of selected fields (57%) – mostly of regions which are rich in galaxies for searching supernovae –, star clusters (16%) and individual galaxies (9%). (It is worth mentioning that in 1995 when the last SN with the Schmidt was recorded the number of catalogued events was about 1000 and out of them 42 were discovered in Piszkéstető.) The distribution of the selected fields according to the name of the constellation is presented in Fig. 6 with Ursa Majoris, Leo and Virgo as the most observed regions on the sky. The observers have given in the logbook the object name for less than 40% of the observations. The distribution by object name is shown in Fig. 7 with M 45 being the most observed object.

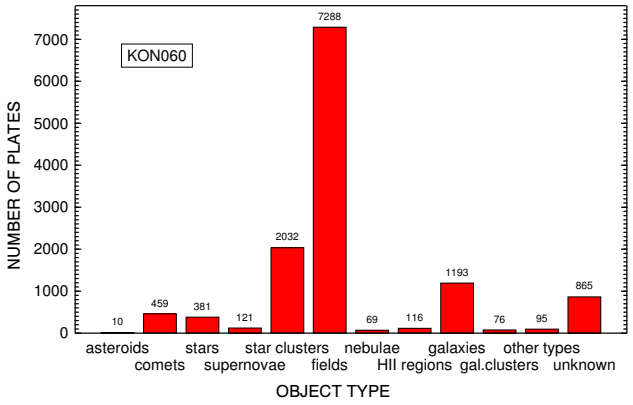

Figure 5: Number of Konkoly plates versus object type.

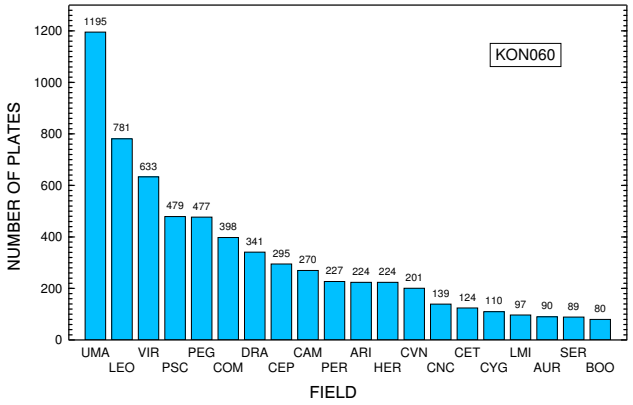

Figure 6: Distribution of Konkoly observations according to field region (constellation).

The examination of the catalogue data shows a total number of 35 observers with the Schmidt telescope. The ordering of the observers by the number of obtained plates (Fig. 8) shows that the most productive observer has more than 5000 plates (Miklós Lovas) and other 3 observers (Lajos G. Balázs, Maria Kun and Gábor Szécsényi-Nagy) have obtained between 1000 and 2000 plates. The first 10 observers according to the number of plates have obtained 96% of all plates (the upper four plus István Jankovics, Imre Tóth, Béla Balázs, Margit Paparó, Zsuzsa Vizi, and János Kelemen).

The check-up of the plate availability made in December 2003 revealed that available in the plate vault of Konkoly Observatory are 8935 plates or 70.3% of all plates, while 3772 plates (29.7%) are not available in the archive. Most of them are still at the observers.

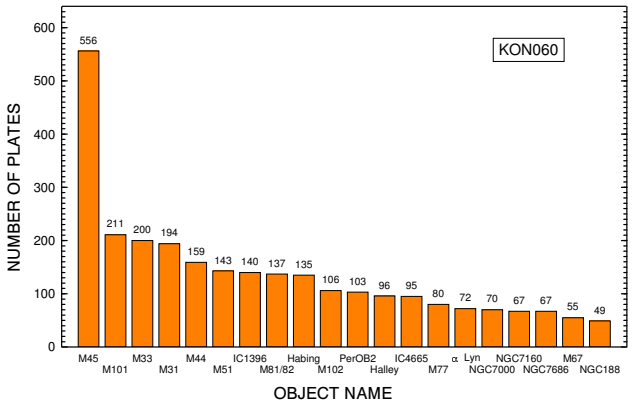

Figure 7: Distribution of Konkoly observations by object name.

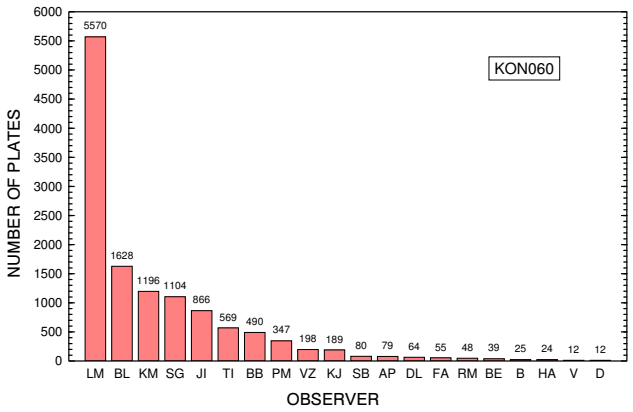

Figure 8: Number of Konkoly plates obtained by different observers.

4. PLATE DIGITIZATION

The Konkoly Observatory has at disposal a flatbed scanner UMAX PowerLook 3000. With it scanning in high resolution mode of 3048 dpi (8 μm) is possible. One Konkoly plate can be scanned for about 20 min in two parts because of the 8 cm wide field of the scanner in this mode. The total volume of the digitized information per plate (with some overlapping of the two parts) is nearly 400 Mb. Up to now only several dozens of selected plates, most of them in the Pleiades region, have been scanned.

5. CONCLUSIONS

More than 13 000 plates were obtained in the period 1962 – 1997 with the 60/90/180 cm Schmidt telescope of Konkoly Observatory, Hungarian Academy of Sciences, as a main observatory instrument for wide-field photographic observations. The data for these plates from the Konkoly plate catalogue were included in the WFPDB and thus made accessible on-line at `http://www.skyarchive.org`. The analysis of the plate catalogue data shows that the majority of plates are devoted to observations of selected fields (57%), mostly for supernova research, star clusters (16%) and individual galaxies (9%). Presently in the plate vault of Konkoly observatory are available 8935 plates or 70.3% of all plates, while 3772 plates (29.7%) are not in the archive – most of them are still at the observers. Selected plates in the Pleiades region have been scanned with the Konkoly Observatory flatbed scanner UMAX PowerLook 3000 which offers good possibilities for plate digitization. The results from the conducted wide-field observations in Konkoly have been published in the contributions of the institute, in IBVS, as well in other known astronomical journals.

Proc. IV Serbian-Bulgarian Astronomical Conference,
Belgrade 21–24 April 2004,
eds. M. S. Dimitrijević, V. Golev, L. Č. Popović, M. Tsvetkov,
Publ. Astron. Soc. "Rudjer Bošković" No 5, 2005, 303 - 308 *Contributed paper*

BAMBERG SOUTHERN PHOTOGRAPHIC PATROL SURVEY: INCORPORATION IN THE WFPDB

M. TSVETKOV[1], K. TSVETKOVA[1], A. BORISOVA[1], D. KALAGLARSKY[2], R. BOGDANOVSKI[2], U. HEBER[3], I. BUES[3], H. DRECHSEL[3] and R. KNIGGE[3]

[1] *Institute of Astronomy, Bulgarian Academy of Sciences, 72 Tsarigradsko Shosse Blvd., 1784 Sofia, Bulgaria*
E–mail tsvetkov@skyarchive.org

[2] *Space Research Institute, Bulgarian Academy of Sciences, 6 Moskovska Str., 1000 Sofia, Bulgaria*
E–mail damyan@skyarchive.org

[3] *Dr. Remeis-Sternwarte Bamberg, Astronomical Institute of the University of Erlangen-Nürnberg, Sternwartstrasse 7, D-96049 Bamberg, Germany*
E–mail heber@sternwarte.uni-erlangen.de

Abstract. The description, cataloging and incorporation in the Wide-Field Plate Database (WFPDB, `http://www.skyarchive.org`) of the Dr. Remeis-Observatory Bamberg Southern Photographic Patrol Survey (22 000 plates) is presented. The survey was taken with 20 cameras (each with $d = 10$ cm), Zeiss camera ($d = 7$ cm), and the Harvard telescopes – $10''$ Metcalf and $3''$ Ross B. The plates stored at present in the observatory stacks were obtained in the period 1963 – 1976 in Boyden Observatory (South Africa), Mount John University Observatory – Lake Tekapo (New Zealand) and San Miguel Observatory (Argentina). The observational programme supported by the Deutsche Forschungsgemeinschaft (DFG) was under the supervision of Prof. Dr. W. Strohmeier – Director of the Bamberg Observatory at that time. For the first time digital CCD preview images of the plates by observational zones are included in the WFPDB and an access to them for the worldwide astronomical community is provided. A special attention is paid to the sub-survey in the LMC region. An opportunity for on site plate digitization with Epson Expression 1640XL flatbed scanner is offered in the observatory since May 2003.

1. INTRODUCTION

In the early 60s German astronomers from Potsdam, Hamburg, Heidelberg, Göttingen, etc. activated their plans to create a southern astronomical observatory (Wolfschmidt, 2002). As a result the ESO (at present the world largest astronomical organization) was founded in 1963 in the framework of the European cooperation. Just in that time the Bamberg astronomers (Strohmeier, 1965) launched a project of monitor- ing the southern sky with 10 cm Kodak multiple astrograph placed at the

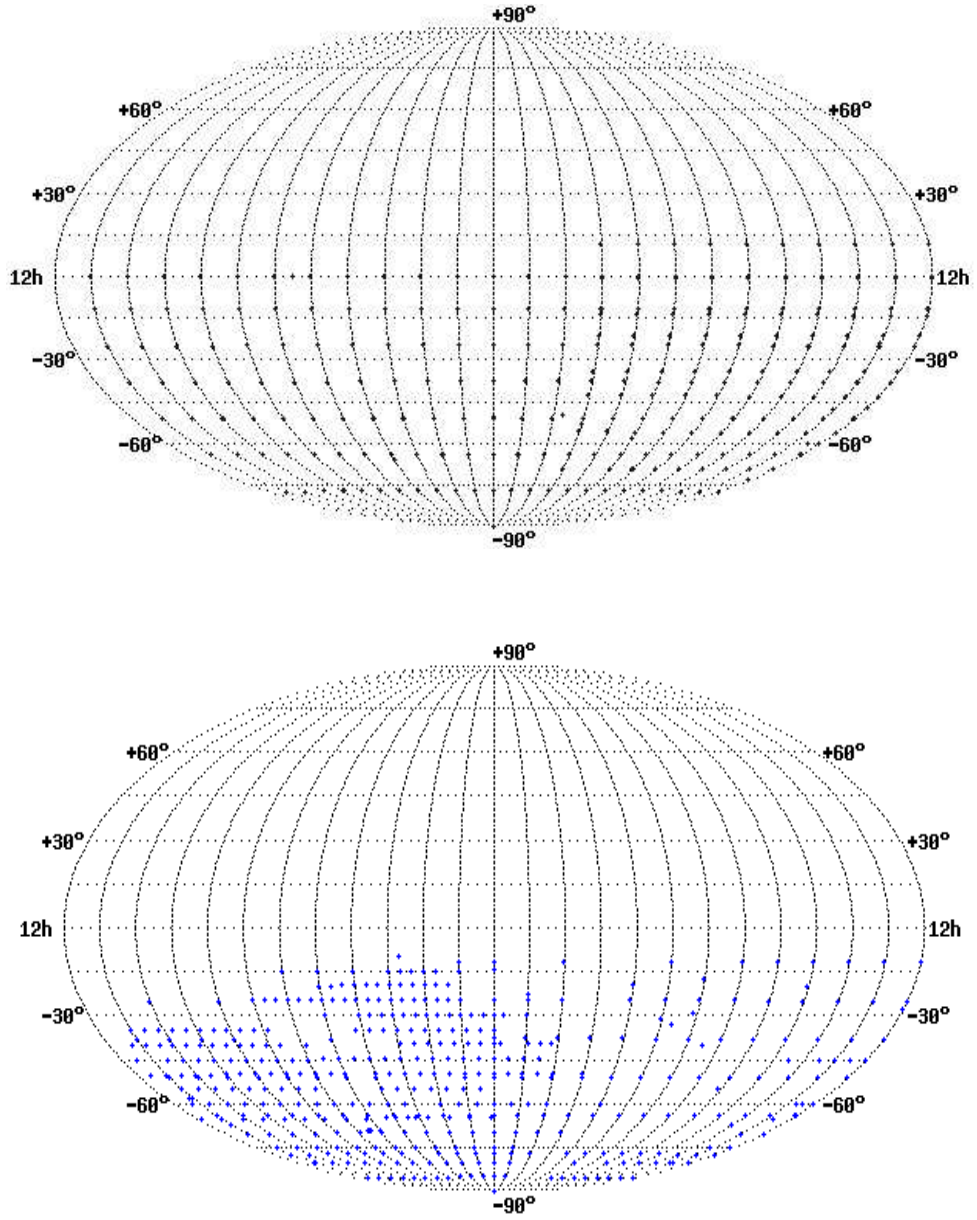

Figure 1: All-sky distribution of the Bamberg Southern Photographic Patrol Survey observations in Molweide projection for BAM010 multiple cameras (upper panel), and HAR025 and HAR008C telescopes (lower panel).

Boyden Station (South Africa). The project chaired by Prof. W. Strohmeier – Director of the Bamberg Observatory at that time, was supported by the Deutsche Forschungsgemeinschaft (DFG) and successfully executed in the period 1963 – 1976. As a result more than 22 000 monitoring plates covering the whole southern sky were received, now well stored in the Bamberg Observatory.

The Bamberg Southern Photographic Patrol Survey (BSPPS) is a unique Southern sky survey as the Harvard sky patrols in South Africa were stopped at that time and other observatories were not still active. That is why for some astronomical tasks the value of this archive now continues to be rather high. Here we present our work on the cataloguing and incorporation into the Wide-Field Plate Database (WFPDB, Tsvetkov 1992, Tsvetkov et al. 1997, `http://www.skyarchive.org`) of the Dr. Remeis-Observatory BSPPS.

2. THE PLATE ARCHIVE

The plates of the Dr. Remeis-Observatory BSPPS were taken in the period 1963 – 1976 with 20 Kodak cameras ($d = 10$ cm, WFPDB identifiers BAM010A, B, C,..., T), the Bamberg 7 cm Zeiss camera (BAM007), and the Harvard telescopes – $10''$ Metcalf (HAR025), and $3''$ Ross B (HAR008C). The emulsions used for the survey were Perutz (for the period 1963 – 1964) and AGFA Astro (for the rest of the monitoring period). In 1973 – 1976 some Kodak emulsions were successfully used mainly for the observations in New Zealand. The plate size is usually 16×16 cm, covering respectively field of 13 sq. deg. The plates in Boyden Observatory (South Africa) were received with the cameras BAM010A, B, C,..., J, in Mount John University Observatory –Lake Tekapo (New Zealand) with the cameras BAM010K, L, M, N, and in San Miguel Observatory (Argentina) with the cameras BAM010O, P, Q, R, S, T. The observational programme was executed manly by R. Knigge and his Bamberg collabor- ators – E. Shöffel, F.-M. Sosna, U. Köhler, and H. Ott, as well as by S. Shaw and J. Sievers from Florida University and the astronomers technicians Fischer and Meier from Boyden Station. In Mount John University Observatory the programme was executed by I. Paterson and M. Clark. In San Miguel Observatory the observations were done by F.-M. Sosna and A. Alarcon.

All plates at present are stored in the observatory plate stacks in very good conditions.

3. INCORPORATION IN THE WFPDB

The computer-readable version of the BSPPS plate catalogue and the database access to it were prepared by the WFPDB team at the Sofia Sky Archive data Center of the Bulgarian Academy of Sciences in the period 1996 – 2002. For this purpose the log books made mainly by R. Knigge were used. For the rest Southern plate collection the information was taken from the plate envelopes.

The all-sky distribution of the BSPPS plates in Molweide projection is presented in Fig. 1a for the Bamberg astrograph with multiple cameras (BAM010) working in Bloemfontain Boyden Station (South Africa), Mount John University Observatory

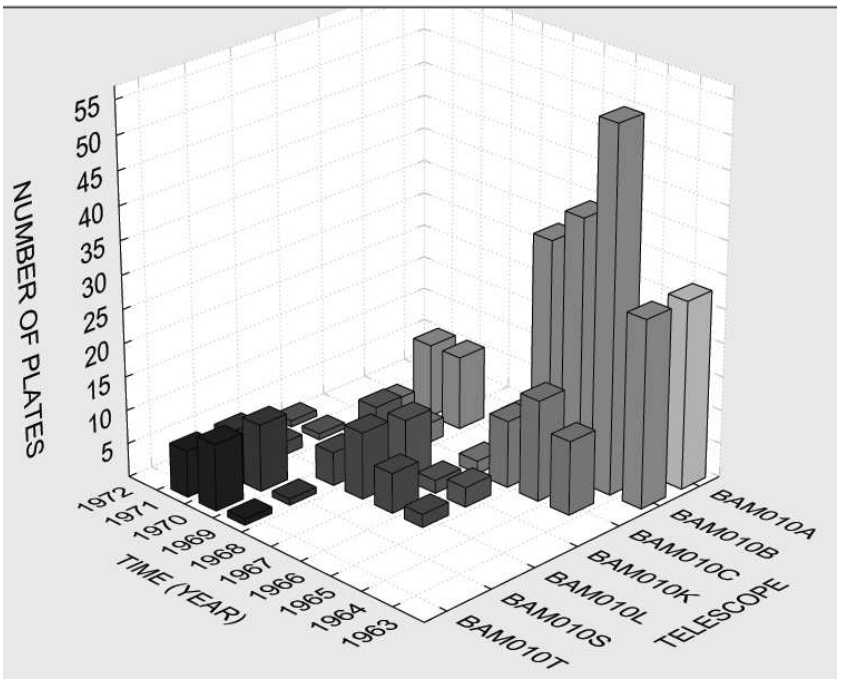

Figure 2: Distribution of the number of LMC plates versus time and instrument.

(New Zealand) and San Miguel Observatory (Argentina), and in Fig. 1b for the Harvard telescopes 10″ Metcalf (HAR025) and 8″ Ross B (HAR008C) in Boyden Station.

The WFPDB Search page now provides not only information for the BSPPS plates needed but also the previews of the plate images taken with a 2 Megapixel SiPiX CCD camera. This is the beginning of the creation of an archive of digitized preview images of the plates in the WFPDB as an unseparated part of the database itself. Besides this an on-line archive of selected digitized plate images is on the way to be prepared.

4. BAMBERG LMC SURVEY

In the frame of the BSPPS a special attention on the monitoring of the Large Magellanic Cloud (LMC) was paid. The Bamberg LMC sub-survey contains about 300 plates received with the astrograph (BAM010) and the Harvard 10″ Metcalf (HAR025) and 8″ Ross B (HAR008C) telescopes.The distribution of the BAM010 LMC plates versus time and instrument is presented in Fig. 2. A preview image of the LMC BSPPS plate (NZ194) scanned with the Bamberg Epson Expression 1640XL flatbed scanner is shown in Fig. 3.

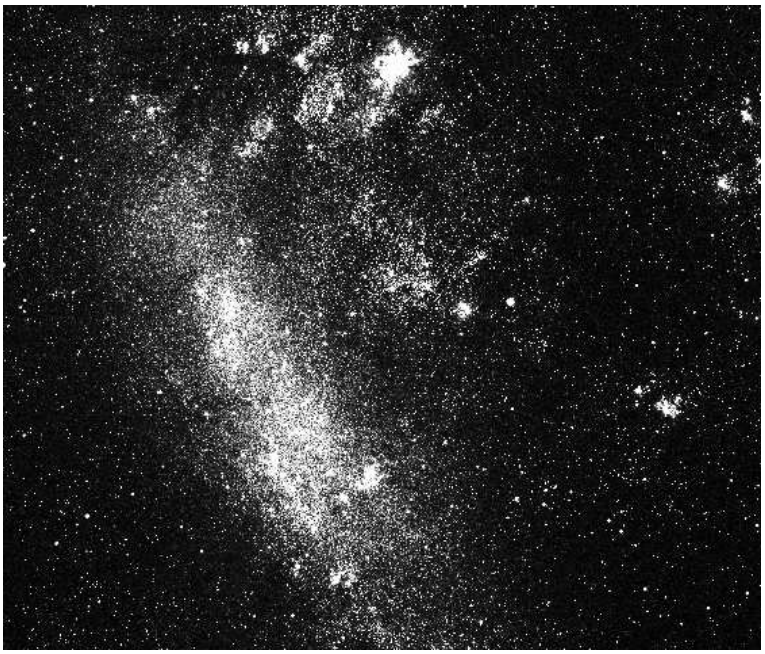

Figure 3: Preview image of the LMC BSPPS plate NZ194.

5. PLATE AVAILABILITY AND DIGITIZATION

The original plates are at disposal in Dr. Remeis-Observatory Bamberg for different astronomical tasks upon request.

The new scanning facility in the Bamberg Observatory Plate Stack provided recently by DFG is a flatbed scanner Epson Expression 1640XL and a powerful PC with DVD writer. It allows to digitize the plates with an optimal resolution of 16 μm with A3 plate size in FITS format. The resolution is good enough for different tasks up to the plate limit, which varies from $11^{\rm m}$ to $14^{\rm m}$ (pg).

Acknowledgements

We acknowledge supports by the Alexander von Humboldt Foundation (2001 – 2003), DFG (2003), BAS/DFG 436-BUL110/120/0-2 project, the Bulgarian National Science Fund grant NFS I-1103/2001 and the IAU Commission 9 "Instruments" Working Group on Sky Surveys. Last year part of this work was coordinated in the frame of COST Action 283 Computational and Information Infrastructure in the Astronomical DataGrid. M.T. and A.B acknowledge the support of the AvH Foundation in the frame of the program Stability Pact for Central and East European Countries.

References

Strohmeier, W.: 1965, Kleine Veroeff. der Remeis Sternwarte, Bd. IV, No. 40, p. 302.
Tsvetkov, M.: 1992, *IAU WGWFI Newsletter*, **2**, 51.
Tsvetkov, M., Stavrev, K., Tsvetkova, K., Semkov, E., Mutafov, A., Michailov, M.-E.: 1997, *Baltic Astron.*, **6**, 271.
Wolfschmidt, G.: 2002, *Astron. Nachr.*, **323**, 548.

Proc. IV Serbian-Bulgarian Astronomical Conference,
Belgrade 21–24 April 2004,
eds. M. S. Dimitrijević, V. Golev, L. Č. Popović, M. Tsvetkov,
Publ. Astron. Soc. "Rudjer Bošković" No 5, 2005, 309 - 315 *Contributed paper*

ARCHIVING OF THE POTSDAM WIDE-FIELD PHOTOGRAPHIC OBSERVATIONS

M. TSVETKOV[1], K. TSVETKOVA[1], K. Y. STAVREV[1], G. M. RICHTER[2], P. BÖHM[2] and K. STAUBERMANN[3]

[1] *Institute of Astronomy, Bulgarian Academy of Sciences, 72 Tsarigradsko Shosse blvd., 1784 Sofia, Bulgaria*
E–mail tsvetkov@skyarchive.org

[2] *Astrophysical Institute Potsdam, An der Sternwarte 16, D-14482 Potsdam, Germany*
E–mail pboehm@aip.de

[3] *University Museum Utrecht, Utrecht, The Netherlands*

Abstract. The inventory of the wide-field plate archives stored in the Astrophysical Institute Potsdam since 1879 is presented. The whole Potsdam plate collection consists of 11 wide-field plate archives obtained in the period 1879 – 1970 (see Catalogue of Wide-Field Plate Archives, version 5.0, March 2004, `http://www.skyarchive.org`) with about 10 000 plates stored not only in Potsdam but in Leiden and Sonneberg, too. The plates contain valuable astronomical information easily to be retrieved. The Potsdam wide-field plate collection reflects also the history and development of the Potsdam Observatory.

1. INTRODUCTION

The archived astronomical wide-field photographic observations are now a part of the existing virtual observatories world-wide. Their importance results from the chance to follow certain astronomical objects with definite coverage in time and space. The possibilities for a quick plate digitization now and the on-line access to the plate information have increased the re-usage of the archived observations. Information about the wide-field photographic archives and their contents can be found in the Wide-Field Plate Database (WFPDB), installed in Strasbourg (`http://vizier.u-strasbg.fr/cats/VI.htx`) and its updated version in Sofia (`http://www.skyarchive.org/`). Many observatories possessing such archives like Asiago Observatory, Royal Observatory of Belgium, Rozhen Observatory, Institute of Astronomy in Cambridge, David Dunlap Observatory, Bamberg Observatory, Royal Observatory Edinburgh, Harvard College Observatory, Maria Mitchell Observatory, Sonneberg Observatory, Midi-Pyrenees Observatory, Valencia Observatory, Main Astronomical Observatory Kiev, etc. have started the execution of projects for scanning of the archival plates.

The accumulated wide-field photographic observations in the Astrophysical Institute Potsdam (AIP) have made well known contributions not only to astronomy, but also to the development of photography itself since the end of the 19th century. In this context we remember many observers from Potsdam like e.g. O. Lohse (since the foundation of the observatory), J. Scheiner (the end of 19th century), J. Hartmann (the beginning of 20th century), E. Hertzsprung and K. Schwarzschild (the 10s of 20th century), G. Eberhard (the 20s and 30s of 20th century). Practically, the Potsdam Observatory was the base for testing new astronomical emulsions, beginning with the dry photographic plates of Schleussner (produced in Frankfurt), to AGFA Enterprise up to 1960 and ORWO after 1960.

The process of archiving the wide-field photographic observations comprises such steps as making of an inventory of the plate collection, preparation of computer-readable versions of the plate catalogues, plate digitization and providing of good storage with suitable temperature, humidity free conditions and easy access to the plates and to the plate digitized information. Here we present this process, running in the AIP.

2. INVENTORY OF THE AIP ARCHIVES

The wide-field plate collection in AIP dates since 1879 when the Astrophysical Observatory Potsdam was put in operation. The beginning of the collection is connected with the name of Oswald Lohse – Haupt-Observator in Potsdam at that time. The wide-field photographic observations, obtained in the period 1879 – 1970, are separated in 11 archives according to the instrument with which they are made. The total number of plates and films in these archives is about 10 000 (including the plates stored in Leiden and Sonneberg).

The plate collection has been stored under relatively good conditions (having in mind such practical problems like humidity, dust, strong illumination, and optimal room temperature) in the building of the Great Refractor (Telegrafenberg), as well as in the new AIP library in Babelsberg (former dome of the 1.22 m telescope) for the archives of Lohse and both Schmidt telescopes.

Table 1 presents an excerpt from the Catalogue of Wide-Field Plate Archives (CWFPA, version 5.0, March 2004, URL: `http://www.skyarchive.org`) and gives some data for the Potsdam Observatory instruments for wide-field photographic observations, as follows: the WFPDB instrument identifier, the main instrument characteristics (type, location, clear aperture, focal length, scale, field size), the years of operation and the number of obtained plates/films. The WFPDB instrument identifier consists of a 3-letter abbreviation of the name of the observatory/institute and the aperture of the telescope in cm. In case of instruments with the same aperture in the same observatory a suffix A, B, C, etc. is added.

3. POTSDAM WIDE-FIELD PLATE ARCHIVES

3.1. THE LOHSE ARCHIVES (POT013B AND POT030A)

The archives contain observations since 1879. According to Lohse's logbook (fortunately found in the library), 217 plates are obtained with the refractor of 30 cm diameter, focal length of 5.4 m, and $38''$/mm scale. The manufacturer of the optics

Table 1: Potsdam Observatory Wide-Field Instruments

WFPDB Instrument Identifier	Type	Location[1]	Clear Aperture [m]	Focal Length [m]	Scale [″/mm]	Field Size [°]	Years of Operation	Number of Plates or Films
POT013A[2]	Rfr	T	0.13	2.10	98		1879-1908	
POT013B	Rfr	T	0.13	1.36	152	5.0	1888-1889	15
POT015[3]	Cam	T	0.15	1.50	137	7.6	1908-1948	3000
POT020[4]	Rfr	T	0.20	3.40	61	1.5	1879-1908	
POT025	Sch	T	0.25/0.30	0.75	275	6.8	1949-1967	405
POT030A	Rfr	T	0.30	5.40	38	1.2	1879-1930	88
POT030B	Rfl	T	0.30	0.90	229		1906-1930	1500
POT032	Rfr	T	0.32	3.40	61	2.7	1889-1920	3000:
POT040A	Rfr	B	0.40	5.50	38	1.7	1917-1938	1436
POT040B[5]	Rfl	T	0.40	0.90	229		1932-1948	
POT050	Sch	T	0.50/0.70	1.72	122	4.5	1952-1970	507

Notes: [1] T – Telegrafenberg, B – Babelsberg. [2] A Steinheil refractor with a tripod manufactured by Pistor and Martin. [3] In 1932 this Zeiss triplet was provided with the 17 cm photovisual objective with 1.20 m focal length. [4] The manufacturer is H. Grubb. In 1908 the Grubb refractor was provided with the 30 cm Steinheil objective for visual photometry of stars. [5] The mirror is parabolic.

was H. Schröder and for the mechanics – A. Repsold. This refractor was called "the Great Refractor" in the period 1879 – 1899 (after 1899 the name "Great Refractor" was ascribed to the new 80 cm refractor, then put in operation). Since 1888 Lohse had sometimes mounted two heliographic objectives with a diameter of 0.13 cm (the first one with 2.1 m focal length, 98″/mm scale, and the second one with 1.36 m focal length, 152″/mm scale, and 5° field size) on the refractor. Lohse's archives made with this telescope and with the attached second heliographic objective are only partly identified till now. They are presented in Tsvetkov et al. (1999a,b).

3.2. THE POTSDAM ZONE CARTE DU CIEL ARCHIVE (POT032)

The Astrographic Catalogue (AC), also known as Carte du Ciel (CdC), was a massive program started in 1887 by 22 observatories with the aim to photograph and measure positions for stars to magnitude $B = 12.5$. The resulting observatory catalogues contain rectangular coordinates of varying precision for over 4.5 million stars, spanning a very wide range of epochs around the average near 1905. These positions, now in computer-readable form, have been reduced to equatorial coordinates nominally in the Hipparcos (ICRS, J2000) system. One of several completed versions is the AC2000. The deep CdC plates with one exposure of 80 min are supposed to be the deepest sky survey available at the end of the 19th century.

The Potsdam Zone of CdC (dec. +31° to +40°) was observed with the double refractor containing one 32 cm photographic objective and one 24 cm visual objective of the manufacturers Steinheil and Repsold. Later on the 32 cm double refractor was replaced by a mirror telescope for spectrographic observations.

The Potsdam CdC archive, containing about 3000 plates, is especially important having in view the started digitization of CdC plates: Cordoba Zone by the UMAX Astra 1220P flatbed scanner (1028 scanned plates, Calderon et al. 2002), Vatican (540 scanned plates, Barbieri et al. 2003), Bordeaux Zone (+11° to +18°) (about 530 scanned plates, Argyle 2002), Sydney Zone (−52° to −64°) (about 360 scanned

plates, Argyle 2002). Plates from the Catania Zone (+47° to +54°), Algiers Zone (+4° to −2°), Brussels and Toulouse have been scanned, too.

Already Fresneau et al. (2001, 2003) made repeated usage of the triple exposure CdC plates and revealed significant opportunities for the detection of flare stars.

3.3. THE HERTZSPRUNG ARCHIVES (POT015, POT030A, AND POT040A)

Some of the Potsdam plates were found by us in Leiden Observatory stored in excellent conditions. These are the plates of Hertzsprung who worked in the Potsdam Observatory from 1909 to 1919 as an observer and moved to Leiden later. A big part of the found Hertzsprung plates - about 460 plates, were obtained with the 15/150 cm Zeiss Triplet located in Telegrafenberg (POT015). The 15/150 cm Zeiss was installed mainly for photographic photometry (Hassenstein, 1941). Another part of the Hertzsprung archive according to the logbook found in Leiden was obtained with the 30/540 cm telescope (POT030A, 36 plates) and the 40 cm Toepfer telescope (POT040A) located in Babelsberg.

3.4. THE 30/90 CM STEINHEIL-SCHMIDT (POT030B) ARCHIVE

The 30/90 cm telescope with the Steinheil objective was installed in 1905 in the west dome of the main building on Telegrafenberg to replace the Grubb refractor. O. Lohse was one of the first observers in January 1905. From October 1905 till February 1906 Bernhard Schmidt mounted on this telescope his 42 cm mirror with a focal lenght of 97 cm and the observatory staff observed obviously with it during Schmidt's work on the Steinheil objective improving. The Steinheil objective was corrected by Schmidt and since March 1906 the observations had been continued by the so called Steinheil-Schmidt optic telescope till October 1930. We found a log book containing information about 1500 plates.

3.5. THE 40 CM REFLECTOR (POT040A) ARCHIVE

The 40 cm reflector located in Babelsberg began its work in 1917. The plates were moved to Sonneberg in order to be re-used in the period of unification of Potsdam and Sonneberg observatories and now are stored there.

3.6. THE BIG SCHMIDT TELESCOPE (POT050) ARCHIVE

The archive contains information for 507 plates obtained in the period 1952 – 1970. The logbook was not found. The first observations (1952) suffered by the mirror astigmatisms and pillar vibrations caused by a nearby railway and the conducted seismographic investigations in Telegrafenberg. Test observations for suitability for spectral and luminosity classification with objective prism spectra with small dispersion (800 Å/mm at Hγ), were done during that period. In 1955 the mirror of the telescope was covered with aluminum and Zeiss Jena made a new correcting plate (1957). The telescope was used for direct or objective prism observations of occasional comets (1956h Arend-Roland, 1957d Mrkos, 1962c Seki-Lines, 1961e Humason). Numerous technical plates were made with the telescope for tests of the technical condition of the telescope, as well as for some technical improvements.

In 1979 the telescope was moved to the Bulgarian National Astronomical Observatory Rozhen as a gift of the Academy of Sciences of DDR to the Bulgarian Academy of Sciences and has been operated since that time by the Rozhen Observatory as a main wide-field instrument.

A special designation system for denoting of the plate serial number on the Big Schmidt telescope plate envelope was used, e.g. S1-007 FOO. S1 stands for the Big Schmidt telescope plates followed by the serial plate number. The last three capital letters were given for quick classification of the plates. The first letter denotes the purpose of the observation: F – for focusing, V – for test plate (from the German "Versuch"), S – for observation of star, N – for nebula, H – for cluster (from "Haufen"), K – for comet ("Komet"), P – small planet, M – Moon. The second letter concerns the use of a filter (with or without). Usually the letters O (stands for "Ohne" – without) and M ("mit" – with) – are used. The third letter stands for method of observation: O for objective (direct) plate, P – for prism, B – not clear to us, H – Hartmann test, R – reflex test picture, Z – for establishment of time scale ("Zeit"), G – not clear to us.[1]

3.7. THE SMALL SCHMIDT TELESCOPE (POT025) ARCHIVE

For the 0.25/0.30 m Schmidt telescope photographic emulsions coated on a glass (291 plates) and film base (119 observations) were used. The telescope was combined with an 8° objective prism with 280 mm diameter. With this telescope mainly spectrophotometric observations of the eclipsing binaries (AR Aur, VV Cep, Zeta Aur, AZ Cas, RS Oph) and comets (Pflug 1967)[2] were made.

The observers identified each plate by a special number, which reflected the observation method used. The designation for observation made on glass is e.g. SP008(S). SP stands for the (S)chmidt telescope (P)late, followed by the serial plate number and in brackets one of the three capital letters (S, V or F). S stands for real observation, usually (S)tar, V – for test observation, F – for focusing.

The designation for observation made on film is e.g. SF012(F). SF stands for the (S)chmidt telescope (F)ilm, followed by the serial plate number. In the brackets one of five letters was used: S – for Star observation, V – for Test plate, F – for Focus plate, H – for Cluster observed, K – for Comet.

4. MAIN OBSERVATIONAL PROGRAMS OF WIDE-FIELD PHOTOGRAPHIC OBSERVATIONS

The main observational programs of the wide-field photographic observations in Potsdam Observatory can be summarized as follows:

– Potsdam Survey of North BD Stars up to 7.5 mag

[1] One can meet a similar designation system later in the Palomar catalogue for the POSS II plates in a simpler form (only two letters used): first letter – S for survey plates, F for focus plates, T for test plates, U for USNO plates and P for different from survey plates; the second letter is used as a rule for designation of the emulsion type.

[2] The work of Pflug (1967) on the comet 1956h Arend-Roland is based on 16 plates. 14 of them are missing in the archive, probably still being kept by the observer.

(G. Müller and P. Kempf, 1886 – 1906)
– Continuation of Potsdam Survey for Weak BD Stars in the Polar Zone
(G. Müller, E. Kron and A. Kohlschütter, 1907 – 1920)
– Potsdam CdC Zone (dec. +31° to +40°)
(J. Scheiner, A. Biehl, O. Birck, 1883 – 1921)
– Photographic Photometry
(J. Scheiner, 1888 – 1891; E. Hertzsprung in the Pleiades and Praesepe, 1912 – 1918)
– Investigations of Double Stars
(J. Scheiner, 1908; E. Hertzsprung, 1914 – 1921; W. Münch, up to 1937)
– Application of Objective Prisms
(E. Hertzsprung, W. Münch, 1910 – 1927)
– Investigations of Dark Nebulae and Stellar Photometry in 115 Southern Kapteyn Selected Areas – the expedition to Bolivia (1928 – 1929)
– Investigations of Mira Type Stars
(R. Müller, 1933 – 1936)
– Investigations of Open Stellar Clusters
(W. Becker, 1935 – 1939)
– Investigations of Eclipsing Binary Stars
(K. Walter, 1937 – 1939)
– Investigations of Comets and Small Planets (up to 1970).

It is seen from the above summary that the Potsdam wide-field plate collection reflects the history and development of the Potsdam Observatory.

5. CONCLUSIONS

As a result of the inventory of the AIP wide-field photographic observations 11 archives obtained in the Potsdam Observatory in the period 1879 – 1970 were included in the Catalogue of Wide-Field Plate Archives. According to this catalogue (version 5.0, March 2004) one of the oldest plate archives in the world made by the former "Potsdamer Haupt-Observator" Oswald Lohse is partly stored in Potsdam. The AIP plate collection, accumulated as a result of different observational programs, contains about 10 000 plates (stored in Potsdam, Leiden and Sonneberg), and reflects the history and development of the Potsdam Observatory. The preservation of this scientific heritage through digitization of the observations is an important task for the future.

Acknowledgements

This work is supported by the National Science Fund at the Ministry of Education and Science of Bulgaria through contract I-1103/2001, by contract 436-BUL110/120/0-2 between Deutsche Forschungsgemeinschaft and the Bulgarian Academy of Sciences, and partly by the EC-COST Action 283.

References

Argyle, R.W.: 2002, in Preservation and Digitization of Photographic Plates, PDPP Newsletter No. 1, Ed. E. Griffin, p. 6.

Barbieri, C., Rampazzi, F., Stagni, R., Omizzolo, A., Bucciarelli, B., Lanteri, L., Marilli, E., Di Paola, A., Licausi, G., Laudi, L., Nesci, R., Rossi, C.: 2003, in Italian National Digitization Project Minutes of the kick-off meeting, Padova, January 20, 2003.

Calderon, J.H., Bustos Fierro, I.H., Willemoes, C., Melia, R.R., Giuppone, C.A.: 2002, *Boletin de la Asociacion Argentina de Astronomia*, **45**, 6.

Fresneau, A., Argyle, R.W., Marino, G., Messina, S.: 2001, *Astron. J.*, **121**, 517.

Fresneau, A., Vaughan, A.E., Argyle, R.W.: 2003, *Astron. J.*, **125**, 1519.

Hassenstein, W.: 1941, Mitteilungen des Astrophysikalischen Observatoriums Potsdam, No. 1.

Pflug, K.: 1967, *Astron. Nachr.*, **290**, 89.

Tsvetkov, M.K., Tsvetkova, K.P., Richter, G., Böhm, P., Scholz, G.: 1999a, *Astron. Nachr.*, **320**, 63.

Tsvetkov, M., Lukarski, H., Budell, R., Tsvetkova, K.: 1999b, Proc. of the Sixth National Conference on Contemporary Problems of Solar Terrestrial Connections, Sofia, 18-19 November 1999.

CIP - Каталогизација у публикацији
Народна Библиотека Србије, Београд

520/524 (082) (0.034.2)

SERBIAN-Bulgarian Astronomical Conference (4 ; 2004 ; Beograd)
Papers, Photos and Videos [Elektronski izvor] / IV Serbian - Bulgrarian Astronomical Conference, Belgrade, Serbia, 21-24 April 2004 ; edited by Milan S. Dimitrijević ... [et.al.]. - Belgrade : Astronomical Society "Rudjer Bošković", 2007 (Belgrade : N. Milovanović : M. S. Dimitrijević). - 1. elektronski optički disk (CD-ROM) ; 12cm

Nasl. sa naslovnog ekrana. - Tiraž 100.

ISBN 978-86-906631-3-2

a) Астрономија - Зборници b) Астрофизика - Зборници
COBISS.SR-ID 139864332